University of Newcastle upon Tyne

School of Electrical, Electronic and Computer Engineering

High Efficient Interleaved Boost Converter with Novel Switch Adaptive Control in Photovoltaic Application

A Thesis submitted for the degree of Doctor of Philosophy

March 2013

Saleh H. Elkelani Babaa

DECLARATIONS

I hereby declare that this thesis is my own work and the submission is in accordance with the University and School guidance on good academic conduct, and I confirm that the wordage is within the prescribed range as advised by my School and Faculty.

Abstract

Energy conversion efficiency is an important factor for the long-term feasibility of photovoltaic systems. Significant work has been carried out into improving the effectiveness of solar arrays in recent years. In addition, there has been substantial research into novel power converter topologies for maximum energy efficiency. However, in photovoltaic applications, even the most promising power converter topologies do not necessarily guarantee optimum performance under all operating conditions. For instance, the efficiency of the power conversion stage may be excellent during periods of high irradiance, but significantly lower in poorer light conditions. This work attempts to address this problem, by seeking to achieve higher energy conversion efficiency under sub-optimal conditions. In this thesis, stand-alone photovoltaic systems using DC-DC boost converters are considered. An interleaved boost converter with novel switch adaptive control scheme is designed to maximise system efficiency over a wider range of real-time operating atmospheric conditions and with different load conditions without incurring significant additional cost.

Acknowledgements

It is a pleasure to acknowledge the contribution of many individuals through the entire PhD years who have directly or indirectly helped my writing of this thesis.

Also, I am grateful to my supervisor Dr Matthew Armstrong for his numerous fruitful discussions and guidance help, thanks a lot. Moreover, I would like to thank my other colleagues Professor Volker Pickert, Gill Webber, the technicians and receptionists in our School for their cooperation and assistance.

Furthermore, I would like to express my deep gratitude to my parents and every member of my family for their endless inspiration, support and guidance throughout my whole life.

Last but not the least; I would like to thank my friends, who have supported me through their encouragement, support and friendship during this period of study.

Table of Contents

List of tables

List of figures

Chapter 5

Abbreviations

AC: Alternating current

ADC: Analogue to Digital converter

AGND: Analogue Ground

AI: Artificial Intelligence

ANN: Artificial Neural Network

ASIC: Application Specific Integrated Circuit

BEP: Best Efficiency Point

CCS: Code Composer Studio

CV: Constant Voltage method

CCM: Continuous current mode

DC: Direct Current

DCM: Discontinuous current mode

dP-P&O: Improved Perturb and Observe method

DGND: Digital Ground

DSP: Digital Single Processer

EPP: Estimate Perturb and Perturb method

FCN: Fuzzy Cognitive Networks

FF: Fill Factor

FLC: Fuzzy Logic Controller

GUI: Graphical User Interface

HIT: Heterojunction with Intrinsic Thin layer

HV: High Voltage

IC: Incremental Conductance

IPM: Intelligent Power Module

LV: Low Voltage

MCU: Microcontroller Unit

MPP: Maximum Power Point

MPPT: Maximum Power Point Tracking

MP&O: Modified Perturb and Observe method

OC: Open Circuit

RCC: Ripple Correlation Control method

Vref: reference voltage

P&O: Perturb and Observe

PC: Personal Computer

PI: Proportional and integral control

PLC: Programmable Logic Controller

PV: Photovoltaic

PWM: Pulse Width Modulation

SC: Short Circuit

USD: United State Dollars

Chapter One

1. Introduction

1.1. Background

For the past 150 years, primarily driven by global industrialisation, the world economy has been running from fossil fuels which were previously relatively cheap and abundant. Fossil fuel supplies are now significantly depleted and it is expected that availability of these resources will become even more scarcer over the next 20 - 40 years [1]. Furthermore, due to their polluting effects, fossil fuels are a major cause of climate change. Energy consumption accounts for more than 60% of the CO2 emitted into the atmosphere [2]. To avoid the anticipated effects of global warming, the only way is to change consumption behaviour and move to low carbon energy systems. For this reason, scientists have considered alternative solutions for the supply of energy which can extract energy with minimal negative impact on human life and the environment [3].

Over the last twenty years the issue of energy supply has been widely discussed due to the shortage in oil and gas, increasing fuel prices, and rapid increase in energy demand due to continued growth in the global population and industrialisation. At recent geopolitical events, talks about alternative sources of energy have gained additional attention and investment in renewable energy is no longer only a means of addressing climate change, but also now plays a very important part in sustainable economic growth over future years [4]. Indeed, 2012 was the international year of sustainable energy as declared by The United Nations General Assembly and Ban Kimono who supported the agenda which sought to mobilise action on three key objectives:(1) to improve the rate of energy efficiency, (2) to double the share of clean energy in the global energy mix and (3) to provide universal access to modern energy services. All three are to be achieved by 2030 [5].

In recent years, application of renewable energy has continued to grow strongly despite economic crises and the Arab Spring which slowed development in North Africa and the Middle East. Investment in renewable energy increased by 17% in 2011, $257 billion which is a new record and six times greater than the figure for 2004, the boom of investment in solar power jumped by 52% to $147 billion and spectacularly surpassed the

largest single sector investment in recent years, wind power [5]. In 2011, the European Union established more renewable energy capacity than ever before. At the year-end of 2011, the top five countries in terms of total installed capacity of solar power were Germany, Italy, Japan, Spain, United States; these were closely followed by the rapidly expanding China.

Also in 2011, other countries saw many significant achievements in the area of off-grid and standalone energy solutions. Access to reliable renewable energy not only counters the environmental and health hazards associated with current energy resources, but can also provide basic energy requirements such as lighting, cooking, cooling and heating. This is especially important to people who live in rural communities and poor urban areas where geographical limitations, unaffordable existing power networks and absence of the grid network are familiar issues. For example, Bangladesh has installed 1.2 million rural domestic solar systems and created about 60,000 jobs in the solar sector to improve the efficiency and quality of life. Moreover, a pilot project was financed by the Word Bank to provide 1,050 lighting systems to rural homes in two of the poorest states in Mexico. In Africa, Botswana provided electricity to 350 villages by means of solar energy and in eastern Zambia, energy supply companies provided 400 photovoltaic (PV) systems to households [5] [6].

Improvement in energy efficiency saved the world about 915 EJ of energy between 1990 and 2007 and in developing countries the potential for further improvement is still vast. Renewable energy can work to reduce the electricity demand on the grid, decrease losses, and cost associated with transmission within the grid network [5].

Photovoltaic power generation is gaining increased importance as a renewable source due to a number of advantages; absence of fuel cost, low maintenance, lack of noise and minimal wear due to absence of moving parts and a pollution-free operation once it is installed [7] [5] [4] . In addition, solar PV Pico systems and home PV systems are very popular for lighting solutions in African villages, rural and urban communities and also in other developed countries that have a considerable amount of solar radiation [5]. As PV systems are required to be of lower cost, smaller size and operate more efficiently, this research focuses on standalone PV systems with the aim of improving system efficiency over a wider range of atmospheric conditions than observed in many existing systems.

1.2. The art of standalone photovoltaic (PV) system

Stand-alone PV systems have become globally accepted as a feasible and practical tool for generating electricity; especially in urban regions where transporting electricity is either very difficult or expensive. The typical standalone PV system, which will be investigated in this study, with minimum system elements is shown in Fig. 1.1. The main elements of the system are a PV array to convert sun light to electricity, maximum power point tracking controller to control PV array output power at the maximum, DC to DC converter to step-up or step-down the voltage and current levels and the DC load of the user. During the last decade, many researchers have been interested in reducing the cost and increasing the efficiency of standalone PV systems. The overall cost has generally declined due to reductions in component costs, especially the PV array. Also, the efficiency of these systems has improved by up to 78% in the current decade [8] [9]. To maximize the efficiency to these systems, the main element needs to be investigated which is the energy conversion system including MPPT algorithm.

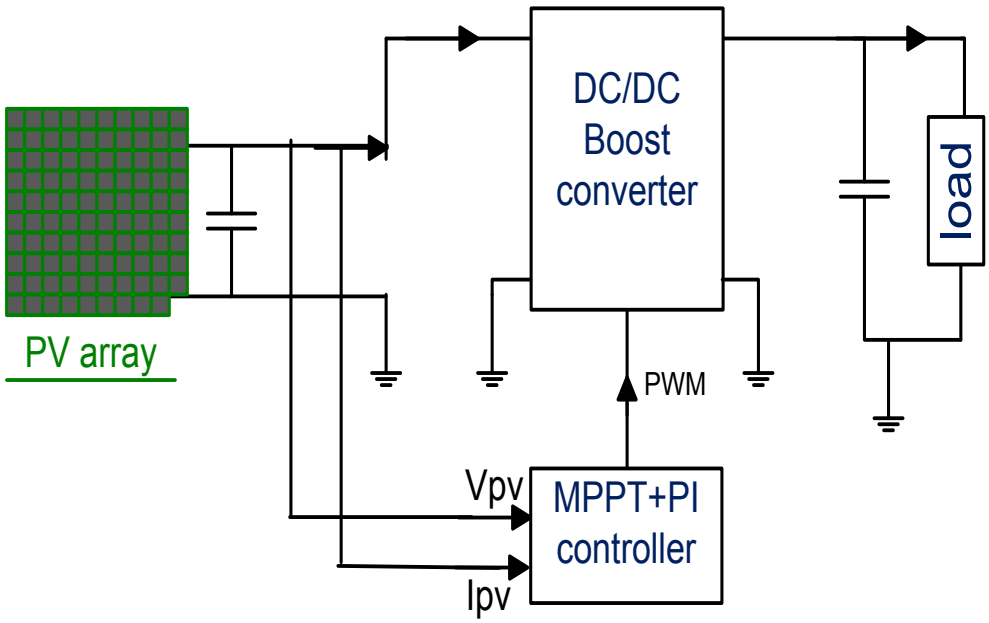

Fig. 1.1, Block diagram of a typical standalone PV system

1.2.1. Photovoltaic (PV) array

PV arrays harness the energy of the sun by converting it into electricity via a photoelectric process. The first generation of silicon semiconductor photovoltaic cells was in 1954 [10]. The photovoltaic solar cell consist of a p-n junction fabricated in a thin wafer, or layer, of semiconductor (usually crystalline silicon). In the dark, the I-V output characteristic of a solar cell has an exponential characteristic similar to that of a diode [11] [12] . When solar energy photons hit the solar cell with energy greater than the band gap energy of the semiconductor, electrons are knocked loose from the atoms in the material, creating electron-hole pairs [12],[13]. These carriers are swept apart under the influence of the internal electric fields of the p-n junction and create a current proportional to the incident radiation. When the cell is short circuited, the current flows in an external circuit, when the cell is open circuit, the current is shunted internally by the intrinsic p-n junction diode. The characteristics of this diode therefore set the open circuit voltage characteristics of the cell [11] [12]. PV materials are either thin film or crystalline, and they are judged on two basic factors: cost and efficiency. The crystalline panel is more efficient and costly in comparison to the thin film panel [14]. Nowadays, different materials are used to manufacture the cell and an efficiency of 16% can be reached [15].

Solar cells, supports, connections and protection components represent the whole assembly for generating photovoltaic (PV) panel power. As the industry makes commercial PV modules of different sizes, a number of photovoltaic modules are usually arranged in parallel and series to meet energy requirements. The typical I-V characteristics of a PV array are shown in Fig. 1.2. When multiplying the current and voltage of the array, a P-V characteristic can be acquired as shown in Fig. 1.3, the maximum power point (MPP) indicates the point of maximum panel power output.

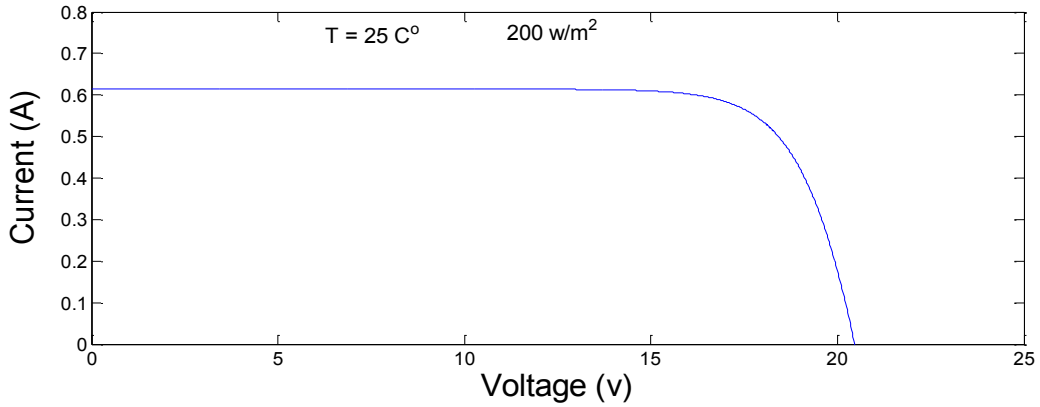

Fig. 1.2, I-V characteristics of a typical PV panel

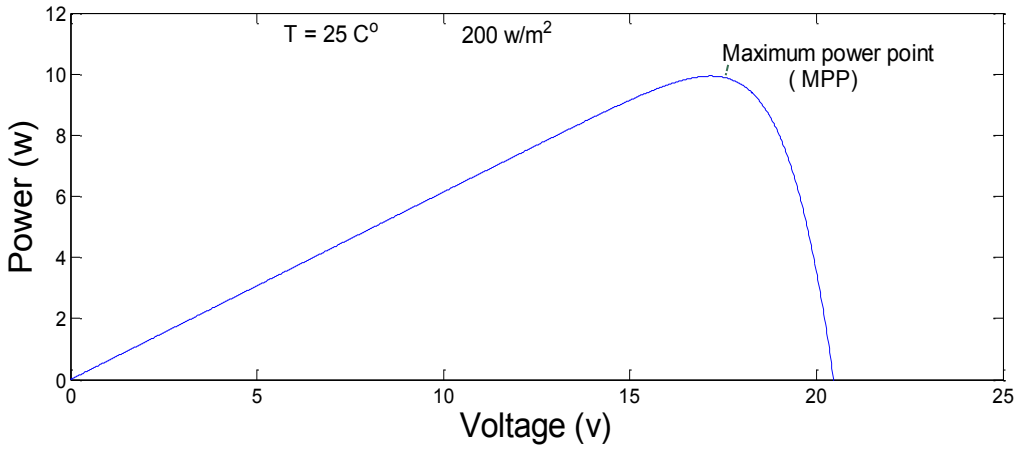

Fig. 1.3, P-V characteristics of a typical PV panel

1.2.2. Maximum power point tracking (MPPT) controller

Since the PV generator exhibits nonlinear characteristics, its maximum power point (MPP) varies with solar insolation, and there is a unique operating point of the PV generator at which its power output is at a maximum as shown in Fig. 1.4. Therefore, for maximum utilization efficiency, it is necessary to use a maximum power point tracking algorithm to generate all available PV panel maximum power under different insolation to the load. For this reason, many maximum power point tracking algorithms have been researched and developed alongside their optimization techniques [16],[17],[18] and indicated that the Perturbation and Observation (P&O) and Incremental Conductance (IC) algorithms are the most efficient [17]. However, in the literature review presented in Chapter two of the thesis, a range of maximum power point tracking methods for standalone systems is discussed. The MPPT selection is based on the following requirements:

- The ability of the algorithm to detect multiple maxima
- Cost of implementation
- Ease of implementation/computational complexity
- Convergence speed
- High efficiency within a wide output PV power range

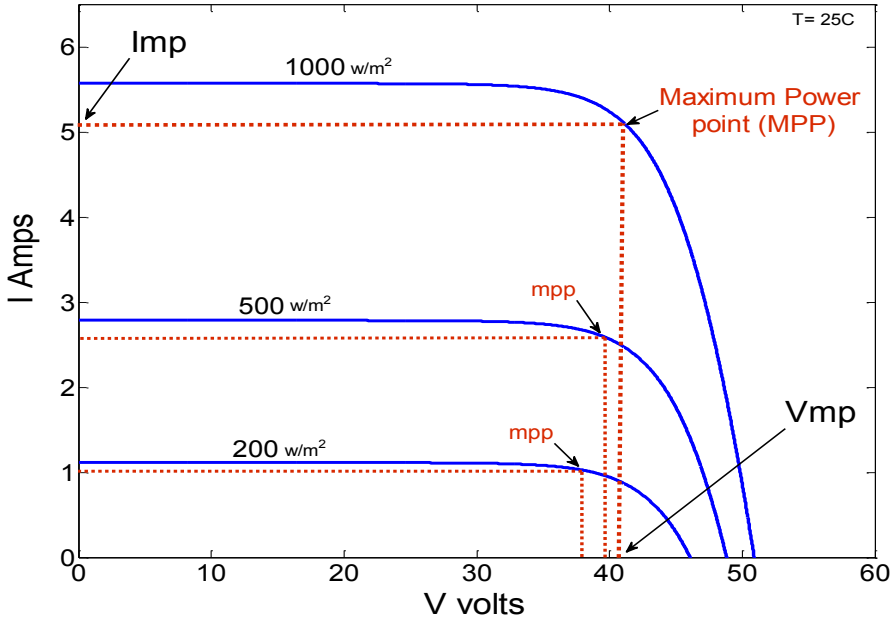

Fig. 1.4, I-V Characteristics of a typical PV panel with MPPT control

1.2.3. DC-DC boost converter

In general, the definition of a power converter is an electronic device which converts the electrical quantities (magnitude, frequency or phase angle) of voltage and current with the help of a switching arrangement to match the load requirement. In order to continuously adjust the voltage, current levels and match the PV source to the load in a standalone PV system, a DC to DC boost converter is typically required. There are two sorts of DC/DC boost converter, an isolated boost converter and a non-isolated boost converter. During the last decade, a large number of DC to DC boost converter topologies have been proposed to maximize the efficiency of PV systems. For example, Dwari [19] has used a common active clamp to achieve high efficiency with an interleaved inductor-coupled boost converter. However, in this topology each phase of the interleaved converter requires an active clamp circuit which leads to an increase in cost, size and complexity [19]. Also, Wuhua [20] used a voltage multiplier cell with an interleaved boost converter to increase the efficiency further, but this is also achieved with extra components and additional cost.In literature, a number of different boost converters are proposed. Chapter two of the thesis investigates applicable boost converter topologies for use in standalone photovoltaic systems. The requirements in the selection process are:

- To achieve high conversion efficiency for a wide PV power range

- Low cost implementation
- Ease of implementation and control
- Limit the current and voltage ripple in the system
- Achievable voltage gain

1.2.4. DC load

A stand-alone PV system directly supplies and operates electrical equipment, unlike grid-connected PV systems which inject electricity back into the grid network. The load in a stand-alone PV system can be one or more of a range of applications, for example, lighting, television, water pumps, motors, electronic gadgets, space satellites, telecommunication devices in remote areas and heating. As such, tand-alone PV systems can be connected to either DC or AC loads. Matching the power requirements of the load to the capabilities of the PV system is essential to optimise the efficiency and cost of the overall system. Furthermore, the type of load (resistive, inductive, capacitive, storage elements) may directly influence the dynamic performance of the PV system.

In this work, only DC load systems will be considered. Therefore, inverter technology will not be considered. Furthermore, it will be assumed that the load does not contain significant storage elements such as batteries. Chemical cells require specific attention and care, and present significant health and safety issues when conducting practical work. DC loads can typically be resistive loads or inductive loads, or both - as in the case of DC motors in fans or pumps. Furthermore, some DC lighting systems, such as fluorescent and low-pressure sodium lamps, are inductive loads. Examples of resistive loads include alternative lighting systems (incandescent lamps, quartz halogen lamps) and resistive heating devices such as toasters, soldering irons, coffee makers, and domestic heating applications such as hot water tanks.

Due to the limitation of equipment available in the lab, the majority of the analysis presented in this thesis will be applied to standalone PV system connected to a simple resistive DC load. However, for completeness, a brief simulation study applied to inductive type loads is provided to demonstrate the versatility of the control schemes presented in the thesis.

Often, the real-time load demand varies according to the time of day and also between working week days and weekends. An example of the change in load profile for a typical application is shown below in Fig. 1.5 [21]. As shown in the figure, there is a significant variation in load demand. This will impact on the control of the stand-alone PV system and typically affect its operation as it attempts to achieve optimum efficiency under all conditions. For this reason, this work considers an experimental standalone PV system which is tested with different load demands to establish the effect on the system efficiency.

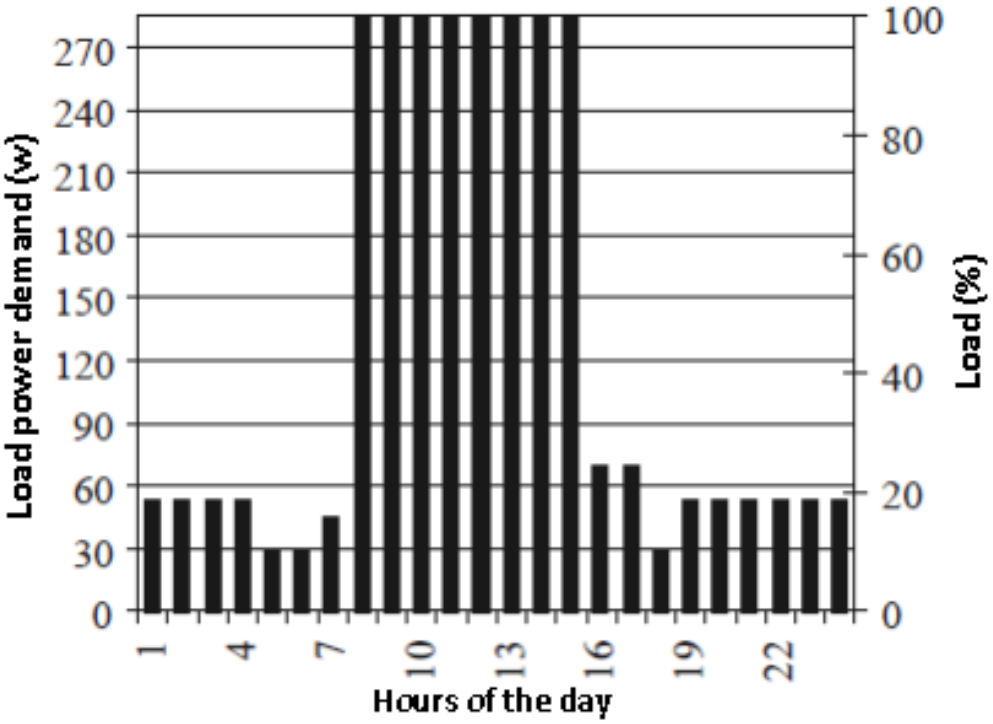

Fig. 1.5, Lighting load profile of public office in Kuwait at different hours of the weekday

1.3. Research objectives

The aim of the research presented in this thesis is to help improve the efficiency of DC/DC boost converter based photovoltaic applications. This goal can be achieved by accurately evaluating and understanding the performance of a standalone PV system over a wide range of operating conditions. Upon performing this analysis, the impact of fluctuating output power is considered. To increase the efficiency level of PV systems, an extensive study is required to consider different boost converter topologies and MPPT algorithms to mitigate the often undesirable impact of real-time power fluctuation in PV systems. Accordingly, the main objectives of the research can be summarized as follows:

1- To simulate and carry out the performance analysis of standalone PV systems in general to meet typical rural/residential demands.
2- To simulate and study the effects of a standalone PV system with and without maximum power point tracking (MPPT) control.
3- To build and study a typical model of a standalone photovoltaic (PV) system with a focus on the photovoltaic PV model, boost converter and maximum power tracker controller. Also to look into improving the efficiency of a DC/DC boost converter with maximum power point tracking (MPPT) by developing a novel control algorithm which will enable the boost converter to operate at higher efficiency over a wider range of input PV conditions.
4- To experimentally confirm the simulation findings on a small DC/DC converter based system. To develop and evaluate a new control strategy to improve the efficiency of the PV system. To test overall system efficiency under different atmospheric conditions by using a programmable power supply acting as a solar panel emulator.

1.4. Outline of thesis

To achieve the aforementioned objectives and facilitate the presentation of the result obtained in this research, the thesis is organized as follows:

1- Chapter one provides a general overview of renewable energy and describes the standalone PV systems. This chapter also looks at the components of a standalone PV system from the solar array to the load and presents the research objectives and outlines the thesis.

2- Chapter two reviews recent achievements and current research activity on DC-DC boost converters and MPPT control algorithms in the field, it discusses the positive and negative aspects that have emerged from the research. As a conclusion, the correct boost converter and MPPT method to be used in the introduced Standalone PV system is selected.

3- Chapter three describes the design, build, and modelling of the software and hardware of the standalone PV system.

4- Chapter four considers the conventional boost converter and investigates its performance with MPPT control. Moreover, chapter four discusses the result with fixed and varied PV insolation (hence array power) and variable load.

5- Chapter five considers the interleaved boost converter and investigates its performance with MPPT control. A similar approach to Chapter four is presented. This chapter also summarises the findings associated with the interleaved boost converter.

6- Based on the results of Chapters four and five, Chapter six presents a new interleaved converter design with novel control strategy. This is a key chapter of the thesis, it presents the main contribution to knowledge and confirms the successful achievement of the initial research objectives.

7- The last chapter, Chapter seven, presents the summary and final conclusions of the work. Suggestions for future work are also provided.

Chapter Two

2. Literature Review

2.1. Review of the methods of Maximum Power Point Tracking (MPPT) controller

Tracking the maximum power point (MPP) of a photovoltaic array is an essential stage to increase the efficiency of most PV systems [22] [23]. It is a technique that is used to obtain the maximum power by measuring and sampling the output voltage and/or current of the solar array, and then controlling a power converter or adjusting the load to ensure maximum power is delivered to the load system for any given atmosphere condition. Many MPPT methods have been introduced and numerous variants of each method have been proposed to overcome specific disadvantages. The large number of methods proposed can make it difficult to determine the best technique to adopt when implementing a PV system [24]. The methods all vary in complexity, number of sensors required, digital or analogue implementation, convergence speed, tracking ability, and cost effectiveness. Furthermore, the type of application can have a significant impact on the selection of MPPT algorithm. For this reason, thesis summarises the most popular MPPT techniques in use today. Two promising methods are then highlighted for consideration when implementing a system which needs to cope well over a wide range of irradiance conditions.

2.1.1. Perturbation and observation (P&O) method

The P&O algorithm [17] [18] as shown below in Fig. 2.1 and Fig. 2.2 operates by increasing or decreasing the array terminal voltage, or current, at regular intervals and then comparing the PV output power with that of the previous sample point. If the PV array operating voltage changes and power increases ($dP/dV_{pv}>0$), the control system adjusts the PV array operating point in that direction; otherwise the operating point is moved in the opposite direction. At each perturbation point, the algorithm continues to operate in the same manner [25] [26].

The main advantage of this approach is the simplicity of the technique. Furthermore, previous knowledge of the PV panel characteristics is not required. In its simplest form, this method generally exhibits good performance provided the solar irradiation does not vary too quickly [17]. At steady state, the operating point oscillates around the MPP voltage and usually fluctuates slightly. For this reason, the perturbation frequency should be low enough so that the system can reach steady state before the next perturbation. Also, the perturbation step size must be sufficient so that the controller is not significantly affected by

measurement noise, and generates a measurable change in the photovoltaic array output [27] [28].

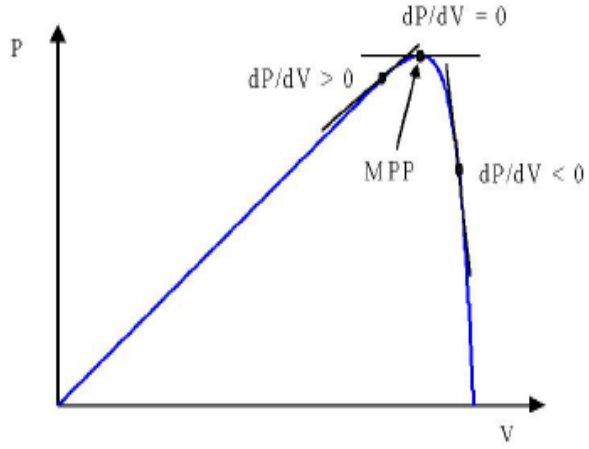

Fig. 2.1, dP/dV at different positions on the power characteristic [18]

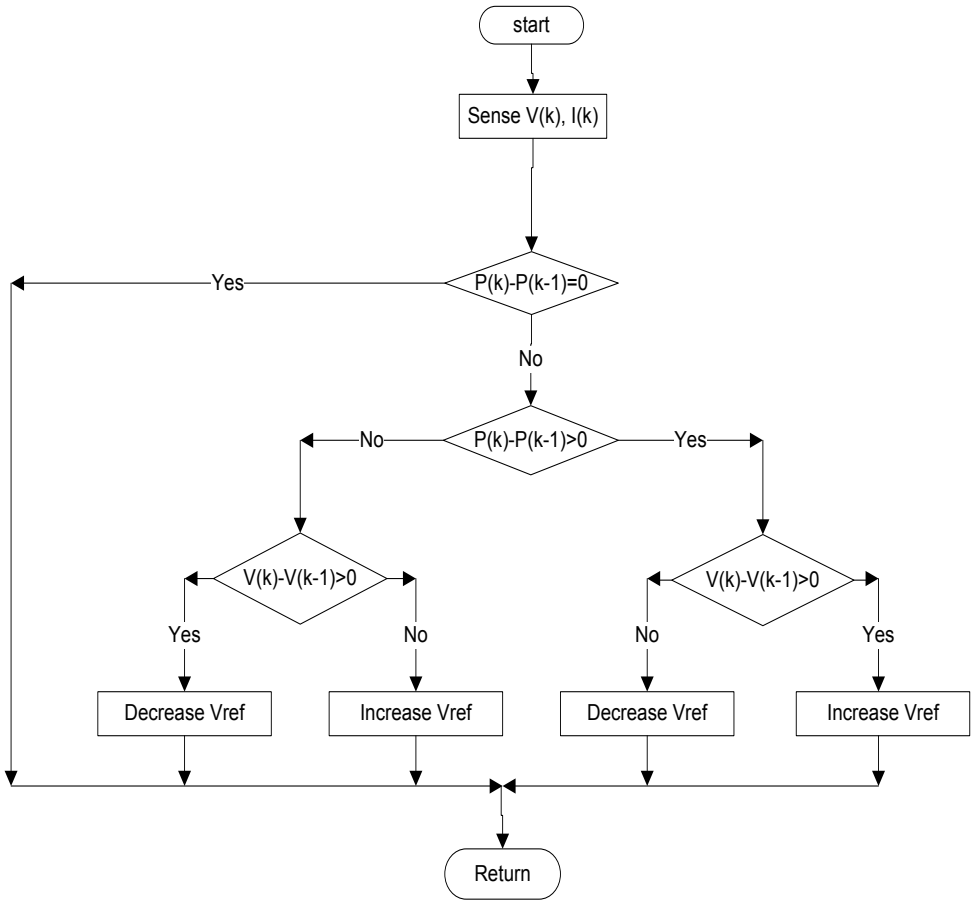

Fig. 2.2, Flowchart of the P&O method

Combined P&O with CV

The classic perturb and observe (P&O) method has the disadvantage of poor efficiency at low irradiation. For this reason, alternative solutions have been proposed. For example, Cristinel, Uffe, and Frede [29] combine a constant voltage (CV) algorithm with a modified P&O method as shown in Fig. 2.3 to track the MPP with high efficiency under both low and high solar irradiation conditions. The algorithm operates by increasing the duty cycle until the PV output voltage is close to the open circuit voltage of the panel (Voc), this is then used as the initial conditions for the MPP tracker. The algorithm then evaluates the current output; if the current is higher than (0.7A) the algorithm adopts the PO method; if it is lower it converts to the CV method. Simulation results demonstrate that overall greater energy can be extracted from the PV panel; efficiency levels of 95% to 99% are quoted over a wide irradiation range [29]. However, there is a complication of combining the two methods.

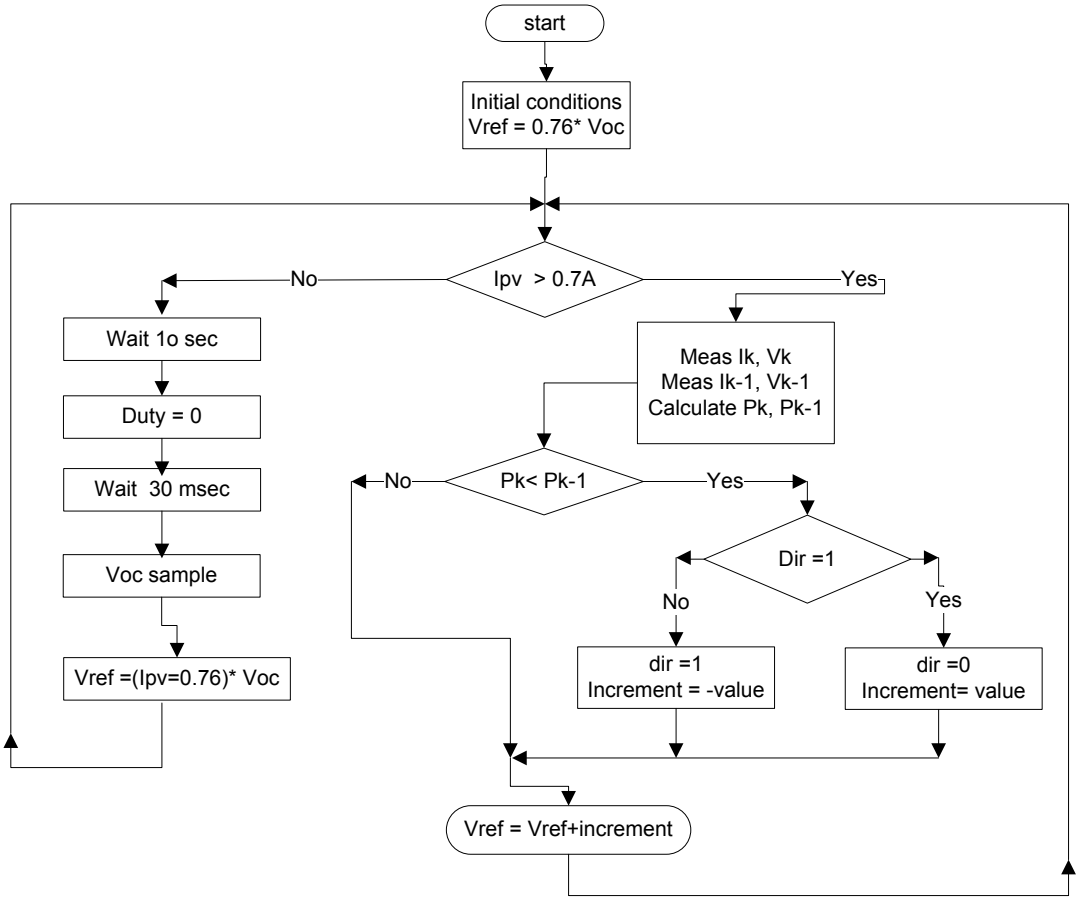

Fig. 2.3, Flowchart of the combined P&O with CV

Modified Perturb and Observe (MP&O) method

The P&O method is also prone to erratic behaviour under rapid variation in light levels. This may result in slow, or incorrect, MPP tracking. C. Liu, R. Cheung [30], and A. Yafaoui, B. Wu [31], introduced a Modified P&O (MP&O) method to solve this problem. The method adds an irradiance-changing estimate process in every perturbation process to measure the amount of power variation caused by the change of conditions. Results show improved performance over the conventional P&O method. However, MP&O has a slow tracking speed which is approximately half of the conventional P&O method.

Estimate, perturb and perturb (EPP) method

To improve the tracking speed of the MP&O method, an Estimate, perturb and perturb (EPP) method is proposed by C. Lui, B. Wu, and R. Cheung [30] . The EPP algorithm uses one estimation step for every two perturbation steps. It has been shown experimentally that, compared to MP&O, the EPP method has faster tracking speed, and with a similar tracking accuracy [31].

Optimization of P&O method

Ultimately, oscillations around the MPP give rise to loss of available energy [32]. To limit the impact of this issue, Nicola Femia shows how the P&O parameters can be optimised for the dynamic behaviour of the specific power converter under investigation [28].

Improved perturb and observe (dP-P&O) method

During rapidly changing irradiation, it is possible for the classic P&O algorithm to become confused and track the MPP in the wrong direction [17] [33] [34]. D. Sera , T. Kerekes , R. Teodorescu, and F. Blaabjerg [18] offer a simple and effective solution to this problem; dP-P&O. In this method, the power measurement is deconstructed to reveal the power coming from different sources. The MPPT is then provided exclusively with the power change created by its own previous instructions. To achieve this, an additional measurement of the solar arrays' power is required. This is carried out at the mid-point of the MPPT sampling period, as shown in Fig. 2.4 and Fig. 2.5. The method has been experimentally tested and compared with the classic P&O method. The results show that the dP-P&O technique is able to prevent the P&O from tracking in the wrong direction during rapidly changing irradiation, and considerably increases tracking speed.

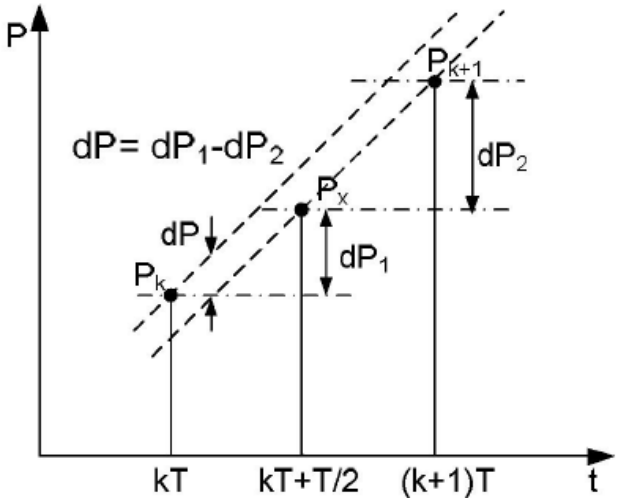

Fig. 2.4, Measurement of the power between two MPPT sampling instances [18]

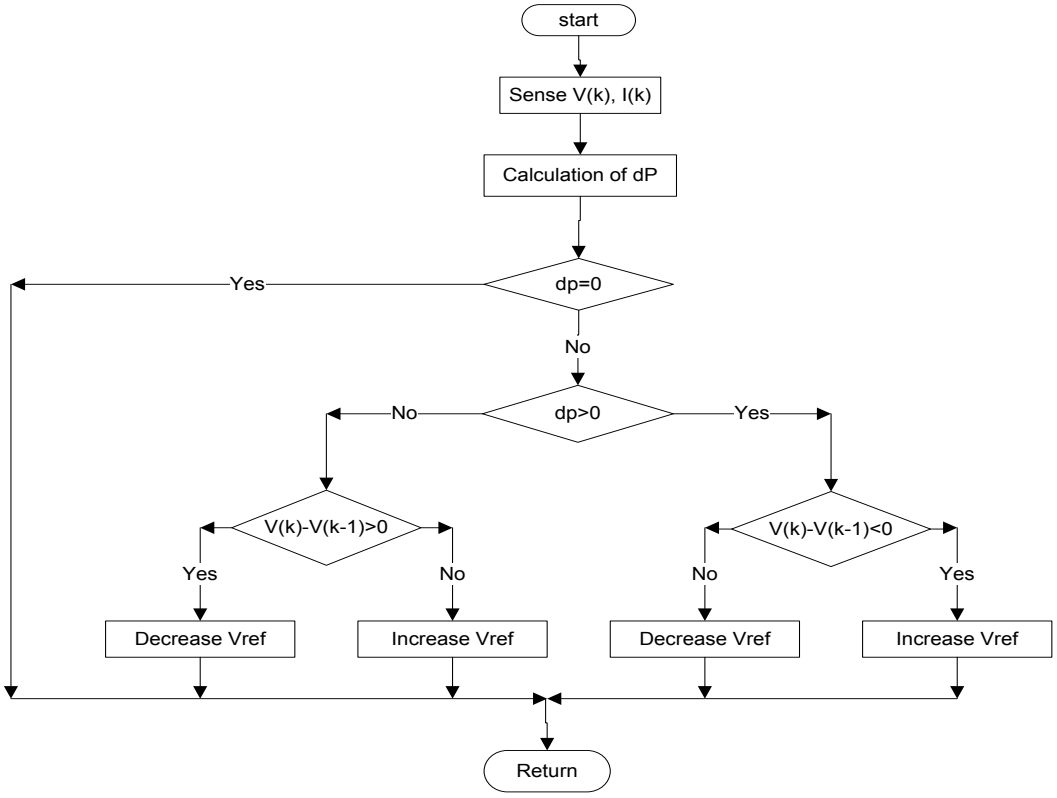

Fig. 2.5, Flowchart of the dp-P&O method

2.1.2. Incremental Conductance (IC) Method

The Incremental Conductance (IC) algorithm, shown in Fig. 2.6, seeks to overcome the limitations of the perturbation and observation algorithm by using the incremental conductance of the photovoltaic. This algorithm works by searching for the voltage

operating point at which the conductance is equal to the incremental conductance. At this point, the system stops perturbing the operating point. The advantage of this algorithm is that it has the ability to ascertain the relative "distance" to the maximum power point (MPP), therefore it can determine when the MPP has been reached. Also, it is capable of tracking the MPP more precisely in highly variable weather conditions [29], and exhibits less oscillatory behaviour around the MPP compared to the P&O method, even when the P&O method is optimized [33]. Nevertheless, the IC algorithm has the disadvantage that instability can result due to the use of a derivative operation in the algorithm. Also under low levels of insolation, the differentiation process difficult and prone to measurement noise; and results can be unsatisfactory [30] .

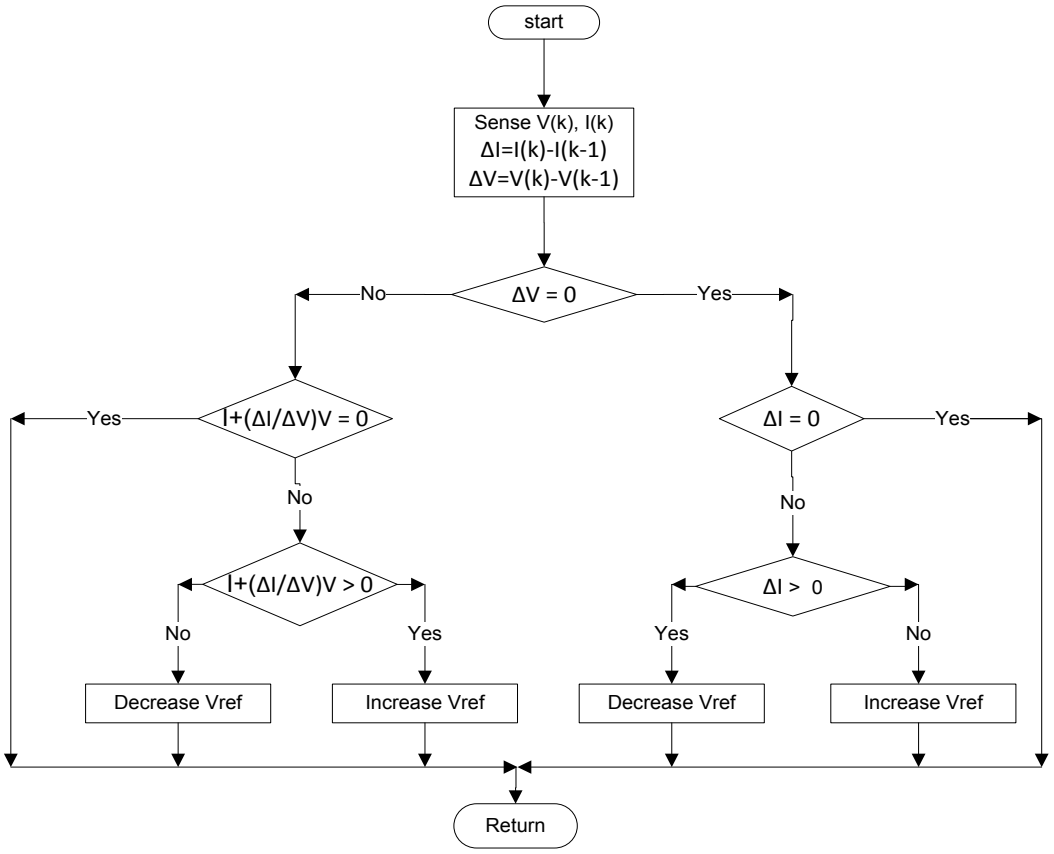

Fig. 2.6, Flowchart of the IC method

There is an alternative IC algorithm presented in [17] which is called the Two-Model MPPT (ICb) algorithm and combines the CV and the IC method. If the irradiation is lower than 30% of the nominal irradiance level the CV method is used, otherwise the IC method is adopted. Therefore this method requires the additional measurement of solar irradiation as shown in Fig. 2.7 [17].

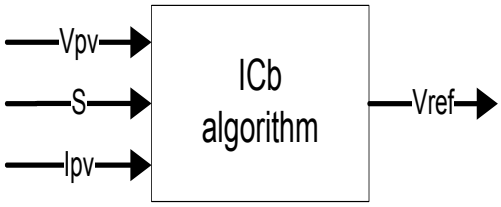

Fig. 2.7, ICb block diagram

Advanced incremental conductance algorithm with a variable step size

In general, the IC tracking approaches use a fixed iteration step size, which is determined by the accuracy and tracking speed requirement. The step size may be increased to improve tracking speed, however, accuracy is decreased. Likewise, reducing the step size improves the accuracy, but sacrifices the speed of convergence of the algorithm. To solve this problem, L. Jae Ho, B. HyunSu, and C. Bo Hyung [35] proposed an IC technique with a variable step size. This approach automatically adjusts the step size to the solar array operating point. When the operating point is judged to be far from the MPP, the algorithm increases the step size to enable the algorithm to operating point of approach quickly towards the MPP. However, when the operating point is close to the MPP, the step size is decreased. Through the variation of the step size, both improved accuracy and speed are accomplished. Experimental results, based on a parallel buck converter system, validate the speed and robustness of the scheme. Furthermore, small signal modelling, confirms the stability of the system in almost all cases [35].

2.1.3. Open Voltage (OV) method

The algorithm is introduced by R. Faranda and S. Leva [17] and is based on the observation that the voltage of the MPP is always close to a fixed percentage of the open circuit voltage. The location of the maximum power point is adjusted by temperature and insolation level within a 2% tolerance band. The open-voltage algorithm technique selects 76% of the open circuit voltage (V_{ov}) as the optimum operating voltage (V_{op}) at which the maximum output power can be obtained as shown in Fig. 2.8. This MPPT controller requires a static switch to be placed in series with the PV array to enable the open circuit voltage to be measured on demand. Whilst measuring the open circuit voltage, the current of the PV panel is zero (I_{pv} = 0), so no power is delivered by the load and so momentarily the energy produced by the photovoltaic system is lost [17].

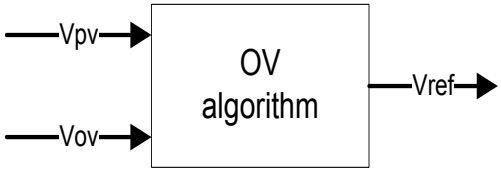

Fig. 2.8, OV block diagram

2.1.4. Constant Voltage (CV) method

The constant voltage (CV) algorithm is one of the simplest MPPT algorithms. The operating point of the photovoltaic array is retained near the maximum power point (MPP) by regulating the solar output voltage to match an unmovable reference voltage V_{ref}. The reference voltage value is set equal to the voltage at the maximum power point (V_{mpp}) of the characteristic photovoltaic array. The algorithm assumes that PV panel variations, such as temperature and irradiation are not significant, and the constant reference voltage is adequate to achieve performance close to the MPP. For this reason, in practice, the CV algorithm may never exactly locate the MPP. During installation, it is usually necessary to gather data to establish the constant voltage reference, as this may change from one location to another. In low insolation conditions, it may be observed that the constant voltage technique is more effective than either the perturb and observe, or the incremental conductance algorithm [36] [17].

2.1.5. Temperature (T) method

A temperature MPPT algorithm is introduced in papers from R. Faranda, S. Leva, [17] and R. F. Coelho [37]. By looking at the V-I characteristics, it is observed that the short-circuit current (I_{sc}) of the solar array is proportional to the irradiance (G) level and is generally steady when the cell temperature changes, whilst the open-circuit voltage (V_{ov}) of solar panel is directly proportional to the PV array temperature (T). This algorithm employs temperature sensors fixed on the back surface of the PV array and voltage sensors. It starts by simultaneously measuring the temperature (T) and the photovoltaic output voltage (V_{vp}) as shown in Fig. 2.9.

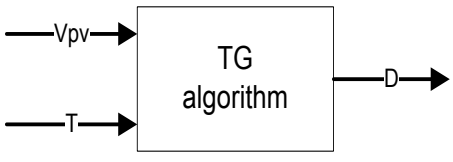

Fig. 2.9, TG block diagram

From the measurement, the value of maximum power point voltage (V_{mpp}) is evaluated using the following equation:

$$V_{mpp}(T) = V_{mpp}(T_{ref}) + u_{vmpp}(T - T_{ref})$$

Where u_{vmpp} is the temperature coefficient of the V_{mpp} from data sheet information, and T_{ref} is the reference temperature.

From this, the incremental duty ratio (D) is determined from the difference between the desired value of V_{mpp} and the measured PV voltage (V_{vp}). This is updated at each sample interval to keep the output voltage of the PV array close to the maximum power point voltage, as shown in Fig. 2.10.

As indicated in the results obtained by Faranda and Leva, the temperature method exhibits lower efficiency compared to the P&O and IC algorithms.[17]. Furthermore, the temperature algorithm requires datasheet information regarding the PV array, and the algorithm has to be updated to ensure accurate operation of the PV system and compensate for parameter changes caused by system aging [37].

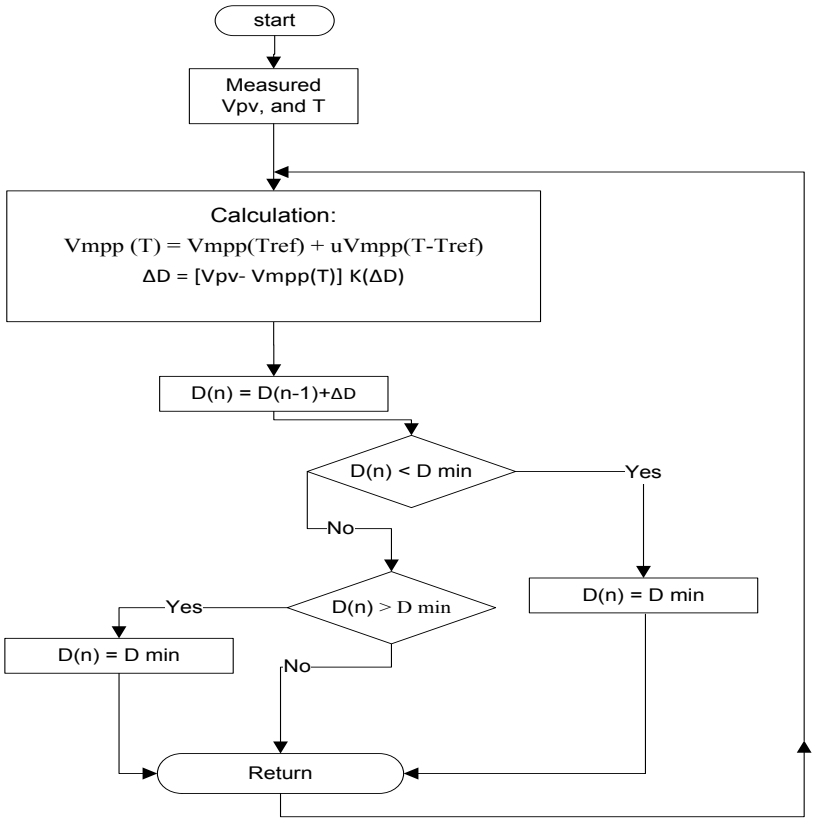

Fig. 2.10, Flowchart of the temperature method

2.1.6. Parasitic capacitance method

The parasitic capacitance algorithm was developed by Branbrilla [38], and it is similar to the incremental inductance (IC) algorithm, except that parasitic junction capacitance (C_{pv}) is included to model charge storage in the P-N junction of photovoltaic cells [39] [40]. This algorithm requires two multiplications with complexity of the control circuit [33].

2.1.7. Forced oscillation method

This algorithm is presented by Tse [36], adding a small 100Hz voltage to the operation voltage of the photovoltaic voltage which leads to ripple power whose phase and amplitude are dependent on the location of the operating point to the MPP [33] as shown in Fig. 2.11. If the modulation takes place in zone A the left side of the MPP the ripple voltage of the power will be in phase. However, if the modulation happens in zone B to the right side of the MPP, with respect to the voltage the curling (wave or ripple) of the power output will be out of phase 180 degrees. If the operation point is exactly the MPP, then output power curling will have very small amplitude with double frequency of the curling of the voltage [33].

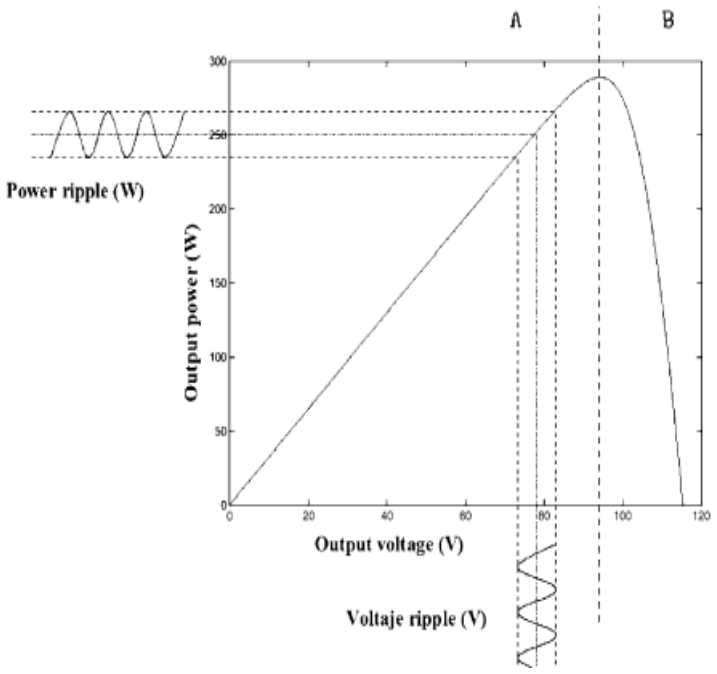

Fig. 2.11,Curve P-V for PV generator with power ripple caused by Vpv modulation [33]

The advantage of this algorithm is that it provides information on the location of the maximum power point when the analysis of the signal amplitude and phase. Moreover, the algorithm allows the operating voltage to be adjusted slowly towards the MPP voltage, so there will be no continuous oscillation around the maximum power point [33]. On the other hand, the oscillation method uses a more complex algorithm and evaluation of the signals at very low amplitude is difficult [33].

2.1.8. Feedback voltage (current) method

A Feedback Voltage (or Current) method has been applied by J. N. H.D. Maheshappa [41] and H. Chihchiang [42], It is used to tie the bus voltage at a constant level. It operates, as shown in Fig. 2.12, by comparing the PV voltage with the constant voltage and adjusting the duty cycle (D) of the converter to operate the PV array at a point close to the MPP. The method is low cost, computationally simple, and only uses one feedback control loop. However, it does not consider the effect of variations in temperature and irradiation [33].

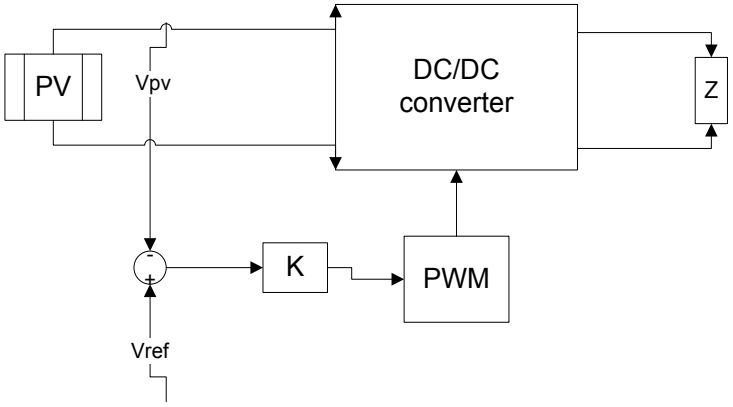

Fig. 2.12, Voltage-feedback with PWM modulation

2.1.9. Ripple Correlation Control (RCC) method

Krein [43] who first proposed the ripple correlation method and it has been modified to resemble RCC by Arcidiacono [44]. The method requires the PV array voltage and current to be measured, and from this power is calculated. The voltage and power measurements are then passed through a low pass filter to remove any high-frequency ripple; before computing dPpv/dVpv. The sign of the derivative is ascertained using a sine function and indicates the operating region of constant voltage or current. An integrator is then used to generate the

reference array voltage, which is compared with the real PV voltage to produce an error signal that is used to suitably adjust the modulation index of PWM [45].

As described in [17], the RCC scheme can be implemented with simple and inexpensive analogue circuits and does not require prior information about PV characteristics. However, it has a lower tracking capability at low insolation levels, and it uses large tracking steps near the MPP[17].

2.1.10. Fuzzy logic control

Fuzzy logic control in MPP applications has become increasingly popular as microcontroller processing power has improved, and costs have reduced [46]. Fuzzy logic controllers have three stages, fuzzification, rule base table lookup, and defuzzification. During fuzzification, numerical input variables are converted into linguistic variables based on a number of defined membership functions (Fig. 2.13). Typically, the greater the number of membership functions used, the more accurately the controller will operate [47] [48]. The input to the fuzzy logic controller is an error signal, E, and the change in error; ΔE. The user has the flexibility of choosing how to compute E and ΔE. These signals are then converted to linguistic variables which define how the system is to be controlled by the user. The advantage of fuzzy logic control is that it does not need an accurate mathematical model of the system, and it is capable of handling system non-linearity.

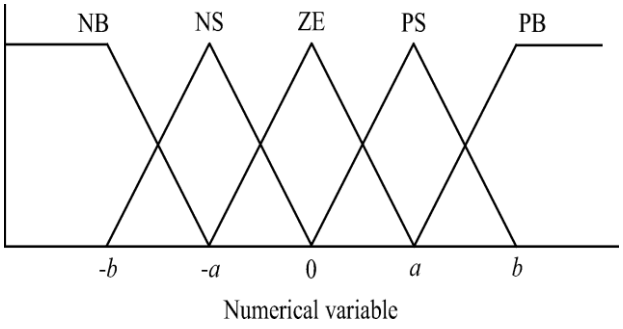

Fig. 2.13, Membership function for inputs and outputs of fuzzy logic controller

The linguistic variables assigned to ΔD for the different combinations of E and ΔE are based on knowledge of the boost converter and the experience of the user. A simple example is shown in Table 2.1. If, for example, the operating point is far to the left of MPP, that is E is PB, and ΔE is ZE, then a large increase duty ratio (ΔD) is required to reach the MPP.

Table 2.1: Example of fuzzy rule-based table

ΔE/E	NB	NS	ZE	PS	PB
NB	ZE	ZE	NB	NB	NB
NS	ZE	ZE	NS	NS	NS
ZE	NS	ZE	ZE	ZE	PS
PS	PS	PS	PS	ZE	ZE
PB	PB	PB	PB	ZE	ZE

The main disadvantage of fuzzy logic control is that the effectiveness depends on user knowledge and competency in choosing the correct error computation and developing a suitable rule base table based on the chosen membership functions [49]. Optimised variants of the fuzzy logic MPPT system have been proposed, including adaptive strategies that tune the membership functions and rule base table in real time [16].

2.1.11. Neural network

A neural network approach is presented by T. Hiyama [50] and L. Zhang [51], To guarantee accurate MPPT operation, the neural network has to be trained to operate with the PV array and adjust for time varying characteristics of the system. Once trained, the neural network does not require detail information about the PV system; it operates like a black box model. The neural network has three layers; input layer, hidden layer, and output layer as shown in Fig. 2.14. The number of nodes in each layer varies and is user dependent. The PV array V_{oc} and I_{sc} are used as the input variables. The output is usually represented by one of several reference signals, or the duty cycle signal used to drive the power converter. The hidden layers act to achieve the MPP; the performance of the system is heavily dependent on how well a neural network has been initially trained [16].

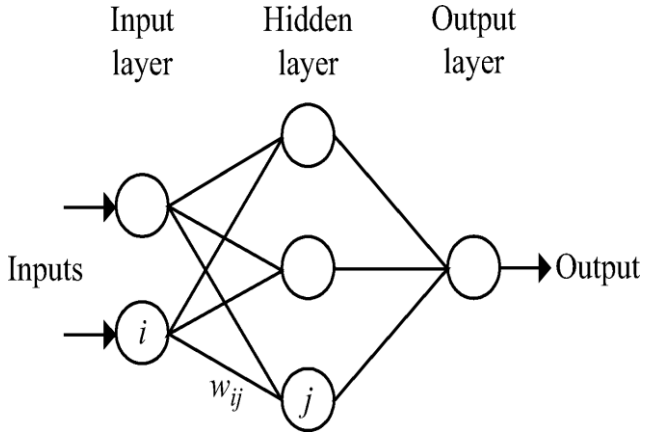

Fig. 2.14, Example of neural network

To guarantee accurate MPPT performance, the neural network has to be trained with the applied PV array characteristics - which change with time. After being trained, the neural network does not require detailed information about the PV system, it operates like a black box model.

Discussion

The review of eleven methods of MPPT, with particular emphasis on variants of the P&O and IC techniques, has been presented to better understand the difference between MPPT algorithms and the impact on system efficiency. In general, during this review, these methods have highlighted positive and negative aspects, for example, the constant voltage (CV) algorithm is more effective than P&O and IC in low insolation conditions, but it provides lower efficiency at a high level of irradiation [52] [17] [29].

By comparing the main six MPPT techniques (P&O, IC, CV, T, OV, SC), as shown in Fig. 2.15 [17], it is evident that despite much research the most widely used methods (P&O and IC) are generally still the preferred algorithms. They offer high efficiency and work at low isolation, and have a modest level of cost to implement. The constant voltage (CV) has a lower efficiency [6], but a lower implementation cost compared to others. The other methods (T, OV, SC) offer "mid-range" performances in contrast to the optimum algorithms and for the purpose of this work are not considered to be optimum MPPT techniques.

Also, with reference to Table 2.2 [16] [52] [53], which shows other introduced MPPT techniques, the table illustrates the major characteristics of the techniques P&O, IC, Voc, Isc, RCC, fuzzy logic and neural network. Among these techniques, it can be seen that P&O, IC and RCC are simple and less expensive to implement. Moreover, with rapidly changeable weather conditions RCC is fast in tracking because it uses large tracking steps near the MPP but during low insolation, RCC shows large power oscillations, while P&O, and IC use small step tracking. While fuzzy logical control and neural network are complex and costly techniques due to their requirements of a digital circuit and periodic tuning, they may work with others systems. In general, considering the review in Table 2.2, and if we look back on the presented knowledge of MPPT methods, most agree that the P&O and IC methods are the preferred option alongside their improvement and optimization techniques.

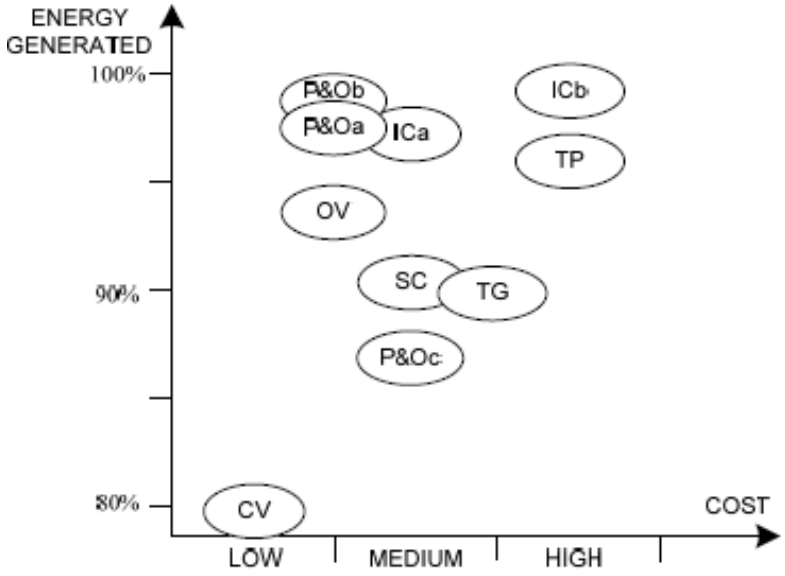

Fig. 2.15, Result of efficiency and cost of some MPPT techniques [17] [52]

Note, P&Oa is the classic perturb and observe method, ICa is the classic incremental conductance method, ICb is combined CV with ICa, SC is a short circuit current, and (TP, TG) are temperature method techniques.

Table 2.2: Major characteristics of some MPPT techniques [16] [53]

MPPT technique	PV array depen -dent?	Impleme -ntation complexi ty	True MPPT ?	Analogue or digital?	Periodic tuning?	Converg -ence speed	Sensed parame- ters
P&O method	No	low	yes	both	no	varies	Voltage current
IC method	No	medium	yes	digital	no	varies	voltage current
Fractional Voc	Yes	low	no	both	yes	medium	Voltage
Fractional Isc	Yes	medium	no	both	yes	medium	Current
RCC method	No	low	yes	analogue	no	fast	Voltage current
Fuzzy logic control	Yes	high	yes	digital	yes	fast	Varies
Neural network	Yes	high	yes	digital	yes	fast	Varies

Summary

Several MPPT techniques have been discussed in this chapter. From this, it is clear that it can be very difficult to choose the best; each MPPT method has its own advantages and disadvantages and the choice is highly application dependent. For example, solar vehicles require fast convergence to the MPP; in this case good options are Fuzzy logic control, and neural network. In orbital stations and space satellites, which involve large cost, the performance and reliability of the MPPT are most important. The tracker must be able to continuously track the true MPP in the minimum amount of time and should not require periodic tuning. In this case, the appropriate methods are O&P/ Hill-climbing and IC.

When using solar panels in residential locations, the objective is to reduce the payback time. To do so, it is necessary to constantly and quickly track the maximum power point. Furthermore, the MPPT should be capable of minimising the ripple around the MPP. Therefore, the two stage IC and optimised P&O methods are suitable. Perturbation and Observation (P&O) and Incremental Conductance (IC) have been evaluated by simulating a standalone PV system, utilising a DC-DC boost converter to connect the PV panel to the load. In particular, the performance of each method has been considered over a wide range of different irradiation conditions. Results show that the Perturb and Observe algorithm exhibits faster dynamic performance and achieves steady state level better than the Incremental Conductance method over a broad range of irradiation settings and load profiles. Therefore, in this work, the Perturb and Observe (P&O) algorithm is selected for use as the maximum power point tracking technique in the introduced standalone PV system.

2.2. A review of DC/DC boost converters

A boost converter is sometimes called a step-up converter, it typically operates by switching one or more semiconductor switches ON or OFF to step up the source voltage up to a higher output voltage which can be used by the load. The objective of this review is to study the technical viability of several classes of DC-DC boost converters for the standalone PV system under consideration in this work. Each converter is evaluated according to economic aspects, efficiency, complexity, and power quality distortion over a wide range of operating conditions.

2.2.1. Conventional boost converter

In electrical power supplies, transforming DC voltages from one level to another is often achieved by using a conventional non-isolated DC-DC power converter. These converters work to transform input DC voltages to output DC voltages at a desired level, and have two modes of operation: continuous current mode operation and discontinuous current mode operation. In some applications, the converter can operate in both modes of operation with different characteristics associated with each.

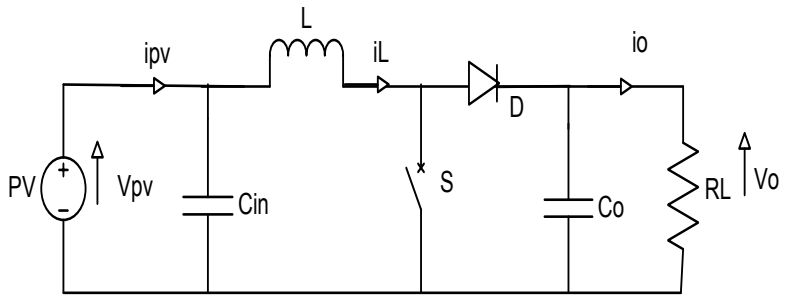

Fig. 2.16, DC -DC conventional boost converter

In brief, the operation of a non-isolated conventional boost converter, as shown in Fig. 2.16, can be described as follows. When the switch (S) is on, the diode (D) is reverse biased and isolates the output side of the converter, energy is then stored in the inductor (L). When the switch is turned off, the load on the output side receives energy from the inductor as well as from the input source. As a result, the output voltage is higher than the input voltage. In addition, the capacitor is assumed very large to keep output voltage constant [1]. The disadvantages of a conventional boost converter are high voltage stress for the switch and the large peak current for the power devices and passive components [54]. This problem can be overcome by using an alternative power converter topology, such as an interleaved converter [55].

2.2.2. Interleaved boost converter

Parallel connection of two or more conventional boost converters is called an interleaved boost converter. With appropriate control, it may be used to improve power conversion efficiency and to better operate the solar cell array at maximum power [56]. Figure 2.17 shows an example interleaved boost converter comprising of two boost converters (two limbs) in parallel.

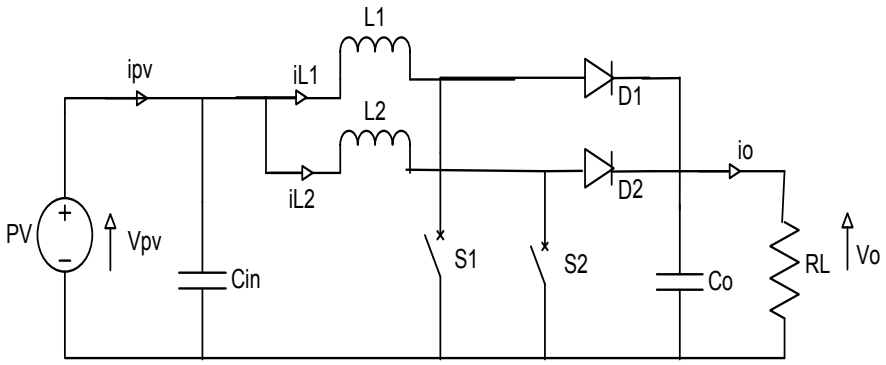

Fig. 2.17, Equivalent circuit of interleaved boost converter

The two limb interleaved boost converter works by operating the PWM of each limb at 180 degrees out of phase to the other limb. Typically, each branch operates in the same fashion as the conventional boost converter previously described. When S2 turns on, the current ramps up in L2 with a slope depending on the input voltage storing energy in L2, D2 is off during this time since the output voltage is greater than the input voltage. When S2 turns off, D2 conducts delivering part of its stored energy to the output capacitor and the load. The current in L2 ramps down with a slope dependent on the difference between the input and output voltage. One half of a switching period later, S1 also turns on completing the same cycle of events.

The main reward of the interleaved boost converter is that it gives lower ripple power at the input and output stages due to an effective increase in switching frequency, therefore there is a chance to minimize the input and output capacitor filters that would be relatively large if a conventional boost were used [56]. Furthermore, higher efficiency may be realized by splitting the input current into two paths, substantially reducing i^2R losses and inductor AC losses. Also it creates lower stresses on the components due to a current split [57] [58] [59] [60]. On the other hand, using an interleaved converter increases the number of system components which may lead to an increase in cost. However, the interleaved boost converter

can use lower rating components due to the shared current to its limbs and in renewable energy systems, long-term improved power generation can help to offset this disadvantage.

2.2.3. New Interleaved isolated boost converter

This converter was presented by Wen [61], it is based on the basic isolated boost converter and it is suitable when high voltage applications are required. It is modified by two cells helping each other in a primary side and secondary side, which is simpler than by paralleling the output side of two basic dual isolated boost converters. In fact to convert DC voltage from a low level to a high level requires the isolated boost converter to create a high current at the input and a high voltage at the output. If two cells connect for the isolated boost converter on a parallel at the input and in series at the output this connection reduces the voltage stress and current stress of switches and the transformer for the converter will reduce by half [61].

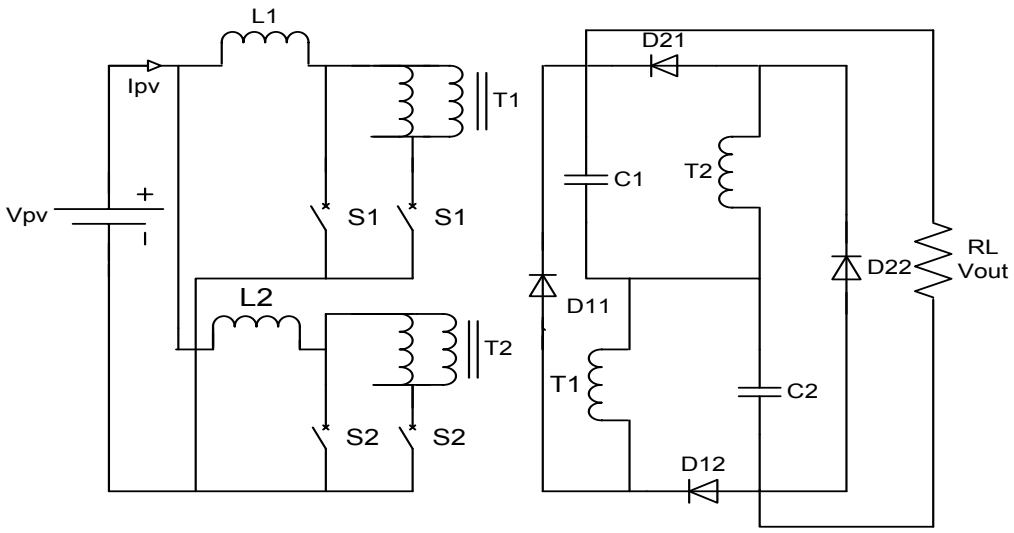

Fig. 2.18, New interleaved isolated boost converter

A new interleaved isolated boost converter, as shown in Fig. 2.18, has two inductors in parallel at the input to share the input current equally, and at the output two capacitors in series sharing the voltage equally. In this way, the new interleaved isolated boost converter has less stress voltage and less stress current on the transformer and switches [62]. All these advantages make the new interleaved isolated boost converter suitable for low to high DC-DC applications [61].

2.2.4. Interleaved boost converter based on the L-type half bridge

The boost converter which is shown in Fig. 2.19 is discussed by Wen, Jin and Smedley [61]. The converter is one of the preferred isolated boost converters for high power applications because of its several advantages such as low current stress on the transformer and inductors, so a small size can be designed, the switches are easy to operate because they are grounded and the circuit is easy to start soft switching. Moreover, circuit configuration is symmetrical so soft switching is easy to implement [61] [62]. On the other hand, this converter has more inductors than other boost converters.

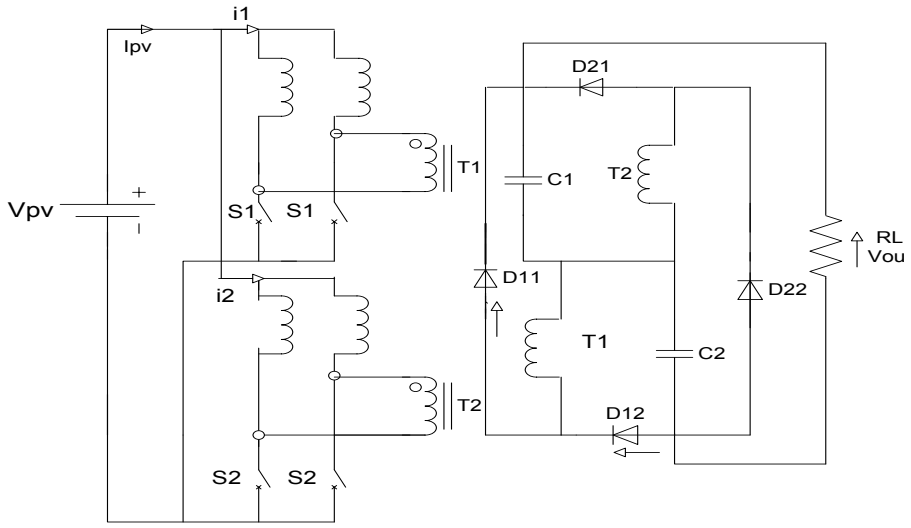

Fig. 2.19, Interleaved isolated boost converter based on the L-type half bridge converter

2.2.5. Push-pull converter

The topology of a push-pull converter was introduced by Wang[63] to meet the requirements of PV systems. As shown in Fig. 2.20 and Fig. 2.21, the first circuit is fed by a voltage mode and the second by a current mode. The advantages and disadvantages of both circuits are summarised below, the advantage in both modes of the push-pull converter is that it has fewer devices in the current path which reduce conduction losses [64]. In the input inductor in current mode operation the switches in the duty cycle are higher than 0.5 [D>0.5], this will reduce the frequency current ripple drawn from solar cells. It safely removes the energy stored in the leakage inductance of the transformer so the auxiliary circuit is desired for the push-pull converter to reduce the voltage stress on the devices [65]. The disadvantage of the push-pull converter is that the switches have to withstand double the input voltage peak, this causes an increase in conduction losses [63].

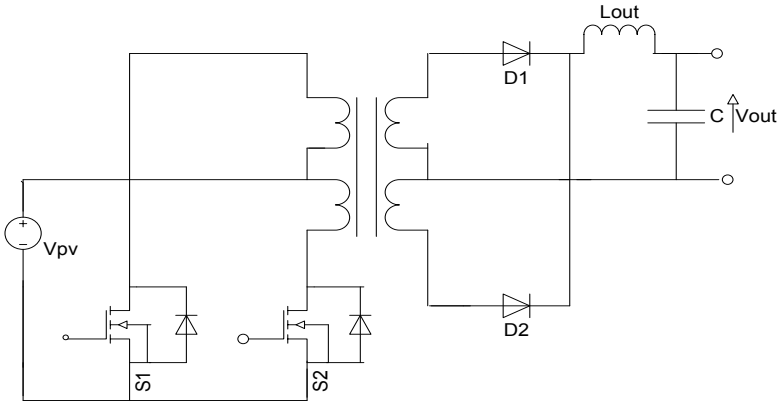

Fig. 2.20, Voltage-fed push-pull converter

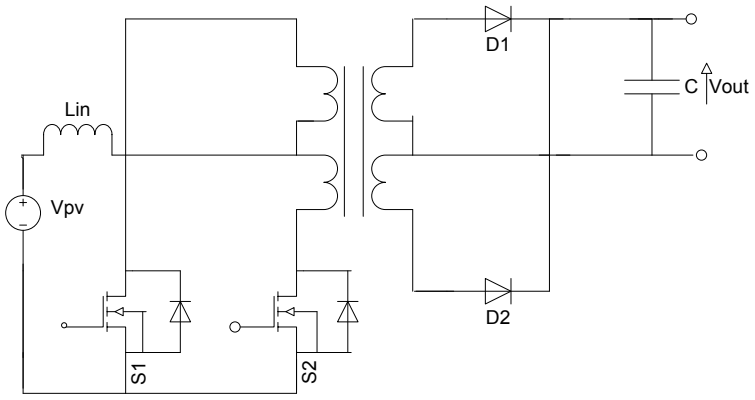

Fig. 2.21, Current-fed push-pull converter

2.2.6. Full and half bridge converter

The half-bridge and full-bridge topologies shown in Fig. 2.22 and Fig. 2.23, which are presented by Wang and Klumpner [63], use untapped primary transformer windings. It is known that such transformers feature better utilization of the copper, also these topologies feature reduced device voltage stress that is equal to the input voltage. The half bridge topology has a split capacitor bus, twice transformer turn ratio and two device current in contrast with the full-bridge leading to increased transformer loss and size. A full bridge is

well suited for applications which require a wide input voltage range [66], and for high power applications [66], also it can be operated in zero voltage switching modes (ZVS) that leads to decreased switching loss at higher frequencies. Furthermore, zero voltage switching can lead to size and cost reduction. In addition, the operation of high frequency gives small size and cost for magnetic components [63]. Although the full-bridge topology requires more switches, it reduces voltage and current stress [63]. Full wave rectifier topology with a centred tapped secondary winding and two diodes are used to maximize the efficiency [67], provide smaller size and lower cost devices, and to make sure lowest voltage drop across the diodes. Nevertheless, the voltage blocking ability of the diodes is twice as high than for a diode bridge rectifier.

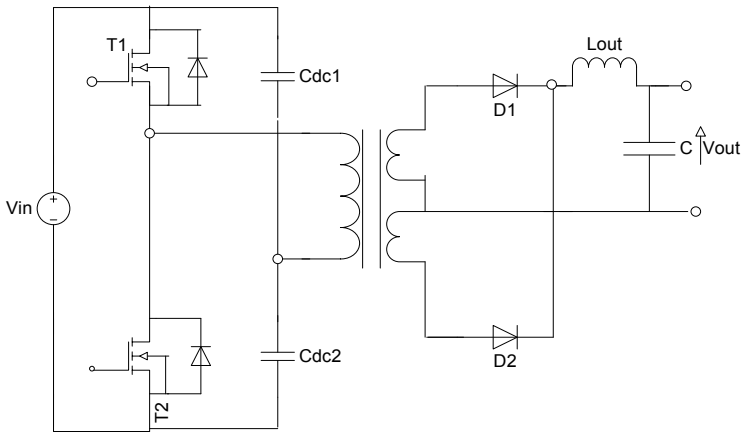

Fig. 2.22, Half-bridge DC/DC converter

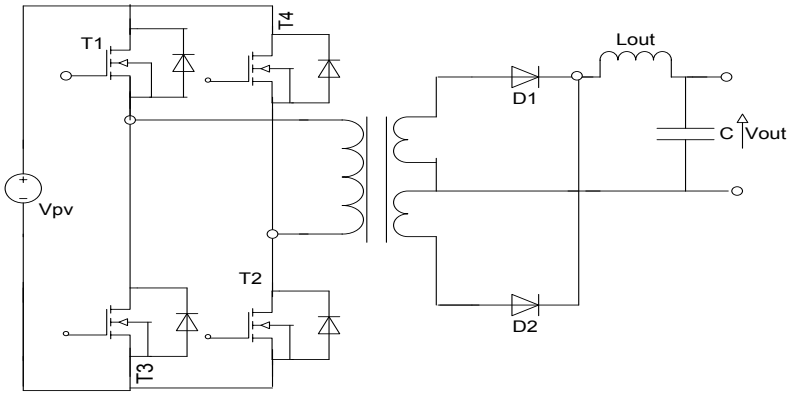

Fig. 2.23, Full-bridge DC/DC converter

2.2.7. Novel high efficiency step-up converter

The novel high step-up converter was proposed by Tseng and Liang [68] [69] to give high efficiency with less voltage stress on diodes, switches, and capacitors. The design of the converter consists of a voltage boost cell and an energy clamp circuit. The function for the proposed converter is as an active clamp circuit to suppress the voltage spike on the power switch during the turn off transient period [68] [69]. In order to increase the output voltage, the fly back converter output terminal and boost converter output terminal are serially connected with a coupled inductor as shown in Fig. 2.24.

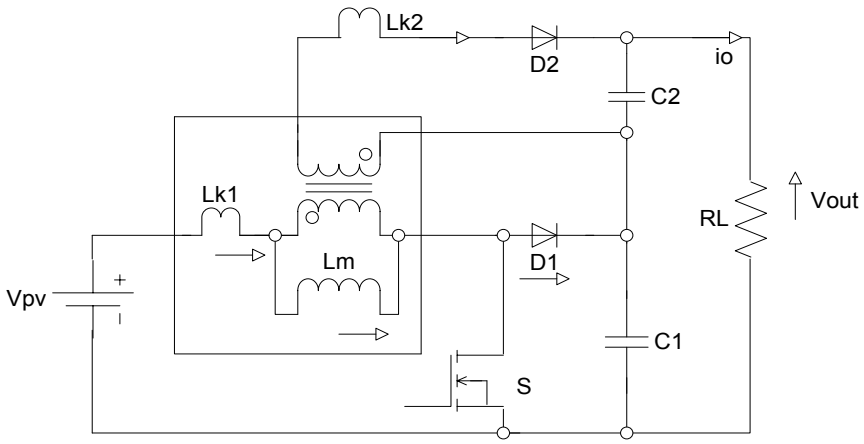

Fig. 2.24, Novel high efficiency step-up converter

The advantages for the proposed converter are that it has a simple control technique of current mode PWM for a duty cycle below 50 % and the leakage energy is recycled to the output. Moreover, voltage stress is reduced on the switching element and high efficiency are achieved by the low Rds(on) voltage. In addition, a lower rating of the power switching device is achieved, also this converter is able to achieve a high step-up ratio[68]. However,, the ripple of the current is still high compared to a conventional interleaved boost converter.

Summary

After reviewing several types of boost converter, it is obvious that most of the step-up DC-DC converters have a weakness negative side such as some converters' design requires an increase in the components which leads to an increase in cost. On the other hand, the step-up DC-DC converters have strong points, for example, approximately all converters have a low stress voltage and a low stress current on the components for each converter's circuit. In discussing several types of step-up DC/DC converters which have a chance to convert energy from a low level voltage to a high level voltage for a solar power standalone system, it becomes clear that the best suitable converter for the standalone PV System cannot be ascertained. The difference in requirements of the standalone photovoltaic system (voltage-location- standalone type), and to choose a converter, it is important to consider both the producer and the consumer requirements. However, in general after comparison of various boost converters, the interleaved boost converter and full bridge converter are preferred for the PV energy conversion because they are relatively easy to implement and control compared to other topologies reviewed, yet still deliver good performance.

Interleaved boost converter technology has been chosen for use in this research due to its benefits in technique such as low ripple amplitude and a high frequency ripple power at the input and output waveforms, therefore there is a chance to minimize the size of inductors and capacitors that would be relatively large if a conventional boost were used. It also creates low stresses on components due to the current split which increases power processing capability. Furthermore, for a similar power rating, the current flowing in each limb of the interleaved converter is lower than a conventional DC-DC converter, hence reducing overall I^2R losses.

The research aims to investigate the interleaved boost converter in comparison with a conventional boost converter to assess the converter's efficiency with a PV system and present a novel control strategy for the interleaved boost converter to improve system efficiency. The requirement of the control is to isolate one limb of the interleaved boost converter as this is necessary to operate the interleaved boost converter at low PV power as a conventional boost converter and at high PV power as an interleaved boost converter. This control will be shown and discussed in Chapter six.

Chapter Three

3. System Description and Modelling

3.1. Introduction

This chapter describes the prototype PV standalone system used for all experimental investigations in this project. The setup comprises of a solar power emulator, a DC-DC boost converter, a maximum power point tracking control and resistive load. In order to maximise efficiency, the conclusions from the literature review on maximum power point tracking algorithms and different DC-DC boost converters are taken into account.

3.2. Description of the experimental setup

The experimental setup involves a 250 Watt system with resistive load, in this project a standalone type without backup batteries is introduced, as shown in Fig. 3.1. In general, the system consists of a single PV generator, DC/DC boost converter, a maximum power point tracker (MPPT) algorithm and a DC resistive load.

A TopCon® DC-DC power supply unit, based on an intelligent power module, was used as a PV emulator Data from a 50 Watt photovoltaic array (KD50SE-1P) was then used to generate the current and voltage profiles of the PV array in simulation (MATLAB) and then programmed into the DC power supply using TopCon® software. This process will be explained in detail in the following discussion. The outputs of the TopCon® DC power supply are measured with Hall Effect Current/Voltage Sensors; LV25-P and LTS15-NP, respectively. The outputs of these sensors were connected to the 12-bit resolution analogue to digital converter (ADC) inputs of a TI TMS320F28335 eZdsp kit used for control and data acquisition. The ADC readings and the sensors outputs were calibrated using a DC power supply and high-resolution digital multimeter prior to testing. A power meter was used to measure the emulated PV power, the load power and the efficiency of the system Furthermore, an A622 current probe and a P5200 high voltage differential probe with a digital oscilloscope Tektronix TDS3014B were used to measure the data of the PV current, PV voltage, inductor current, voltage and current of load. The load was varied manually from zero to its maximum value (200 ohm) via a sliding variable resistor.

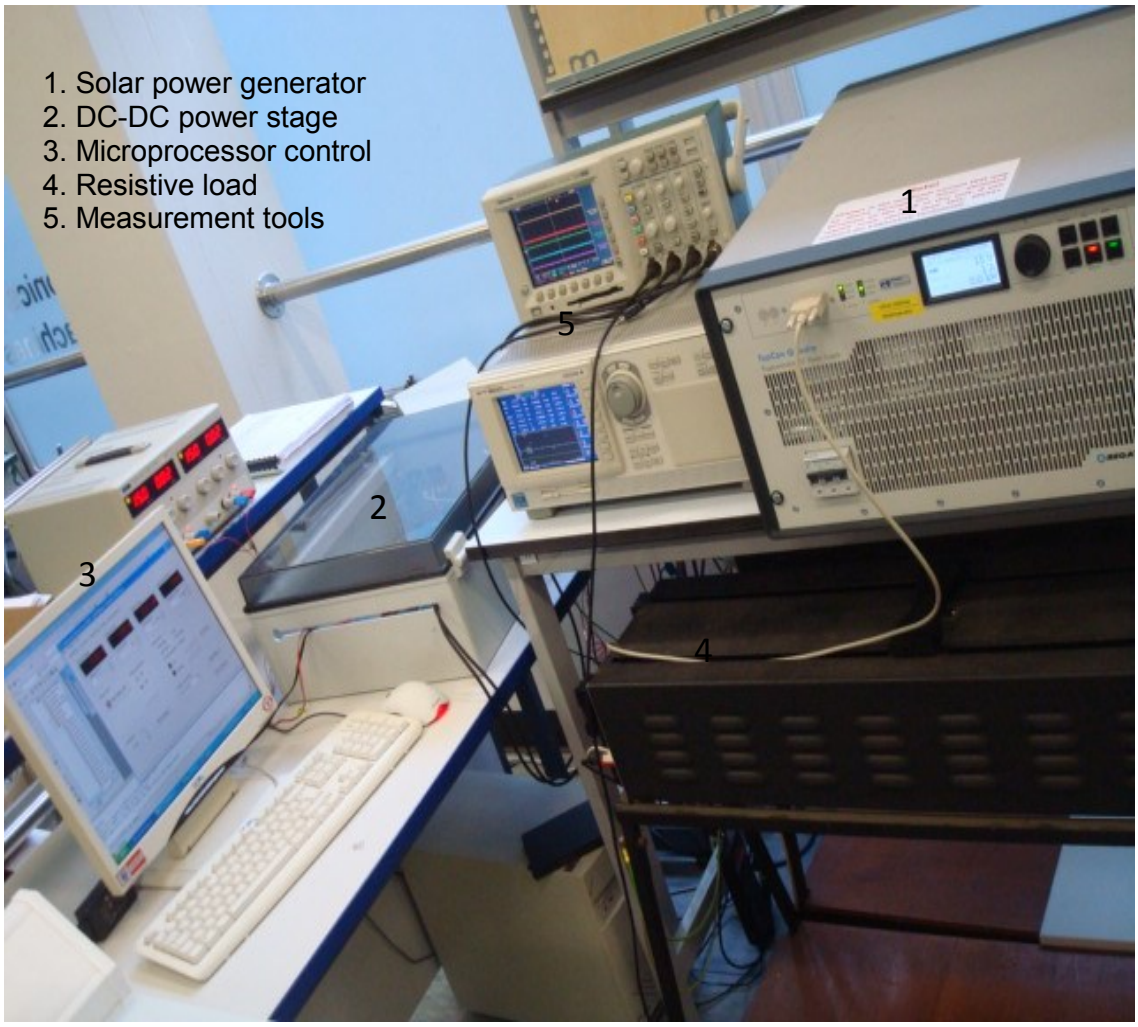

Fig. 3.1, Experiment Standalone PV system setup

3.3. Photovoltaic (PV) modelling and data generation

Photovoltaic panels consist of several PV cells in parallel and series connection. Parallel connection is accountable for increasing the current of the PV panel whereas the series connection is responsible for increasing the voltage of the PV panel. The photovoltaic cell can be presented by the circuit shown below in Fig. 3.2 which is a simple equivalent circuit which consists of series resistance, parallel resistance (usually neglected because its effect is less noticeable compared to series resistance) and diode in parallel with a current source. The output of the current source is directly proportional to the light falling on the cell (photocurrent Iph). When light hits the solar cell, the energy of the photons generates free charge carriers. The current source produces the photoelectric current Iph. Since the current is dependent upon the radiance while the voltage of the cell depends approximately on the temperature.

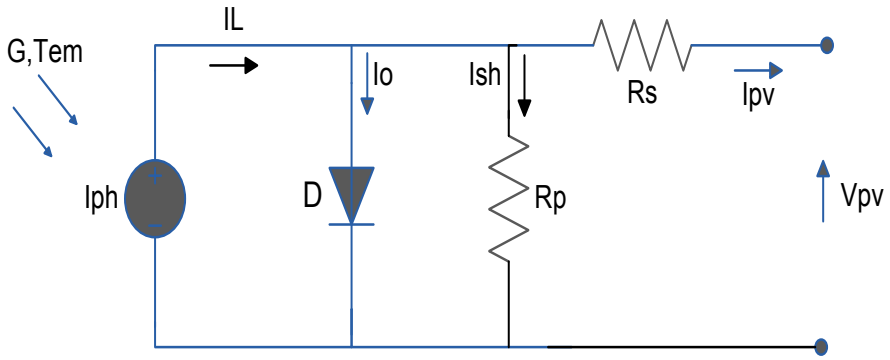

Fig. 3.2, Equivalent circuit of PV solar cell

The series resistance Rs, which is in a range of a few milliohms, describes the voltage drop that occurs as the charge carriers migrate from the semiconductor to the electrical contacts. The parallel resistance Rp describes the leakage current (neglected). With series resistance, it is possible to calculate characteristic curves for current or voltage of solar cells at different temperatures and irradiance. The characteristics of the PV cell are described in the equations (3.1-3.8) given below [70] [71] [72] [12]. In the analysis; I_L is photo current, R_S is cell series resistance, I_O is cell reverse saturation current, T is temperature, V_{OC} is open circuit voltage , I_{SC} is short circuit current. Q is electronic charge (q = 1.602e-19), *K* is Boltzmann's constant (K = 1.381e-23), N is the diode ideality factor (1 < n< 2).

$$I = I_L - I_O(e^{q(V+IR_S)/nkT} - 1) \quad (3.1)$$

$$I_L = I_L(T_1) + K_O(T - T_1) \quad (3.2)$$

$$I_{L(T_1)} = G.\, I_{SC}(T_{1,nom})/G_{(nom)} \quad (3.3)$$

$$K_O = (I_{SC}(T_2) - I_{SC}(T_1))/(T_2 - T_1) \quad (3.4)$$

$$I_O = (I_O(T_1).\left(\frac{T}{T_1}\right)^{\frac{3}{n}}.\, e^{qV_q(T_1)/nk(\left(\frac{1}{T}-\frac{1}{T_1}\right))} \quad (3.5)$$

$$I_O(T_1) = \frac{I_{SC}(T_1)}{e^{qV_{OC}(T_1)/nk(T_1)}} - 1 \quad (3.6)$$

$$R_S = \frac{dV}{dI_{voc}} - (\frac{1}{X_V}) \quad (3.7)$$

$$X_V = I_O(T_1)\left(\frac{q}{nk(T_1)}\right) e^{qV_{OC}(T_1)/nk(T_1)} - (\frac{1}{X_V}) \quad (3.8)$$

All constants in the equations are determined by examining the manufacturer's ratings of the PV array. The industry has made commercial PV modules of different sizes from about 50W to 200W; they consist of a number of photovoltaic cells that are usually arranged in parallel and in series to meet energy requirements. Typical module data, a HIT photovoltaic module HIP-210NH1-BO-1 [73] [72 cells, maximum 210 Watts] and a KD50SE-1P module [74] [36 cells, maximum 50 Watts] are tested in simulation and emulated, as shown in Table 3.1.

Table 3.1: Key data of the KD50SE-1P PV model and of the HIP-210NH1-BO-1, PV model

	HIP-210NH1-BO-1	**KD50SE-1P**
	G=1000w/m², T=25C°	G=1000w/m², T=25C°
Maximum power	210 (W)	50 (W)
Short circuit current	5.57 (A)	3.07 (A)
Open circuit voltage	50.9 (V)	22.1 (V)
Max. power current	5.09 (A)	2.8 (A)
Max. power voltage	41.3 (V)	17.9 (V)

3.3.1. PV generation in Matlab software

For the purposes of the simulation study, data is taken directly from the manufacturers' published data sheets and applied in Matlab. Details of the data used are shown in Table 3.1. The results of Matlab software generation to PV module models are shown in Figs. 3.3, 3.4, 3.5 and 3.6, these outputs of Matlab function are revealed for various irradiations levels and disclose excellent correspondence with the chosen model data.

The current and voltage (I-V) curves of the Sanyo HIP-210NH1-BO-1 solar module and the KD50SE-1P solar module which are used in this research at different solar irradiance levels as provided in the module datasheet are shown in Fig.3.3 and Fig. 3.4, the short circuit current of the module is proportional to the solar irradiance while its open circuit voltage increases slightly with the irradiance level at constant array temperature. The photovoltaic (PV) generator can be approximated to a current source if it is operated near its short circuit condition and can be approximated to a voltage source if it is operated near its open circuit condition. At the knee area of the curve where the maximum power point lies, the PV generator cannot be accurately approximated to either type of source. The PV generator must be operated in this area to make use of the maximum possible generated power.

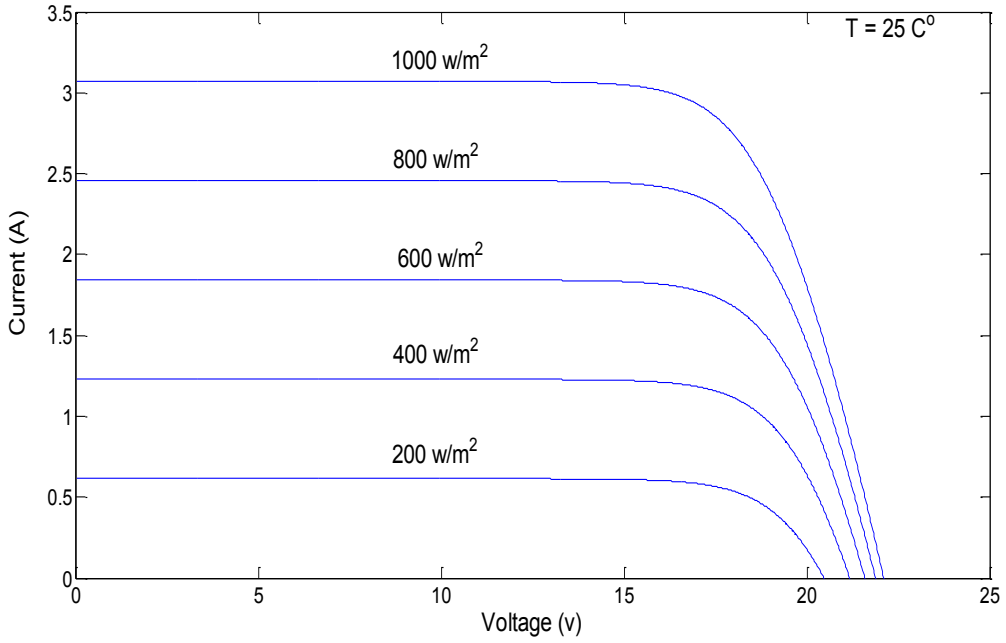

Fig. 3.3, Influence of solar irradiance on the I-V characteristics of the KD50SE-1P solar module

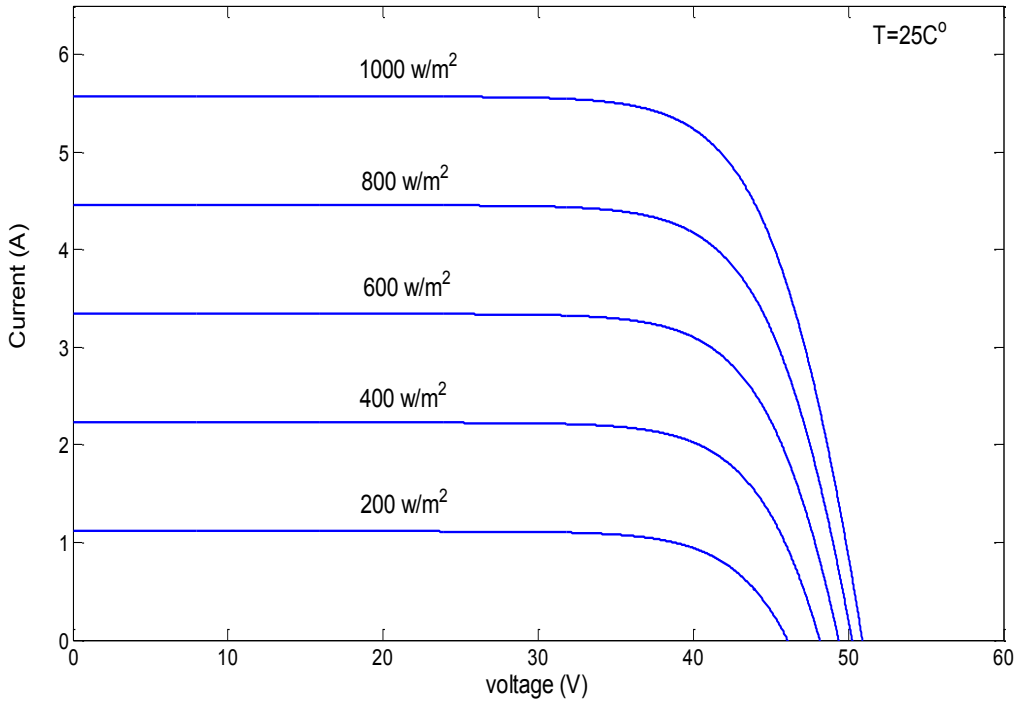

Fig. 3.4, Influence of solar irradiance on the I-V characteristics of HIP-210NH1-BO-1solar module

The power and voltage (P-V) curves of the Sanyo HIP-210NH1-BO-1 solar module and the KD50SE-1P solar module which are used in this research are shown in Fig.3.5 and Fig. 3.6. The results are in good agreement with the graphs presented in the manufacturers' datasheets. Clearly, for maximum utilization efficiency, it is necessary to use a maximum power point tracking algorithm to operate the system at the optimum point

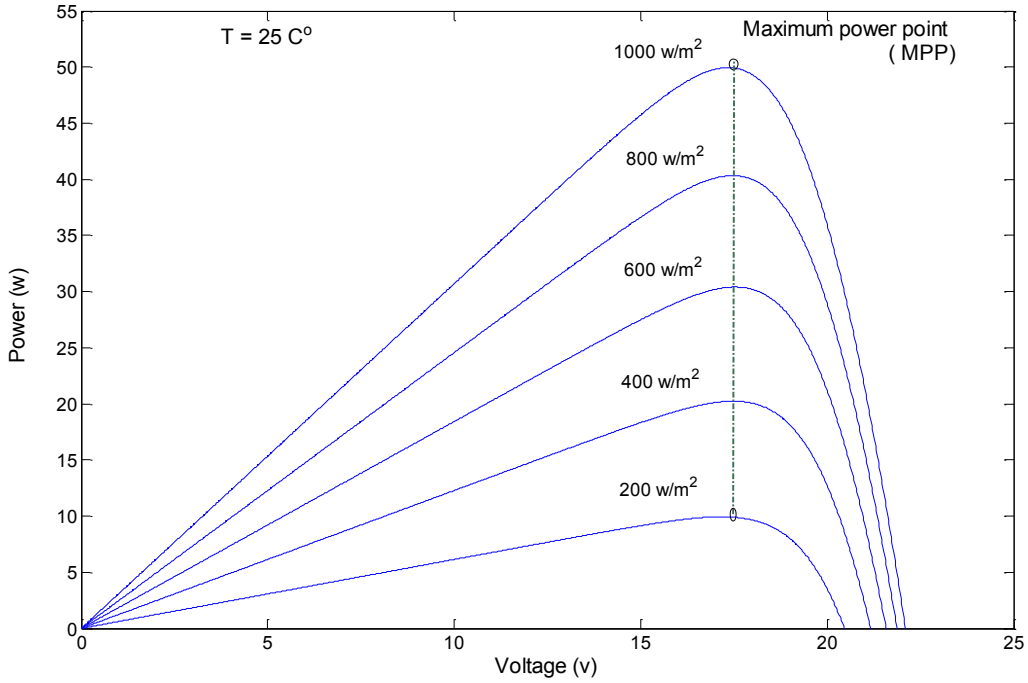

Fig. 3.5, Influence of solar irradiance on the P-V characteristics of the KD50SE-1P solar module with MPP

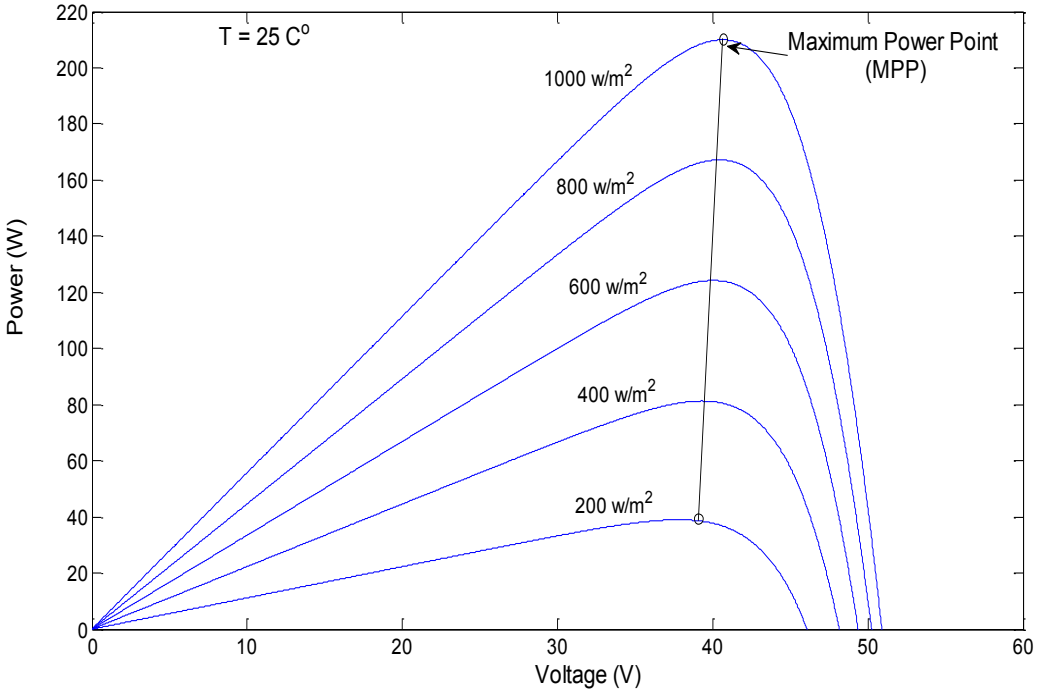

Fig. 3.6, Influence of solar irradiance on the P-V characteristics of HIP-210NH1-BO-1solar module with MPP

3.3.2. PV generation in experiment

The characteristics generated by the Matlab simulation model are then used to program the TopCon Solar Array Simulation (SAS) software, providing the foundation for the experimental work. The DC power supply, shown in Fig. 3.7, is able to emulate solar arrays with its Application Area Programming (AAP) feature which permits the loading, editing and storing of hundreds of current - voltage curves.

Fig. 3.7, TopCon DC power supply

3.4. Controller of the standalone system

The MPPT microprocessor control strategy for the standalone PV system is shown in Fig. 3.8. It is used to improve efficiency by ensuring high throughput of power at low and high insolation. The PI controller is used to adjust the duty ratio and to improve the converter transient response. The ratio of output voltage and input voltage is controlled by varying the on-off duty cycle of the converter switch. Moreover, since the output voltage of the converter in PV applications is fixed by the battery that is usually connected in parallel with the load, output voltage control is not required.

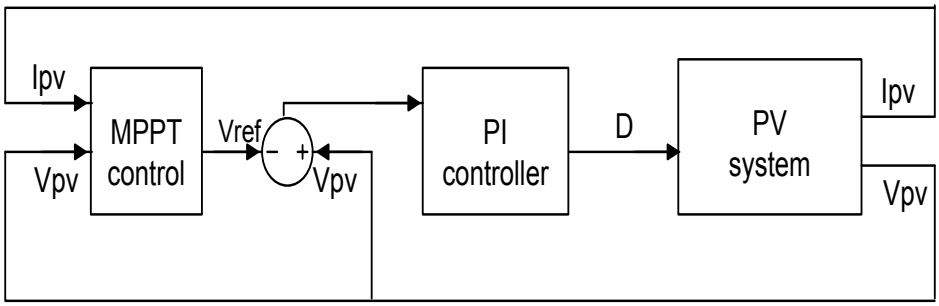

Fig. 3.8, Block diagram of standalone PV system microprocessor control

3.4.1. Maximum power point tracking (MPPT) controller

Since the PV generator exhibits nonlinear characteristics as shown in Fig. 3.9, its maximum power point varies with the solar insolation, and there is a unique operating point of the PV generator at which its power output is at a maximum. Therefore, for maximum utilization efficiency, it is necessary to use a maximum power point tracking algorithm to generate all available PV panel maximum power under different insolation to the load. The literature review in Chapter two makes reference to maximum power point tracking methods, it concludes by recommending the use of the well-known perturbation and observation (P&O) algorithm for tracking the maximum power point in this project.

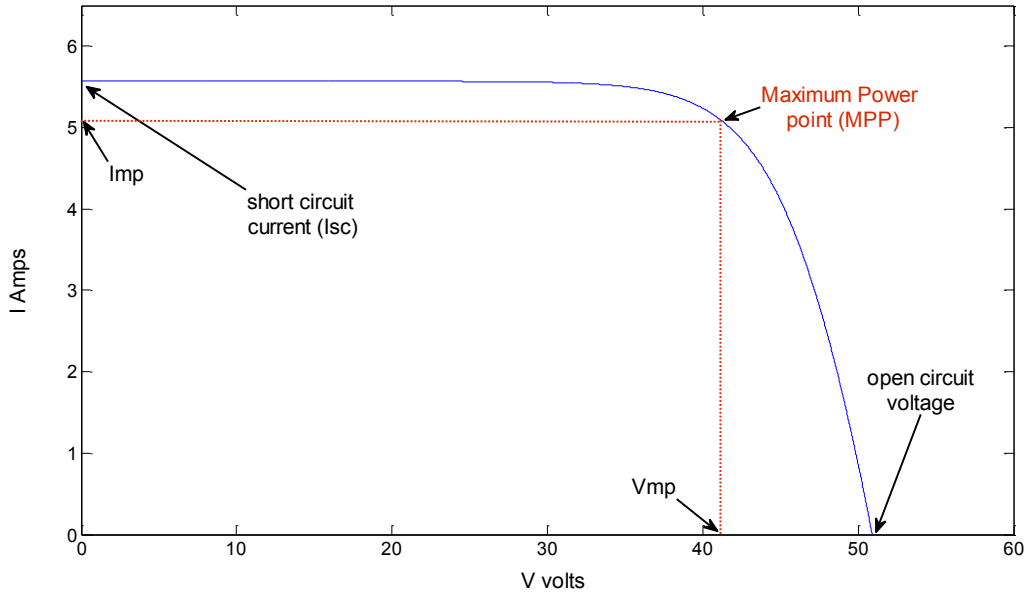

Fig. 3.9, I-V Characteristics of a typical PV panel with MPPT control

The P&O algorithm is chosen due to its ease of implementation in its basic form and its advantages compared to other methods. It operates by periodically perturbing (incrementing or decrementing) the array terminal voltage, as shown in Fig. 3.9, and comparing the PV output power with that of the previous perturbation cycle. If the PV array operating voltage changes and power increases, the control system moves the PV array operating point in that direction, otherwise the operating point is moved in the opposite direction. In the next perturbation cycle the algorithm continues in the same way [75] [26]. The main advantage of this method is the relative simplicity of the algorithm. Furthermore, previous knowledge of

the PV system characteristics is not required if the irradiation does not vary too quickly, this method generally works well alongside its optimization techniques, it is one of the most efficient [17] and continuously tracks the true MPP in a minimum amount of time [16].

3.4.2. Proportional and integral (PI) controller

The maximum power point tracker MPPT takes measurement of the PV module current and voltage and calculates the reference voltage (Vref) where the PV operating voltage should move to. The task of the MPPT control is to set reference voltage only and it is repeated periodically with a slow rate 1-15 samples per second. Then there is another control loop that is the proportional-integral (PI) control that regulates the input voltage of the DC-DC converter. The PI control job is to minimize the error between the measured voltage of PV and reference voltage that is calculated by the MPPT algorithm by adjusting the duty cycle. The digital PI control operates rapidly and provides a good dynamic system response. Digital PI controller use sample and hold circuitry to convert analogue signal to digital signal and vice versa. To tune the discrete PI controller, there are many stability-analysis tuning techniques available; such trial and error tuning, Ziegler Nichols, pole placement, and so on. This research had used the trail-and-error tuning method to tune the discrete PI control in the system, due to its simple yet effective approach. Using the trial-and-error tuning method, the proportional gain (k_p) is set at 1 and the integral gain (k_i) is set at 800. The controller's block diagram is shown in Fig. 3.10. In considering Fig 3.10, the equations defining the digital controller are as follows (3.9-3.11):

$$C(z) = PI \tag{3.9}$$

u is the controller output

e is the error input to the controller

k_p is the proportional gain

k_i is the integral gain

T is sample time

$$\mathrm{K}_P = \mathrm{K} - \frac{\mathrm{KT}}{2\mathrm{T}_i}, \mathrm{K}_I = \frac{\mathrm{KT}}{\mathrm{T}_i} \tag{3.10}$$

$$\frac{U_{(z)}}{E_{(z)}} = C_{(z)} = \mathrm{K}_P + \frac{\mathrm{K}_I}{1 - z^{-1}} \tag{3.11}$$

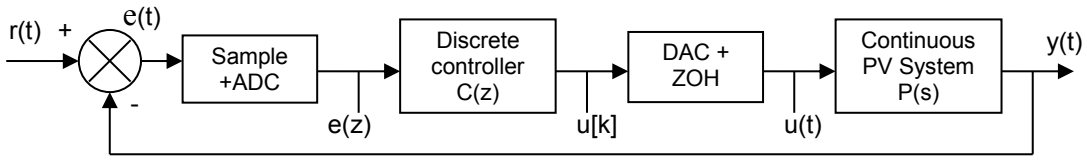

Fig. 3.10, Block diagram of digital PI controller

3.4.3. Matlab software control

Matlab software is used for testing the selected photovoltaic arrays KD50SE-1P module and the HIP-210NH1-BO-1 module with manufactured data under different irradiations of atmosphere condition with and without maximum power point tracking control (Perturb & Observe algorithm). In Fig. 3.11, as can be seen on the PV power chart of the HIP-210NH1-BO-1 module, the shown PV power without the MPPT (Perturbs & Observe algorithm) the curve is far from the maximum power points under a changeable irradiation condition. However, when the MPPT control (Perturb and Observe algorithm) is connected in the system, the power of the PV array with MPPT is on the maximum power point even with changeable atmospheric conditions. For example, at 1000w/m^2, the shown PV power curve with MPPT control is 210 Watts but the PV power array without the MPPT control is about 170 Watts, also under a different level of irradiation of 200w/m^2 the maximum PV power array with MPPT control is 40 Watts, however the PV power array without MPPT control is about 20 Watts.

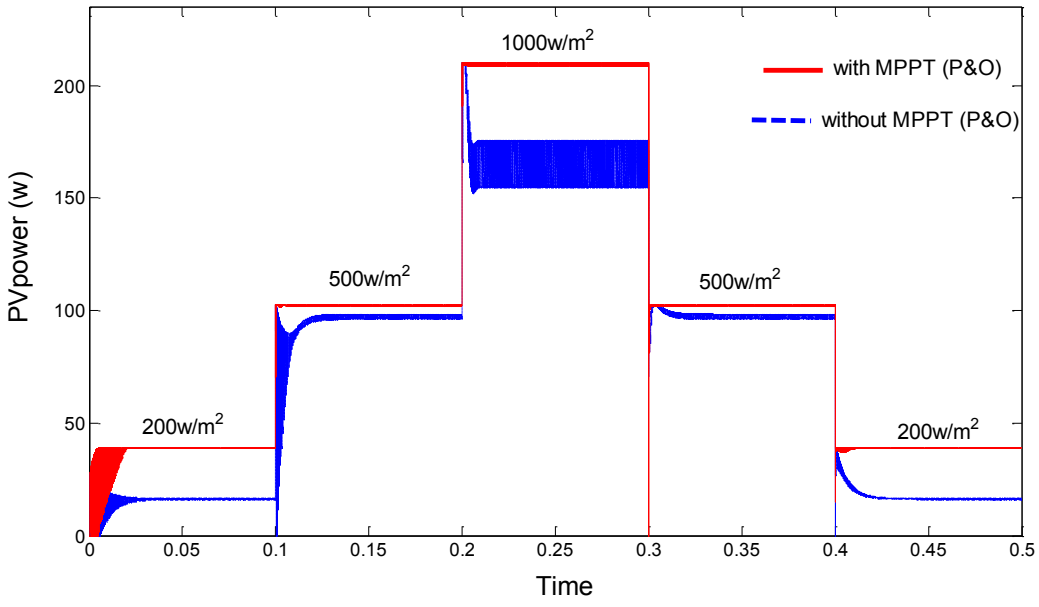

Fig. 3.11, PV power of HIP-210NH1-BO-1solar array without and with MPPT (Perturb & Observe) control under changeable irradiation levels of weather conditions

3.5. DC-DC Boost Converter

To complete control of the power flow using a boost converter, the input voltage must lie between zero and output voltage, that allows the boost converter to always operate at the MPP in all load conditions. In addition, compared with a buck converter which needs another element of diode to block the reverse current flow when the panel voltage is less than the battery voltage, the boost converter naturally has this diode as part of its structure, which eradicates an additional source of power loss and voltage drop. In the review, Chapter two addressed different types of boost converter and advocates the use of the conventional and interleaved boost converters in this project. To combine the advantages of both converters, an interleaved boost converter with novel switch adaptive control is proposed. The hardware developed for this project is shown in Fig. 3.12. The proposed topology is required to isolate one limb of the interleaved boost converter and force it to operate as a conventional boost converter at low PV power levels.. This topology will be shown and discussed in Chapter six.

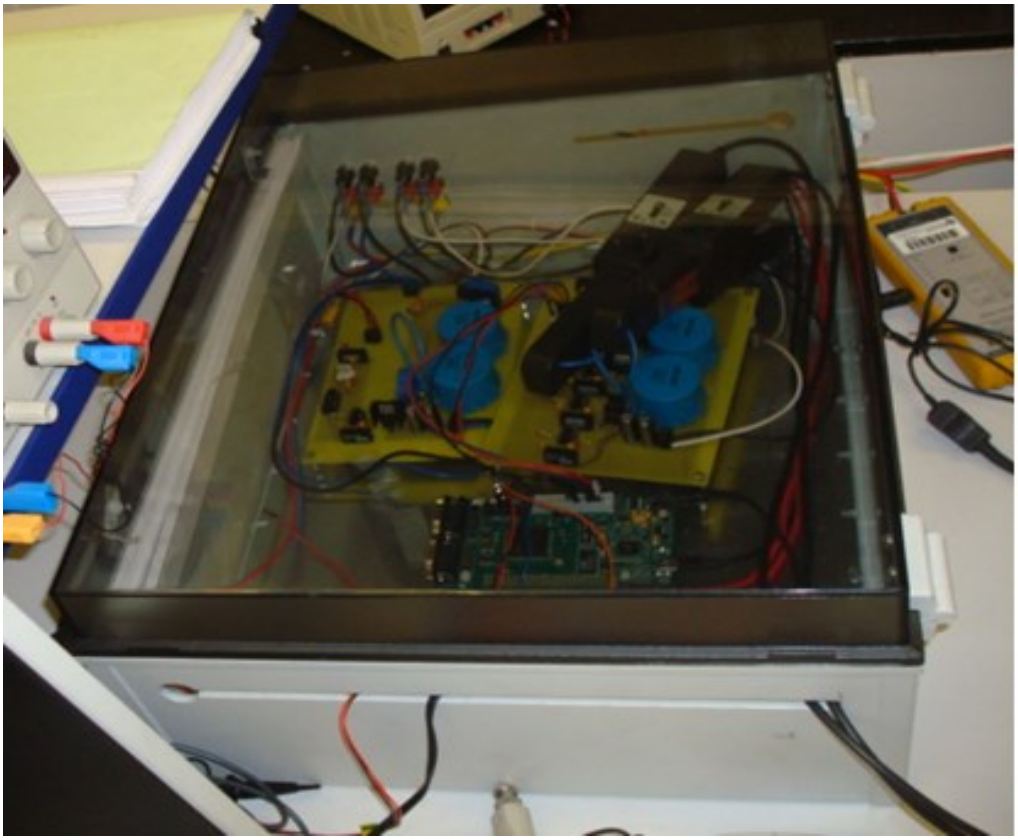

Fig. 3.12, DC-DC boost converter unit of instructed stand-alone PV system

3.5.1. Efficiency issue

After research into boost converters, it is evident that to assess the conventional boost converter and conventional interleaved boost converter fully, it is important to consider the design of both converter topologies. It is essential to consider losses, cost and size within the introduced system.

3.5.1.1. Power losses

Inductor losses consist of copper loss and core loss, the current exchange affects only the copper loss which is expressed in equation (3.12) [57]:

$$P_{inductor\ copper\ loss} = \left(\frac{i_{in}}{N}\right)^2 . r_L \tag{3.12}$$

Where, i_{in} is the input current, R_L is the inductor resistor and N number of phases. From formula (3.12) inductor loss can be calculated in the conventional boost converter as below:

$$P_{inductor\ copper\ loss}1 = \left(\frac{i_{in}}{1}\right)^2 . r_L = {i_{in}}^2 . r_L \tag{3.13}$$

Also from equation (3.1) inductor loss in the interleaved boost converter can be calculated as below [7]:

$$P_{inductor\ copper\ loss}2 = 2.\left(\frac{i_{in}}{2}\right)^2 . r_{L1} + 2.\left(\frac{i_{in}}{2}\right)^2 . r_{L2}$$

$$= \frac{{i_{in}}^2}{2} . (r_{L1} + r_{L2}) \tag{3.14}$$

As can be seen from equation (3.14) the interleaved halves the inductor losses compared to the conventional boost converter. Furthermore, there is more opportunity to reduce inductor loss in the interleaved converter by effectively splitting the inductor value of the conventional boost converter across each phase of the interleaved boost converter, switching loss also has a large impact on system efficiency. In semiconductor devices, power loss appears in the form of switching loss (equation (3.15)) and conduction loss (equation (3.16)).

$$P_{Switch-switching\ loss} = \frac{1}{2} V_o \frac{i_{in}}{N} \left(t_{on} + t_r + t_{off} + t_f\right) f_S \tag{3.15}$$

$$P_{Switch-conduction\ loss} = R_{ds(on)} . D \left(\frac{i_{in}}{N}\right)^2 \tag{3.16}$$

$$P_{gat-loss} = V_g\ Q_g f_s$$

Where, t_{on} is the turn-on time, t_{off} the turn-off time, t_r current rise time, t_f voltage fall time,V_o the voltage, f_s switching frequency, $R_{ds(on)}$ turn-on resistor and D duty ratio.

From equation (3.15) and (3.16) the switching loss in a conventional boost is:

$$P_{Switc-switching\ loss}1 = \frac{1}{2} V_o\ i_{in}\left(t_{on} + t_r + t_{off} + t_f\right) f_S \tag{3.17}$$

$$P_{Switch-conduction\ loss}1 = r_{ds(on)}.D(i_{in})^2 \tag{3.18}$$

$$P_{gat-loss}1 = V_g\ Q_g f_s$$

Also using equations (3.6) and (3.7), the switching loss in the interleaved boost converter is:

$$P_{Switch-switching\ loss}2$$

$$= 2.\frac{1}{2} V_o \frac{i_{in}}{2}\left(t_{on} + t_r + t_{off} + t_f\right) f_S$$

$$= \frac{1}{2} V_o\ i_{in}\left(t_{on} + t_r + t_{off} + t_f\right) f_S \tag{3.19}$$

$$P_{Switch-conduction\ loss}\ 2 = (2\ ).r_{ds(on)}.D\left(\frac{i_{in}}{2}\right)^2$$

$$= r_{ds(on)}.D(i_{in})^2 \tag{3.20}$$

$$P_{gat-loss}2 = 2.V_g\ Q_g f_s$$

From equations (3.17), (3.18), (3.19) and (3.20), it is clear that switching losses are identical in both converter topologies. However, with the interleaved converter it is possible to use clever switching strategies to effectively divide the switching across limbs and reduce the switching loss further. Diode losses can be evaluated in formulas (3.21) and (3.22), where V_{out} is the output voltage, t_{rr} is reverse recovery time and V_F is forward voltage drop.

$$P_{Diode-reverse\ recovery\ loss} = \frac{1}{2} V_{out} i_{RM} t_{rr} f_S \tag{3.21}$$

$$P_{Diode-conduction\ loss} = V_F \frac{i_F}{N}(1 - D) \tag{3.22}$$

From equation (3.21) and (3.22) the diode loss in the conventional boost converter can be evaluated as below:

$$P_{Diode-reverse\ recovery\ loss}1 = \frac{1}{2} V_{out} i_{RM}\ t_{rr} f_s \tag{3.23}$$

$$P_{Diode-conduction\ loss}1 = V_F.i_F.(1-\ D) \quad (3.24)$$

In the interleaved boost converter diode loss is:

$$P_{Diode-reverse\ recovery\ loss}2 = 2.\frac{1}{2}V_{out}i_{RM}t_{rr}f_s$$

$$= V_{out}i_{RM}\ t_{rr}f_s \quad (3.25)$$

For diode conduction losses, the forward current is equal to the inductor current ($I_F = i_L$), so the diodes losses in the interleaved boost converter are:

$$P_{Diode-conduction\ loss}2 = 2.V_F\frac{i_F}{2}D$$

$$P_{Diode-conduction\ loss}2 = V_F.i_F.(1-D) \quad (3.26)$$

Comparing the two power converter topologies, the diode losses in both converters show identical conduction loss as given in equations (3.24, 3.26), whilst the diode switching losses (reverse recovery losses) are different in both converters. In summary, this simplified power loss analysis shows that the interleaved boost converter has lower inductor losses, but there is little difference in switching and diode losses compared to the conventional boost converter, assuming the same switching frequency is applied in each case (It is accepted that this may not always be the case).

3.5.1.2. Switching Frequency

The choice of switching frequency is generally more subjective. If the requirement of the system is a small power circuit and there is less distortion, then high switching frequency is required while, at the same time, the switching frequency must be low enough to keep the efficiency high.

3.5.1.3. Selection Switching Device

Selecting the switches is based on current and voltage ratings, and should take into consideration any potential losses. For this, $R_{ds(on)}$ must be low enough to minimize conduction loss and V_F should be as low as possible at the maximum output current specification to minimize conduction losses. Moreover, t_{rr} reverse recovery time should be

as low as possible to minimize switching loss. Note that the interleaved boost converter has the choice of using a low rating current component due to the current split in its branches.

3.5.1.4. Selection of Inductance and Capacitance

The appropriate choice of inductor value can be determined using equation (3.27) [76] [77]:

$$L = \frac{V_{in}.D}{\Delta i_L.f} \tag{3.27}$$

As this shows, a smaller output current ripple requires larger inductor values leading to increased cost. From equation (3.27), the conventional boost converter inductor value can be determined as:

$$\mathrm{i_{pv-max}} = \mathrm{i_{in}} = \mathrm{i_L}$$

$$L = \frac{V_{in}.D}{\Delta i_L.f}$$

For the interleaved boost converter, inductor values L_1, L_2 can be calculated as:

$$\mathrm{i_{pv-max}} = \mathrm{i_{in}} = \frac{\mathrm{i_{L1}}}{2} = \frac{\mathrm{i_{L2}}}{2}$$

$$L_1 = L_2 = \frac{V_{in}.D}{2\Delta i_L.f}$$

With respect to the output capacitor, this is determined by equation (3.28) as follows:

$$C = \frac{V_{out}.D.f}{\Delta V_{out}.R}$$

(3.28)

As shown, larger capacitor values lead to smaller output voltage ripple and taking into consideration the equivalent series resistance (ESR), a smaller ESR value results in less loss in the capacitor.

3.5.1.5. Continuous and Discontinuous Current Mode

Based on the amount of energy that is delivered to the load during each switching period, the boost converter can be classified into continuous (CCM) or discontinuous current mode (DCM). In the discontinuous current mode, the inductor current mode ramps down to zero during the switching off time, if not the converter operates in a continuous current mode.

The disadvantages of DCM switch and output diode peak currents are larger when the converters operate in DCM. Furthermore, the larger peak currents cause greater EMI/RFI problems. Also, larger peak currents necessitate using larger current and power dissipation rated diodes and switches [76]. In DCM the switching losses dominate, whilst in CCM the induction losses dominate [19]. Therefore, the efficiency of a DC-DC boost converter that operates in continuous current mode is likely to remain very high [78].The problem facing the interleaved boost converter is that when the amount of energy delivered to the load is small, the interleaved boost converter operates in DCM due to a split of the small amount of input current between its branches. For that reason, when there is small input current, the novel control operates the interleaved boost converter as a conventional boost converter to avoid DCM, by pushing the total amount of current into one branch and isolating the other one. When there is a high amount of energy, the interleaved boost converter with a switch adaptive control is ordered to operate as the interleaved boost converter.

3.6. Summary

In this chapter, the prototype PV standalone system used for all experimental investigations in this project has been introduced. The setup comprise of a 50 Watt PV array emulator connected to 200 ohm resistive load via a power DC-DC converter. Real-time control and data acquisition are performed utilizing a TI TMS320F28335 eZdsp Kit.

The characteristics of the individual components comprising this prototype PV standalone system were measured and compared to those given in the manufacturer's datasheets. Based on these measured characteristics, accurate models have been developed for the PV emulator. The component models were combined to simulate the overall system on the Simulink/Matlab environment. The requirement for accurate MPPT algorithms has been validated in this Chapter. From this, a Perturb and Observe algorithm has been developed and verified experimentally providing a foundation for the research work.

Chapter Four

4. Conventional Boost Converter

Typically, in electrical power supplies, transforming the DC voltage from one level to another is achieved through the use of a controlled DC to DC switch mode power converter [1]. These converters, which work to transform input DC voltages to controllable output DC voltages, are often used to regulate the output of DC power supplies and drive DC motor applications. The boost converter transforms a low input voltage to a higher magnitude output voltage, usually with the same polarity as the input [79] [80].

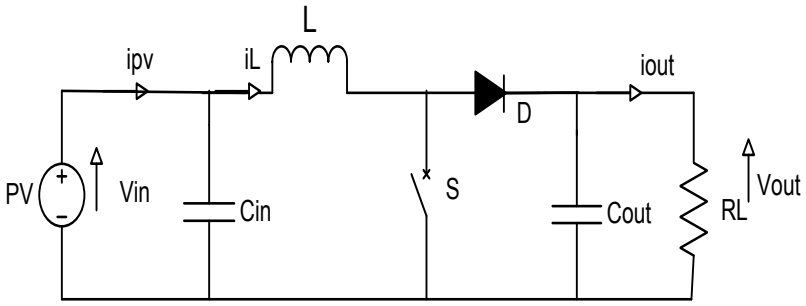

Fig. 4.1, Non-isolated conventional boost converter

The operation of a non-isolated conventional boost converter is shown in Fig. 4.1: when the switch is turned on, the supply voltage is applied across the inductor (L) and the diode (D) is reversed which isolates the output side, and the energy source is stored in the inductor. After the switch is turned off, the load or the output side receives energy from the inductor in addition to the input source. Due to this, the output voltage becomes greater than the input voltage [79]. Moreover, this converter has two modes of operation: continuous current condition and discontinuous current condition, in practice the converter could operate in both modes of operation with different characteristics. For analysis, the capacitor is assumed to be very large to keep the output voltage constant [1], also the input voltage is assumed to be constant and the inductor current is then linear [79].

Continuous-conduction mode

In continuous current mode (CCM) the inductor current [i_L (t) > 0] never falls to zero within a switching cycle but there is oscillation in the DC value due to the switching state being on (t_{on}) and off (t_{off}) as the waveforms as shown in Fig. 4.2. In this case the inductor has to be large to give a lower peak current and this results in a small ripple on the output which leads to the advantage of reducing device stresses [81] [80].

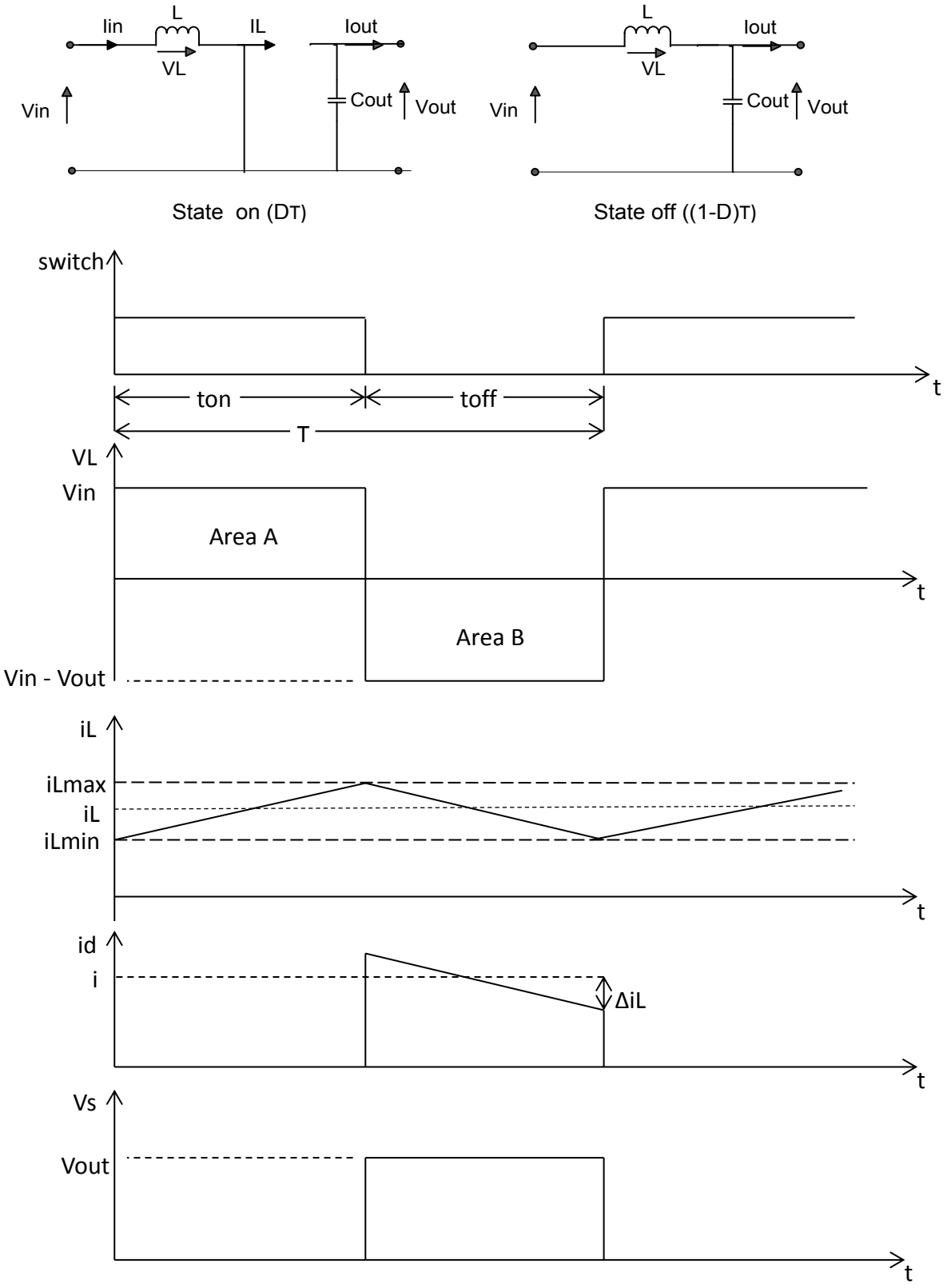

Fig. 4.2, Conventional boost converter waveforms at continuous conduction mode: (A) switch on, (B) switch off

Fig. 4.2, depicts the equations analysis which is the official expression of the operation of the boost converter in continuous conduction mode:

Area A = area B and

$$T = \frac{1}{f}$$

$$T = t_{on} + t_{off}$$

$$t_{off} = T - t_{on}$$

$$t_{on} = DT$$

$$t_{off} = T - DT = (1 - D)T$$

$$D = \frac{t_{on}}{T}$$

Where D is the duty ratio, T is the time period through the switching cycle, t_{on} is the switching on time, t_{off} is the switching off time, f is the frequency, and V_{out} is the output voltage and V_{in} is the input voltage. If Area A is equal to area B, then the output voltage expression is as follows:

$$V_{in}DT = (V_{in} - V_{out})(1 - D)T$$

$$V_{in}D = V_{in} - V_{out} - V_{in}D + V_{out}D$$

$$V_{out} - V_{out}D = V_{in} - V_{in}D - V_{in}D$$

$$V_{out}(1 - D) = V_{in}$$

Then

$$\frac{V_{out}}{V_{in}} = \frac{1}{(1 - D)} \tag{1.4}$$

Discontinuous conduction mode

As shown in Fig. 4.3, discontinuous conduction mode occurs when the inductor current falls to zero in the off state (t_{off}) before the end of the switching cycle. This may be due to minimized inductor size or small input current [79, 80]. Discontinuous conduction mode in a boost converter has the advantage of a lower transistor switching-on loss and a lower boost-rectifier reverse-recovery loss [54].

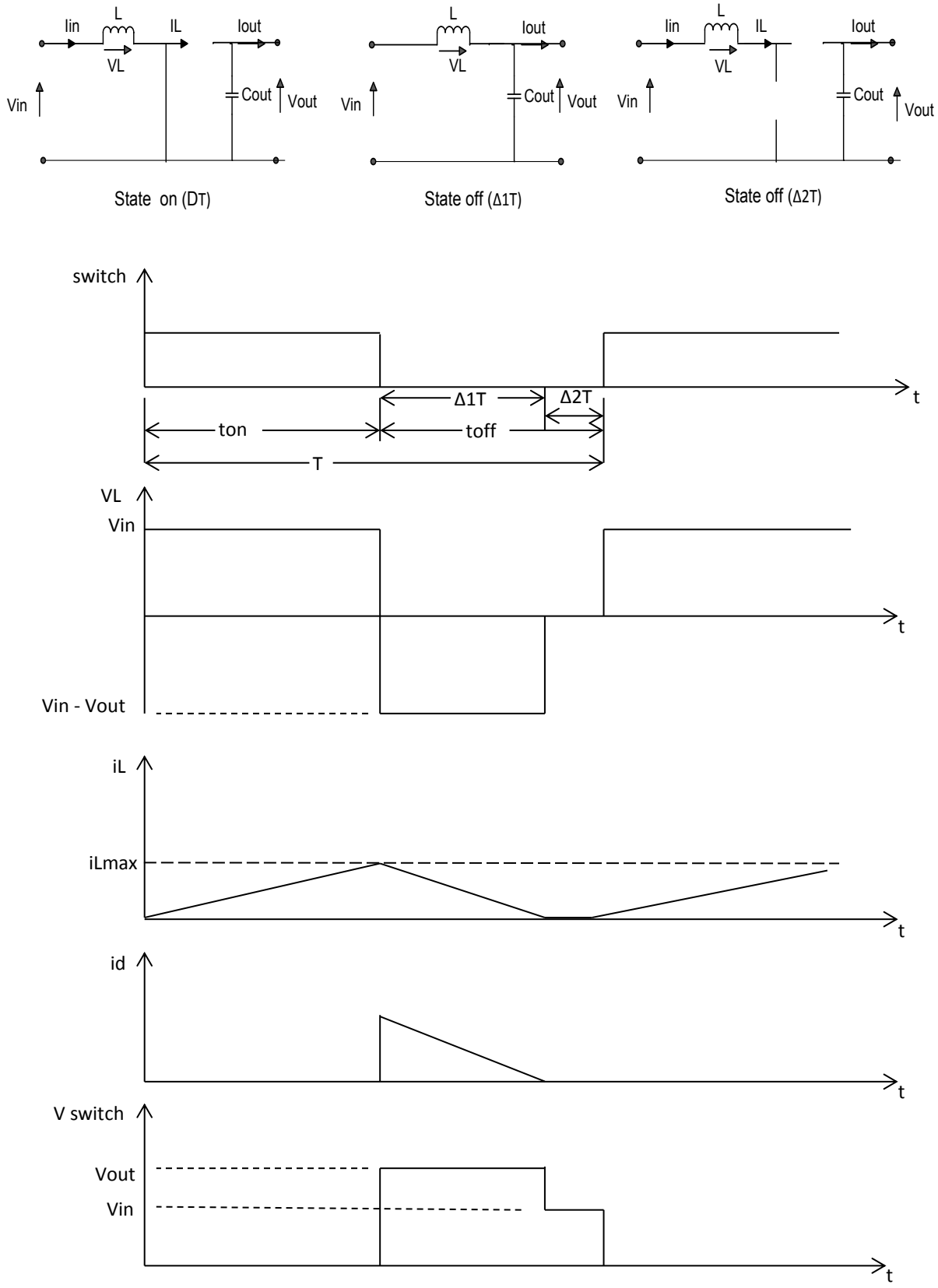

Fig. 4.3, Conventional boost converter waveforms at discontinuous conduction mode

From Fig.4.3 in discontinuous conduction mode

$t_{on} = DT$ and $\mathrm{t_{off}} = \Delta_1 \mathrm{T} + \Delta_2 \mathrm{T}$

When the switch is turned on

$$V_L = L\frac{di}{dt}$$

$$V_{in} = L\frac{i_{Lmax}}{DT} \tag{4.2}$$

When the switch is turned off i_L falls to zero

$$V_L = L\frac{di}{dt}$$

$$V_{in} - V_{out} = L\frac{i_{Lmax}}{\Delta_1 T} \tag{4.3}$$

From equation 4.2

$$i_{Lmax} = \frac{V_{in}DT}{L}$$

From equation 4.3

$$i_{Lmax} = \frac{(V_{out} - V_{in})\Delta_1 T}{L}$$

$$\therefore \frac{V_{in}DT}{L} = \frac{(V_{out} - V_{in})\Delta_1 T}{L}$$

$$\therefore \Delta_1 T = \frac{V_{in}DT}{V_{out} - V_{in}} \tag{4.4}$$

The load current (i_{out}) is the average value of the diode current

$$\therefore i_{out} = \frac{1}{2}\Delta_1 T\frac{i_{Lmax}}{T}$$

From equation 4.4

$$i_{out} = \frac{i_{Lmax}}{2T}.\frac{DTV_{in}}{(V_{out} - V_{in})}$$

$$i_{out} = \frac{1}{2LT} \cdot \frac{(DTV_{in})^2}{(V_{out} - V_{in})} \quad (4.5)$$

From equation 4.4

$$(V_{out} - V_{in}) = \frac{1}{2LT} \cdot \frac{(DTV_{in})^2}{i_{out}}$$

$$V_{out} = V_{in} + \frac{1}{2LT} \cdot \frac{(DTV_{in})^2}{i_{out}}$$

$$\therefore \frac{V_{out}}{V_{in}} = 1 + \frac{D^2 V_{in} T}{2L i_{out}}$$

Where V_{out} is the output voltage, D is the duty ratio, V_{in} is the input voltage, L is the inductor and i_{out} is the load current. In discontinuous conduction mode the voltage transfer function is not a simple function of duty ratio (D), it depends upon the size of the inductor, the output current and the switching frequency as expressed in the equation above.

Output voltage ripple:

The peak-to-peak output voltage ripple can be calculated from the waveforms shown in Fig. 4.4. In continuous mode operation it is assumed that all the components of the ripple current for the diode current go through the capacitor C, and its average value through the load resister is shown in the shaded area (ΔQ) of the waveforms [80].

By assuming a constant load current, the peak-peak output voltage ripple is given as follows:

$$\Delta V_{out} = \frac{\Delta Q}{C}$$

$$\Delta V_{out} = \frac{t_{on} i_{out}}{C} = \frac{t_{on} V_{out}}{CR} \qquad (4.6)$$

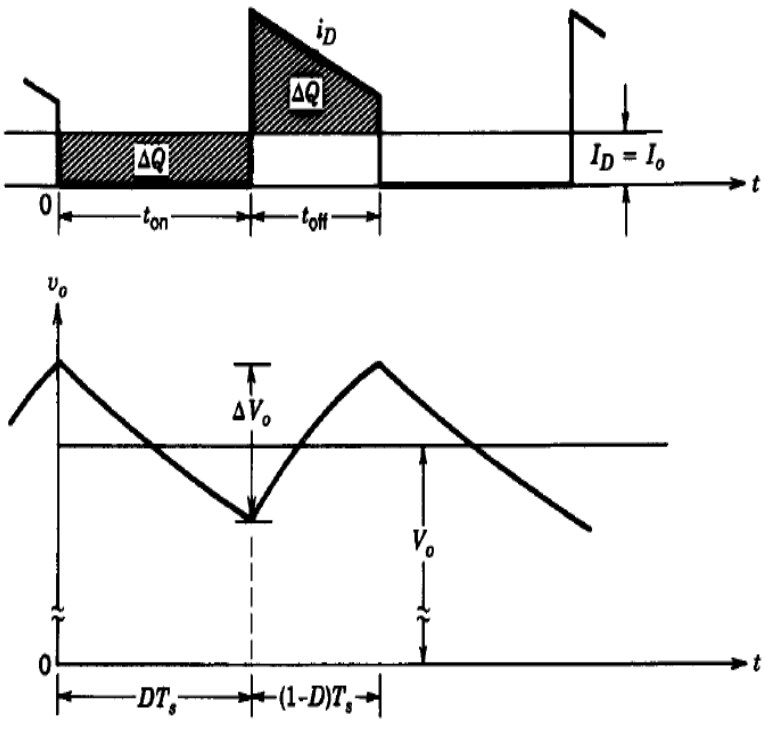

Fig. 4.4, Conventional boost converter output voltage ripples [1]

4. 1. Design of conventional boost converter

In this section, the thesis determines the elements of the conventional boost converter shown in Fig. 4.5, with rated power 210 Watts to be structured as follows and used with an introduced Stand-alone PV system.

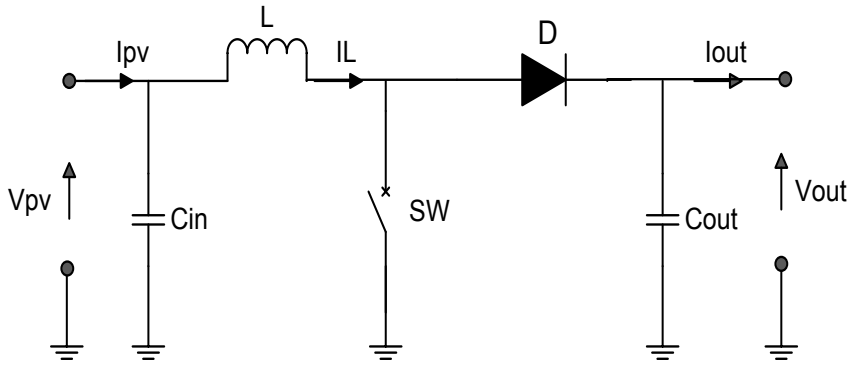

Fig. 4.5, Structure of conventional boost converter

Assuming the 210 Watt panel is used in temperature (T =25C°), irradiance (G = 1000w/m²) and it is working at its maximum power using an MPPT controller from the enclosed reference data sheet: The output power of the PV panel with G=1000 w/m² and T= 25 C° gives a maximum power (P_{pv-max}) = 210 W, a maximum power voltage (v_{pv-max}) = 41.3V and a maximum power current (i_{pv-max}) = 5.09 A. In a standalone PV system with a maximum power point tracking control using a conventional boost converter:

$i_{pv-max} = i_{in} = 5.09A$

i_L is the inductor current, i_{in} is the input current

$V_{pv-max} = V_{in} = 41.3V$

$P_{pv-max} = P_{in} = 210W$

$$i_{pv-max} = \frac{P_{pv-max}}{V_{pv-max}} \quad (4.7)$$

$$i_{out} = \frac{V_{out}}{R_{Load}} \quad (4.8)$$

The following parameters are needed to calculate the power stage conventional boost converter:

The input voltage range: $V_{in(\min)}$ = 0V, and $V_{in(max)}$= 41.3V

Maximum resistive load: R_{Load} = 195 ohm

Switch frequency of the converter: f = 20 kHz

Estimated input current ripple: Δi_{in} = 9%

Estimated output voltage ripple: ΔV_{out}= 0.24%

The frequency (f) is chosen to be 20 kHz

Assuming efficiency (η) of the converter is 100%

$T = \frac{1}{f}$, thus the time period of one cycle switching is (T) = 50 µsec

t_{on} is the time when the switch is on, f is the frequency, D is the duty cycle, t_{off} is the time when the switch is off, T is the total time period of one cycle of witching.

$$T = t_{on} + t_{off}$$

$$t_{on} = DT$$

$$V_{out} = \frac{V_{pv-max}}{1-D} \quad (4.9)$$

Due to the assumption that the efficiency is 100%, the output power is equal to the input power and the output voltage of the converter under PV panel with G=1000 w/m² is:

$$P_{out} = \frac{{V_{out}}^2}{R_{Load}}$$

$$V_{out} = \sqrt{210 \times 195} \cong 203\ volt$$

$$i_{out} = \sqrt{\frac{210}{195}} \cong 1.04\ Amps$$

$$D = 1 - \frac{V_{pv-max}}{V_{out}} = 1 - \frac{41.3}{203} \cong 0.8$$

This tells us, that that in this system with a full resistive load 195 ohm, the duty cycle will be from zero to approximately 0.8.

Diode selection

The diode is a semiconductor device that is controlled by its own voltage and current. When a diode is forward biased, it starts to conduct with a small forward voltage (V_F) across it. It turns off when the current flow into the device becomes zero. When the diode is reverse biased it stays in the off state. The diode is simulated by a resistor, an inductor and a DC

voltage source connected in series with a switch. The switch operation is controlled by the voltage and the current. The diode can also contain a series Resistance-Capacitor snubber circuit that can be connected in parallel with the diode device, however in this system the snubber circuit of the diode is neglected to avoid losses. The diode selection is based on the current and voltage rating, and to minimize losses the reverse recovery time and voltage forward should be as low as possible [82], adding the 30% of safety factor to the output voltage rating [83]. The chosen diode is (IRFB4321PBF) which was selected to be used in the simulation software and in the hardware experiment, it has a low forward voltage (V_F) = 0.895 V and very good reverse recovery time (t_{rr}) = 25 ns.

Inductor selection

The inductor will be selected based on the requirement of the current ripple system and power losses. When the switch is on, the voltage across the inductor is given by:

$$V_L(t) = L\frac{di(t)}{dt} = V_{in}$$

$$\frac{di(t)}{dt} = \frac{V_L(t)}{L} = \frac{V_{in}}{L}$$

The inductor current increases with a constant slope $\frac{V_{in}}{L}$

When the switch is off, the voltage across the inductor is given by

$$V_L(t) = L\frac{di(t)}{dt} = V_{in} - V_{out} - V_d$$

$$\frac{di_L(t)}{dt} = \frac{V_L(t)}{L} = \frac{V_{in} - V_{out} - V_d}{L}$$

V_d is the voltage dropped on the diode

The change in the inductor current during one cycle is:

$$2\Delta i_L = \frac{V_{in}}{L}t_{on} + \frac{V_{in} - V_{out} - V_d}{L}t_{off}$$

The inductor current ripple

$$\Delta i_{Lp} = 9\%\ i_L = 5.09 \times \frac{9}{100} = 0.4581A$$

The peak-to-peak current

$\Delta i_{Lp-p} = 2\Delta i_L = 0.9162$ A

The following equation 4.10 is good for estimating the right inductor:

$$L = \frac{V_{in}}{\Delta i_{Lp-p}} DT \qquad (4.10)$$

$$L = \frac{41.3}{0.9162 \times 20000} \times 0.8 = 1.8mH \cong 2mH$$

However, if the system ordered $\Delta i = 4\%$

$$\Delta i_{Lp} = 4\%\ i_L = 5.09 \times \frac{4}{100} = 0.2036A$$

$$L = \frac{41.3}{2 \times 0.2036 \times 20000} \times 0.8 = 4mH$$

Therefore, looking at both values of the inductors it will be seen that with less value of inductance there is more current ripple. A large value of inductance will reduce the current ripple and discontinuous current mode will be surely avoided. However,, using a high value of inductor will be associated with high inductor resistance, large size and high cost. To improve the efficiency of the converter the resistance of the inductor should be sufficiently small. The inductor selected (B82615B2502M001) was used in the simulation to validate the results of the experimental work; it has a low resistance inductor (r_L) = 0.15 ohm, and inductance value is $(L) = 1\ mH$. Due to component availability, two B82615B2502M001 inductors were connected in series to give a total inquired inductor value ($(L) = 2\ mH$, (r_L) = 0.3Ω).

Determine Output capacitor value

The output filter capacitor is mainly used to meet the output voltage ripple and converter stability requirement. The ripple voltage is related to the capacitance and equivalent series resistance of capacitor. The output capacitor supplies the entire load current during the time when the switch is on. Assuming the equivalent series resistance with capacitor is zero:

$$i_C(t) = C\frac{dV_C}{dt}$$

When the switch is on, the capacitor supplies the load current

$$i_C(t) = -\frac{V_{out}(t)}{R} = C\frac{dV_C(t)}{dt}$$

$$\frac{dV_C(t)}{dt} = -\frac{V_{out}(t)}{RC}$$

When the switch is off

$$i_C(t) = i_L - \frac{V_{out}(t)}{R} = C\frac{dV_C(t)}{dt}$$

$$\frac{dV_C(t)}{dt} = R\, i_L - \frac{V_{out}(t)}{RC}$$

From equation (4.6) the change in capacitor voltage during one cycle can be determined by

$$\Delta V_C = \frac{V_{out}}{RC} t_{on}$$

$$\Delta V_C = 0.24\%,\ \Delta V_{out} = \frac{0.24}{100} \times 203 = 0.48V$$

In this case

$$C = \frac{V_{out}}{2\Delta V_C R}\, t_{on}$$

$$t_{on} = DT = \frac{D}{f}$$

$$C = \frac{203}{2 \times 0.48 \times 195 \times 20000} \times 0.8 \cong 44\mu F$$

If $\Delta V_C = 1\%$

$$\Delta V_C = 1\%\ V_{out} = 203 \times 1\% = 2.5V$$

$$C = \frac{203}{2 \times 2.03 \times 195 \times 20000} \times 0.8 \cong 10\mu F$$

Therefore, it can be seen that with less value of capacitance there is more voltage ripple, a large capacitor will reduce the voltage ripple and help the output stability, however the output voltage will be slow to reach a steady state level. The chosen output capacitor to be used is (EEUED2C220) which has the value 22µF, two of these are connected in parallel to give a total 44µF.

Input capacitor selection

The benefit of inserting this capacitance is to eliminate the undesirable effect of the current harmonics and make the current extracted from the PV module practically constant with a small amount of ripple. The minimum value for the input capacitor is usually given in the data sheet, this minimum value is necessary to stabilize the input voltage due to the peak current requirement of switching power supply. To reduce the capacitor losses, the best

method is to use low equivalent series resistance (ESR) ceramic capacitors. The chosen input capacitor to be used is a (TR3D475M063C0700) ceramic capacitor which has a value of 4.7μF and (ESR = 0.7Ω), two of these are connected in parallel to give a total 9.4μF.

Switching device selection

Choosing the right switch is an important part in power electronic devices, here in the design for the converter the efficiency is important so less power losses is required. IGBT and MOSFET can both be applied as the main switch in the boost converter, but if consideration is given to the main characteristics of the switch, max-current, max-voltage and max-frequency, Mosfet is selected to be used as the main switch in the power conventional boost converter stage because the Mosfet switch has a moderately cost, low switching losses and does not need complex operation requirements. While IGBT switches can be used in a high voltage application because its maximum voltage is 6 kV, there is a wide variety of power Mosfet switches available from various vendors. One can choose the most suitable for the system's needs by looking at the rate of the current and voltage pulse and the safety factor is 30%, also by looking at low losses of Mosfet then $R_{ds(on)}$ must be low enough to minimize conduction loss. The chosen diode is (BYW29EX-200) which was selected to be used for the diode. Also, the power Mosfet switch that is selected to be used is (IPP075N15N3 G) which meets the above-mentioned requirements.

Analysis and loss calculation for conventional boost converter

Calculation of loss analysis is as follows: (assuming the output power of the PV panel with G=1000 w/m² and T= 25 C° this gives maximum power (P_{pv-max}) = 210W, maximum power voltage (v_{pv-max}) = 41.3V and maximum power current (i_{pv-max}) = 5.09A.)

Inductor Loss

The resistance (r_L) of the used inductor $2mH$ is 0.3Ω

Then power losses on the inductor with Δi = 9 % can be calculated as follows:

$i_{L-peak} = i_L + \Delta i_{Lp}$ = 5.09 + 0.4581 = 5.5481A

$P_{loss-L} = (i_{L-peak})^2 \times r_L$ = $(5.5481)^2 \times (0.3)$ = 9.234 W

If it is assumed that the resistance (r_L) of the inductor $4mH$ is 0.6Ω with Δi = 4 %.Then power losses on the inductor can be calculated as follows:

$i_{L-peak} = i_L + \Delta i_{Lp}$ = 5.09 + 0.2036 = 5.2936 A

$P_{loss-L} = (i_{L-peak})^2 \times r_L$ = $(5.2936)^2$ × (0.6) = 18.468 W

Hence, it is demonstrated that with a small inductor value there are lower losses However, a large inductor value gives lower current ripple and vice versa. Therefore, an engineering compromise is necessary.

Mosfet Loss

$$P_{Switc-switching\ loss} = \frac{1}{2} V_o\ i_{in}\left(t_{on} + t_r + t_{off} + t_f\right) f_S$$

$$= \tfrac{1}{2}(203)(5.09)\left((38 + 52 + 69 + 21)(10^{-9})\right).\ 20 \times 10^3 = 1.859 \text{ Watt}$$

$$P_{Switch-conduction\ loss} = r_{ds(on)}.\ D(i_{in})^2$$

$$= (7.3 \times 10^{-3})(0.8)(5.09)^2 = 0.151 \text{ Watt}$$

$$P_{gat-loss} = V_g\ Q_g f_s$$

$$= 20 \times (35 \times 10^{-9}) \times 20 \times 10^3 = 0.014 \text{ Watt}$$

Diode Loss

$$P_{Diode-reverse\ recovery\ loss} = \frac{1}{2} V_{out} i_{RM}\ t_{rr}\ f_s$$

$$= \tfrac{1}{2}(203)(0.2)(25 \times 10^{-9})\ (20 \times 10^3) = 0.01 \text{ Watt}$$

$$P_{Diode-conduction\ loss} = V_F i_F (1 - D)$$

Here the forward current is equal to the maximum inductor current $(I_F = i_L)$

$$P_{Diode-conduction\ loss} = (0.895)(5.09)(1 - 0.8) = 0.911 \text{ Watt}$$

The efficiency of the conventional boost converter with PV panel output power of under G=150 w/m² and T= 25 C° is: (assuming the output power of the PV panel with G=150 w/m² and T= 25 C° this gives maximum power (P_{pv-max}) = 28.5W, maximum power voltage (v_{pv-max}) = 36.7V and maximum power current (i_{pv-max}) = 0.779A.)

$$\eta = \frac{P_{pv-max} - (P_{inductor} + P_{switch} + P_{diode})}{P_{pv-max}} \times 100\%$$

$$\eta = \frac{210 - (9.23 + (1.859 + 0.151 + 0.014) + (0.01 + 0.911))}{210} \times 100\% = 94.2$$

$$P_{out} = \frac{{V_{out}}^2}{R_{Load}}$$

$$V_{out} = \sqrt{28.5 \times 195} \cong 74.5\ volt$$

$$i_{out} = \sqrt{\frac{28.5}{195}} \cong 0.382\ Amps$$

$$D = 1 - \frac{V_{pv-max}}{V_{out}} = 1 - \frac{36.7}{74.5} = 0.5$$

Inductor Loss

The inductor loss, with Δi = 9 %, can be calculated as follows:

$i_{L-peak} = i_L + \Delta i_{Lp}$= 0.779 + (0.07) =0.849 A

$P_{loss-L} = (i_{L-peak})^2 \times r_L$ = $(0.849)^2$ × (0.3) = 0.216 Watt

Mosfet Loss

$$P_{Switch-switching\ loss} = \frac{1}{2} V_o\ i_{in}\left(t_{on} + t_r + t_{off} + t_f\right) f_S$$

$$= \tfrac{1}{2}(74.5)(0.779)\left((38 + 52 + 69 + 21)(10^{-9})\right)20 \times 10^3 = 0.104 \text{ Watt}$$

$$P_{Switch-conduction\ loss} = r_{ds(on)} D (i_{in})^2$$

$$= (7.3 \times 10^{-3})(0.5)(0.779)^2 = 2.214 \times 10^{-3} \text{ Watt}$$

$$P_{gat-loss} = V_g\ Q_g f_s$$

$$= 20 \times (35 \times 10^{-9}) \times 20 \times 10^3 = 0.014 \text{ Watt}$$

Diode Loss

$$P_{Diode-reverse\ recovery\ loss} = \frac{1}{2} V_{out} i_{RM}\ t_{rr}\ f_s$$

$$= \tfrac{1}{2}(74.5)(0.2)(25 \times 10^{-9})(20 \times 10^3) = 3.725 \times 10^{-3} \text{ Watt}$$

$$P_{Diode-conduction\ loss} = V_F i_F (1 - D)$$

Here, the forward current is equal to the maximum inductor current $(I_F = i_L)$

$$P_{Diode-conduction\ loss} = (0.895)(0.779)(1 - 0.5) = 0.348 \text{ Watt}$$

Efficiency of the conventional boost converter with an output power of the PV panel under G=150 w/m² and T= 25 C° is:

$$\eta = \frac{P_{pv-max} - (P_{inductor} + P_{switch} + P_{diode})}{P_{pv-max}} \times 100\%$$

$$\eta = \frac{28.5 - (0.216 + (0.104 + 2.214 \times 10^{-3} + 0.014) + (3.725 \times 10^{-3} + 0.348))}{28.5} \times 100\% = 97.58$$

From this, the power loss and overall efficiency of the conventional boost converter under changeable irradiation conditions is shown in Table 4.1.

Table 4.1: Efficiency and power losses of conventional boost converter

		Inductor losses	switch losses			Diode losses		
Irradiation w/m^2	P_{pv-max} (Watt)	(Watt)	P_{SSloss} (Watt)	P_{SCloss} (Watt)	$P_{gatloss}$ (Watt)	$P_{DS\ loss}$ (Watt)	P_{DCloss} (Watt)	efficiency %
150	28.6	0.216	0.104	2.214×10^{-3}	0.014	3.725×10^{-3}	0.348	97.58
300	59.99	0.855	0.301	5.69×10^{-3}	0.014	5.4×10^{-3}	0.485	97.22
700	145.7	4.664	1.097	0.0363	0.014	8.4×10^{-3}	0.777	95.47
1000	210	9.23	1.859	0.151	0.014	0.01	0.911	94.2

4. 2. Controller design

To operate the Mosfet switch of the conventional boost converter, a Pulse-Width Modulation (PWM) is used as shown in Fig. 4.6. The PWM employs a constant switching time period (i.e. fixed frequency) and adjusts the on period of the switch to control the average output voltage, V_{pv}. The control voltage signal is obtained by the difference between the actual output voltage V_{pv} and its reference voltage V_{ref} value that is calculated by MPPT. The maximum power point tracking (MPPT) algorithm is used to calculate the reference voltage towards which the photovoltaic operating voltage should move next to obtain maximum power point [84], this process is repeated periodically with a slow rate of around 1-10 samples per second.

The instantaneous voltage error between the reference voltage and the measured PV voltage is fed to the Proportional-Integral (PI) controller. The PI controller is tuned using a trial and error tuning method to determine the values of integral time (T_i) and proportional gain (k_p) based on the system transient response characteristics. Using this method, the integral gain is set at 800 and the proportional gain is set at 1 to ensure good dynamic and steady state performance, with acceptable stability margin. The integral gain (k_i) improves the tracking by reducing the error between the actual voltage V_{pv} and the reference voltage V_{ref} that is calculated by the maximum power point tracking controller. In general, the system employs the PI controller towards minimizing the error between the measured voltage and V_{ref} by varying the duty cycle (D) [85]. The PWM frequency is kept constant (20 kHzl. When the amplified error signal, which varies slowly relative to the switching frequency dynamics, is greater than the triangular waveform, the switch control signal becomes higher, causing the switch to turn on, otherwise, the switch is off [80].

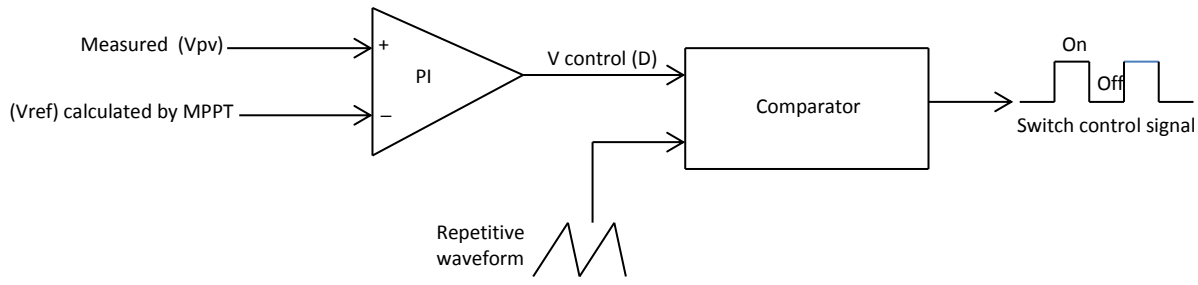

Fig. 4.6, Pulse Width Modulator control for conventional boost converter

4. 3. Results and discussion

To validate the theoretical analysis of the introduced standalone photovoltaic system using a conventional boost converter, a perturb and observe based maximum power point tracking algorithm is used to guarantee maximum PV power is extracted from the panel. Both simulation and experimental systems are developed to evaluate the conventional boost converter with the introduced system. Tests are carried out at several power levels for two possible photovoltaic panels (KD50SE-1P and HIP-210NH1-BO-1; details first presented in Table 3.1) under a variety of atmospheric conditions. Furthermore, the investigation considers the impact of different load levels. In addition, to validate the results, key design constraints and parameters are used on the conventional boost converter in both the software and hardware as shown in Table 4.2. In the following discussion, the results of the simulation using Matlab (Simulink) are shown from Fig. 4.7 to Fig. 4.14, and then the experimental results and discussion are presented in Fig. 4.15 to Fig. 4.23.

Table 4.2: Parameters for conventional boost converter

f = 20 kHz, D=0.1&0.9	Conventional boost converter
Capacitor (Cin)	9.4 μF
Inductors	L1= 2 mH
Frequency	20kHz
Capacitor (Cout)	44μF
Maximum Resistive load	200Ω
Mosfet	IPP075N15N3 G
Diode	BYW29EX-200

4. 3.1. Simulation results and discussion

Here, the conventional boost converter is tested when connected to a resistive load. Two dissimilar power panels are used to supply the DC-DC conventional boost converter; they have different maximum power ratings of 50 Watts and 210 Watts. The corresponding results for load power (output power) and PV power are shown in Figs. 4.8 and 4.11. The following describes these results in more detail.

4.3.1.1. Conventional converter with 50% load under solar panel of 50 Watt

The conventional boost converter, tested with 100 ohm load, and supplied by solar array of rate maximum 50 Watts with changeable atmospheric conditions is shown in Figs 4.7, 4.8 and 4.9. The results show that the conventional converter has a low efficiency of 90% at irradiation of $1000\text{w/m}^2, 25\text{C}^o$ but when the maximum PV power is decreased due to a drop of irradiation, the efficiency of the conventional boost converter rises, as is reaches 95% at an irradiation of $150\text{w/m}^2, 25\text{C}^o$.

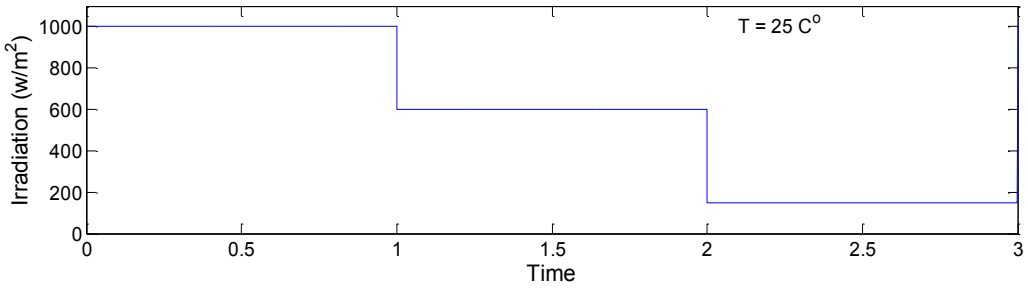

Fig. 4.7, Changeable irradiation over 50 Watt PV panel

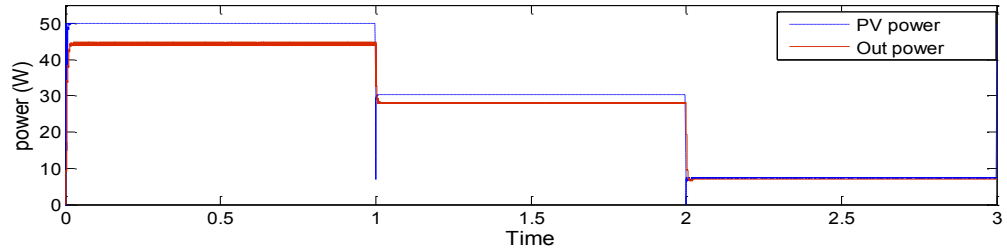

Fig. 4.8, Power of conventional boost converter under changeable irradiation supplying load (100Ω)

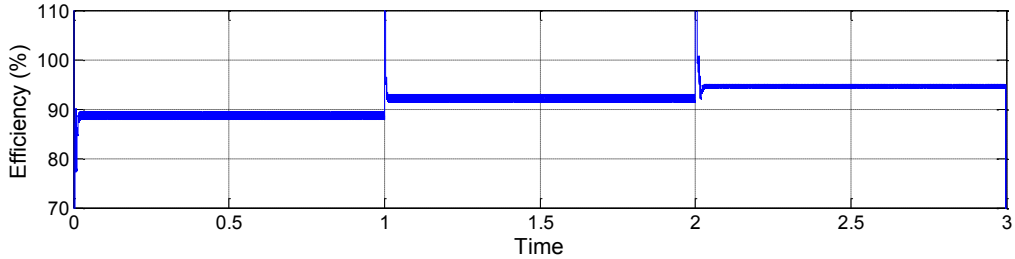

Fig. 4.9, Efficiency of conventional boost converter with load (100Ω) under changeable irradiation conditions

4.3.1.1. Conventional converter with 100% load under solar panel of 210 Watts

The conventional boost converter, tested with load 195 ohm, and supplied by a solar array of maximum 210 Watt rating is shown in Figs 4.10, 4.11 and 4.12. The result figures show that the conventional converter has a high efficiency around 95% at irradiation $200w/m^2, 25C^o$, but when the maximum PV power rises due to a rise in irradiation weather conditions, the efficiency of the conventional boost converter falls, it reaches 91% at irradiation of $1000w/m^2, 25C^o$.

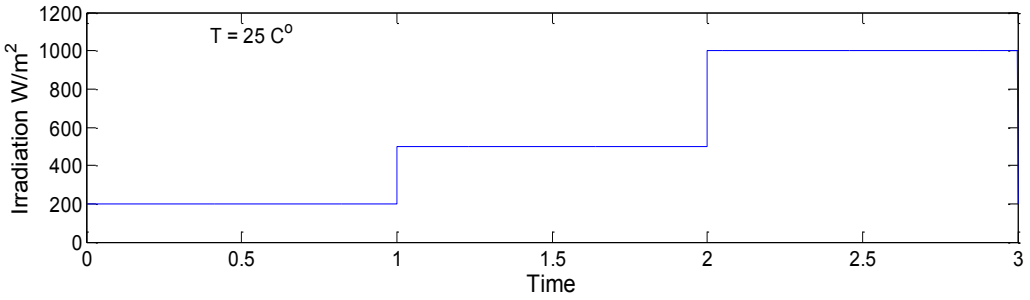

Fig. 4.10, Changeable irradiation over 210 Watt PV panel

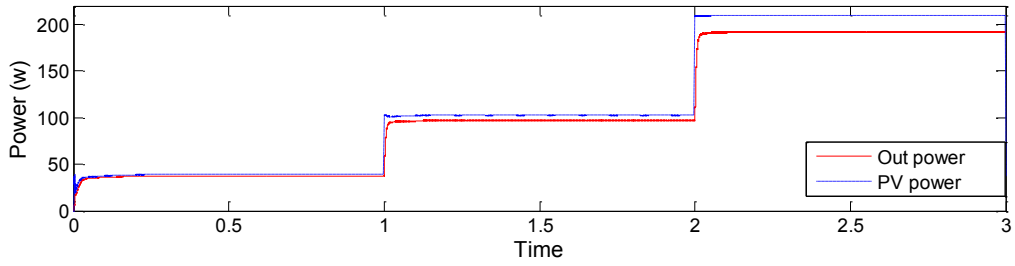

Fig. 4.11, Power of conventional boost converter under changeable irradiation supplying load (195Ω)

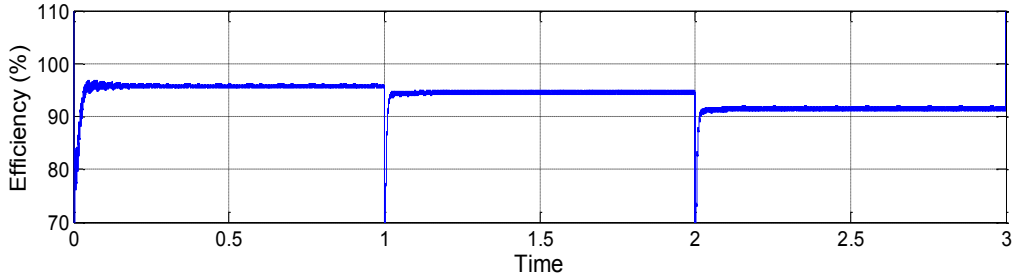

Fig. 4.12, Efficiency of conventional boost converter with load (195Ω) under changeable irradiation conditions

Output power ripple of conventional boost converter:

The output power of the conventional boost converter is obtained under different irradiation conditions. As shown in Fig. 4.13, and Fig. 4.14, the conventional boost converter has about 0.9 W output power ripple under irradiation $500\text{w/m}^2, 25\text{C}^\text{o}$. Also, the conventional boost converter shows an output power ripple of 0.9 W at $100\text{w/m}^2, 25\text{C}^\text{o}$. The conventional boost converter shows low power losses under $100\text{w/m}^2, 25\text{C}^\text{o}$. However, the conventional boost converter shows high power losses over $500\text{w/m}^2, 25\text{C}^\text{o}$. This shows and proves that the conventional boost converter has small power losses at low power levels and large power losses at high power levels.

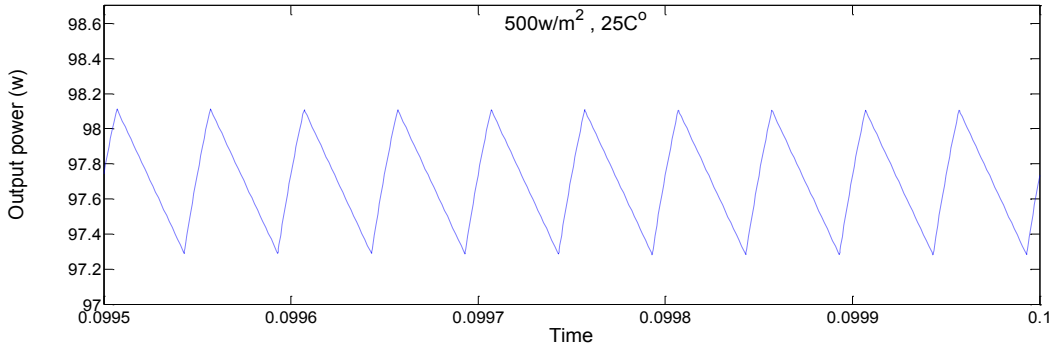

Fig. 4.13, Output power ripple of conventional boost converter under $500\text{w/m}^2,\ 25\text{C}^\text{o}$

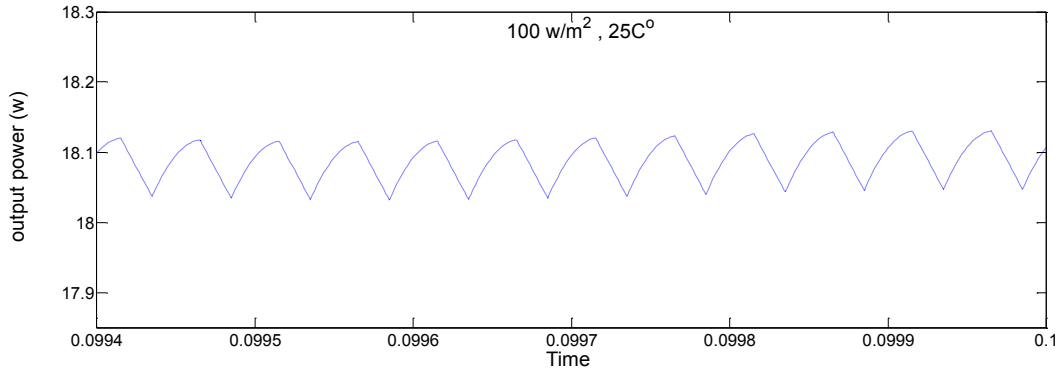

Fig. 4.14 Output power ripple of conventional boost converter under $100\text{w/m}^2,\ 25\text{C}^\text{o}$,

4. 3.2. Experimental results and discussion

The experimental results of the conventional converter supplied with a PV panel of maximum power rating 50 Watts is used to supply the DC-DC conventional boost converter. The solar panel is essentially a current source as the irradiation increases the PV output, the current will be higher and so the PV power is expressed as in equations (4.11, 4.12). The power of the solar array is defined as follows:

$$p_{pv} = i_{pv}\, v_{pv} \tag{4.11}$$

$$p_{pv-max} = i_{pv-max}\, v_{pv-max} \tag{4.12}$$

Output power of load identify as follow

$$p_{out-load} = i_{out-load}\, v_{out-load} \tag{4.13}$$

The efficiency (η) expression as follows:

$$\eta = \frac{P_{pv-max} - (P_{inductor} + P_{switch} + P_{diode})}{P_{pv-max}} \times 100\%$$

$$\eta = \frac{P_{out-(load)}}{P_{pv-max}} \times 100\% \tag{4.14}$$

The pulse width modulation signal to drive the power Mosfet switch is shown in Fig. 4.15 and also shows the inductor current with time on and off time periods using 20 kHz frequency.

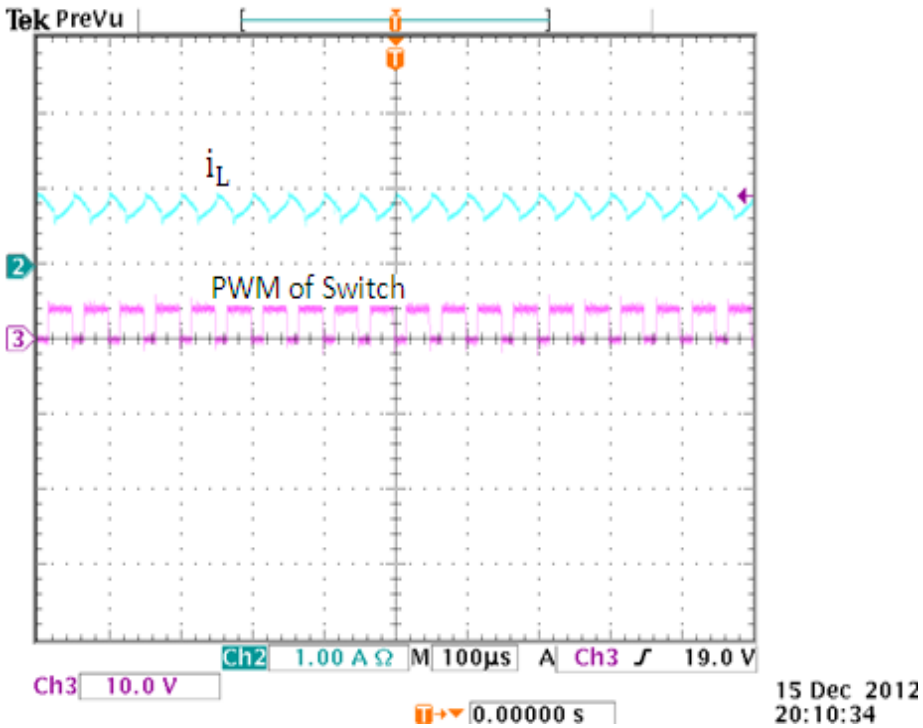

Fig. 4.15, Power Mosfet switching and inductor current in conventional boost converter

The transient response of the conventional boost converter is indicated in Fig. 4.16. As can be seen the conventional boost converter is slow in reaching steady state, and also shows high input current ripple amplitude at maximum PV power and inductor current. The result indicates that the input current ripple amplitude of the conventional boost converter is large and has a low output ripple frequency. The inductor ripple is less than the maximum PV current because of the input capacitor filter used in the converter.

At $150\text{w/m}^2, 25\text{C}^o$, as shown in Fig 4.17, the conventional boost converter displays a maximum PV current of 0.355 Amps [channel 1] and with ripple approximately 0.075 Amps and frequency of 20 KHz, inductor current is 0.310 Amps [channel 3] and clearly remains in continuous conduction mode. The graph also shows a maximum PV voltage of 16.5 Volts [channel 4] with ripple of 0.039 Volts. Fig. 4.18 shows the load characteristics of conventional boost converter at weather condition $150\text{w/m}^2, 25\text{C}^o$, the figure displays the load current is 0.130 Amps [channel 1] with ripple approximate 0.003 Amps, and shows a load voltage is 35.3 Volts with ripple of about 0.09 Volts [channel 4].

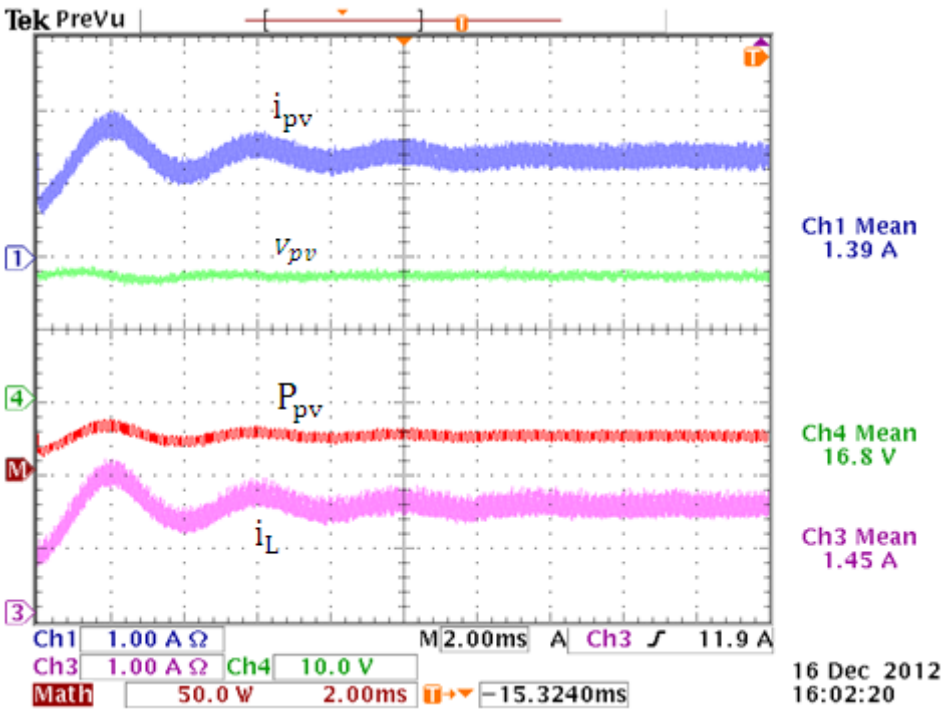

Fig. 4.16, Transient response of conventional boost converter with inductor' current

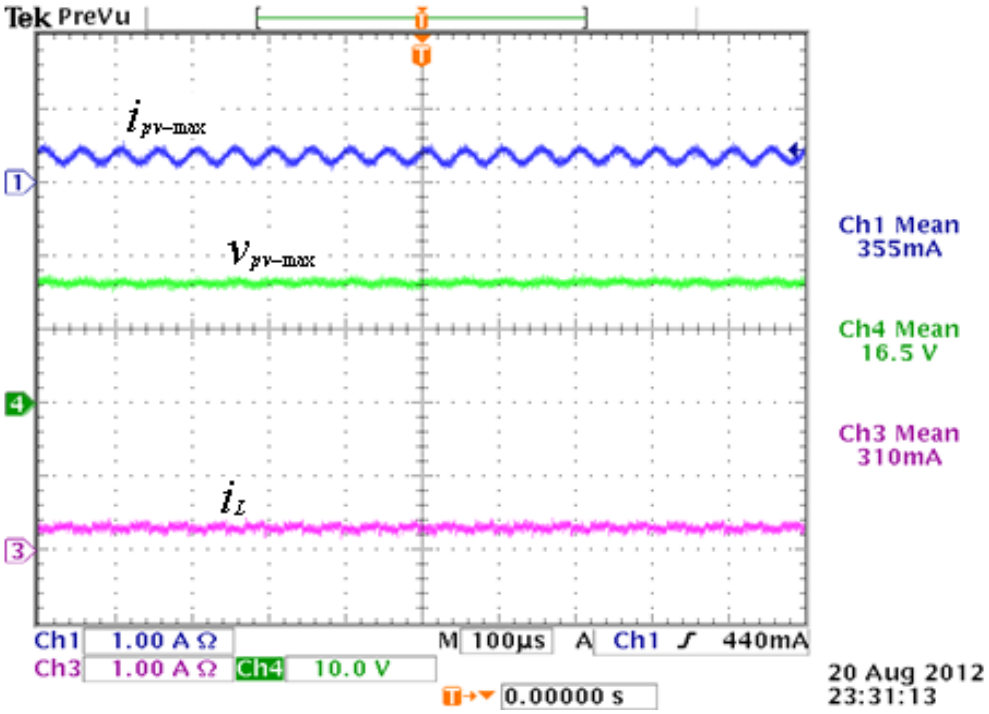

Fig. 4.17, Conventional boost converter with PV power under irradiation=150w/m^2, 25C^o

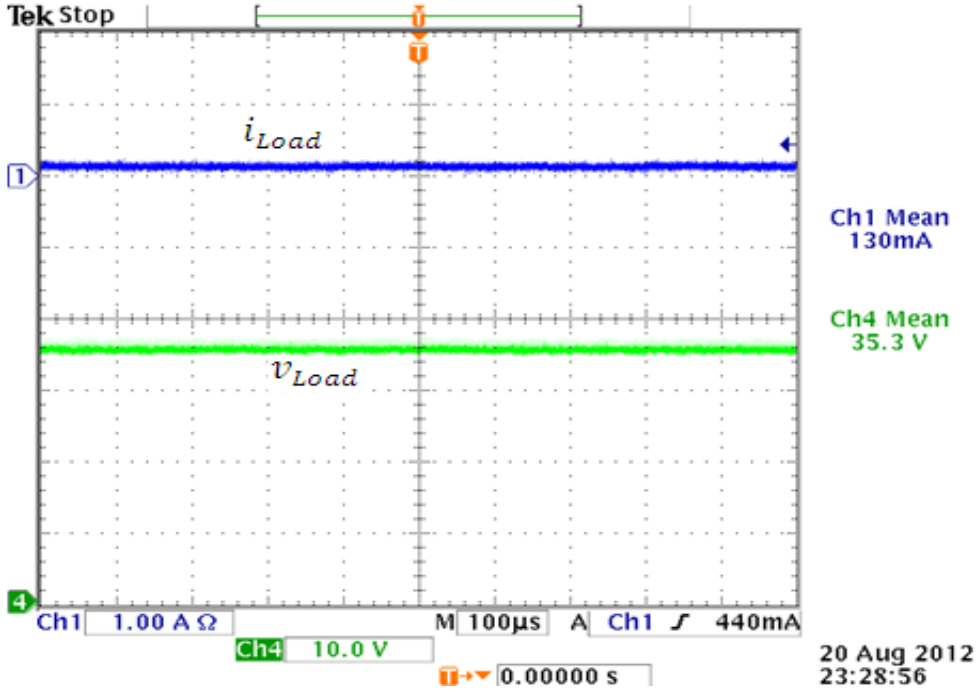

Fig. 4.18, Output current and voltage of conventional boost converter with PV power under irradiation=150w/m^2, 25C^o

The conventional boost converter at 400w/m^2, 25C^o, shown in Fig 4.19, presents a maximum PV current is 1.02 Amps with ripple of approximately 0.1 Amps at 20khz [channel 1], an inductor current is 1.11 Amps [channel 3], and a maximum PV voltage is 17

Volts with ripple approximates 1.5 Volts [channel 4]. Furthermore, Fig. 4.20 shows the load characteristics of the conventional boost converter at 400w/m^2, 25C^o, the graph shows the load current is 0.268 Amps with ripple about 0.006 Amps [channel 1], and shows a load voltage is 59.4 Volts with ripple approximates 0.14 Volts [channel 2].

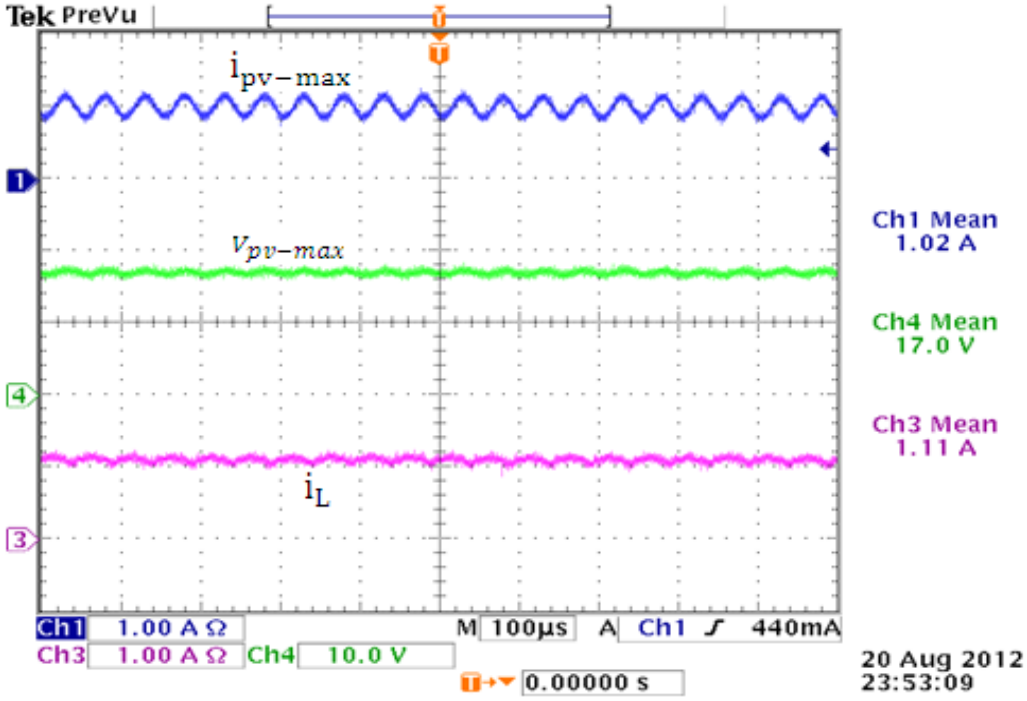

Fig. 4.19, Conventional boost converter with PV power under irradiation = 400w/m^2, 25C^o

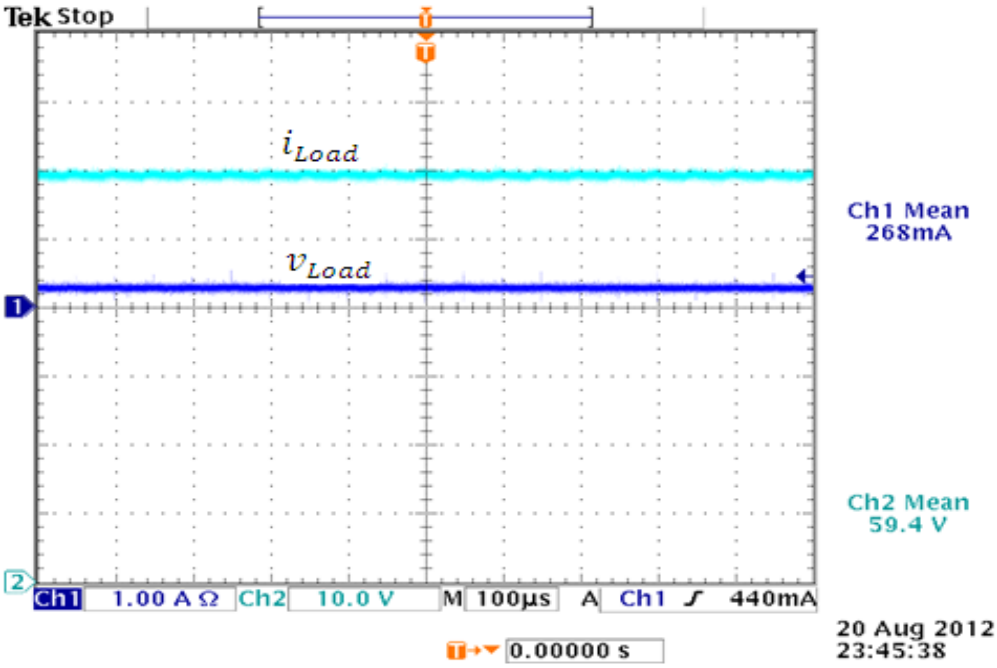

Fig. 4.20, Output current and voltage of conventional boost converter with PV power under irradiation = 400w/m^2, 25C^o

Conventional boost converter at 1000w/m^2, 25C^o , as shown in Fig 4.21, highlights a maximum PV current of 2.83 Amps [channel 1] with ripple approximately 0.45 Amps and frequency of 20 KHz, inductor current is 2.87 Amps [channel 3], a maximum PV voltage is 16.7 Volts [channel 4] with ripple of 1.5 Volts. Furthermore, Fig. 4.22 displays the load characteristics of conventional boost converter at weather condition 1000w/m^2, 25C^o, the figure shows the load current is 0.5 Amps [channel 1] with ripple about 0.0012 Amps, and shows a load voltage is 91.2 Volts [channel 2] with ripple of 0.218 Volts. As can be seen from all waveforms results of conventional boost converter under varied weather condition, the conventional boost converter has high ripple amplitude at the inputs and the outputs.

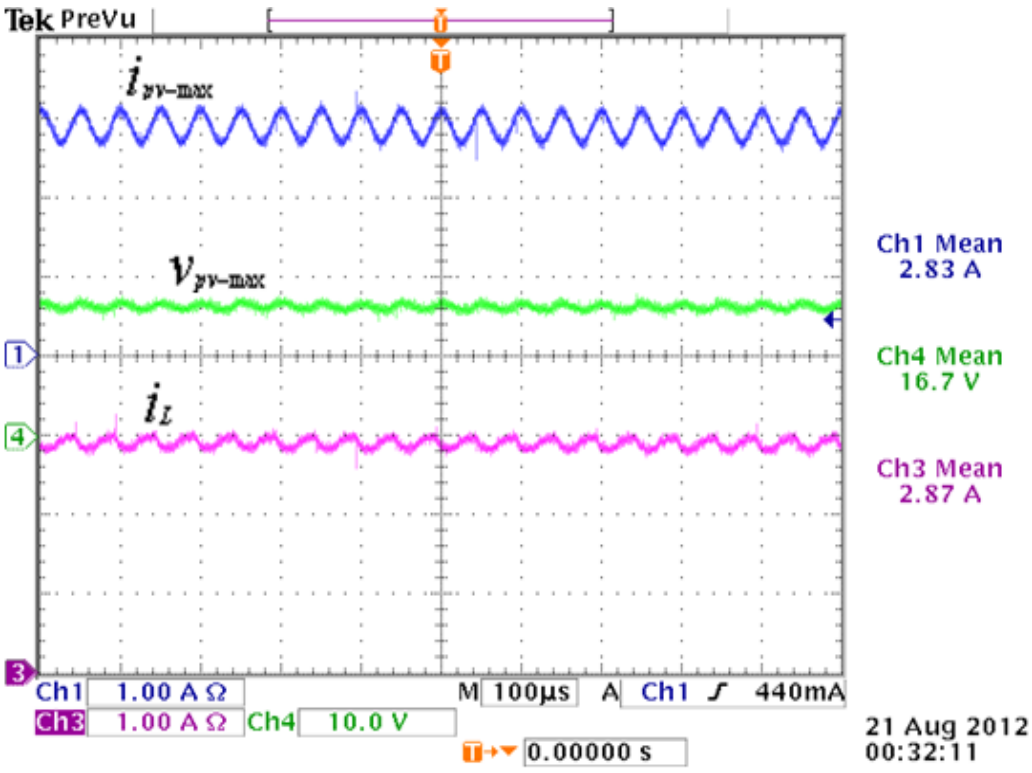

Fig. 4.21, Conventional boost converter with PV power under irradiation = 1000w/m^2, 25C^o

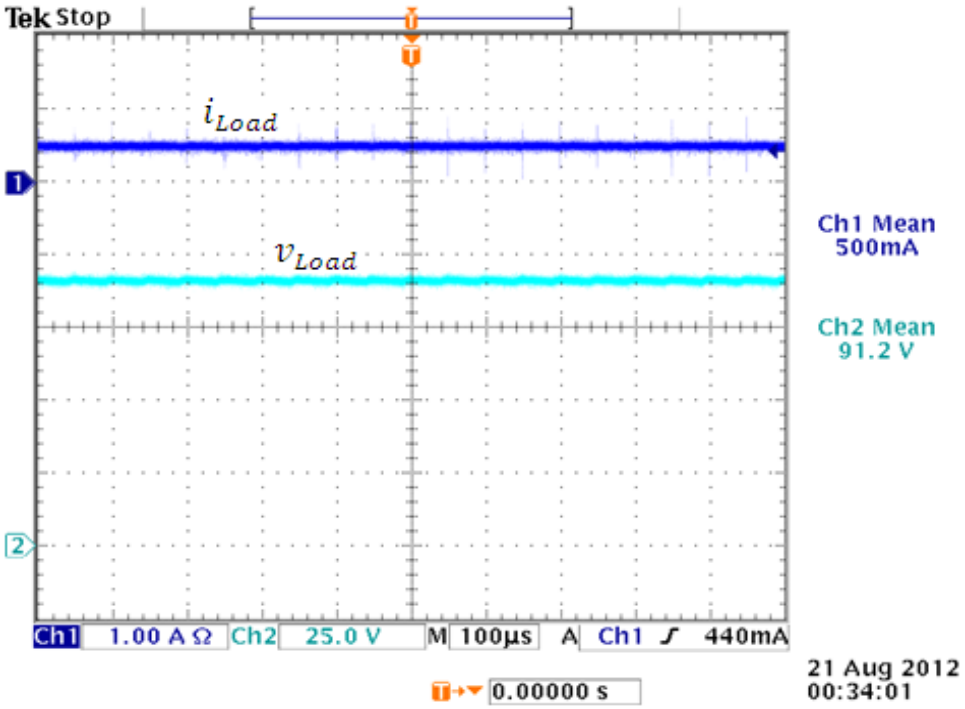

Fig. 4.22, Output current and voltage of conventional boost converter with PV power under irradiation=1000w/m², 25C°

Measured efficiency

Table 4.3: Conventional boost converter measured hardware experiment efficiency

	Conventional boost converter efficiency (%)	
Irradiation (w/m^2)	Load = 195Ω	load = 100Ω
150	91.73	92.66
200	91.98	92.98
300	92.27	92.73
400	92.33	92.53
500	92.19	91.99
600	91.39	91.59
700	90.91	90.85
800	90.34	89.54
900	89.55	89.11
1000	89.08	87.94

Discussion

The experimental efficiency results for the conventional boost converter under various conditions are shown in Fig. 4.23 and table 4.3. The axis (x) represents the maximum PV power that goes up as the irradiation weather rises which is shown on the right axis (y). While the left axis (y) represents the efficiency of the conventional boost converter with different load percentage. The efficiency of the conventional boost converter; with its load of about 100% (195 ohms) and at low irradiation $150w/m^2, 25C^o$ (available PV power of 7 Watts), is 91.73% . At $250w/m^2, 25C^o$ (available PV power of 12 Watts), the efficiency is steady until $550w/m^2, 25C^o$. As the irradiation and maximum PV power continue to rise, the efficiency of the converter starts to decline until it reaches 89.08% at irradiation $1000w/m^2, 25C^o$ (available PV power of 50 Watts). With 50% load (100 ohm), the converter shows a similar trend, the converter shows high efficiency 92.98 % at irradiation $200w/m^2, 25C^o$ with maximum obtainable array power 9.93 Watts. Then, the converter efficiency starts to decrease as the maximum PV power increases. Eventually, when the irradiation is at $1000w/m^2, 25C^o$ available PV power of 50 Watts), the efficiency of the converter is at its lowest level of 87.94%.

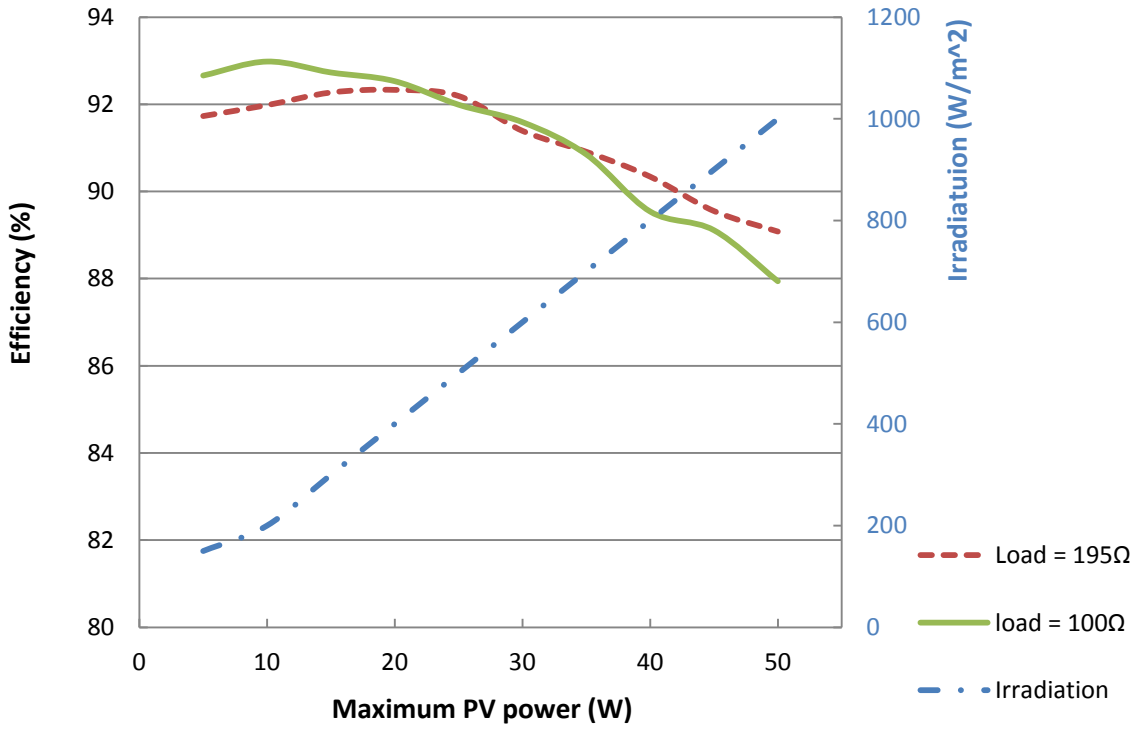

Fig. 4.23, Efficiency results of experiment to conventional boost converter with different load value under irradiation atmosphere condition

4.4. Summary

This chapter has set out to investigate the conventional boost converter stage of the electronic power in standalone PV systems; therefore the simulation and experiment are built to see the performance of a conventional boost converter in a standalone PV system under changeable atmospheric conditions. The performance characteristics of the conventional boost converter are carried out by using the same value of parameters in both tests (simulation and experiment). The switching device, and the diode are chosen after an extensive calculation of key design considerations, particularly, when cost and efficiency are essential factors in any power plant generation.

This study has found, and confirmed that through both simulation and experiment, the conventional boost converter drops in efficiency at a high power of PV panel when there is a higher insolation of weather available. By looking at the I-V characteristics of the solar panel in Chapter one (Fig. 1.2, Fig. 1.4), it can be seen that the current is a major factor of solar energy, so it is expected that the losses will increase as the PV current array climbs due to the rise of insolation, However, the efficiency of the conventional boost converter rises when the power of the PV solar decreases due to a fall of irradiation weather. In the case of a changeable load, the conventional boost converter with different percentages of its resistive load still has low efficiency when receiving a high PV array power and shows high efficiency as the obtained photovoltaic power decreases. Moreover, the study confirming that through the simulation and experimental work, the conventional boost converter shows a high PV power ripple and a high load power ripple.

In discussing the results of the simulation and experiment, a conventional boost converter could be a good choice for a standalone PV system that requires operating in low insolation conditions. Also, a conventional boost converter can be selected if the key consideration is to have a low cost boost converter that is a non-complicated circuit to operate and the efficiency and current ripple are not the main priority.

Chapter Five

5. Interleaved Boost Converter

A two-limb parallel connected conventional boost converter is shown in Fig. 5.1 this is typically called an interleaved boost converter. This converter is used to improve power conversion capability, and one of its applications is to match the photovoltaic system to the load and to operate the solar cell array at maximum power at all insolation [3].

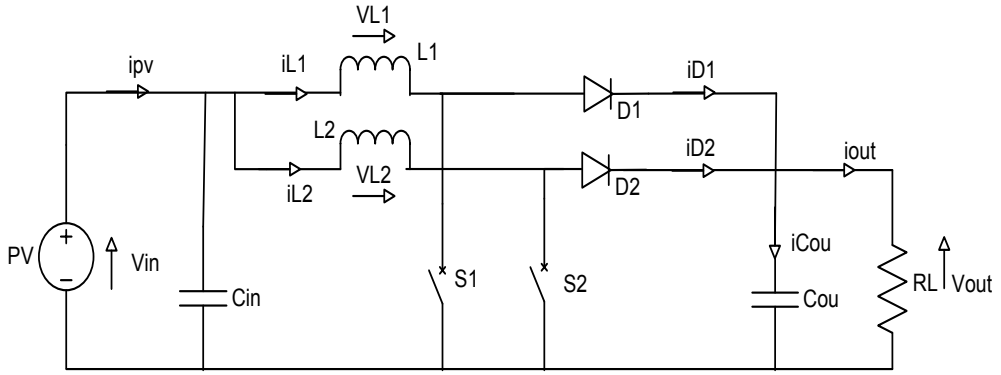

Fig. 5.1, Non-isolated interleaved boost converter

For a step-up application, an equivalent interleaved boost converter offers several advantages over a conventional boost converter; such as a lower current ripple on the input and output stages. Therefore, there is there is the opportunity to minimise the output capacitor filter that is often quite large in the conventional boost [20] [86] [87]. In addition, it effectively increases the switching frequency without increasing the switches losses. Furthermore, it provides a fast transient response to load changes and improves power handling capabilities. A higher efficiency may be realized by splitting the input current into two paths, substantially reducing i^2R losses and inductor AC losses. This also gives low stresses on components due to the current split which increases the power processing capability [9], [22], [23]. However, using an interleaved converter increases the number of power handling components and circuit complexity which may lead to an increase in cost. However, in renewable energy systems, long-term improved power generation can help to offset this disadvantage [9]. The topology of the interleaved boost converter consists of two limbs operating at 180 degrees out of phase from each other. Typically, each branch operates in the same fashion as a conventional boost converter previously described in Chapter four. When S1 turns on, the current ramps up in L1 with a slope depending on the input voltage storing energy in L1, D1 is off during this time since the output voltage is greater than the input voltage. When S2 turns off, the L2 inductor delivers part of its stored energy to the

output capacitor and the load, the current in L2 ramps down with a slope dependent on the difference between the input and output voltage. One half of a switching period later, S2 also turns on, completing the same cycle of events.

Continuous conduction mode

For analysis, assuming the interleaved converter is operating with 50% of duty ratio in a continuous current mode (CCM) the inductor currents (L1 and L2) never fall to zero within a switching cycle as shown in Fig. 5.2

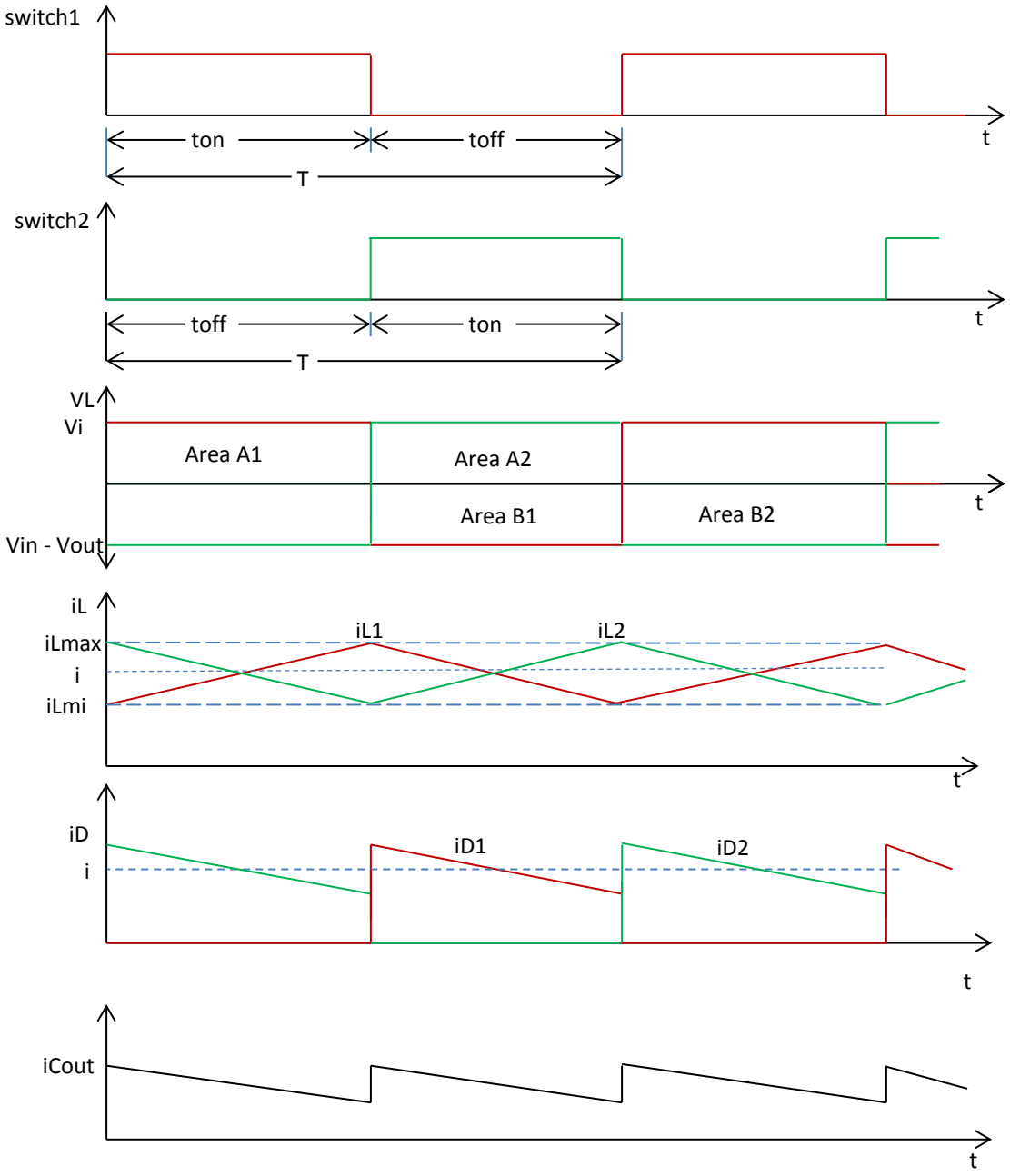

Fig. 5.2, Interleaved boost converter waveforms at continuous conduction mode

The equation below is derived to confirm that with duty ratio $D_1 = D_2 = D$, the same expression that is obtained with a conventional boost converter in CCM is achieved.

Considering figure 5.2, when Area $A_2 = \text{area } B_1$, and if the switching on time is $t_{on} = DT$ and the switching off time is $t_{off} = (1 - D)T$, then;

$$V_{in}D_2T = (V_{in} - V_{out})(1 - D_1)T$$

$$V_{in}D_2 = V_{in} - V_{out} - V_{in}D_1 + V_{out}D_1$$

$$V_{out} - V_{out}D_1 = V_{in} - V_{in}D_2 - V_{in}D_1$$

$$V_{out}(1 - D_1) = V_{in}(1 - D_2 - D_1)$$

And then

$$\frac{V_{out}}{V_{in}} = \frac{(1 - D_2 - D_1)}{(1 - D_1)}$$

Here if

$$D_1 = D_2 = D$$

Then

$$V_{out} = \frac{V_{in}}{(1 - D)}$$

Discontinuous conduction mode

Waveforms for the DCM interleaved boost converter are shown in Fig. 5.3. Here, the inductor current waveforms are phase delayed by 180^o from each other and assumed to be operating with 50% duty ratio.

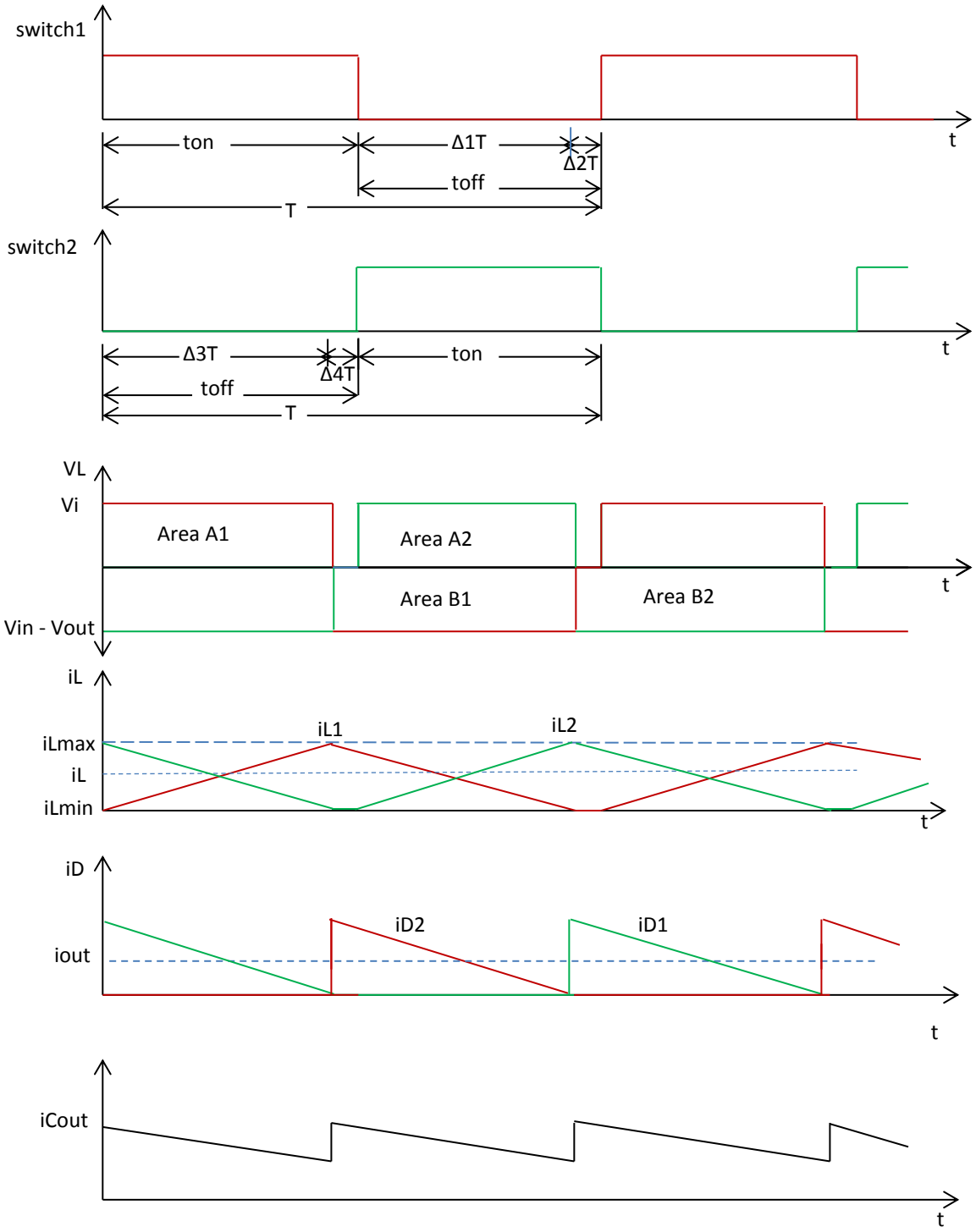

Fig. 5.3, Step-up interleaved boost converter wave forms at discontinuous condition mode

From Fig.5.3, it is possible to consider the discontinuous conduction mode analysis. In the following, D_1 is the duty ratio of switch one, V_{out} is the output voltage, D_2 is the duty ratio of switch two, V_{in} is the input voltage, L_1 is the inductor one, L_2 is the inductor two, i_{out} is the load current.

For switch one:

$t_{on} = D_1 T$, and $\mathrm{t_{off}} = \Delta_1 \mathrm{T} + \Delta_2 \mathrm{T}$

When switch one is turned on

$$V_{L1} = L_1 \frac{di}{dt}$$

$$V_{in} = L_1 \frac{i_{L1-max}}{D_1 T} \quad (5.1)$$

When switch one is turned off i_{L1} falls to zero

$$V_{L1} = L_1 \frac{di}{dt}$$

$$V_{in} - V_{out} = L_1 \frac{i_{L1-\max}}{\Delta_1 T} \quad (5.2)$$

From equation 5.1

$$i_{L1-max} = \frac{V_{in} D_1 T}{L_1}$$

From equation 5.2

$$i_{L1-max} = \frac{(V_{out} - V_{in})\Delta_1 T}{L_1}$$

$$\therefore \frac{V_{in} D_1 T}{L_1} = \frac{(V_{out} - V_{in})\Delta_1 T}{L_1}$$

$$\therefore \Delta_1 T = \frac{V_{in} D_1 T}{V_{out} - V_{in}} \quad (5.3)$$

For switch two:

$t_{on} = D_2 T$, and $\mathrm{t_{off}} = \Delta_3 \mathrm{T} + \Delta_4 \mathrm{T}$

When switch two is turned on

$$V_{in} = L_2 \frac{i_{L2-max}}{D_2 T} \quad (5.4)$$

When switch one is turned off i_{L2} falls to zero

$$V_{in} - V_{out} = L_2 \frac{i_{L2-\max}}{\Delta_3 T} \tag{5.5}$$

$$\therefore \frac{V_{in} D_2 T}{L_2} = \frac{(V_{out} - V_{in})\Delta_3 T}{L_2}$$

$$\therefore \Delta_3 T = \frac{V_{in} D_2 T}{V_{out} - V_{in}} \tag{5.6}$$

From equations (5.1), (5.3), (5.4) and (5.6), the load output current (i_{out}) is the average value of the total diodes current

$$\therefore i_{out} = \Delta_1 T \frac{i_{L1-max}}{4T} + \Delta_3 T \frac{i_{L2-max}}{4T}$$

$$i_{out} = \frac{1}{4L_1 T} . \frac{(D_1 T V_{in})^2}{(V_{out} - V_{in})} + \frac{1}{4L_2 T} . \frac{(D_2 T V_{in})^2}{(V_{out} - V_{in})}$$

$$(V_{out} - V_{in}) = \frac{1}{4L_1 T} . \frac{(D_1 T V_{in})^2}{i_{out}} + \frac{1}{4L_2 T} . \frac{(D_2 T V_{in})^2}{i_{out}}$$

If $D_1 = D_2 = D$, and $L_1 = L_2 = L$

$$\therefore (V_{out} - V_{in}) = \frac{(DTV_{in})^2}{4LTi_{out}} + \frac{(DTV_{in})^2}{4LTi_{out}}$$

$$(V_{out} - V_{in}) = \frac{2(DTV_{in})^2}{4LTi_{out}}$$

$$V_{out} = V_{in} + \frac{(DTV_{in})^2}{2LTi_{out}}$$

$$\therefore \frac{V_{out}}{V_{in}} = 1 + \frac{D^2 V_{in} T}{2Li_{out}}$$

In discontinuous conduction mode the voltage transfer function is not a simple function of duty ratio, it depends upon the size of the inductor, output current and switching frequency as the expression showing on a conventional boost converter at discontinuous current mode.

5.1. Design of interleaved boost converter

The interleaved boost converter circuit is shown in Fig. 5.4, this part is provided to design and determine the elements and parameters of the circuit based on frequency switches operation and on energy from a photovoltaic source as follows.

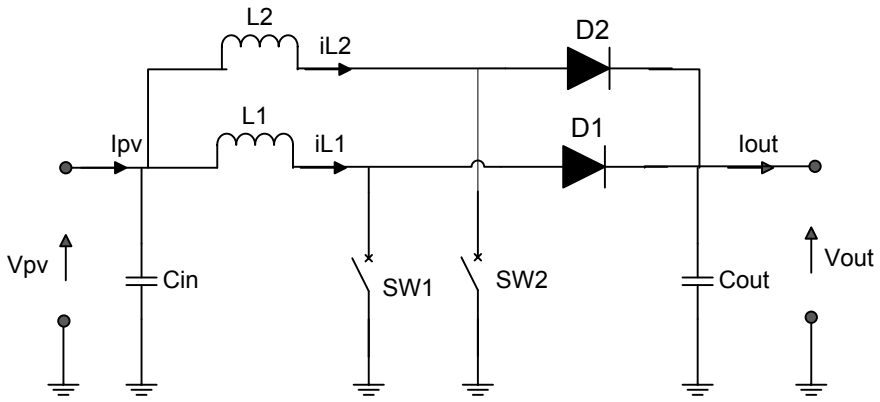

Fig. 5.4, Structure of interleaved boost converter

In designing an interleaved boost converter, a typical constraint is the maximum output ripple. Once the frequency, input voltage, and output voltage are defined, this ripple is directly related to the inductor value. The design specifications and procedure are the same as the conventional boost converter presented in Chapter four. The following parameters are also needed: The photovoltaic voltage V_{pv} is the input voltage of the converter range: $V_{in(\min)}$ = 0 V, and $V_{in(max)}$= 41.3V. Assumption of efficiency is 100 %, maximum resistive load: R_{Load} = 195 ohm, switch frequency of the converter: f = 20 kHz, estimated photovoltaic current ripple Δi_{pv} which is the input current of the converter: Δi_{in} = 9%, estimated output voltage ripple: ΔV_{out}= 0.24%.

Inductor selection

The input current is the sum of the two inductor currents as the inductor's ripple current are 180^{o} out of phase, they cancel each other out and reduce the input current ripple that the boost inductors cause. However, the interleaved boost converter has the same input current ripple requirement as the conventional boost converter, each inductor of the interleaved boost converter carries half of the input current. From equation 4.9

$$D = 1 - \frac{V_{pv-max}}{V_{out}} = 1 - \frac{41.3}{203} = 0.8$$

$$i_{pv-max} = i_{in} = i_{L1} + i_{L2} = 5.09 \text{ A}$$

$$i_{L1} = i_{L2} = \frac{i_{pv-max}}{2} = \frac{i_{in}}{2} = \frac{5.09}{2} = 2.545A$$

If Δi = 9%, then the inductor ripple current is:

$$\Delta i_{Lp} = 9\%\ i_L = 5.09 \times \frac{9}{100} = 0.4581A$$

The peak-to-peak current ripple is:

$$\Delta i_{Lp-p} = 2\Delta i_L = 0.9162\ \text{A}$$

Then using equation 4.10 :

$$L_1 = L_2 = \frac{L_{conv}}{2} = \frac{V_{in}-V_d}{2\Delta i_{Lp-p}} DT = \frac{41.3}{2 \times 0.9162 \times 20000} \times 0.8 \cong 1mH$$

The inductor (B82615B2502M001) which is selected for use in the simulation software and in experiment has a low resistance inductor (r_L) = 0.15 ohm and the inductor value is (L) = 1 mH.

Selection of output and input capacitors

Since the desired output voltage ripple (ΔV = 0.24%) of the interleaved boost converter is the same as the conventional boost converter, from the calculation the capacitors have the same value gained in the conventional boost converter. Therefore, the same chosen output capacitor is used (EEUED2C220) and has the value 22μF. Two of them connected in parallel give a total output capacitor of 44μF. Also the same chosen input capacitor is used (TR3D475M063C0700) and has a value 4.7μF and ESR = 0.7Ω; two of these connected in parallel give a total of 9.4μF.

Selection of switching devices and diodes

Because the interleaved boost converter consists of two phases which require two inductors, two power Mosfets switches and two diodes are required. These extra components will increase cost but will share current which results in a low amplitude ripple and reduced losses. The specification of switching devices and diodes will be the same as that used in the

conventional boost converter. The power Mosfet switch that is selected for use is the same for switch one and switch two (IPP075N15N3 G). The chosen diode is (BYW29EX-200).

Analysis and loss calculation for the interleaved boost converter

Calculation of loss analysis is as follows: When the output power of the PV panel with G=1000 w/m² and T= 25 C° this gives maximum power (P_{pv-max}) = 210W, maximum power voltage (v_{pv-max}) = 41.3V and maximum power current (i_{pv-max}) = 5.09A.

Inductor losses:

$$r_{L1} = r_{L2} = \frac{r_{L-conv}}{2} = \frac{0.3}{2} = 0.15\Omega$$

$$P_{inductor\ copper\ loss} = \left(\frac{i_{PV}}{N_{numb.\ of\ phases}}\right)^2 . r_{resi.of\ inductor} \quad (5.7)$$

$$i_{L1-peak} = i_{L1} + \Delta i_{L1} = 2.545 + (2.545\times(9/100)) = 2.77405A$$

$$P_{loss-L1} = (i_{L1-peak})^2 \times r_{L1} = (2.77405)^2 \times 0.15 = 1.1543W$$

$$i_{L2-peak} = i_{L2} + \Delta i_{L2} = 2.545 + 0.22905 = 2.77405A$$

$$P_{loss-L2} = (i_{L2-peak})^2 \times r_{L2} = (2.77405)^2 \times 0.15 = 1.1543W$$

Overall inductor loss for the interleaved boost converter is as follows

$$P_{loss-Lw} = P_{loss-L1} + P_{loss-L2} = 1.1543 + 1.1543 = 2.3086\ W$$

As can be seen, these are lower losses compared to the previously calculated inductor loss for the conventional boost converter.

Mosfet Losses:

$$P_{Switch-switching\ loss}$$

$$= 2\frac{1}{2}V_o\frac{i_{in}}{2}(t_{on} + t_r + t_{off} + t_f)f_S$$

$$= \frac{1}{2}V_o\, i_{in}(t_{on} + t_r + t_{off} + t_f)f_S$$

$$= \frac{1}{2}(203)(5.09)\left((38 + 52 + 69 + 21)(10^{-9})\right)20 \times 10^3 = 1.859\ \text{Watt}$$

$$P_{Switch-conduction\ loss} = 2\left(r_{ds(on)}D\right)\left(\frac{i_{in}}{2}\right)^2$$

$$= 2(7.3 \times 10^{-3})(0.8)(5.09/2)^2 = 0.0756 \text{ Watt}$$

$$P_{gat-loss}2 = 2V_g\ Q_g f_s$$

$$= 2 \times 20 \times (35 \times 10^{-9}) \times 20 \times 10^3 = 0.028 \text{ Watt}$$

Diodes losses:

$$P_{Diode-reverse\ recovery\ loss} = 2\frac{1}{2}V_{out}(i_{RM})t_{rr}f_s$$

$$= (203)(0.2)(25 \times 10^{-9})(20 \times 10^3) = 0.0203 \text{ Watt}$$

$$P_{Diode-conduction\ loss} = (2)V_F\frac{i_F}{2}(1 - \mathrm{D})$$

Here the forward current is equal to the inductor current $(I_F = i_L)$

Then, $P_{Diode-conduction\ loss} = 2 \times (0.895)(5.09/2)(1 - 0.8) = 0.911$ Watt

Efficiency of an interleaved boost converter at G=1000 w/m² and T= 25 C° is illustrated below:

$$\eta = \frac{P_{pv-max} - (P_{inductor} + P_{switch} + P_{diode})}{P_{pv-max}} \times 100\%$$

$$\eta = \frac{210 - (2.308 + (1.859 + 0.0756 + 0.028) + (0.0203 + 0.911))}{210} \times 100\% = 97.52$$

Loss analysis is as follows: When the output power of the PV panel with G=150 w/m² and T=25C°, this gives maximum power (P_{pv-max}) = 28.5W, maximum power voltage (v_{pv-max}) =36.7V, and maximum power current (i_{pv-max}) = 0.779A. Moreover, with the assumption that efficiency is 100% then the output power is equal to the input power. The analysis considers the output voltage of the converter when the PV panel operates with G=150 w/m²:

$$P_{out} = \frac{{V_{out}}^2}{R_{Load}}$$

$$V_{out} = \sqrt{28.5 \times 195} \cong 74.5\ volt$$

$$i_{out} = \sqrt{\frac{28.5}{195}} \cong 0.382\ Amps$$

$$D = 1 - \frac{V_{pv-max}}{V_{out}} = 1 - \frac{36.7}{74.5} = 0.5$$

Inductor losses:

Then power losses in the inductor with $\Delta i = 9$ % can be calculated as follows:

$$i_{L1} = i_{L2} = \frac{i_{pv-max}}{2} = \frac{i_{in}}{2} = \frac{0.779}{2} = 0.389A$$

$$i_{L1-peak} = i_{L1} + \Delta i_{L1} = 0.389 + (0.389 \times (9/100)) = 0.424A$$

$$P_{loss-L1} = (i_{L1-peak})^2 \times r_{L1} = (0.424)^2 \times 0.15 = 0.0269W$$

$$i_{L2-peak} = i_{L2} + \Delta i_{L2} = 0.389 + 0.035 = 0.424A$$

$$P_{loss-L2} = (i_{L2-peak})^2 \times r_{L2} = (0.424)^2 \times 0.15 = 0.0269W$$

Whole losses on inductors of the interleaved boost converter are as follows:

$$P_{loss-Lw} = P_{loss-L1} + P_{loss-L2} = 0.0269 + 0.0269 = 0.0538 \text{ W}$$

Mosfet Losses:

$$P_{Switc-switching\ loss} = 2\frac{1}{2}V_o\left(\frac{i_{in}}{2}\right)\left(t_{on} + t_r + t_{off} + t_f\right)f_S$$

$$= \frac{1}{2}(74.5)(0.779)\left((38 + 52 + 69 + 21)(10^{-9})\right) \times 20 \times 10^3 = 0.104 \text{ Watt}$$

$$P_{Switch-conduction\ loss} = 2(r_{ds(on)}D)\left(\frac{i_{in}}{2}\right)^2$$

$$= 2(7.3 \times 10^{-3})(0.5)\left(\frac{0.779}{2}\right)^2 = 1.107 \times 10^{-3} \text{ Watt}$$

$$P_{gat-loss} = 2V_g\ Q_g f_s$$

$$= 2 \times 20 \times (35 \times 10^{-9}) \times 20 \times 10^3 = 0.028 \text{ Watt}$$

Diodes losses:

$$P_{Diode-reverse\ recovery\ loss} = 2\frac{1}{2}V_{out} i_{RM}\ t_{rr}\ f_s$$

$$= (74.5)(0.2)(25 \times 10^{-9})\ (20 \times 10^3) = 7.45 \times 10^{-3} \text{ Watt}$$

$$P_{Diode-conduction\ loss} = 2V_F\frac{i_F}{2}(1 - D)$$

Here the forward current is equal to the maximum inductor current $(I_F = i_L)$

$$P_{Diode-conduction\ loss} = 2(0.895)(0.779/2)(1-0.5) = 0.348 \text{ Watt}$$

Efficiency of the interleaved boost converter with PV panel output power of G=150 w/m² and T= 25 C˚ is:

$$\eta = \frac{P_{pv-max} - (P_{inductor} + P_{switch} + P_{diode})}{P_{pv-max}} \times 100\%$$

$$\eta = \frac{28.5 - \left(0.053 + (0.104 + 1.107 \times 10^{-3} + 0.028) + (7.45 \times 10^{-3} + 0.348)\right)}{28.5} \times 100\% = 98\%$$

Using a similar approach, the power loss and efficiency of the interleaved boost converter under various irradiation conditions is shown in Table 5.1:

Table 5.1: Efficiency and power losses of interleaved boost converter power

		Inductor losses	switch losses			Diode losses		
Irradiation w/m^2	P_{pv-max} (Watt)	(Watt)	P_{SSloss} (Watt)	P_{SCloss} (Watt)	$P_{gatloss}$ (Watt)	$P_{DS\ loss}$ (Watt)	P_{DCloss} (Watt)	efficiency %
150	28.5	0.053	0.104	1.107×10^{-3}	0.028	7.45×10^{-3}	0.348	98
300	59.99	0.214	0.301	5.69×10^{-3}	0.028	0.0108	0.485	98.2
700	145.7	1.164	1.097	0.0363	0.028	0.0168	0.777	97.85
1000	210	2.308	1.859	0.0756	0.028	0.0203	0.911	97.52

For completeness, the power loss and efficiency of the interleaved boost converter at low irradiation conditions, when operating in discontinuous current mode, is shown in Table 5.2. In discontinuous current mode, the peak and RMS value of the current are high [88] [89]. For the reasons outlined earlier, this results in the Mosfet losses dominating [90]. In calculating the data in Table 5.2, at low irradiation, the current has been divided by two as the RMS and peak current are expected to be higher when it operates in discontinuous current mode.

Table 5.2: Efficiency and power losses of interleaved boost converter considering DCM

		Inductor losses	switch losses			Diode losses		
Irradiation w/m^2	P_{pv-max} (Watt)	(Watt)	P_{SSloss} (Watt)	P_{SCloss} (Watt)	$P_{gatloss}$ (Watt)	$P_{DS\ loss}$ (Watt)	P_{DCloss} (Watt)	efficiency %
150	28.5	0.053	0.208	4.428×10^{-3}	0.028	7.45×10^{-3}	0.696	96.5
300	59.99	0.214	0.602	11.38×10^{-3}	0.028	0.0216	0.97	96.9
700	145.7	1.164	1.097	0.0363	0.028	0.0168	0.777	97.85
1000	210	2.308	1.859	0.0756	0.028	0.0203	0.911	97.52

5. 2. Controller design

The generation of two interleaved duty ratio commands is accomplished using two PWM units which are controlled by a two bit shift register [91]. This register sequentially resets each pulse width modulation ramp and corresponding output key, resulting in a phase delay between PWM signals of $2\pi/2$ as shown in Fig. 5.5. The two PWMs employ constant frequency and control the turning on period of the switches to control the average output voltage V_{pv}. Constant switching time period: $T = \mathrm{t}_{\mathrm{on}} + \mathrm{t}_{\mathrm{off}}$

The signal of the control voltage is obtained by the difference between the actual output voltage V_{pv} and its reference voltage V_{ref} value that is calculated by MPPT. The maximum power point tracking (MPPT) algorithm is used to calculate the reference voltage towards which the photovoltaic operating voltage should move next to obtain a maximum power point [84], this process is repeated periodically with a slow rate of around 1-10 samples per second.

The instantaneous voltage error between the V_{ref} and measured PV voltage is fed to the proportional-integral (PI) controller. The PI controller is tuned using a trial and error tuning method for determining the values of integral time (T_i) and proportional gain (k_p) . Using this method, the integral gain is set at 800 and the proportional gain is set at 1 to ensure a fast stability rate. The integral gain (k_i) improves the tracking by reducing the error between the actual voltage V_{pv} and the reference voltage V_{ref} that is calculated by the maximum power point tracking control. In general, the system employs the PI controller towards minimizing the error between the measured voltage and V_{ref} by varying the duty cycle (D1 and D2) [85]. The frequency is kept constant (20 kHz) in both a pulse-width modulation (PWM) control and is chosen not to be low to avoid high noise and not high to evade the high switching losses. When the amplified error signal, which varies slowly with time relative to the switching frequency, is greater than the triangular waveform, the switch control signal becomes higher, causing the switch to turn on, otherwise, the switch is off [80]. Controlling Mosfet switches in the interleaved boost converter can be operated by pulses shown in Fig. 5.6 with 20 kHz frequency and delay between the two PWM signals is 180^{o}.

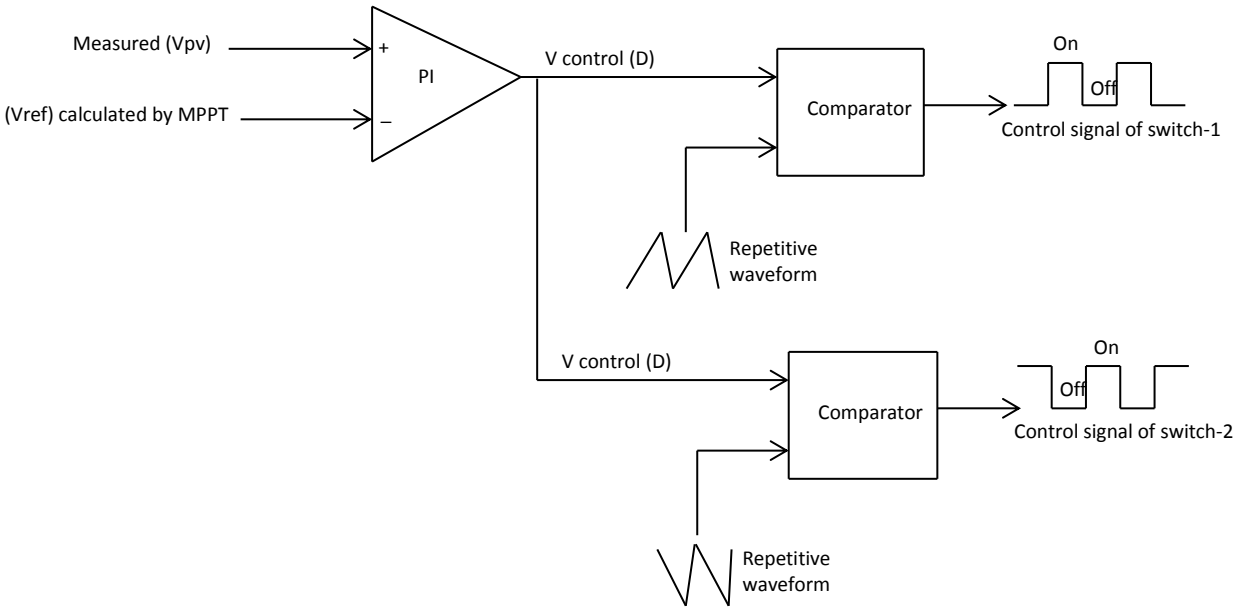

Fig. 5.5, Pulse Width Modulator control for interleaved boost converter

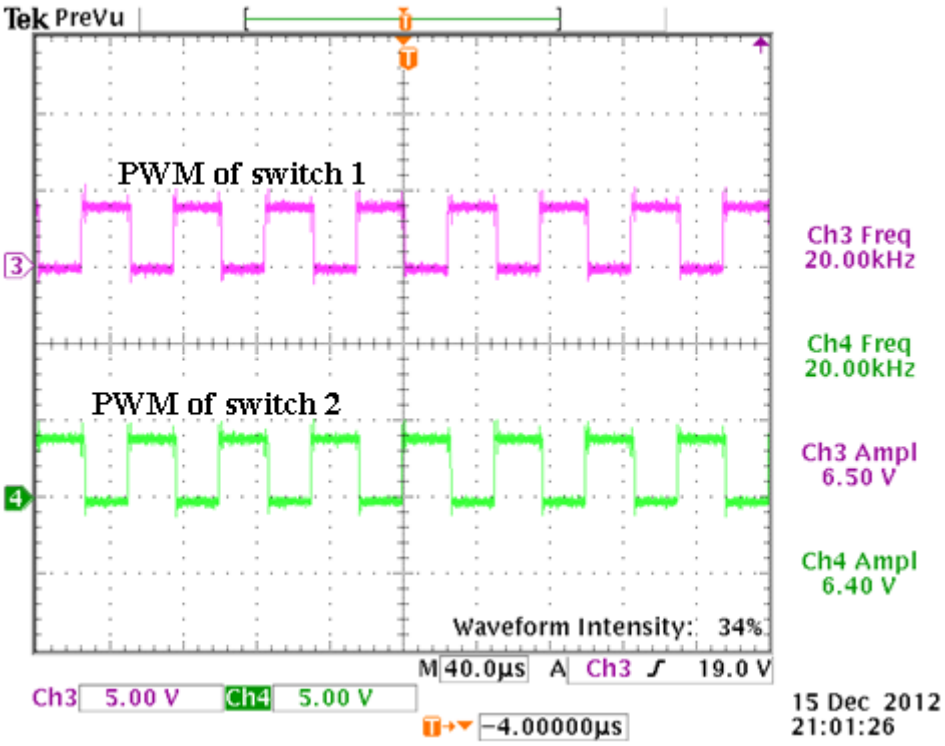

Fig. 5.6, Hardware pulses of the switches of interleaved boost converter with shift 180^{o}

5. 3. Results and discussion

The simulation and experimental set up of the interleaved boost converter is used to validate the theoretical analysis of the introduced standalone photovoltaic system using the power stage of an interleaved boost converter. A perturb and observe MPPT algorithm is used to guarantee the maximum power of the PV panel engaged to the converter. The simulation and experimental are built to evaluate the interleaved boost converter with the introduced system; tests are carried out with two different power level photovoltaic panels (HIP-210NH1-BO-1) and (KD50SE-1P) under a variety of atmospheric conditions (details in Table 3.1). Also, the tests are run with different loading. In addition, to validate the results, similar considered key design constraints and parameters are used on the interleaved boost converter in both the software and hardware as shown in Table 5.3.

Table 5.3: Parameters for interleaved boost converter

f = 20 kHz D = 0.1- 0.9	Interleaved boost converter
Capacitor (Cin)	9.4 μF
Inductors	L1= 1 mH
	L2=1 mH
Frequency	20kHz
Capacitor (Cout)	44 μF
Resistive load	100 & 195Ω
Mosfets	IPP075N15N3 G
Diodes	BYW29EX-200

5.3.1. Simulation results and discussion

The interleaved boost converter as active power stage fed to load, load power (output power) and PV power are shown in Figs 5.8 and 5.11. Two dissimilar power panels are used to supply the DC-DC interleaved boost converter; they have different maximum power rates of 50 Watts and 210 Watts.

5.3.1.1. Interleaved converter with 50% load under solar panel of 50 Watts

The interleaved boost converter is tested with 100 ohm load (50% rating) and supplied by a solar array rated at 50 Watts. The atmospheric conditions are varied shown in Fig 5.7 and the response of the system is summarised in Figs 5.8, and 5.9. The results show that the interleaved boost converter has a high efficiency of 95.6% at $1000\text{w/m}^2, 25\text{C}^o$, but when the maximum PV power is decreased, the efficiency of the interleaved boost converter also falls; it collapses to 93% at an irradiation of $150\text{w/m}^2, 25\text{C}^o$ with maximum accessible PV power.

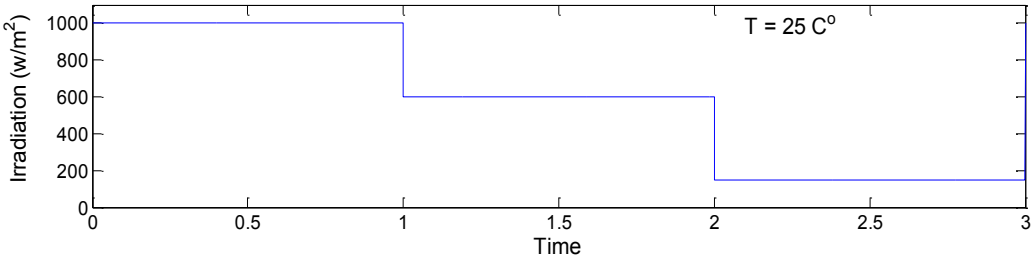

Fig. 5.7, Changeable irradiation with 50 Watt PV panel

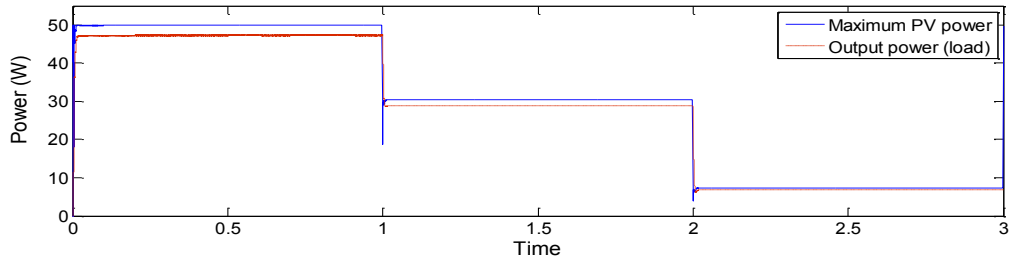

Fig. 5.8, Power of interleaved boost converter under changeable irradiation (load100 ohm)

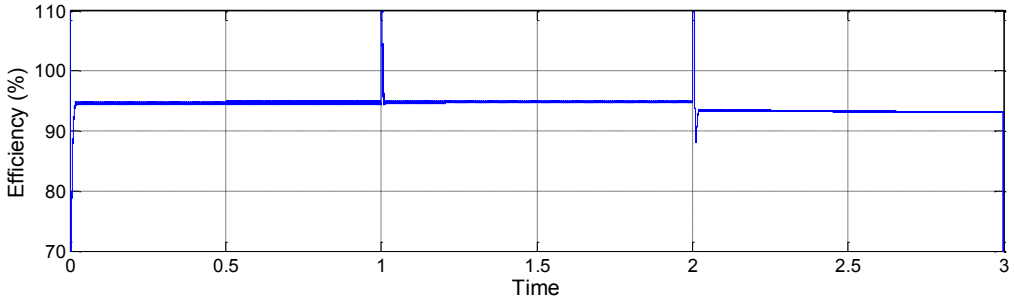

Fig. 5.9, Efficiency of interleaved boost converter with load (100Ω) under changeable irradiation conditions

5.3.1.2. Interleaved converter with 100% load under solar panel of 210 Watts

The interleaved boost converter, tested with 195 ohm load and supplied by a solar array rated at 210 Watts maximum, and subject to changeable atmospheric conditions, is shown in Figs (5.10, 5.11, and 5.12). The figures show that the interleaved boost converter has relatively low efficiency (around 90%) at $200\text{w/m}^2, 25\text{C}^\text{o}$, but when the maximum PV power rises due to increasing irradiation the efficiency of the interleaved boost converter also rises; it reaches 95.8% at $1000\text{w/m}^2, 25\text{C}^\text{o}$.

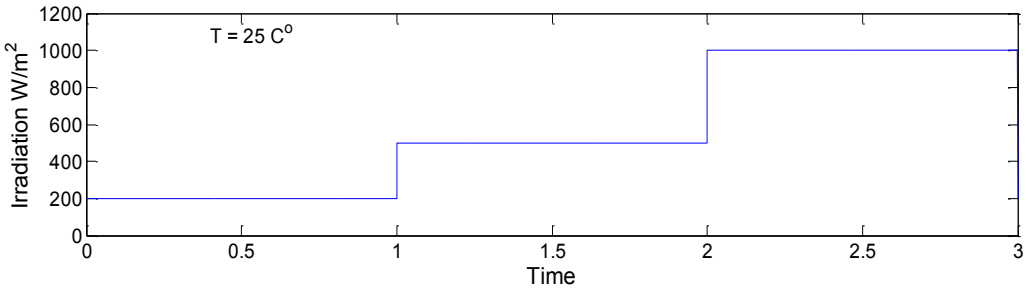

Fig. 5.10, Changeable irradiation over 210 Watt PV panel

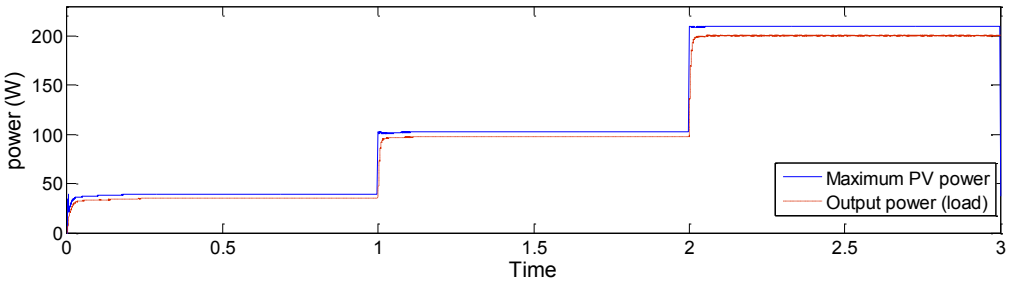

Fig. 5.11, Power of interleaved boost converter under changeable irradiation supplying load (195Ω)

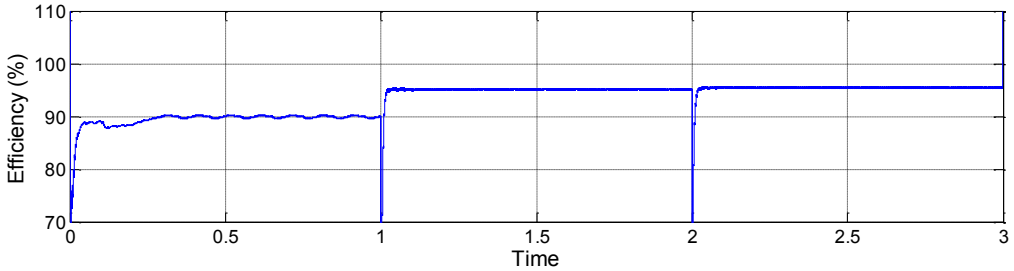

Fig. 5.12, Efficiency of interleaved boost converter with load (195Ω) under changeable irradiation conditions

Output ripple of interleaved boost converter:

The output power of the interleaved boost converter is obtained under different irradiation conditions. As shown in Fig. 5.13, and Fig. 5.14, the interleaved boost converter has 0.23 W output power ripple amplitude at $500\text{w/m}^2, 25\text{C}^\text{o}$. Also, the interleaved boost converter shows an output power ripple amplitude of 0.23 W under $100\text{w/m}^2, 25\text{C}^\text{o}$. The interleaved boost converter shows high power losses at $100\text{w/m}^2, 25\text{C}^\text{o}$, however, it has low power losses at $500\text{w/m}^2, 25\text{C}^\text{o}$. This proves the interleaved boost converter has high power losses at low PV power levels and low power losses at high PV power levels.

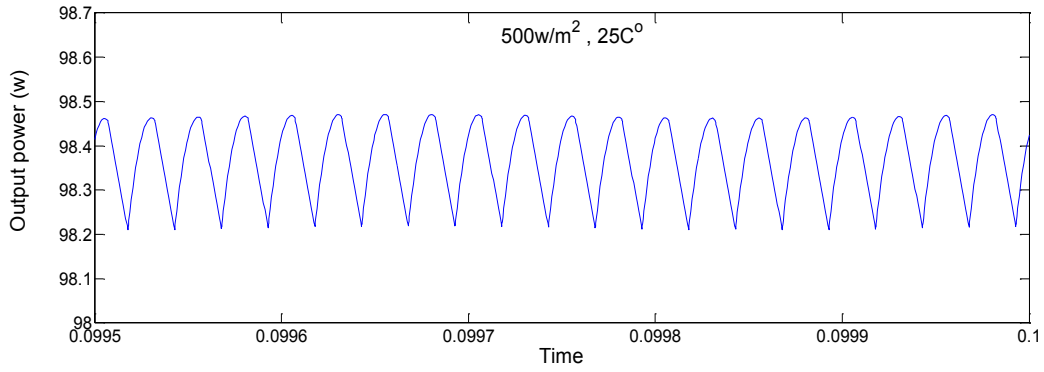

Fig. 5.13, Output power ripple of interleaved boost converter under $500\text{w/m}^2,\ 25\text{C}^\text{o}$

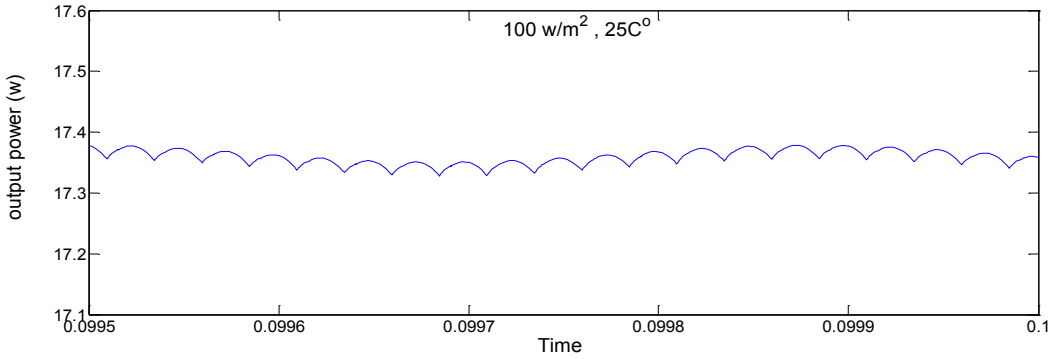

Fig. 5.14, Output power ripple of interleaved boost converter under $100\text{w/m}^2,\ 25\text{C}^\text{o}$

5.3.2. Experimental results and discussion

The experimental results of the interleaved boost converter are obtained using a PV emulator designed set for 50 Watts maximum output power. This is used to supply the input of the DC-DC interleaved boost converter. Consider the photovoltaic power, and efficiency expressions in equations (4.11, 4.12, 4.13, and 4.14); the interleaved boost converter has two phases operating 180 degrees out of phase from each other as shown in Fig. 5.15. Two PWMs are used to drive the gate voltage to Mosfet, and one Mosfet should be turned on half a period time delay from the other one. Furthermore, the figure shows the characteristic of the switches and inductors' in the interleaved boost converter when operating at 20 kHz frequency.

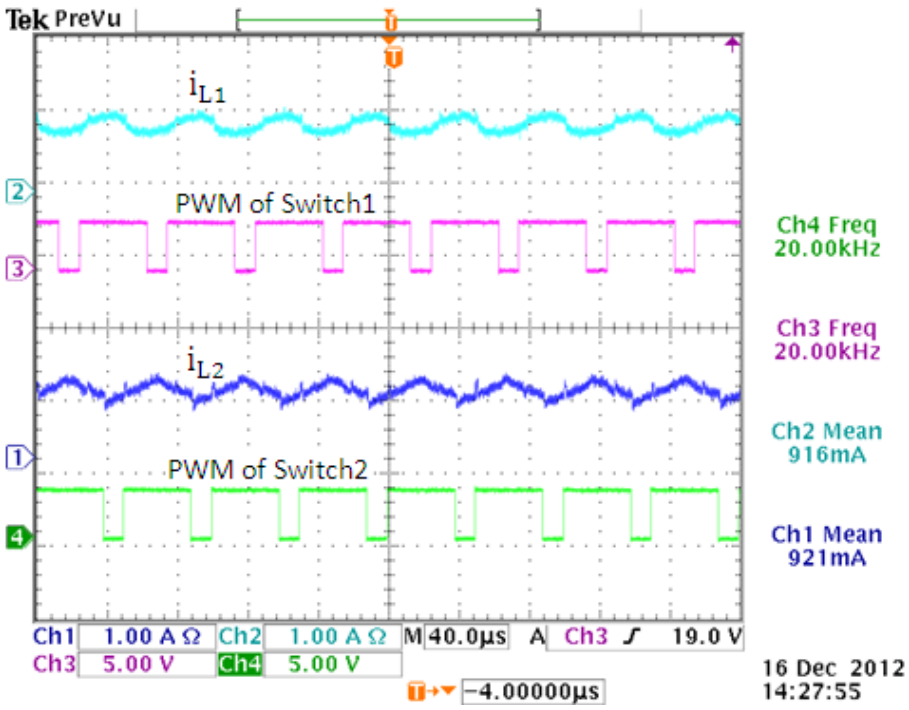

Fig. 5.15, Characteristic of switches and inductors' current in interleaved boost converter

In Fig. 5.16, the interleaved boost converter shows a dynamic response, and as it can be seen that the input current ripple amplitude of the interleaved boost converter is small and has a high output ripple frequency and the inductor ripple is less than the maximum PV current because of the used input capacitor filter in the converter. Generally, the interleaved boost converter has shown fewer ripples in the inputs and outputs of its waveforms in comparing with the conventional boost converter waveforms characteristics in chapter four.

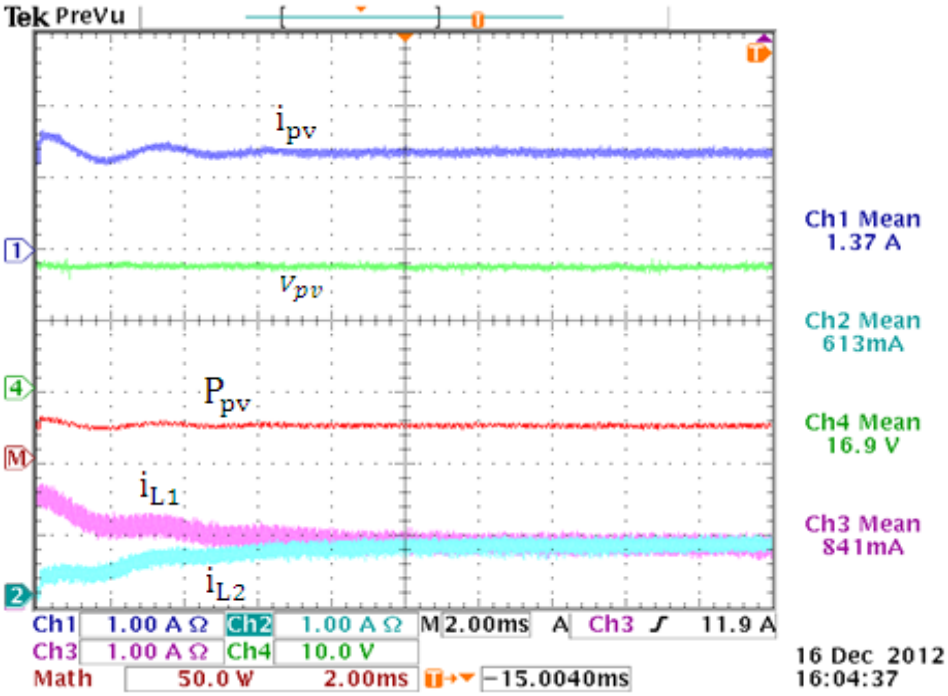

Fig. 5.16, Transient response of interleaved boost converter with inductors' current

Discussion

As can be seen from the results, as the irradiation increases the maximum PV panel current increases while the maximum PV panel voltage is almost constant, these characteristics inform us the solar power is behaving as a current source. It also shows a rise in load power, load current and load voltage as the irradiation soars. At $150w/m^2, 25C^o$, as shown in Fig 5.17, the interleaved boost converter displays a maximum current panel of 0.394 Amps with approximate ripple of 0.035 Amps at 10 KHz [channel 1], a maximum voltage panel of 17.7 Volts with ripple is about 1.5 Volts [channel 4], a maximum PV power of about 10 Watts, inductor 2 current of 0.179 Amps [channel 2], and shows a current of inductor 1 is 0.176 Amps [channel 3]. In addition, the graph show the inductors 'current are in discontinuous conduction mode. Furthermore, Fig. 5.18 shows the load characteristics of interleaved boost converter at weather condition $150w/m^2, 25C^o$, the figure displays the load current is 0.193 Amps with ripple is about 0.004 Amps in channel (1), a load voltage is 35 Volts with ripple of 0.085 Volts [channel 4] and the load power is about 7 Watts.

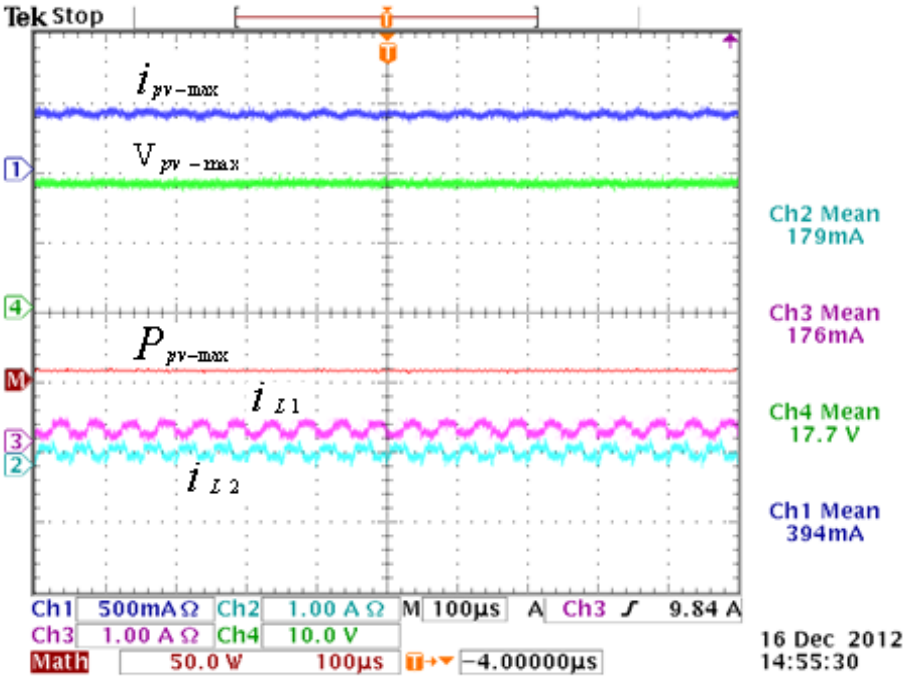

Fig. 5.17, Interleaved boost converter with PV power under Irradiation=150w/m^2, 25C^o

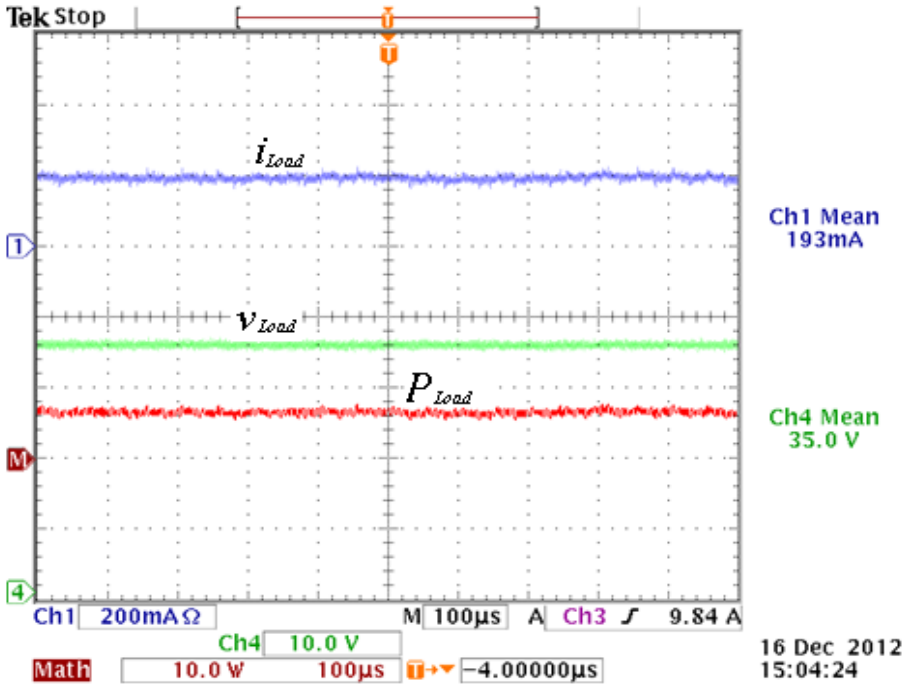

Fig. 5.18, Load current and voltage of interleaved boost converters with load power under irradiation=150w/m^2, 25C^o

At 500w/m^2, 25C^o, as highlighted in Fig 5.19, the interleaved boost converter presents a maximum PV current is 1.42 Amps with ripple approximates 0.126 Amps and frequency about 10 KHz [channel 1], inductor 2 current is 0.720 Amps [channel 2], inductor current 1

is 0.723 Amps [channel 3], a maximum PV power is about 25 Watts, maximum PV voltage is 16.9 Volts with 1.48 Volts ripple [channel 4]. Furthermore, Fig. 5.20 shows the load characteristics at $500w/m^2, 25C^o$, the graph shows the load current is 0.350 Amps [channel 1] with ripple of 0.008 Amps, load power is about 20 Watts, and load voltage is 65.3 Volts with approximate ripple 0.156 Volts [channel 4].

At $1000w/m^2, 25C^o$, shown in Fig 5.21, the interleaved boost converter shows a maximum PV current is 2.89 Amps with 0.26 Amps ripple [channel 1], inductor 2 current is 1.46 Amps [channel 2], inductor current 1 is 1.48 Amps [channel 3], maximum PV voltage is 16.3 Volts with ripple of 1.5 Volts [channel 4].. Furthermore, Fig. 5.22 displays the load characteristics at $1000w/m^2, 25C^o$, the figure shows the load current is 0.488 Amps with 0.0011 Amps ripple [channel 1], load voltage is 91.2 Volts with 0.21 Volts ripple [channel 4], and shows a load power is about 44.5 Watts.

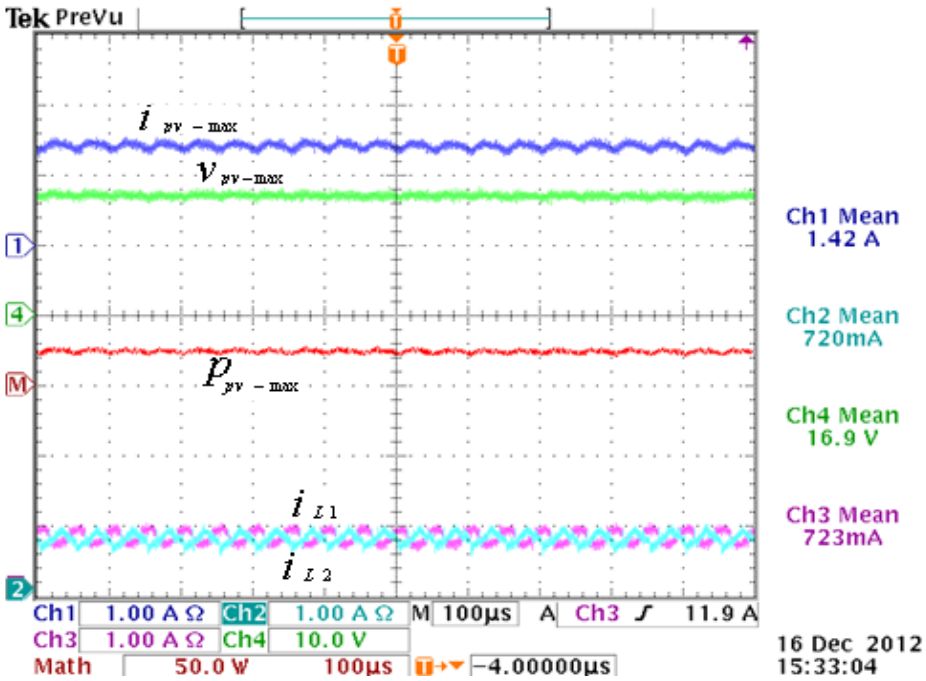

Fig. 5.19, Interleaved boost converter with PV power under irradiation = $500w/m^2, 25C^o$

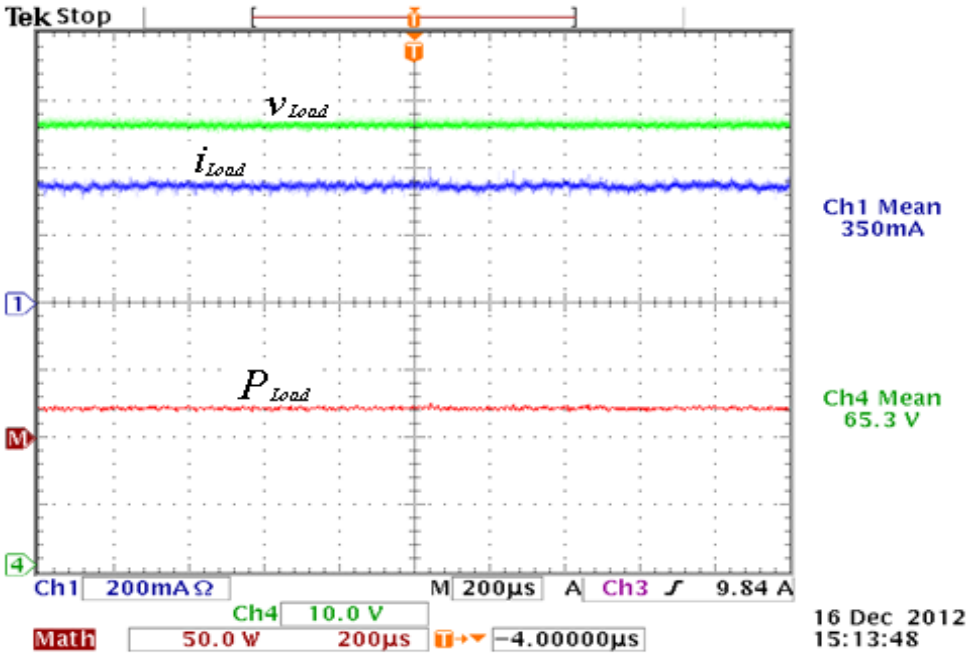

Fig. 5.20, Load current and voltage of interleaved boost converters with load power under irradiation=500w/m^2, 25C°

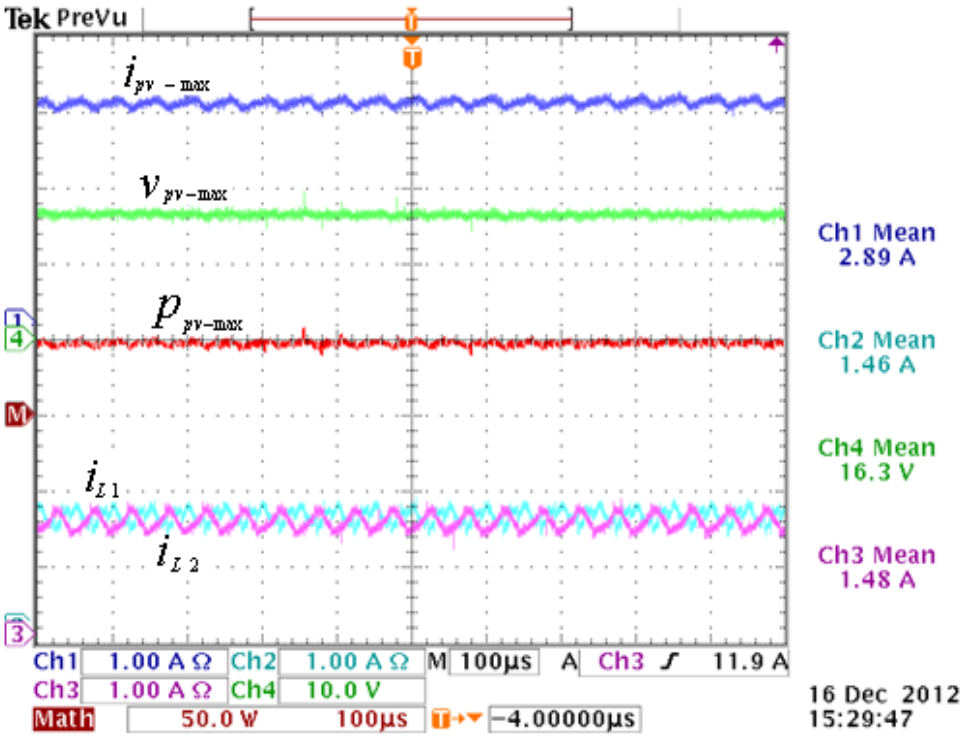

Fig. 5.21, Interleaved boost converter with PV power under irradiation=1000w/m^2, 25C°

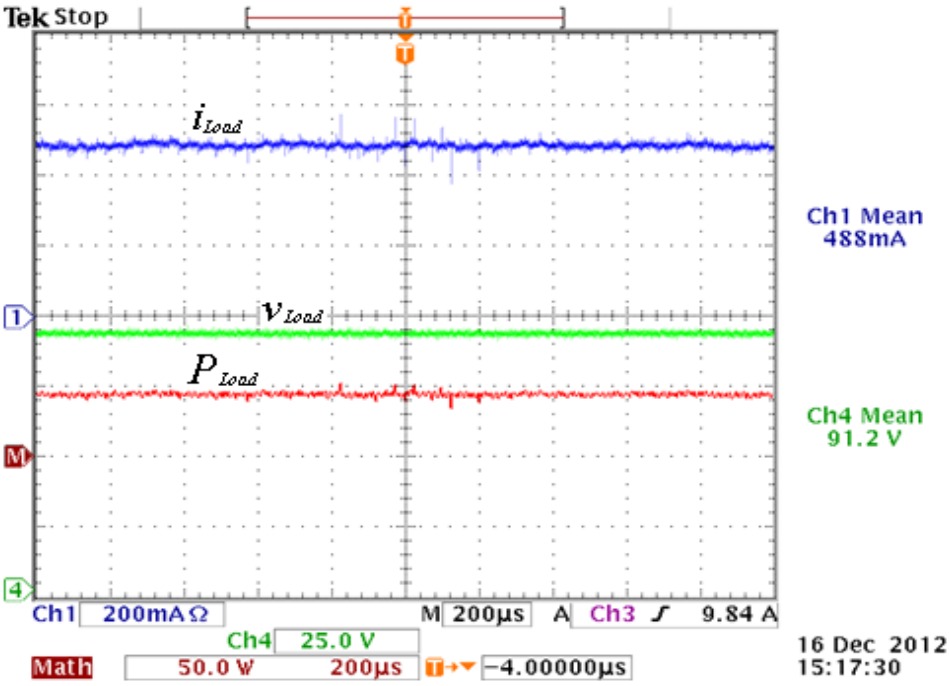

Fig. 5.22, Load current and voltage of interleaved boost converters with load power under irradiation=1000w/m^2, 25C^o

Measured efficiency

Table 5.4: Interleaved boost converter; measured experimental efficiency

	Interleaved efficiency (%)	
Irradiation (w/m^2)	Load = 195Ω	load = 100Ω
150	88.28	90.02
200	88.72	90.88
300	89.81	91.76
400	90.7	92.05
500	91.33	91.95
600	91.5	92.11
700	91.68	91.93
800	91.75	91.88
900	91.67	91.63
1000	91.54	91.48

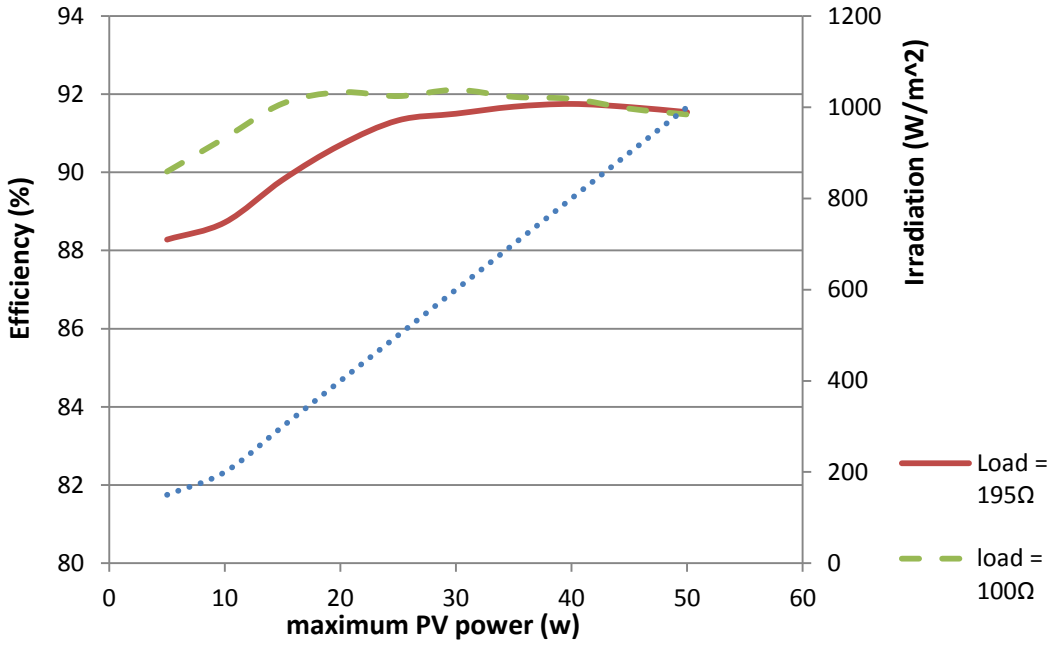

Fig. 5.23, Efficiency results of interleaved boost converter with different load value under irradiation conditions

Discussion

The results from the interleaved boost converter are presented in Fig. 5.23 and in Table 5.4. The left axis (y) represents the efficiency of the interleaved boost converter with different load percentages and axis (x) presents the maximum PV power that rises as the irradiation weather rises which is shown on the right axis (y). As the result on the whole figure indicates, the efficiency of the interleaved boost converter with its load of about 50 % (100 Ohms), at low irradiation $150\text{w/m}^2, 25\text{C}^\text{o}$ with available generated maximum PV power of about 7 Watts, the converter shows low efficiency of 90.02% and after a slight climb at $250\text{w/m}^2, 25\text{C}^\text{o}$ that produced the available maximum PV power of 12 Watts, after that the high level efficiency nearly starts to be steady as can be seen at irradiation levels $400\text{w/m}^2, 25\text{C}^\text{o}$, $500\text{w/m}^2, 25\text{C}^\text{o}$, at $750\text{w/m}^2, 25\text{C}^\text{o}$ as the obtained maximum PV power rises until the efficiency of the converter reaches 91.48 % at irradiation $1000\text{w/m}^2, 25\text{C}^\text{o}$ and maximum PV power 50 Watts. Also, the converter with (195 Ohm) 100 percentage of its load shows nearly the same trace, the converter has shown a high efficiency level around 91.60 % at irradiation $600\text{w/m}^2, 25\text{C}^\text{o}$, $700\text{w/m}^2, 25\text{C}^\text{o}$, $800\text{w/m}^2, 25\text{C}^\text{o}$ and $900\text{w/m}^2, 25\text{C}^\text{o}$ with maximum obtainable array power, but the converter shows a low efficiency when the maximum PV power reduces due to the decrease of the irradiations, for example, at $150\text{w/m}^2, 25\text{C}^\text{o}$ with gained maximum power 7 Watts, the efficiency of the converter goes to the lowest level of 88.28%.

5.4. Summary

This chapter has set out to investigate the interleaved boost converter stage of the electronic power in standalone PV systems, so the simulation and experiment are built to see the performance of an interleaved boost converter in a standalone PV system under changeable atmospheric conditions. The performance of the interleaved boost converter is carried out using the same value of parameters in both tests (software and hardware). The switching devices and diodes are chosen to be the same as that used with the conventional boost converter which is selected after an extensive calculation of key design considerations. Especially when cost and efficiency are essential factors in any power plant generation.

This section of study has confirmed that through both the software and hardware, the interleaved boost converter shows a low ripple of PV power and a low ripple of load power in comparison with the conventional boost converter. Furthermore, the study has found that the interleaved boost converter has high efficiency at a high power of PV panel when more insolation of weather is available. However, the efficiency of the interleaved boost converter declines when the power of the PV solar panel decreases due to a plunge in irradiation weather. In the case of a changeable load, the interleaved boost converter with different percentages of its resistive load still also has low efficiency when receiving low PV array power and shows a high efficiency as the obtained photovoltaic power increases. Looking to the system at low irradiation, it can be seen that a small PV current is shared between interleaved limbs. Therefore, the system operates in discontinuous current mode (DCM). Since the peak and RMS value of the current are high in DCM, higher losses result and greater current stress appears on the switches and for this reason the switching loss becomes dominant. Furthermore, because the interleaved converter has two switches, the efficiency will drop in comparison with a conventional boost converter.

To draw a conclusion on the results of the simulation and hardware, an interleaved boost converter could be good choice for a standalone PV system that requires operating energy in a high insolation climate. Also, the interleaved boost converter may be selected if the key consideration is to have a boost converter that has a non-complicated circuit to operate and high efficiency, a low current ripple and has moderate cost.

Chapter Six

6. Interleaved Boost Converter with Novel Switch Adaptive Control

After investigation, with reference to the conventional boost converter in Chapter four and to an interleaved boost Converter in chapter five, assessment of both converters has found that each converter exhibits a significant drop in efficiency at different stages of PV power output. For example, the efficiency of the conventional boost converter decreases at high power levels, whilst the efficiency of the interleaved boost converter decreases at low PV power levels. Therefore, this chapter aims to make a contribution to knowledge by combining the performance of both the discussed converters to improve the overall efficiency of the standalone PV system over a wide range of operating conditions. Specifically, the proposed scheme aims to improve the efficiency of the interleaved boost converter at low power levels by operating it as a conventional boost converter, but retaining the interleaved operation at high photovoltaic power levels.

To achieve this, a new switch adaptive control strategy is proposed as shown in Fig. 6.1. At high power, it operates normally as an interleaved converter, following the switch control rules already described in Chapter five. However, at low power (low irradiance) one phase of the interleaved cell is isolated by an auxiliary-switch (Sc) and all the current is controlled to flow in one phase of the interleaved converter. Fundamentally, the interleaved converter is now operating as a conventional boost converter (single inductor, single switch). At low power levels, the current is obviously low. However, by controlling all of the current into one leg of the interleaved boost converter, it reduces the risk of operating in discontinuous current mode. So long as the converter operates in a continuous current mode, the efficiency of the converter will be greater.

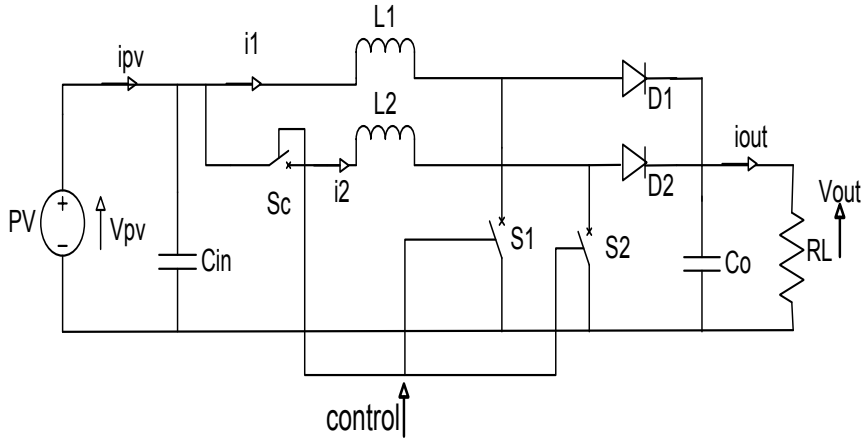

Fig. 6.1, Interleaved boost converter with novel switch adaptive control

The proposed adaptive switching strategy is highlighted in Fig. 6.2. It has several advantages, in particular it minimises system losses and helps the interleaved converter to operate with maximum power conversion efficiency at all times under a wide range of atmospheric conditions [92]. Moreover, the control scheme can be achieved with no significant additional hardware, and in terms of microprocessor implementation it is computationally light.

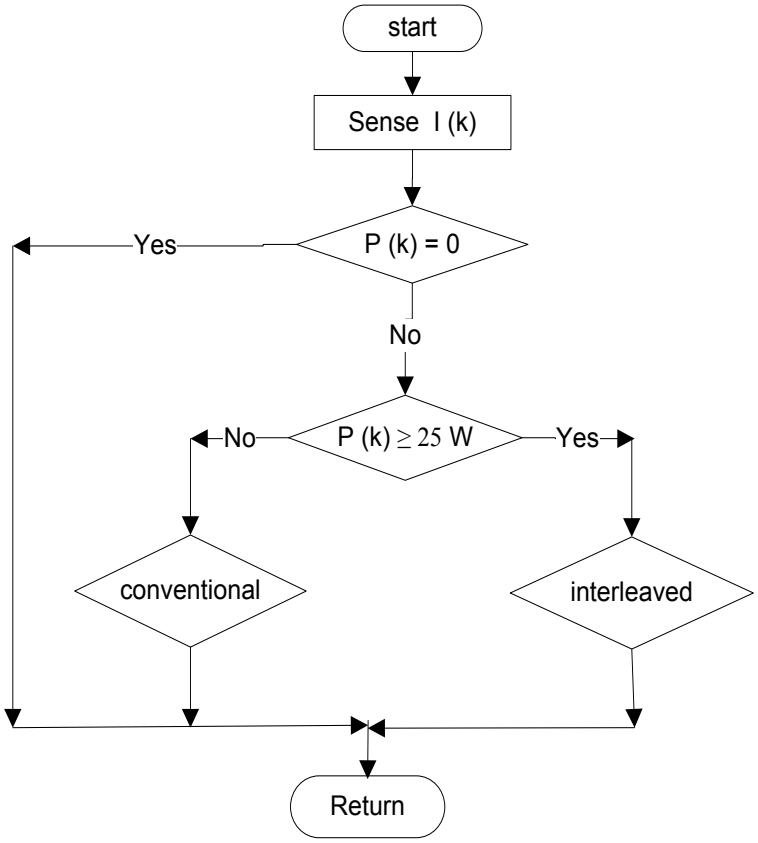

Fig. 6.2, Flow chart of novel switch adaptive control

The controller measures the PV current and PV voltage to monitor the PV power and follows a very simple request to operate the converter as an interleaved boost converter (switch ON) at high PV power when the power is over a 25 Watt level, and as a conventional boost converter (switch OFF) at low PV power when the PV power is lower than 25 Watts. The need for the auxiliary switch is not immediately obvious at first. However, its inclusion is very important to the successful operation of the proposed scheme. To justify the use of the auxiliary switch, consider the simulation shown in Fig. 6.3, Fig. 6.4, and Fig.6.5.

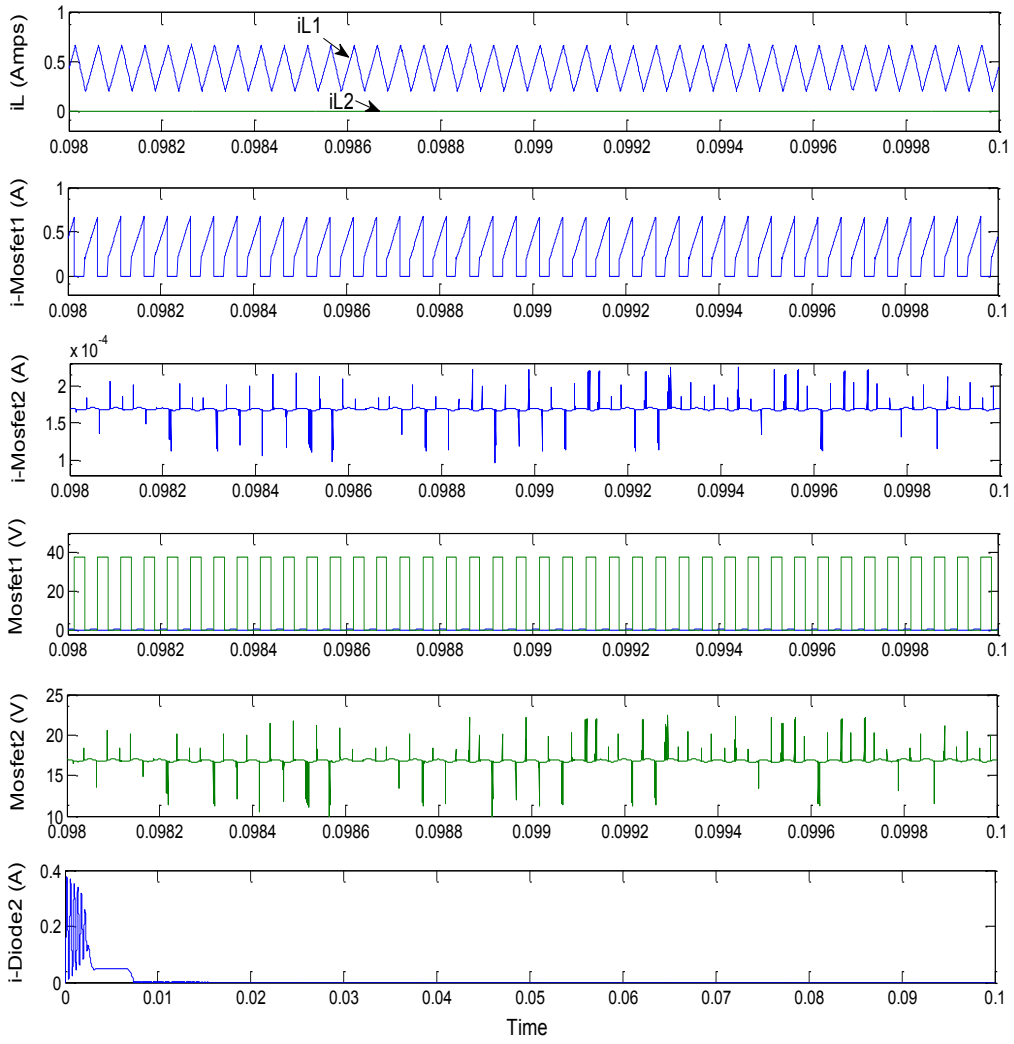

Fig. 6.3, Characteristics of proposed interleaved boost converter with novel switch adaptive control without auxiliary switch

The performance of the proposed interleaved boost converter, with novel switch adaptive control, and without auxiliary the switch is shown in Fig. 6.3. This figure shows there is a high leakage current, high voltage and current stress on switch two (Mosfet and diode). This causes significant heat generation in switch two and quickly leads to failure of the switch two device.

Using the external auxiliary switch to isolate limb two ensures no current is flowing in the second interleaved boost converter limb. By using this strategy, there is a significant improvement in the characteristic performance of the converter, as shown in Fig. 6.4, there is measurable leakage current and significantly less current and voltage stress on the switch

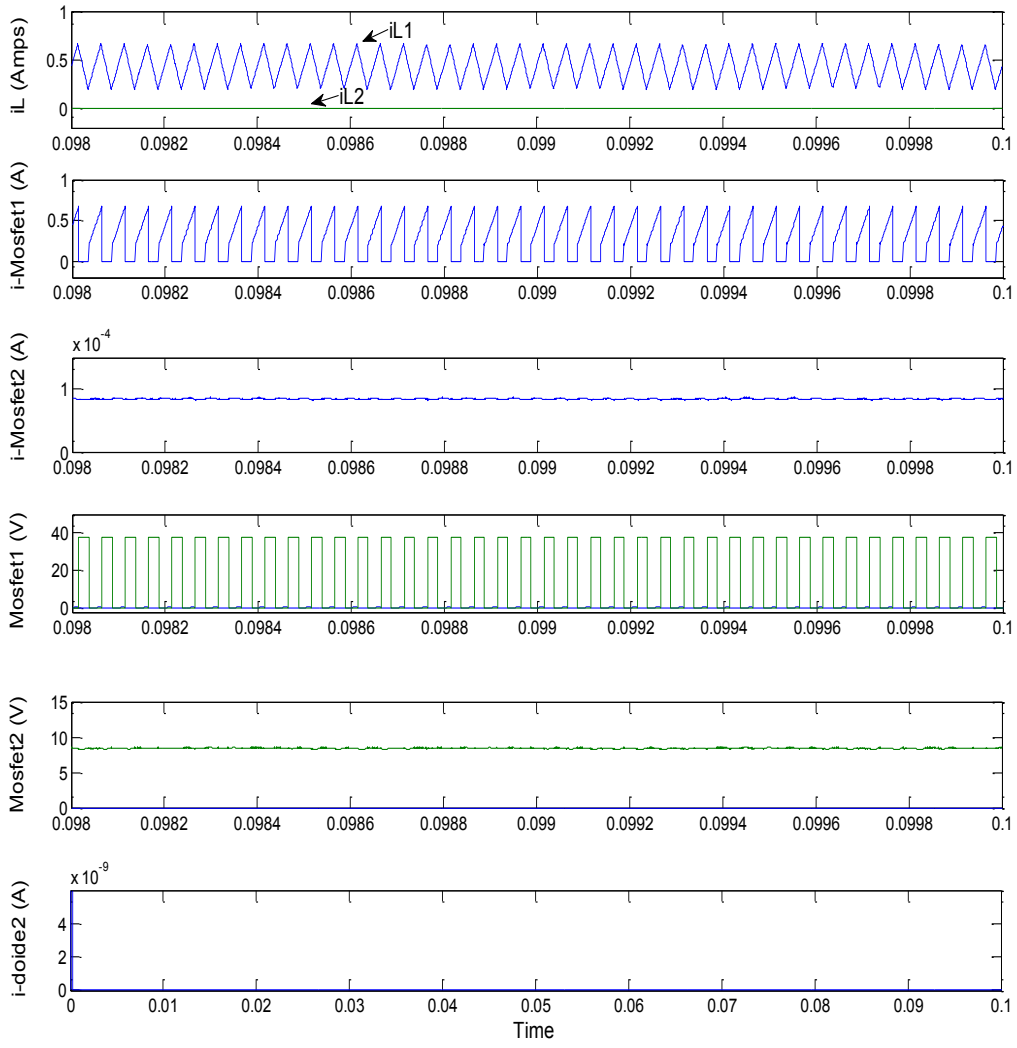

Fig. 6.4, Characteristics of the proposed interleaved boost converter with novel switch adaptive control with auxiliary switch

Here, Fig. 6.5, shows the efficiency of the interleaved boost converter with novel switch adaptive control; with and without the additional switch. As can be seen from the graph, it shows slightly better efficiency characteristics compared to the converter with the auxiliary switch, approximately (95.5%), compared to (95.2%). However, this is a compromise on efficiency which must be accepted in order for the converter to operate successfully under the proposed scheme. As described later in the thesis, one of the areas for future investigation is developing a strategy to mitigate the need for this auxiliary switch.

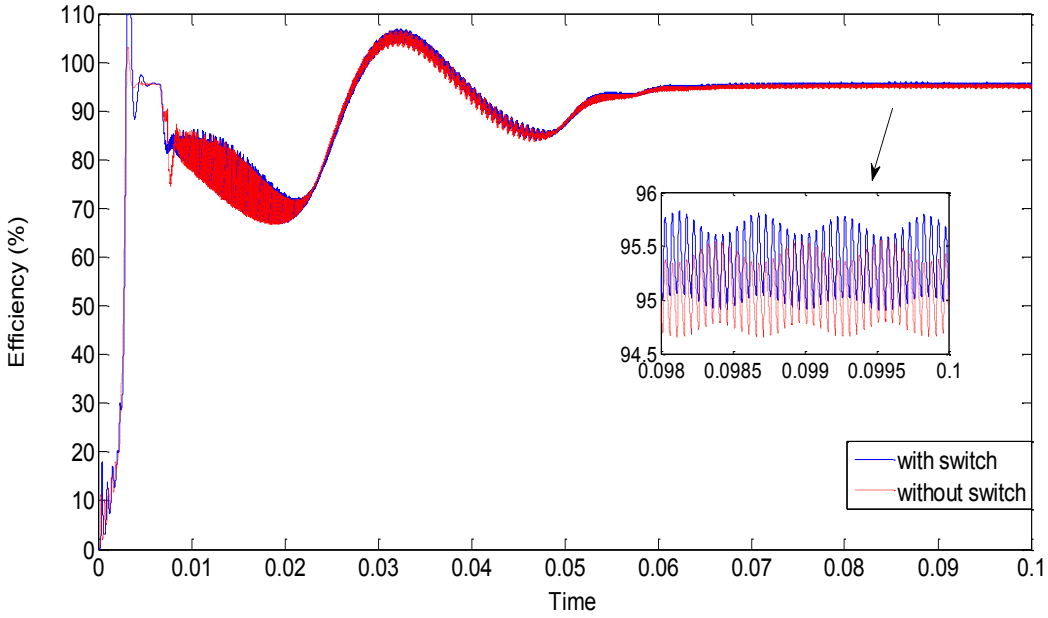

Fig. 6.5, Efficiency of the proposed interleaved boost converter with novel switch adaptive control with and without additional switch

6.1. Design of interleaved boost converter with novel switch adaptive control

The interleaved boost converter with novel switch adaptive control combines all the principles of the discussed interleaved boost converter in Chapter five, but operates with both conventional and the interleaved boost converter modes of control, as required.

Analysis and loss calculation for the interleaved boost converter with novel switch adaptive control

The loss analysis of the proposed converter is the same as the loss analysis of the conventional boost converter below $500\text{w/m}^2, 25\text{C}^\text{o}$, and its loss analysis is very similar to the interleaved boost converter above $500\text{w/m}^2, 25\text{C}^\text{o}$. However, the auxiliary switch that is

used to turn ON and OFF the second limb of the interleaved boost converter must be considered; this switch does not operate under fast PWM operation so the switching loss of the auxiliary switch is almost zero. The conduction loss of the auxiliary switch can be calculated as follows:

$$P_{Ex-Switch-conduction\ loss} = (r_{ds(on)})\left(\frac{i_{in}}{2}\right)^2$$

Loss analysis of interleaved boost converter with novel switch adaptive control under loading condition above 500w/m^2, 25C^o: Using Table 5.2, Table 6.1 and by adding power loss of extra switch under loading condition.

The efficiency of an interleaved boost converter with novel switch adaptive control at PV output power of G=1000 w/m² and T= 25 C˚, is illustrated below:

$$P_{Ex-Switch-conduction\ loss} = (0.003)\left(\frac{5.09}{2}\right)^2 = 0.0194\ Watts$$

$$\eta = \frac{210 - (2.308 + (1.859 + 0.0756 + 0.028 + 0.0194) + (0.0203 + 0.911))}{210} \times 100\%$$

$$= 97.51$$

The efficiency of the interleaved boost converter with novel switch adaptive control at output power of PV panel under G =700 w/m² and T= 25 C˚, is illustrated below:

$$P_{Ex-Switch-conduction\ loss} = (0.003)\left(\frac{3.618}{2}\right)^2 = 0.0098\ Watts$$

$$\eta = \frac{145.7 - (1.164 + (1.097 + 0.0363 + 0.028 + 0.0098) + (0.0168 + 0.777))}{145.7}$$

$$\times 100\% = 97.852$$

From the above analysis, the proposed converter, which uses an extra switch, has similar efficiency to the interleaved boost converter when operating under high irradiation conditions.

6.2. Control design of the interleaved boost converter with novel switch adaptive control

The novel adaptive control switch of the interleaved boost converter is structured to isolate one limb by using a controlled switch before inductor two. The structure is also able to switch the limb on or off of the switch's two signals as shown in Fig. 6.6. This control structure measures the PV current and PV voltage to monitor the PV power and follows a very simple request to operate as an interleaved boost converter (switch ON) at high PV power when the power is over a 25 Watts level and as a conventional boost converter (switch OFF) at low PV power when the PV power is lower than 25 Watts. The PWM unit generation with MPPT control in an interleaved boost converter with novel switch adaptive control is presented in Chapter four when the converter is operated as a conventional boost converter and is presented in chapter five when the converter is operated as an interleaved boost converter. This control policy works well as shown in Fig. 6.7, following the change of PV power point.

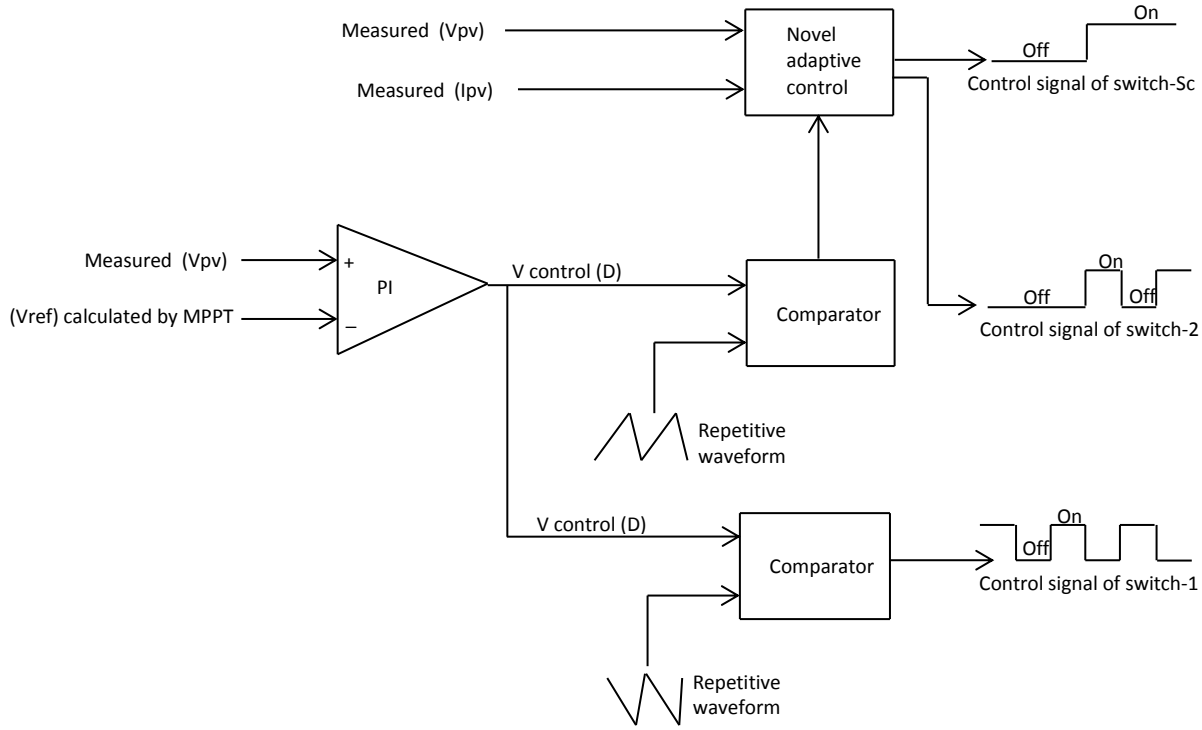

Fig. 6.6, Pulse width modulator control for interleaved boost converter with novel adaptive control scheme

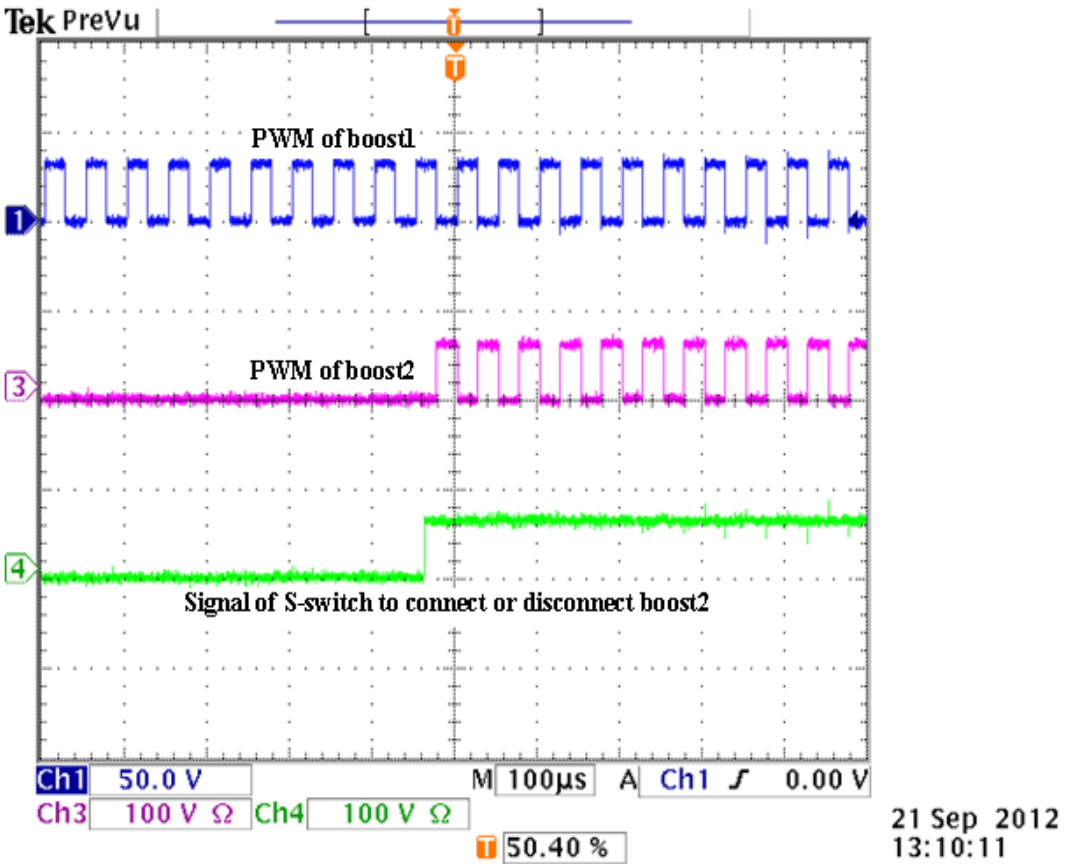

Fig. 6.7, Interleaved boost converter switching signals with novel adaptive control

6. 3. Results and discussion

The interleaved boost converter with novel switch adaptive control is set up in simulation and an experiment to validate the theoretical analysis of the introduced standalone photovoltaic system. A maximum power point tracking (MPPT) control of perturb and observe algorithm is used to guarantee that the maximum power of a PV panel is engaged to the converter. The software and hardware are built to evaluate the interleaved boost converter with novel switch adaptive control in the introduced system, therefore tests are done with a mixture of power levels of photovoltaic panels (KD50SE-1P) and (HIP-210NH1-BO-1) in Table 3.1 under a variety of atmospheric condition. Also, the tests are run with different load percentages. In addition, to validate the results, similar considered key design constraints and parameters are used on the interleaved boost converter with novel switch adaptive control in both software and hardware as shown in Table 6.1. It is evident that the interleaved boost converter with adaptive switching control topology is similar to the interleaved boost converter parameters.

The results and discussion of simulation using Matlab (SimPower System) are shown from Fig. 6.8 to Fig. 6.29, then the experiment results and discussion from Fig. 6.30 to Fig. 6.38. The interleaved boost converter with adaptive switching control is simulated using the introduced method control to operate it at high efficiency at all times under different irradiation atmospheric condition.

Table 6.1: Parameters for interleaved boost converter with novel switch adaptive control

Frequency = 20 kHz, Duty ratio = 0.1- 0.9	Interleaved boost converter with novel switch adaptive control
Capacitor (Cin)	9.4 µF
Inductors	L1= 1 mH
	L2=1 mH
Frequency	20kHz
Capacitor (Cout)	44 µF
Resistive load	100 & 195 Ω
Mosfets	IPP075N15N3 G, (Ex-S = IRFB3077PBF)
Diodes	BYW29EX-200

6. 3.1. Simulation results and discussion

The relation of converter efficiency with its current inductor mode, in Fig. 6.8 with $150\text{w/m}^2, 25\text{C}^o$, shows that when it is operated as an interleaved boost converter, the low input current of the PV panel is shared between its limbs and the inductor current operates in discontinuous current mode that leads to a low efficiency level. However, when it is operated as a conventional boost converter, all of the input current of the PV panel is in one leg and the inductor current operates in continuous current mode that provides a high efficiency level. Fig. 6.9 shows the opposite with $1000\text{w/m}^2, 25\text{C}^o$ when the extracted current of the PV is high, when the converter is operated as interleaved, the input current is divided between its limbs and the current inductor still operates in continuous current mode which gives a high efficiency level compared to when the converter is operated as a conventional converter.

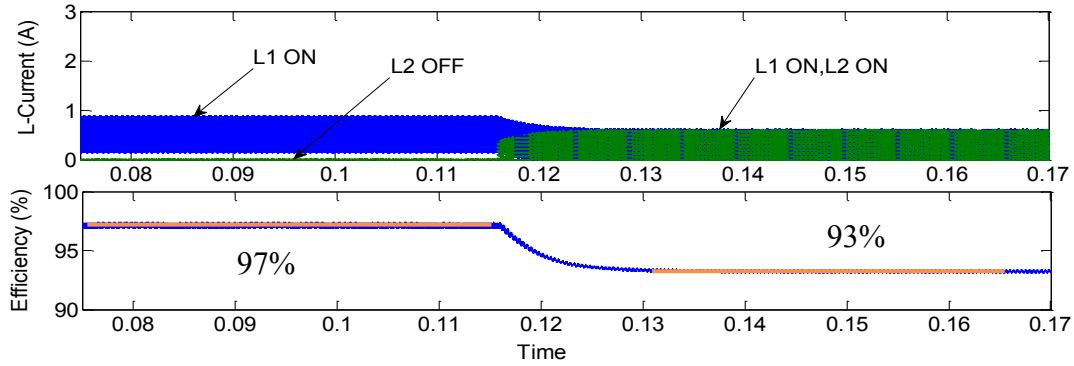

Fig. 6.8, Efficiency with inductor current of interleaved boost converter with novel switch adaptive control at $150\text{w/m}^2, 25\text{C}^o$

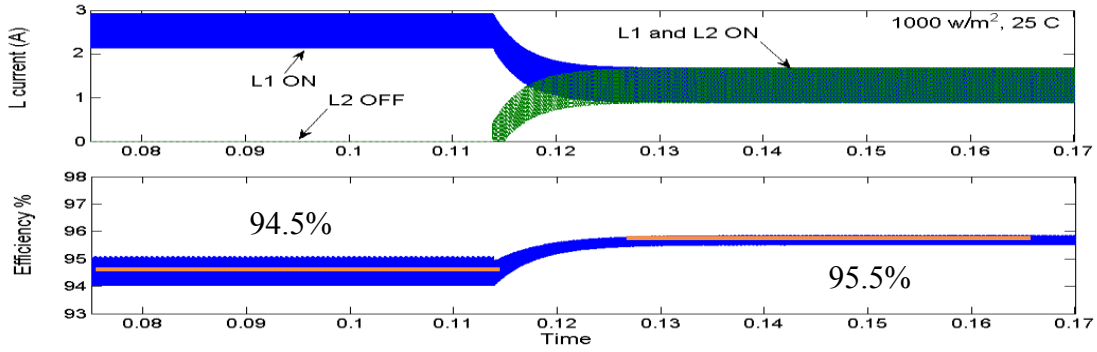

Fig. 6.9, Efficiency with inductor current of interleaved boost converter with novel switch adaptive control at $1000\text{w/m}^2, 25\text{C}^o$

6.3.1.1. Boost converters under PV panel of 50 Watts and with resistive load

The discussed converters are tested with load 195 Ohm and supplied by a solar array rated at 50 Watts maximum with a rising irradiation profile as shown in Figs (6.10, and 6.11). As can be seen in Fig. 6.12, the conventional boost shows a reduction in efficiency when the PV power reaches approximately 24 Watts, whilst the interleaved boost still shows an improving efficiency characteristic when the PV power increase. Fig. 6.13 shows that the interleaved boost converter with novel switch adaptive control has a stable efficiency of around 95%.

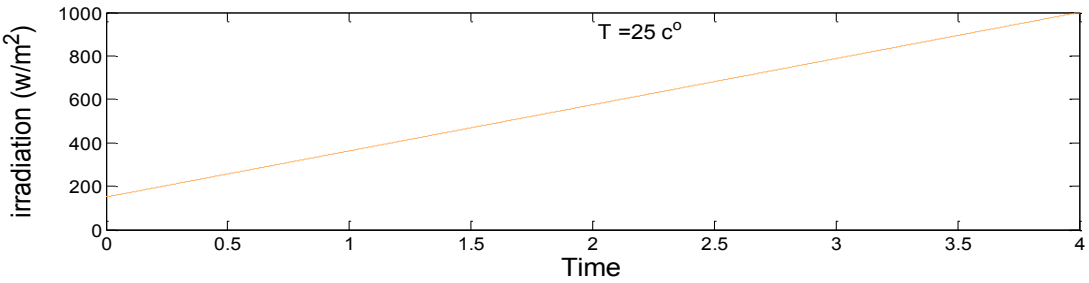

Fig. 6.10, Rise in irradiation over 50 Watt PV panel

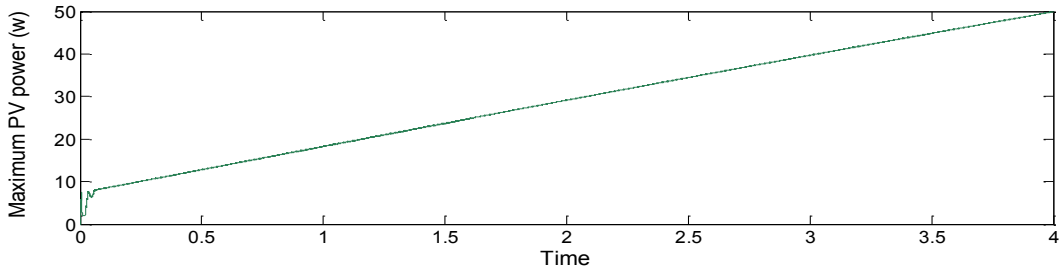

Fig. 6.11, Power of PV panel 50 Watt under raised irradiation conditions

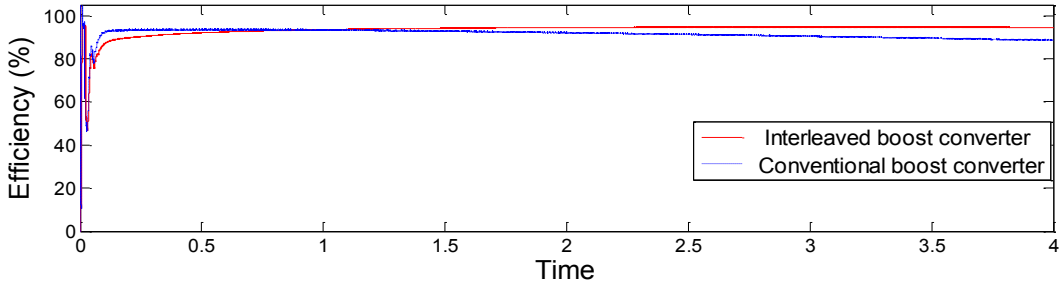

Fig. 6.12, Efficiency of interleaved and conventional boost converters under increased irradiation conditions

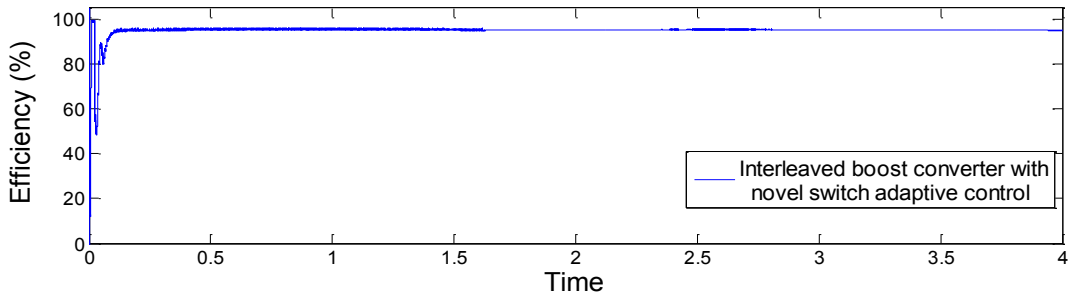

Fig. 6.13, Efficiency of interleaved boost converter with novel switch adaptive control under increased irradiation conditions

The discussed converter is then tested under a fall in irradiation using the same solar panel of rate maximum 50 Watts with load 195 Ohm are shown in Figs (6.14 and 6.15). As seen in Fig. 6.16 the conventional boost converter shows a rise in efficiency when the PV power reaches approximately 25 Watts whilst the interleaved boost converter starts to demonstrate a drop in efficiency. Fig. 6.17 shows that the interleaved boost converter with novel switch adaptive control has a stable high efficiency of about 95% under a decrease in maximum PV power.

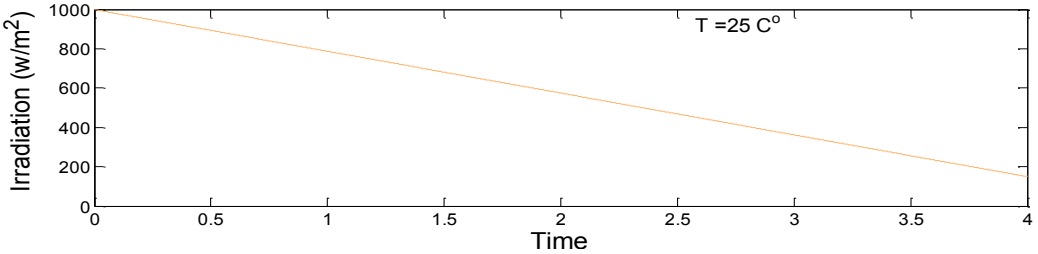

Fig. 6.14, Decrease in irradiation over 50 Watt PV panel

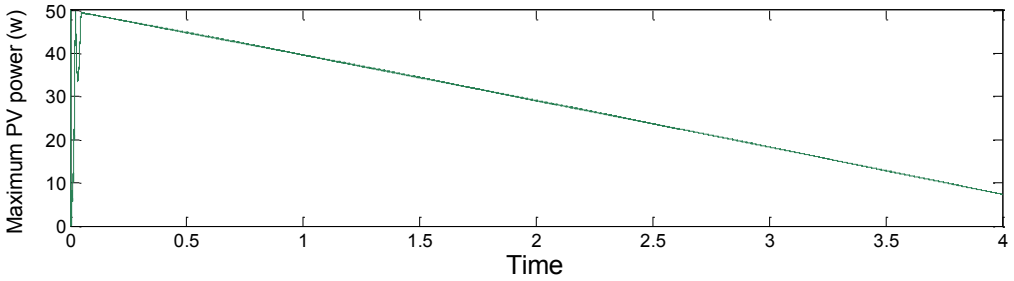

Fig. 6.15, Power of PV panel 50 Watts under decreased irradiation

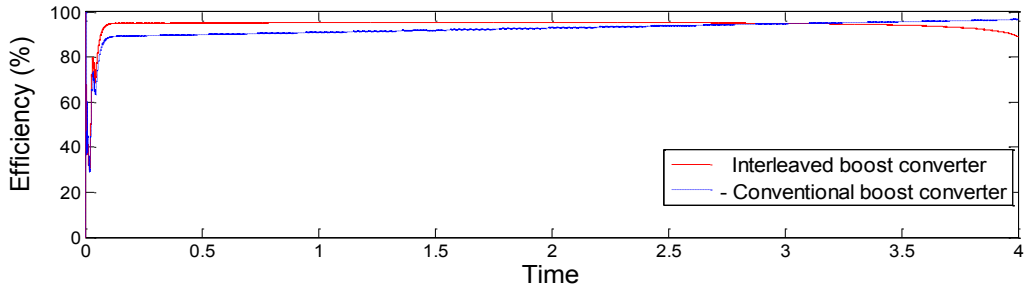

Fig. 6.16, Efficiency of interleaved and conventional boost converters under a drop in irradiation conditions

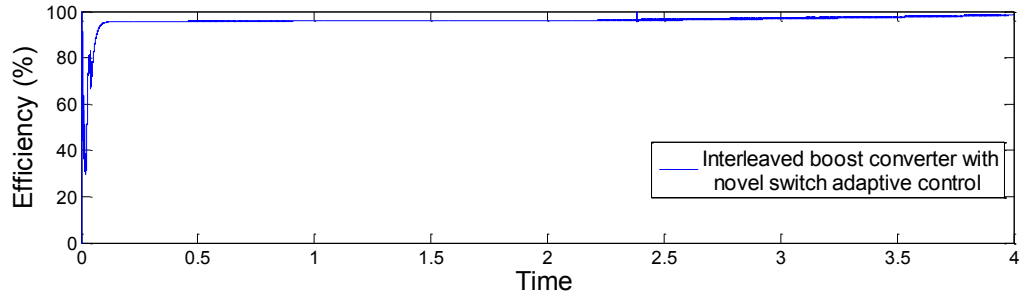

Fig. 6.17, Efficiency of interleaved boost converter with novel switch adaptive control under a drop in irradiation conditions

6.3.1.2. Boost converters under PV panel of 210 Watts and with resistive load

In Fig. 6.20 it can be seen that the conventional boost shows a drop in efficiency when PV power reaches about the 100 Watts level while the interleaved boost still shows higher efficiency. Moreover, the graph in Fig. 6.21 shows the interleaved boost converter with novel switch adaptive control has a stable high efficiency of about 95% under a rise of maximum PV power all the time.

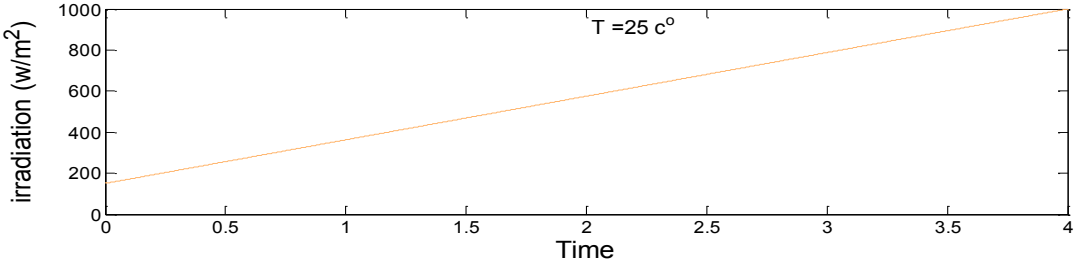

Fig. 6.18, Rise in irradiation over 210 Watts of PV panel

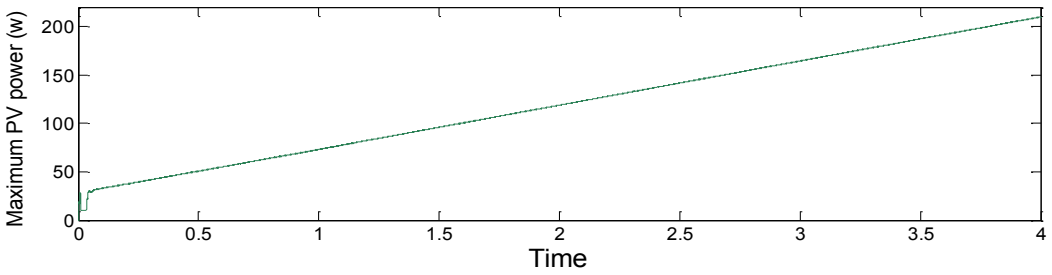

Fig. 6.19, Power of PV panel 210 Watts under increased irradiation conditions

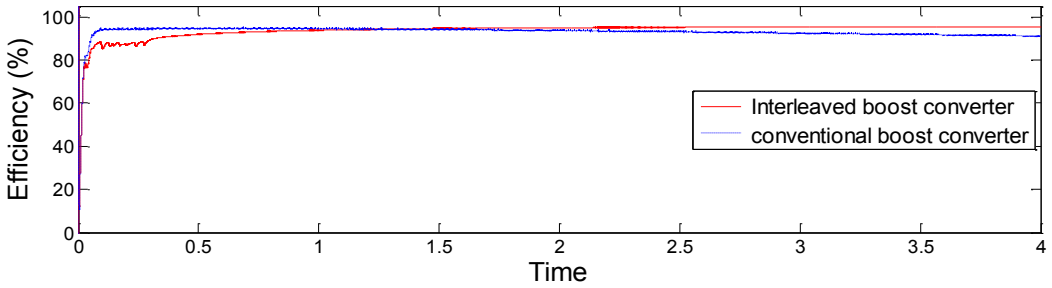

Fig. 6.20, Efficiency of interleaved and conventional boost converter under arise in irradiation conditions

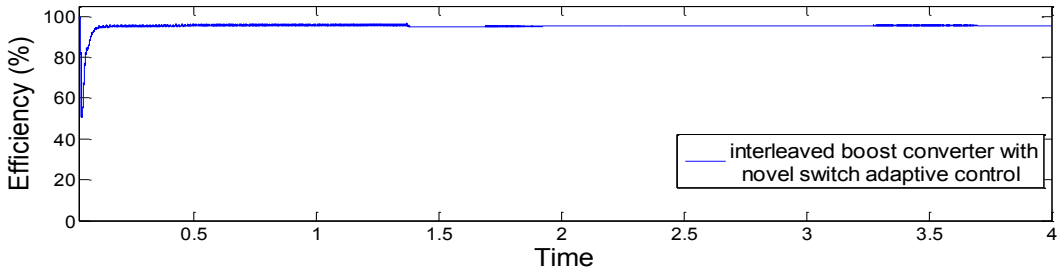

Fig. 6.21, Efficiency of interleaved boost converter with novel switch adaptive control under a rise in irradiation conditions

The presented converters are then tested under a fall in irradiation still using the same solar array of maximum 210 Watts rating and load 195 Ohm, as shown in Figs (6.22, and 6.23). In Fig. 6.24 it can be seen that the conventional boost shows a rise in efficiency when the PV power reaches about 98 Watts power while the interleaved boost converter begins to show a drop in efficiency level. Fig. 6.25 shows that the interleaved boost converter with novel switch adaptive control has high efficiency of 95% under a decrease in maximum PV power.

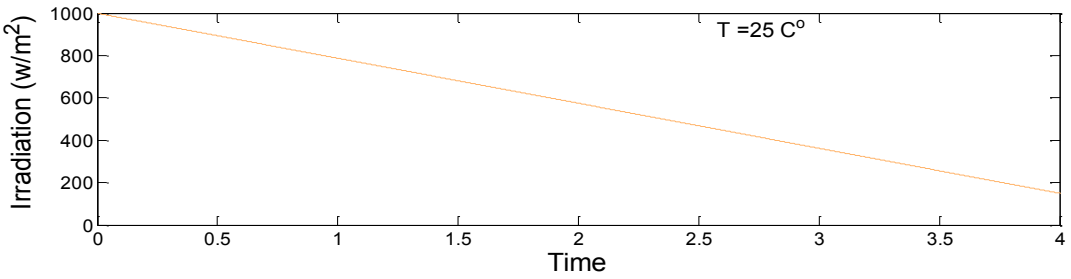

Fig. 6.22, Fall in irradiation over 210 Watts PV panel

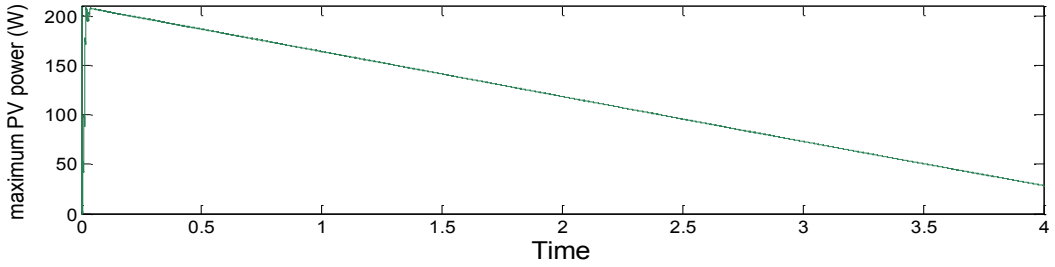

Fig. 6.23, Power of PV panel 210 Watts under decreased irradiation conditions

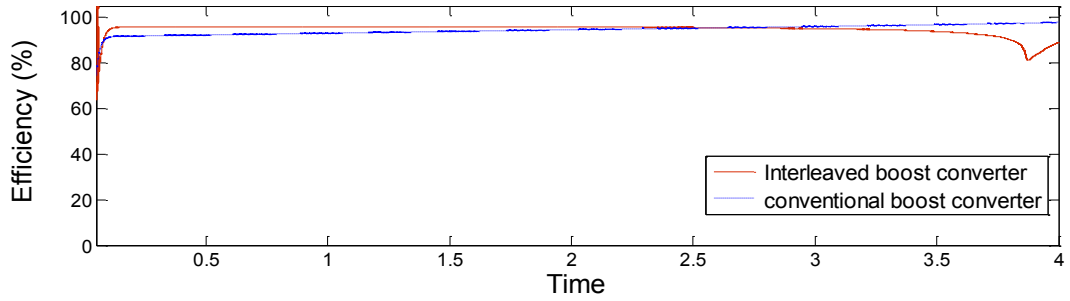

Fig. 6.24, Efficiency of interleaved and conventional boost converter under a drop in irradiation conditions

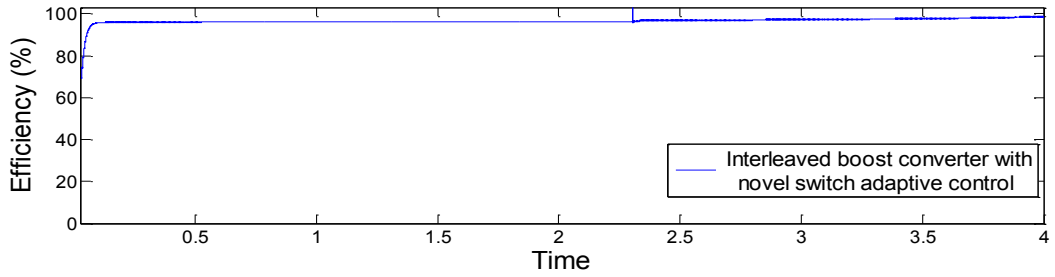

Fig. 6.25, Efficiency of interleaved boost converter with novel switch adaptive control under a drop in irradiation conditions

6.3.1.3. Boost converters with inductive load

The introduced boost converters are tested with inductive load (L=50 mH, R=80 Ohm), and supplied by a solar array of rate maximum 50 Watts with a rise in irradiation of atmospheric conditions are shown in Figs (6.26, and 6.27). In Fig. 6.28, it can be seen that the conventional boost shows a drop in efficiency when PV power reaches about the 25 Watt level, the interleaved boost shows a drop in efficiency when the PV power below 25 Watts and growth in efficiency level when the PV power over 25 Watts. Moreover, the graph in Fig. 6.29 shows the interleaved boost converter with novel switch adaptive control has a stable high efficiency of about 95% all the time under a rise of maximum PV power.

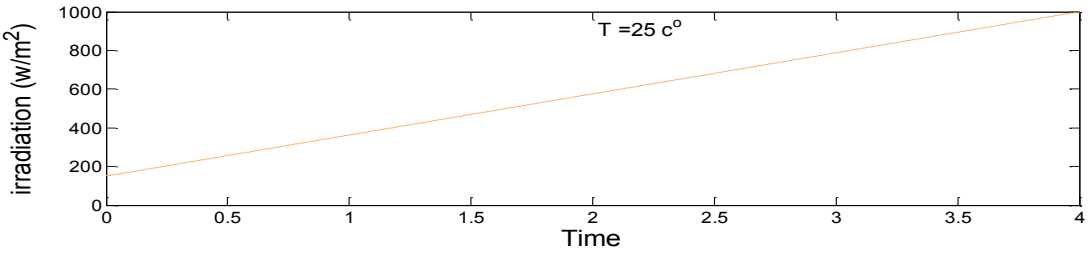

Fig. 6.26, Rise in irradiation over 50 Watts PV panel

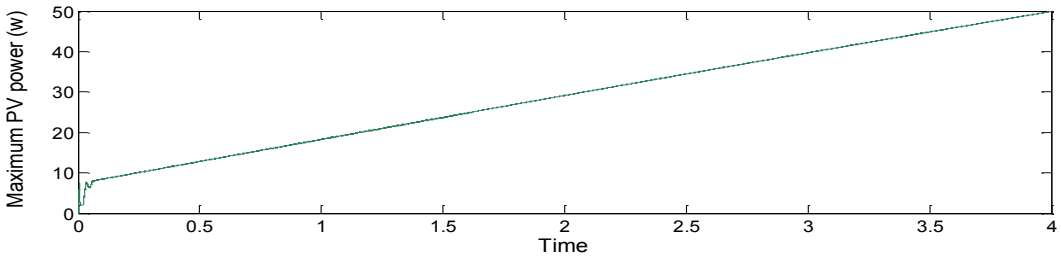

Fig. 6.27, Power of PV panel 50 Watts under raised irradiation conditions

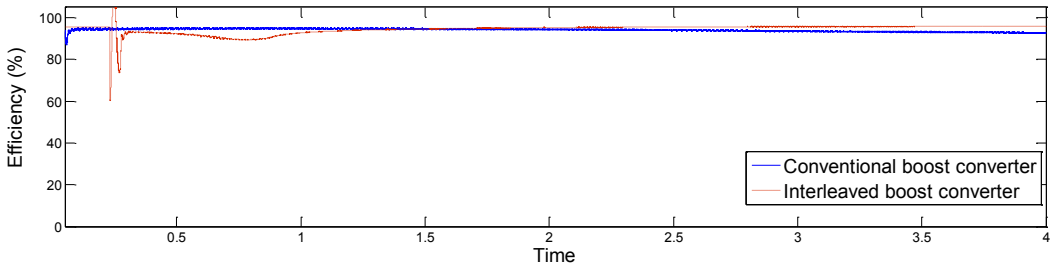

Fig. 6.28, Efficiency of interleaved and conventional boost converters under increased irradiation conditions and with inductive load

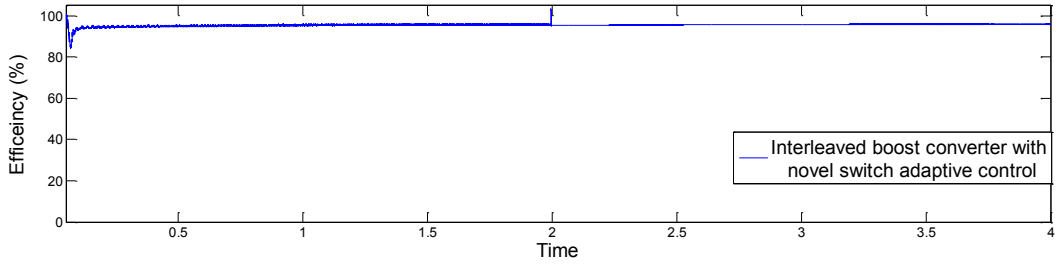

Fig. 6.29, Efficiency of interleaved boost converter with novel switch adaptive control under increased irradiation conditions and with inductive load

6. 3.2. Experimental results and discussion

The interleaved boost converter with novel switch adaptive control is tested with a solar panel of maximum power rate 50 Watts. For laboratory safety reasons the 210 Watts solar array has not been used. With its switch control, the converter uses only one phase when it is operating in conventional boost converter mode and two phases operating 180 degrees out of phase with each other when operating in interleaved boost converter mode. Pulse width modulation pins of the DSP are programmed to switch the gate voltage of the power Mosfet switch (Sc-switch) ON and OFF to isolate one of the limbs as shown in Fig. 6.7. The maximum power, current and voltage of the PV panel using an interleaved boost converter with novel switch adaptive control are obtained under different irradiation condition levels $150w/m^2, 25C^o$, $500w/m^2, 25C^o$, $1000w/m^2, 25C^o$ respectively.

At weather condition of $150w/m^2, 25C^o$ in Fig.6.30, the interleaved boost converter with novel switch adaptive control shows [channel 1] a maximum current array of 0.444 Amps with ripple of 0.039 Amps with ripple frequency of 10 KHz, maximum voltage array of 16.3 Volts with ripple of 1.47 Volts [channel 4], inductor 2 current at zero when limb two is isolated by the novel switch adaptive control [channel 3], and the current of inductor 1 in continuous conduction mode is 0.650 Amps [channel 2].

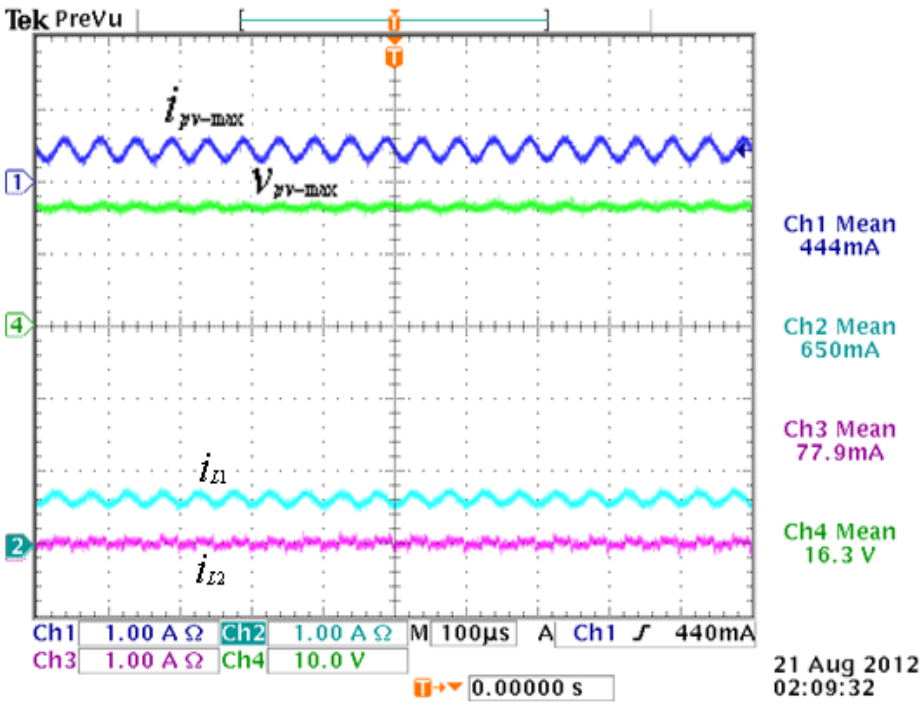

Fig. 6.30, Interleaved boost converter with novel switch adaptive control at irradiation $=150w/m^2, 25C^o$

In addition, Fig 6.31, shows the proposed boost converter at weather condition of 150w/m^2, 25C^o, with load current of 0.224 Amps with ripple approximates 0.0005 Amps [channel 1], and load voltage of 35.2 Volts with ripple is about 0.081 Volts [channel 4].

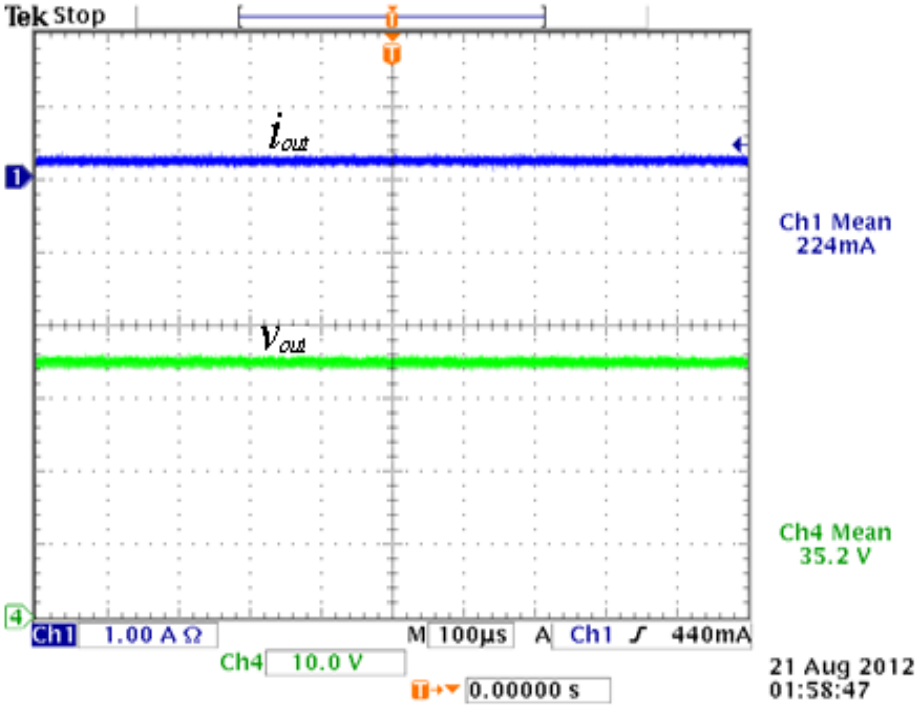

Fig. 6.31, Output current and voltage of interleaved boost converters with novel switch adaptive control at irradiation =150w/m^2, 25C^o

At irradiance levels of 500w/m^2, 25C^o, as seen in Fig. 6.32, the proposed boost converter control system operates at around 25 Watts. Results demonstrate a good dynamic response which adapts well to power variations during to operating conditions. Furthermore, the PV voltage quality is not affected by both transition periods and no significant distortion is observed in the voltage. The proposed converter reveals a maximum PV power of about 25 Watt, maximum current of 1.2 Amps [channel 1] a maximum PV voltage of 16.4 Volts [channel 4], inductor 2 current of 0.208 Amps [channel 3] when the limb two is non-isolated by the novel switch adaptive control, and inductor 1 current of 0.948 Amps [channel 2]. Also, Figs 6.33 shows the load characteristics waveforms at the time of response to the proposed boost converter' novel switch adaptive control at around operating point level of the maximum PV, shows load current of 0.350 Amps [channel 1], a load voltage of 65.2 Volts [channel 4], and load power of approximately 20 Watts.

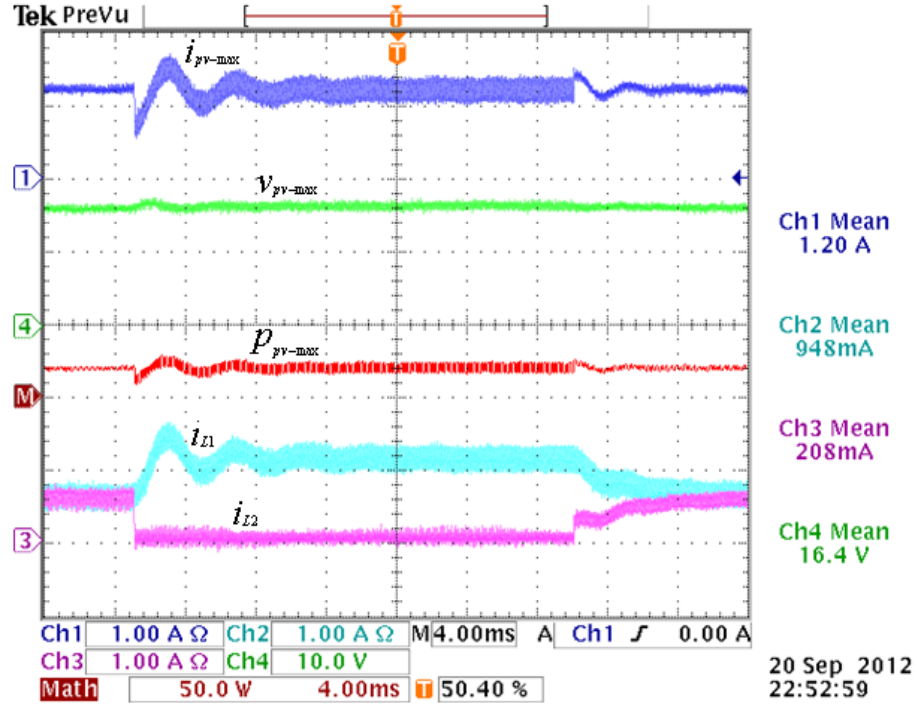

Fig. 6.32, Interleaved boost converter with novel switch adaptive control responses to PV power change around irradiation of 500w/m^2, 25C^o

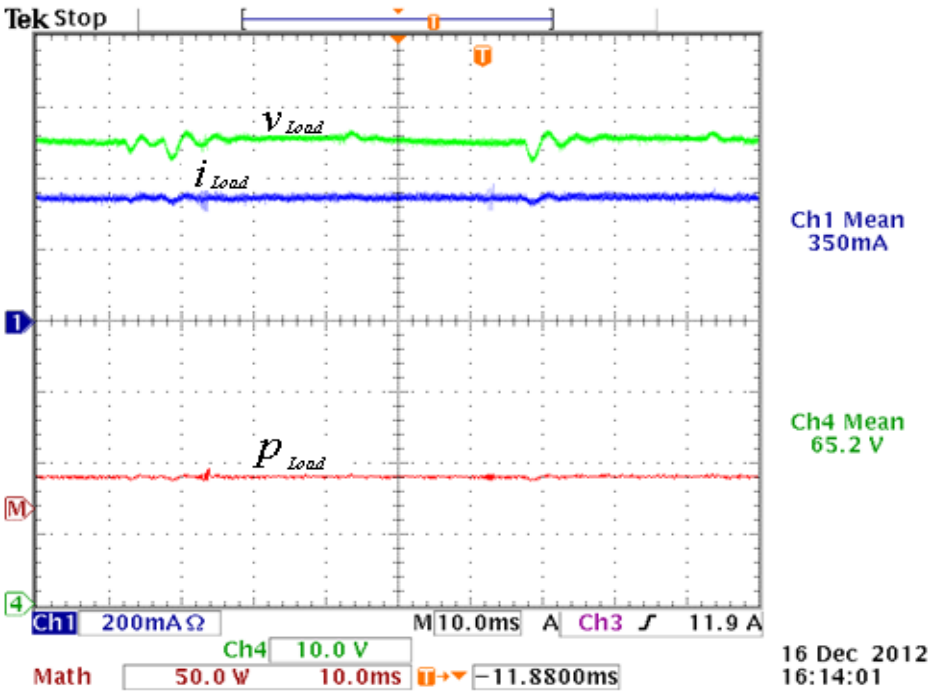

Fig. 6.33, Outputs response of interleaved boost converter with novel switch adaptive control under PV power change around irradiation of 500w/m^2, 25C^o

Fig. 6.34 shows the change of the proposed boost converter from conventional boost converter mode to interleaved boost converter mode at irradiation $500\text{w/m}^2, 25\text{C}^o$ which is achieved via the novel switch adaptive control to operate. The proposed boost converter shows a maximum current array of 1.2 Amps [channel 1], inductor 1 current of 0.730 Amps in [channel 2], inductor 2 current of 0.436 Amps [channel 3] when the limb two is connected by the novel switch adaptive control, a maximum voltage array of 17.2 Volts in [channel 4], and the maximum PV power is 25 Watt.

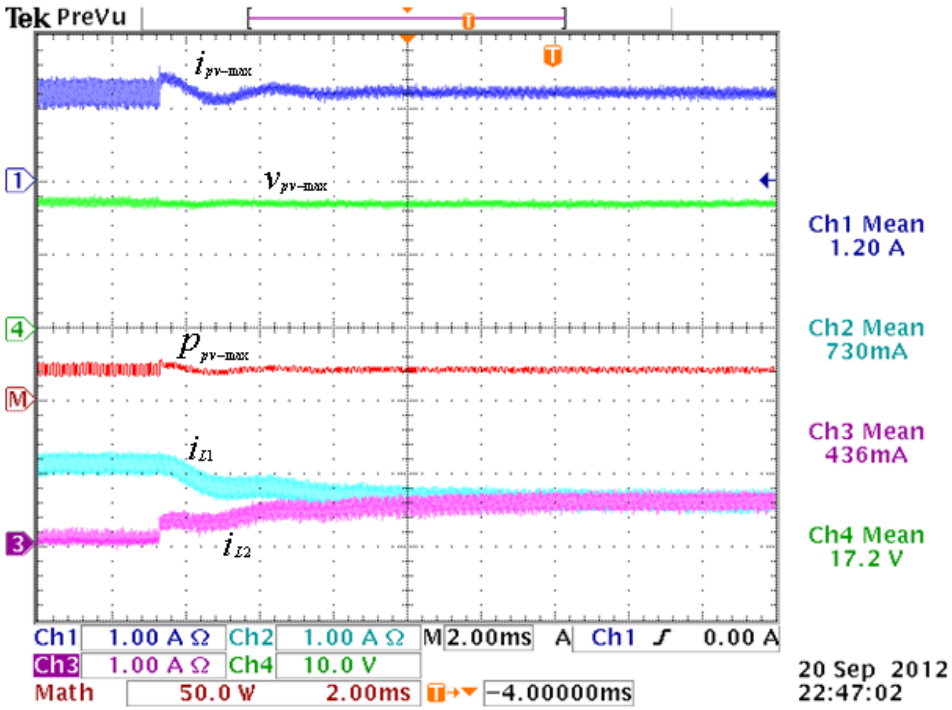

Fig. 6.34, Interleaved boost converter with novel switch adaptive control responses to transition from conventional to interleaved mode at irradiation of $500\text{w/m}^2, 25\text{C}^o$

A shown in Fig 6.35, with conditions of $1000\text{w/m}^2, 25\text{C}^o$, the proposed boost converter draws a PV panel current of 2.88 Amps with 0.25 Amps ripple and frequency of 10 KHz [channel 1] inductor current 1 is 1.43 Amps [channel 2], inductor current 2 is 1.38 Amps [channel 3],, and the maximum panel output voltage of 16.1 Volts with 1.4 Volts ripple [channel 4]. Furthermore, Fig. 6.36 shows the load characteristics of the interleaved boost converter with novel switch adaptive control at weather condition $1000\text{w/m}^2, 25\text{C}^o$; the load current is 0.495 Amps with 0.001 Amps ripple [channel 1] and the load voltage is 91.8 Volts with 1.45 Volts ripple [channel 4]. The output current and voltage of the interleaved

boost converter with novel switch adaptive control have very little ripple, as shown in figure 6.33.

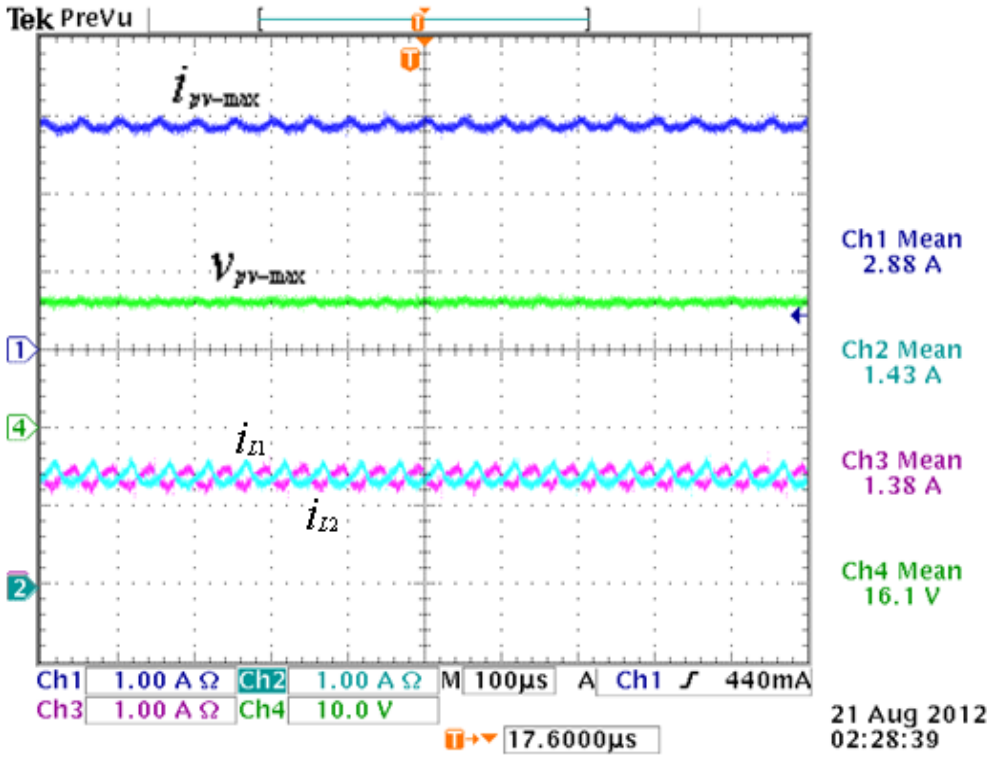

Fig. 6.35, Interleaved boost converter with novel switch adaptive control at irradiation of 1000w/m^2, 25C^o

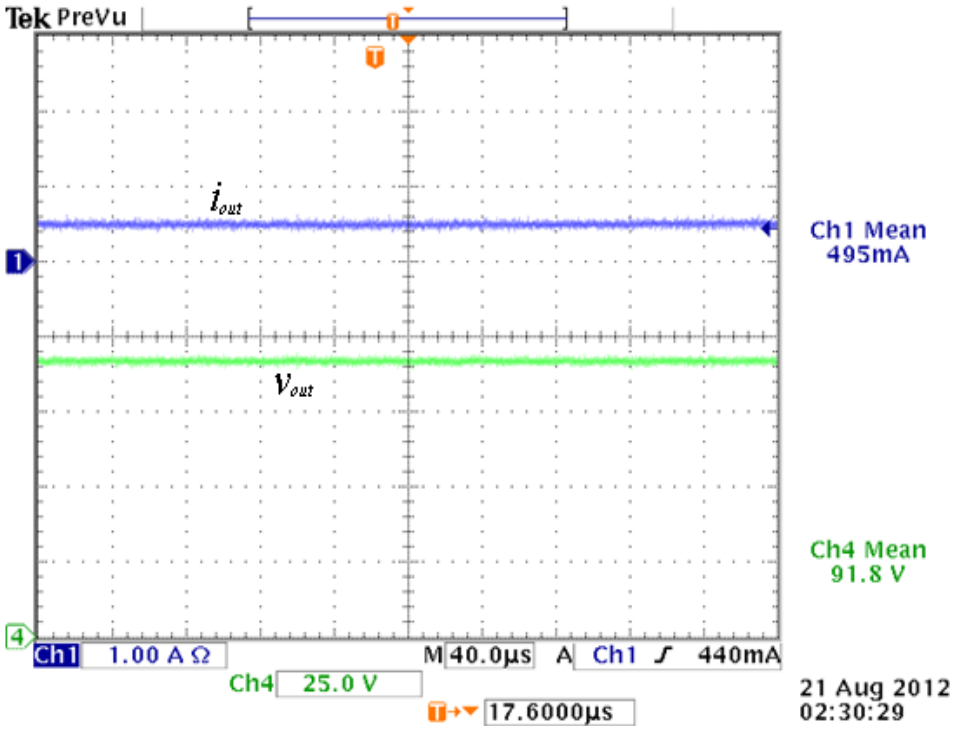

Fig. 6.36, Output current and voltage of Interleaved boost converter with novel switch adaptive control at irradiation=1000w/m^2, 25C^o.

Measured efficiency:

Table 6.2: Measured experimental efficiency of interleaved boost converter with novel switch adaptive control

		Interleaved boost converter with novel switch adaptive control efficiency (%)	
Irradiation (w/m^2)	PV power	Load = 195Ω	Load = 100Ω
150	7.5	90.93	92.14
200	10	91.12	92.38
300	15	91.86	92.5
400	20	92.12	92.48
500	25	91.92	91.76
600	30	91.79	91.74
700	35	91.81	91.84
800	40	91.63	91.56
900	45	91.59	91.35
1000	50	91.84	91.46

Table 6.3: Comparison of measured experimental efficiency

Irradiation (w/m^2)	Solar power (W)	Conventional boost converter efficiency (%)	Interleaved boost converter efficiency (%)	Interleaved with novel switch adaptive control efficiency (%)
100	5	91.51	87.51	90.69
150	7.5	92.2	87.81	90.72
200	10	92.52	88.49	91.22
300	15	92.8	89.51	92.06
400	20	92.77	90.59	92.4
500	25	92.35	91.51	92.54
600	30	92.11	91.8	92.39
700	35	91.2	91.95	91.97
800	40	90.77	91.9	91.89
900	45	90.06	91.85	91.59
1000	50	89.45	91.84	91.84

Discussion

Efficiency results for the interleaved boost converter with novel switch adaptive control (under various tests of atmospheric conditions and variable resistive load) are shown in Fig. 6.37 and in Table 6.2. As can be seen, the left axis (y) represents the efficiency of the converter with different load percentages, and axis (x) represents the maximum PV power that rises as the irradiation weather takes off that is shown on the right axis (y). The efficiency of the interleaved boost converter with novel switch adaptive control under 50 % (100 ohms) of its load, with low irradiation $150\text{w/m}^2, 25\text{C}^\text{o}$ and maximum available PV power of about 7 Watts, is 92.14%. After climbing to $300\text{w/m}^2, 25\text{C}^\text{o}$ and maximum available PV power of 15 Watts, the high efficiency level starts remain steady; as can be seen by similar results at irradiation levels of $450\text{w/m}^2, 25\text{C}^\text{o}$ and $600\text{w/m}^2, 25\text{C}^\text{o}$. At $1000\text{w/m}^2, 25\text{C}^\text{o}$, at near maximum PV power, the efficiency of the converter reaches 91.46 %. Moreover, with 100 percentage (195 ohm) a similar trend is observed; the converter shows the efficiency level to be around 91.9% at irradiation $400\text{w/m}^2, 25\text{C}^\text{o}$, $600\text{w/m}^2, 25\text{C}^\text{o}$, and $900\text{w/m}^2, 25\text{C}^\text{o}$ with maximum obtainable array power, but the converter shows a lower efficiency of 91.9% at $150\text{w/m}^2, 25\text{C}^\text{o}$ and $200\text{w/m}^2, 25\text{C}^\text{o}$ when the maximum PV power reduces due to the decrease in irradiation.

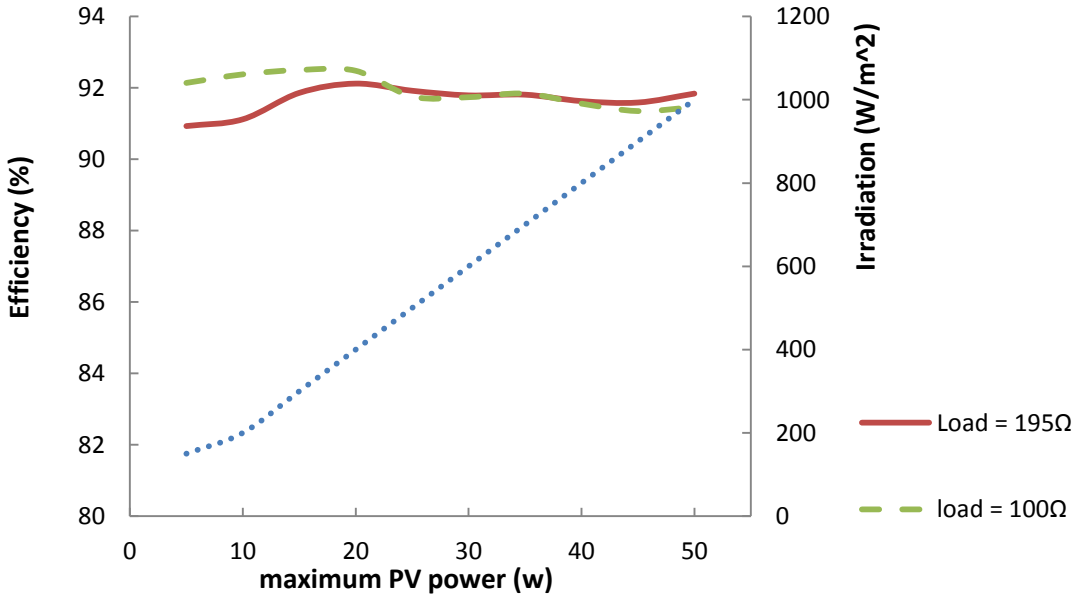

Fig. 6.37, Efficiency results of the experimental in the interleaved boost converter with novel switch adaptive control under irradiation atmosphere condition and load percentages

The results from the conventional power converters discussed in Chapter five and Chapter six, and the proposed topology (interleaved boost converter with novel switch adaptive control), are compared in Table 6.3. As can be seen in Fig. 6.38, the conventional boost converter drops in efficiency at high power; this scenario is expected by looking at equation (3.12), and has high efficiency at low power due to less current in the PV array. However, the interleaved boost converter shows the opposite, high efficiency at a high PV power level but shows a drop in efficiency at a low PV power level when the small current amount of PV is shared between interleaved limbs, operating in discontinued current mode (DCM), when switching loss dominates. Because the interleaved boost converter has two switches, the efficiency drops with a small PV panel current as compared to the conventional boost converter. The proposed, interleaved boost converter with novel switch adaptive control gives high efficiency with low and high PV power levels after combining the advantages of both a conventional and interleaved boost converter in the new projected converter scheme.

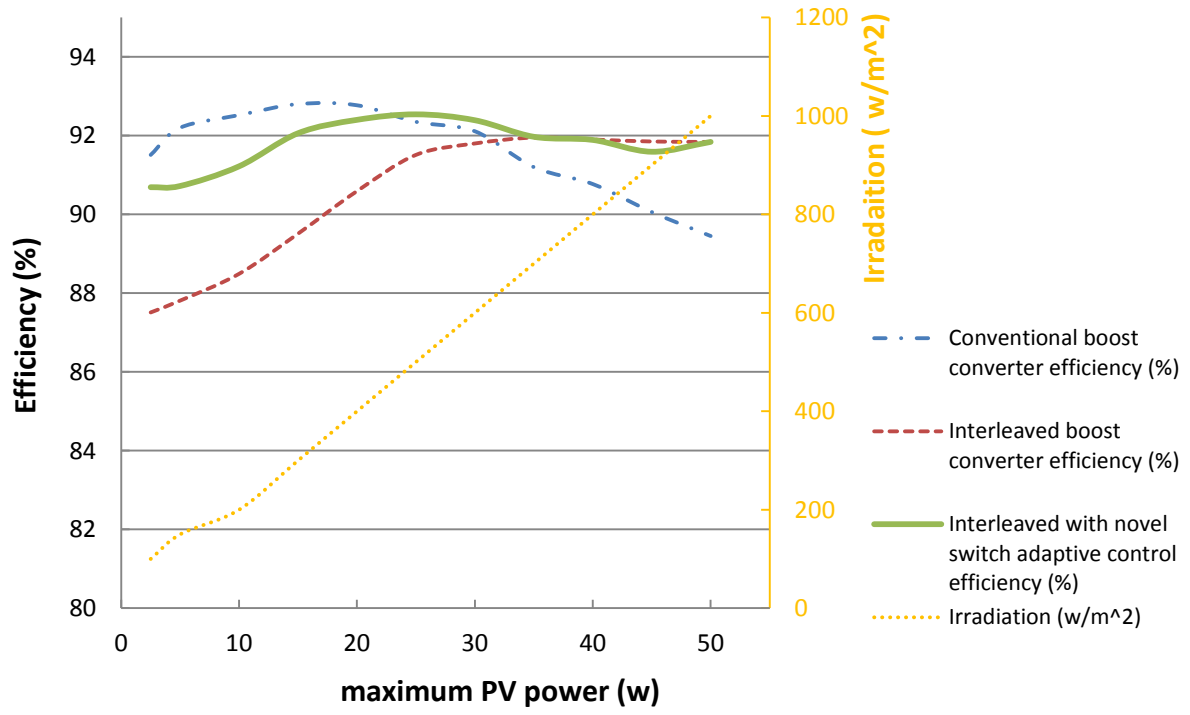

Fig. 6.38, Experimental efficiency results of discussed boost converters with different power levels of PV under atmospheric conditions

Annual energy gain

To convert power (kW) to energy (kWh), we assume the described converter will provide load power (49 Watts) for about 5 hours per day with irradiation 1000w/m^2, 25C^o , 365 days a year. With this example, the standalone PV system will produce 89.425 kWh energy per annum. Using the efficiency expression, the gained load power of discussed converter can be calculated as follows:

$P_{out-(load)} = P_{pv-max} \times \eta\,\%$

From this, the annually energy gained can be calculated as follows:

Annual energy gained = (Gained load power of the standalone PV system) × (five hours of day at different irradiation level) × (365days of the year)

Using this approach, similar energy gain figures can be calculated for different irradiance conditions for all three converter topologies; conventional boost converter, interleaved boost converter, and interleaved boost converter with novel switch adaptive control. The results are summarised in Table 6.4. Whilst a fairly simplistic approach, the results show that the interleaved boost converter with novel switch adaptive control achieves notable energy gain over the year given that the system will typically experience all irradiation conditions.

Table 6.4: evaluated experimental of gained energy of presented boost converters

Irradiation (w/m^2)	Max-PV power (w)	Conventional boost converter		Interleaved boost converter		Interleaved boost converter with novel switch adaptive control		Percentage improvement (%)
		Load power (w)	Annual energy gain (kwh)	Load power (w)	Annual energy gain (kwh)	Load power (w)	Annual energy gain (kwh)	
150	7.5	6.915	12.619	6.585	12.017	6.804	12.417	3.328
300	15	13.92	25.404	13.426	24.502	13.809	25.201	2.852
700	35	31.92	58.254	32.182	58.732	32.189	58.744	0.841
1000	50	44.725	81.623	45.92	83.804	45.92	83.804	2.672

6.4. Summary

The chapter has set out to combine the advantages of a conventional boost converter and an interleaved boost converter in a stage of the electronic power of standalone PV systems, so simulation and experimental are built to see the performance of the new proposed design in a standalone PV system under changeable atmospheric conditions.

The design performance of the interleaved boost converter with novel switch adaptive control is carried out by using the same value of parameters in both tests (software and hardware). The switch devices and the diodes are chosen the same that are used with the conventional boost converter and interleaved boost converter which are selected after an extensive calculation of key design considerations. Mainly, the cost and efficiency are essential factors in any power plant generation. However, in this scheme extra switch (Sc-switch) is added to the interleaved circuit to connect one of its limbs when it is needed. The requirement for an auxiliary switch in one limb of the proposed interleaved boost converter has been justified in simulation. It is also worth noting that this was also validated experimentally - the circuit failed (Mosfet failure) without this device!

This part of the study has created a design and confirmed that through both via simulation and hardware experiments, the projected interleaved boost converter with novel switch adaptive control exhibits high efficiency at both low and high power of PV panel when there is a changeable level in weather insolation. In the case of different loads, the interleaved boost converter with novel switch adaptive control with changeable load conditions has a high efficiency when receiving a low PV array power and also a high efficiency as the obtained photovoltaic power increases. Furthermore, the proposed circuit promises to operate in continuous current mode with different levels of used photovoltaic power and shows worthy produced gained energy through the year.

To conclude, the interleaved boost converter with novel switch adaptive control is a good choice for a standalone PV system that requires operating energy in a changeable insolation climate. Also, the interleaved boost converter with novel switch adaptive control can be selected if the key consideration is to have a boost converter that has a non-complicated circuit to operate, a low current ripple, moderate cost and high efficiency.

Chapter Seven

7. Conclusion

The aim of this project has been to conduct research into high efficiency standalone PV systems. This thesis has proposed a new control methodology which can be applied to interleaved DC-DC converters systems to improve the efficiency yield in PV systems over a wide range of operating conditions, including low irradiance conditions where interleaved converters typically struggle due to the potential for discontinuous current mode operation.

In order to achieve a high efficiency system, initial research into different MPPT algorithms was carried out. The survey revealed that there although significant research has been carried out into a vast number of different methods, the perturbation and observation (P&O) and incremental conductance (IC) based algorithms remain some of the most efficient and widely applied techniques on offer. For this reason, P&O was selected as the preferred method for achieving a high efficiency system in this work. Unfortunately, maximum power point tracking alone cannot overcome efficiency short falls in the power converter stage. Therefore, in order to transfer maximum power to the load, the DC-DC converter efficiency must also be improved. Literature review shows that much research has been carried out into developing new power converter topologies for high efficiency operation. However, this work has revealed that many of these solutions suffer from similar drawbacks; either the proposed solutions adds extra components and thus a rise in cost, controller complexity is significantly greater, or the power converter is optimised for maximum efficiency over a limited range. For this reason, this work set out to develop a simple power electronic and control solution, which offered excellent performance over both low and high irradiance conditions.

After a full review of typical power converter topologies, the interleaved boost converter was selected for this work. The benefits of the interleaved boost converter technique include low ripple amplitude and high frequency ripple power at the input and output waveforms due to an effective increase in switching frequency. Therefore, there is a chance to minimize the size of inductors and capacitors that would be relatively large if conventional boost converter technology is used. Furthermore, for a similar power rating, the current flowing in each limb of the interleaved converter is lower than a conventional DC-DC converter, hence reducing overall ($\mathbf{i^2r}$) losses. Unfortunately, operating an interleaved power converter under

low power conditions can lead to discontinuous current mode due to the split current in the separate branches. In photovoltaic applications this is a likely scenario under low irradiance conditions. At low power level where the switching losses dominate the interleaved converter will show low efficiency. In this case the presented conventional boost converter which has one branch to the current with fewer switches offers better efficiency.

For this reason, this thesis presents an interleaved power converter with a novel, yet simple, adaptive control strategy. The circuit behaves as a normal interleaved boost converter under high solar irradiance conditions, but under low irradiance levels the switching pattern is adjusted in real time so as to behave in the same way as a conventional boost converter. To achieve this dual mode of operation, it is shown that a single additional switch is required in the circuit. Simulation results show that this additional switch is necessary to protect the circuit when one of the limbs of the interleaved converter is inactive. Practical work also confirms this, as the boost converter fails (MOSFET fails) if this protection is not provided. At the initial outset of this research, it was not expected that this additional switch would be necessary. A future research goal from this work is to develop new strategies to remove the need for this auxiliary switch. Simulation and experimental research has demonstrated that the proposed interleaved boost converter controller is capable of achieving maximum power conversion efficiency at all times, under a wide range of atmospheric conditions and with different levels of load conditions. In this way, one of the major objectives of the research has been successful. To quantify the improvement of the system, results from this proposed power converter solution have been compared to a conventional DC/DC boost converter and a conventionally controlled interleaved boost converter. The following conclusions are made from the work:

Conventional boost converter: The study has found and confirmed through both simulation and experimental work that the conventional boost converter demonstrates the greatest PV panel output ripple and ripple in the power delivered to the load. Importantly, compared to the interleaved power converter, the conventional boost converter has a drop in efficiency at high power levels when there is higher insolation. However, the efficiency of the conventional boost converter increases when the output power of the PV solar panel drops due to a sudden fall of irradiation. In the case of a changeable load, the conventional boost converter with variable resistive load shows higher efficiency as the output photovoltaic power decreases, but it still has a low efficiency when receiving high PV array power. Looking at the I-V characteristics of a typical solar panel, it can be seen that the

current is a major factor in solar energy, so it is expected that the losses will increase as the PV array current rises due to the increase in insolation. Simulation and experiment results show that the conventional boost converter could be a good choice for a standalone PV system that regularly operates in low insolation conditions. Also the conventional boost converter can be selected if the key consideration is low cost and simple circuit operation.

Interleaved boost converter: The study has found, and confirmed through software and hardware experiments, that the interleaved boost converter exhibits lower output voltage/current ripple in comparison with the conventional boost converter. Furthermore, the interleaved boost converter has highest efficiency at high levels. However, the efficiency of the interleaved boost converter decreases when the power of the PV solar panel declines due to a plunge of irradiation. Looking at the system under low irradiation conditions, it can be seen that only a small current is present in the circuit, and this is shared between interleaved limbs. Therefore, the circuit is prone to entering discontinuous current mode (DCM), where switching loss dominates. An important conclusion from this stage of the work is that the efficiency characteristics are opposite to that of the conventional boost converter with respect to high/low irradiance conditions.

Interleaved boost converter with novel switch adaptive control: Here, the research set out to combine the advantages of a conventional boost converter and an interleaved boost converter. Importantly, the proposed circuit extends the range whereby the circuit operates in continuous conduction mode to much lower irradiance conditions. The operation of the circuit has been confirmed in simulation and practically. Additionally, in the case of different loads (resistive load or inductive load), the interleaved boost converter with novel switch adaptive control has shown high efficiency operation. The proposed boost converter has very attractive features, such as low current ripple at the input and output stages, low device stress. It promises to operate in continuous current mode over a wider range of operating conditions, and offers optimised high efficiency under all input and output conditions. In general, the circuit is a good choice for standalone PV systems that requires high efficiency operation in unpredictable weather conditions, or in locations which experience extended periods of time with low irradiance conditions.

Suggestions for Future work

The research in this thesis has considered the performance and efficiency of standalone PV systems. Based on the work presented in this thesis, areas for future work and consideration are summarized as follows:

1. The main area of future research lies in addressing the effect of the auxiliary switch which is added to the proposed of interleaved boost converter topology. Ideally, research into the control strategy may reveal a method for removing this switch. At present, such a method has not been developed. Alternatively, it may be possible to use a bidirectional interleaved boost converter to isolate one limb of the interleaved circuit. This can be achieved by controlling the four MOSFET switches and dead band between the two switches of one limb is needed and this may add extra losses of energy. This study can be compared with the proposed interleaved boost converter in this work.
2. A further study can be carried out to the proposed interleaved boost converter with novel switch adaptive control including active-clamp circuits or zero-voltage transmission ZVT commutation. With these circuits, it may be possible to further improve efficiency.
3. Investigation could be extended to the work carried out in this research for other standalone PV system loads such as inductive and capacitive loads. The work could also be employed and investigated for grid connected photovoltaic applications and with renewable energy sources. Another application area for consideration is battery storage systems.

References

[1] M. N. p, *converter application and design* vol. .et al(eds). : .[CD-Rom], 1989.

[2] M. L. a. C. Greenwood, "Green investing: Towards a clean energy infrastructure," World Economic Forum USA Inc. January 2009.

[3] E. A. O. a. F. Al-Ragom, "the effect of glazing and code compliance," in *Applied Energy*. vol. vol. 71, A. Energy, Ed., 2002, pp. pp. 75-86.

[4] M. L. a. A. Gurung, "Green Investing 2011," Reducing the Cost of Financing, World Economic Forum USA Inc April 2011.

[5] E. Martinot and J. L. Sawin, "Renewables 2012 global status report," Renewable Energy Policy Network for the 21st Century REN21 2012.

[6] E. Martinot and J. L. Sawin, "Renewables global status report 2009 update," Renewable Energy Policy Network for the 21st Century REN21 2009.

[7] H. Chihchiang, L. Jongrong, and S. Chihming, "Implementation of a DSP-controlled photovoltaic system with peak power tracking," *Industrial Electronics, IEEE Transactions on,* vol. 45, pp. 99-107, 1998.

[8] S. R. H. Hadi, S. Tokuda, "Evaluation of performance of photovoltaic system with maximum power point (MPP)," in *Solar Energy Materials and Solar Cells*. vol. vol. 75, 2003, pp. PP.673-678.

[9] B. D. R. Barlow, "Status and experience of solar PV pumping in developing countries," in *10th European Photovoltaic Solar Energy Conference*, 1991.

[10] C. S. F. D. M. Chapin, and G. L. Pearson, "A New Silicon p-n Junction Photocell For Converting Solar Radiation into Electrical Power," *Journal of Applied Physics,* vol. Vol. 25, May 1954.

[11] G. Walker, "Evaluating MPPT converter topologies using a MATLAB PV model," *Journal of Electrical & Electronics Engineering, Australia, IEAust,* vol. vol.21, pp. pp.49-56, 2001.

[12] F. M. G.-. longatt, "Model of Photovoltaic Module in Matlab," in *2do Congreso Iberoamericano De Estudianttes De Indenieria Electrica, Electronica Y Compucion* Maracay,Estado Aragua, Venezuela,, II CIBELEC 2005.

[13] E. Lorenzo, "Solar Electricity Engineering of Photovoltaic Systems," *Artes Graficas Gala, S.L., Spain,* 1994.

[14] H. S. Rauschenbach, *Solar Cell Array Design Handbook. New York*. New York: Van Norstrand Reinhold., 1980.

[15] a. V. U. H. A. Goetzberger, "Photovoltaic Solar Energy Generation," *Springer Series in Applied Science,* 2005.

[16] T. Esram and P. L. Chapman, "Comparison of Photovoltaic Array Maximum Power Point Tracking Techniques," *Energy Conversion, IEEE Transactions on,* vol. 22, pp. 439-449, 2007.

[17] Roberto Faranda and S. Leva, "Energy comparison of MPPT techniques for PV Systems," *WSEAS Transactions on Power Systems,,* vol. Volume 3, pp. 447-455, June 2008.

[18] D. Sera, T. Kerekes, R. Teodorescu, and F. Blaabjerg, "Improved MPPT method for rapidly changing environmental conditions," in *Industrial Electronics, 2006 IEEE International Symposium on*, 2006, pp. 1420-1425.

[19] S. Dwari and L. Parsa, "An Efficient High-Step-Up Interleaved DC–DC Converter With a Common Active Clamp," *Power Electronics, IEEE Transactions on,* vol. 26, pp. 66-78.
[20] L. Wuhua, Z. Yi, D. Yan, and H. Xiangning, "Interleaved Converter With Voltage Multiplier Cell for High Step-Up and High-Efficiency Conversion," *Power Electronics, IEEE Transactions on,* vol. 25, pp. 2397-2408.
[21] N. Shaban, "Development of typical meteorological year for Kuwait," Kuwait Institute for Scientific Research, Report KISR 5857, Kuwait 2000.
[22] N. Femia, G. Lisi, G. Petrone, G. Spagnuolo, and M. Vitelli, "Distributed Maximum Power Point Tracking of Photovoltaic Arrays: Novel Approach and System Analysis," *Industrial Electronics, IEEE Transactions on,* vol. 55, pp. 2610-2621, 2008.
[23] A. Ali, M. H. Saied, M. Z. Mostafa, and T. M. Abdel-Moneim, "A survey of maximum PPT techniques of PV systems," in *Energytech, 2012 IEEE*, Cleveland, OH, pp. 1-17.
[24] B. Subudhi and R. Pradhan, "A Comparative Study on Maximum Power Point Tracking Techniques for Photovoltaic Power Systems," *Sustainable Energy, IEEE Transactions on,* vol. 4, pp. 89-98, Jan, 2013.
[25] M. Barakati, M. Kazerani, and D. Aplevich, "Maximum power tracking control for a wind turbine system including a matrix converter," in *Power & Energy Society General Meeting, 2009. PES '09. IEEE*, 2009, pp. 1-1.
[26] C. Liang-Rui, T. Chih-Hui, L. Yuan-Li, and L. Yen-Shin, "A Biological Swarm Chasing Algorithm for Tracking the PV Maximum Power Point," *Energy Conversion, IEEE Transactions on,* vol. 25, pp. 484-493.
[27] M. A. Elgendy, B. Zahawi, and D. J. Atkinson, "Assessment of Perturb and Observe MPPT Algorithm Implementation Techniques for PV Pumping Applications," *Sustainable Energy, IEEE Transactions on,* vol. 3, pp. 21-33.
[28] N. Femia, G. Petrone, G. Spagnuolo, and M. Vitelli, "Optimization of perturb and observe maximum power point tracking method," *Power Electronics, IEEE Transactions on,* vol. 20, pp. 963-973, 2005.
[29] C. Dorofte, U. Borup, and F. Blaabjerg, "A combined two-method MPPT control scheme for grid-connected photovoltaic systems," in *Power Electronics and Applications, 2005 European Conference on*, 2005, pp. 10 pp.-P.10.
[30] C. Liu, B. Wu, and R. Cheung, "Advanced algorithm for MPPT control of photovoltaic systems," in *Canadian Solar Buildings Conference* Montreal, August 20-24, 2004.
[31] A. Yafaoui, B. Wu, and R. Cheung, "Implementation of maximum power point tracking algorithm for residenial photovoltaic systems," *2nd Canadian Solar Buildings Conference Calgary,* June 10 – 14, 2007.
[32] A. Giustiniani, G. Petrone, G. Spagnuolo, and M. Vitelli, "Low-Frequency Current Oscillations and Maximum Power Point Tracking in Grid-Connected Fuel-Cell-Based Systems," *Industrial Electronics, IEEE Transactions on,* vol. 57, pp. 2042-2053.
[33] V. Salas, E. Olias, A. Barrado, and A. Lazaro, "Review of the maximum power point tracking algorithms for stand-alone photovoltaic systems," *Solar Energy Materials and Solar Cells,* vol. 90, pp. 1555-1578, 2006.
[34] K. Yeong-Chau, L. Tsorng-Juu, and C. Jiann-Fuh, "Novel maximum-power-point-tracking controller for photovoltaic energy conversion system," *Industrial Electronics, IEEE Transactions on,* vol. 48, pp. 594-601, 2001.

[35] L. Jae Ho, B. HyunSu, and C. Bo Hyung, "Advanced Incremental Conductance MPPT Algorithm with a Variable Step Size," in *Power Electronics and Motion Control Conference, 2006. EPE-PEMC 2006. 12th International*, 2006, pp. 603-607.

[36] K. K. Tse, H. S. H. Chung, S. Y. R. Hui, and M. T. Ho, "A novel maximum power point tracking technique for PV panels," in *Power Electronics Specialists Conference, 2001. PESC. 2001 IEEE 32nd Annual*, 2001, pp. 1970-1975 vol. 4.

[37] R. F. Coelho, F. M. Concer, and D. C. Martins, "A MPPT approach based on temperature measurements applied in PV systems," in *Industry Applications (INDUSCON), 2010 9th IEEE/IAS International Conference on*, pp. 1-6.

[38] A. Brambilla, M. Gambarara, A. Garutti, and F. Ronchi, "New approach to photovoltaic arrays maximum power point tracking," in *Power Electronics Specialists Conference, 1999. PESC 99. 30th Annual IEEE*, 1999, pp. 632-637 vol.2.

[39] D. P. H. a. M. E. Ropp, "Comperative Study of Maximum Power Point Tracking Algorithms," SD. 57007-2220, USA.

[40] I. Laird, H. Lovatt, N. Savvides, D. Lu, and V. G. Agelidis, "Comparative study of maximum power point tracking algorithms for thermoelectric generators," in *Power Engineering Conference, 2008. AUPEC '08. Australasian Universities*, 2008, pp. 1-6.

[41] J. N. H.D. Maheshappa, M.V. Murthy, "An improved maximum power point tracker using a step-up converter with current locked loop," Renewable Energy, 13 (2) (1998) 195–201.

[42] H. Chihchiang and S. Chihming, "Comparative study of peak power tracking techniques for solar storage system," in *Applied Power Electronics Conference and Exposition, 1998. APEC '98. Conference Proceedings 1998., Thirteenth Annual*, 1998, pp. 679-685 vol.2.

[43] P. T. Krein, "Ripple correlation control, with some applications," in *Circuits and Systems, 1999. ISCAS '99. Proceedings of the 1999 IEEE International Symposium on*, 1999, pp. 283-286 vol.5.

[44] S. C. V. Arcidiacono, and L. Lambri, "Maximum power point tracker for photovoltaic power plants," in *in Proc. IEEE Photovoltaic Spec. Conf.* vol. pp. 507–512, 1982.

[45] S. Jain and V. Agarwal, "Comparison of the performance of maximum power point tracking schemes applied to single-stage grid-connected photovoltaic systems," *Electric Power Applications, IET,* vol. 1, pp. 753-762, 2007.

[46] R. M. Hilloowala and A. M. Sharaf, "A rule-based fuzzy logic controller for a PWM inverter in photo-voltaic energy conversion scheme," in *Industry Applications Society Annual Meeting, 1992., Conference Record of the 1992 IEEE*, 1992, pp. 762-769 vol.1.

[47] A. M. A. Mahmoud, H. M. Mashaly, S. A. Kandil, H. El Khashab, and M. N. F. Nashed, "Fuzzy logic implementation for photovoltaic maximum power tracking," in *Industrial Electronics Society, 2000. IECON 2000. 26th Annual Confjerence of the IEEE*, 2000, pp. 735-740 vol.1.

[48] A. M. A. Mahmoud, H. M. Mashaly, S. A. Kandil, H. El Khashab, and M. N. F. Nashed, "Fuzzy logic implementation for photovoltaic maximum power tracking," in *Robot and Human Interactive Communication, 2000. RO-MAN 2000. Proceedings. 9th IEEE International Workshop on*, 2000, pp. 155-160.

[49] N. Patcharaprakiti and S. Premrudeepreechacharn, "Maximum power point tracking using adaptive fuzzy logic control for grid-connected photovoltaic system," in *Power Engineering Society Winter Meeting, 2002. IEEE*, 2002, pp. 372-377 vol.1.

[50] T. Hiyama, S. Kouzuma, and T. Imakubo, "Identification of optimal operating point of PV modules using neural network for real time maximum power tracking control," *Energy Conversion, IEEE Transactions on,* vol. 10, pp. 360-367, 1995.

[51] L. Zhang, B. Yunfei, and A. Al-Amoudi, "GA-RBF neural network based maximum power point tracking for grid-connected photovoltaic systems," in *Power Electronics, Machines and Drives, 2002. International Conference on (Conf. Publ. No. 487)*, 2002, pp. 18-23.

[52] R. Faranda, S. Leva, and V. Maugeri, "MPPT techniques for PV Systems: Energetic and cost comparison," in *Power and Energy Society General Meeting - Conversion and Delivery of Electrical Energy in the 21st Century, 2008 IEEE*, 2008, pp. 1-6.

[53] A. N. A. Ali, M. H. Saied, M. Z. Mostafa, and T. M. Abdel-Moneim, "A survey of maximum PPT techniques of PV systems," in *Energytech, 2012 IEEE*, pp. 1-17.

[54] L. Po-Wa, L. Yim-Shu, D. K. W. Cheng, and L. Xiu-Cheng, "Steady-state analysis of an interleaved boost converter with coupled inductors," *Industrial Electronics, IEEE Transactions on,* vol. 47, pp. 787-795, 2000.

[55] M. Veerachary, T. Senjyu, and K. Uezato, "Neural-network-based maximum-power-point tracking of coupled-inductor interleaved-boost-converter-supplied PV system using fuzzy controller," *Industrial Electronics, IEEE Transactions on,* vol. 50, pp. 749-758, 2003.

[56] M. Veerachary, T. Senjyu, and K. Uezato, "Maximum power point tracking of coupled inductor interleaved boost converter supplied PV system," *Electric Power Applications, IEE Proceedings -,* vol. 150, pp. 71-80, 2003.

[57] A. Berasategi, C. Cabal, C. Alonso, and B. Estibals, "European efficiency improvement in photovoltaic applications by means of parallel connection of power converters," in *Power Electronics and Applications, 2009. EPE '09. 13th European Conference on*, 2009, pp. 1-10.

[58] B. Bidoggia, G. Spiazzi, S. Buso, T. Lequeu, and L. Ventura, "Design of a fuel cell based backup system for telecoms applications," in *Telecommunications Energy Conference, 2008. INTELEC 2008. IEEE 30th International*, 2008, pp. 1-8.

[59] D. J. Perreault and J. G. Kassakian, "Distributed interleaving of paralleled power converters," *Circuits and Systems I: Fundamental Theory and Applications, IEEE Transactions on,* vol. 44, pp. 728-734, 1997.

[60] L. Ching-Ming, P. Ching-Tsai, and C. Ming-Chieh, "High-Efficiency Modular High Step-Up Interleaved Boost Converter for DC-Microgrid Applications," *Industry Applications, IEEE Transactions on,* vol. 48, pp. 161-171.

[61] W. Jun, T. Jin, and K. Smedley, "A new interleaved isolated boost converter for high power applications," in *Applied Power Electronics Conference and Exposition, 2006. APEC '06. Twenty-First Annual IEEE*, 2006, p. 6 pp.

[62] C. Hanju, C. Jungwan, and H. Byung-moon, "A new three-phase interleaved isolated boost converter with active clamp for fuel cells," in *Power Electronics Specialists Conference, 2008. PESC 2008. IEEE*, 2008, pp. 1271-1276.

[63] Y. Wang and C. Klumpner, "Optimal design of a DC/DC converter for photovoltaic applications," in *Industrial Electronics Society, 2005. IECON 2005. 31st Annual Conference of IEEE*, 2005, p. 6 pp.

[64] W. Jianqiang, L. Jingxin, and Z. Weige, "Interleaved push-pull converter with very low input and high output," in *Power Electronics and Intelligent Transportation System (PEITS), 2009 2nd International Conference on*, 2009, pp. 247-249.

[65] L. Tsorng-Juu, C. Ren-Yi, C. Jiann-Fuh, and T. Wei-Jin, "Buck-type current-fed push-pull converter with ZCS for high voltage applications," in *TENCON 2007 - 2007 IEEE Region 10 Conference*, 2007, pp. 1-4.

[66] D. Vinnikov, T. Jalakas, and M. Egorov, "Feasibility study of half- and full-bridge isolated DC/DC converters in high-voltage high-power applications," in *Power Electronics and Motion Control Conference, 2008. EPE-PEMC 2008. 13th*, 2008, pp. 1257-1262.

[67] L. Chuang, G. Bin, L. Jih-Sheng, W. Mingyan, J. Yanchao, C. Guowei, Z. Zheng, C. Chien-Liang, Z. Cong, and S. Pengwei, "High-Efficiency Hybrid Full-Bridge–Half-Bridge Converter With Shared ZVS Lagging Leg and Dual Outputs in Series," *Power Electronics, IEEE Transactions on,* vol. 28, pp. 849-861.

[68] K. C. Tseng and T. J. Liang, "Novel high-efficiency step-up converter," *Electric Power Applications, IEE Proceedings -,* vol. 151, pp. 182-190, 2004.

[69] C. Shih-Kuen, L. Tsorng-Juu, C. Jiann-Fuh, and Y. Lung-Sheng, "Novel High Step-Up DC–DC Converter for Fuel Cell Energy Conversion System," *Industrial Electronics, IEEE Transactions on,* vol. 57, pp. 2007-2017.

[70] Y. Yusof, S. H. Sayuti, M. Abdul Latif, and M. Z. C. Wanik, "Modeling and simulation of maximum power point tracker for photovoltaic system," in *Power and Energy Conference, 2004. PECon 2004. Proceedings. National*, 2004, pp. 88-93.

[71] S. Chowdhury, S. P. Chowdhury, G. A. Taylor, and Y. H. Song, "Mathematical modelling and performance evaluation of a stand-alone polycrystalline PV plant with MPPT facility," in *Power and Energy Society General Meeting - Conversion and Delivery of Electrical Energy in the 21st Century, 2008 IEEE*, 2008, pp. 1-7.

[72] D. Kun, B. XinGao, L. HaiHao, and P. Tao, "A MATLAB-Simulink-Based PV Module Model and Its Application Under Conditions of Nonuniform Irradiance," *Energy Conversion, IEEE Transactions on,* vol. 27, pp. 864-872.

[73] "HIP Photovoltaic module," H. 210NH1-BO-1, Ed.: SANYO.

[74] H.-e.-m.-p. module, "Kd50se-1p, data sheet," in *Kyocera Fineceramics GmbH* Fritz-Mueller-Straße 27: 73730 Esslingen/Germany.

[75] S. M. Barakati, M. Kazerani, and J. D. Aplevich, "Maximum Power Tracking Control for a Wind Turbine System Including a Matrix Converter," *Energy Conversion, IEEE Transactions on,* vol. 24, pp. 705-713, 2009.

[76] R.Seyezhai, "Design Consideration of Interleaved Boost Converter for Fuel Cell Systems," *International Journal of Advanced Engineering Sciences and Technologies.Ssn College of Engineering, Chennai , India,* vol. Vol No. 7, Issue No. 2, 323 - 329, 2011.

[77] C. Gyu-Yeong, K. Hyun-Soo, L. Byoung-Kuk, and L. Won-Yong, "Design consideration of interleaved converters for fuel cell applications," in *Electrical Machines and Systems, 2007. ICEMS. International Conference on*, 2007, pp. 238-243.

[78] Z. Qun and F. C. Lee, "High-efficiency, high step-up DC-DC converters," *Power Electronics, IEEE Transactions on,* vol. 18, pp. 65-73, 2003.

[79] B. W. Williams, *Power electronics : devices, drivers, applications and passive components* 2nd ed.. ed.: Basingstoke, Hampshire England : Macmillan, 1992

[80] T. M. U. Ned Mohan, William P Robbins *Power electronics converters, applications, and design* Hoboken, NJ : John Wiley & Sons, c2003

[81] M. Veerachary, T. Senjyu, and K. Uezato, "Maximum power point tracking control of IDB converter supplied PV system," *Electric Power Applications, IEE Proceedings -,* vol. 148, pp. 494-502, 2001.

[82] M. H. Rashid, *Power Electronics - Circuits, Devices, and Applications* 3rd Edition ed.: Pearson Education, 2004.

[83] Taufik, "EE410 Power Electronics I - Lecture Note " Cal Poly State University: San Luis Obispo, 2004.

[84] A. Thenkani and N. Senthil Kumar, "Design of optimum Maximum Power Point Tracking algorithm for solar panel," in *Computer, Communication and Electrical Technology (ICCCET), 2011 International Conference on*, pp. 370-375.

[85] M. A. G. de Brito, L. Galotto, L. P. Sampaio, G. de Azevedo e Melo, and C. A. Canesin, "Evaluation of the Main MPPT Techniques for Photovoltaic Applications," *Industrial Electronics, IEEE Transactions on,* vol. 60, pp. 1156-1167.

[86] S. S. R. Gulam Amer1, "Estimation of Reliability of a Interleaving PFC Boost Converter," *Serbian Journal of Electrical Engineering* vol. Vol. 7, No. 2,, pp. 205-216, November 2010.

[87] O. Hegazy, J. Van Mierlo, and P. Lataire, "Analysis, Modeling, and Implementation of a Multidevice Interleaved DC/DC Converter for Fuel Cell Hybrid Electric Vehicles," *Power Electronics, IEEE Transactions on,* vol. 27, pp. 4445-4458.

[88] K. Dong-Hee, C. Gyu-Yeong, and L. Byoung-Kuk, "DCM Analysis and Inductance Design Method of Interleaved Boost Converters," *Power Electronics, IEEE Transactions on,* vol. 28, pp. 4700-4711, Oct, 2013.

[89] G. Amer Sandepudi and S. Rao, "Estimation of Reliability of a Interleaving PFC Boost Converter," *Serbian Journal of Electrical Engineering,* vol. Vol. 7, No. 2, , pp. 205-216, November 2010, .

[90] K. A. Praveen, A. Gulam, and R. S. Srinivasa, "Reliability Estimation for Power Factor Correction Circuits," *Asian Power Electronics Journal,,* vol. Vol. 3, No. 1,, Sept 2009.

[91] B. A. Miwa, D. M. Otten, and M. E. Schlecht, "High efficiency power factor correction using interleaving techniques," in *Applied Power Electronics Conference and Exposition, 1992. APEC '92. Conference Proceedings 1992., Seventh Annual*, 1992, pp. 557-568.

[92] A. Sayal, "MPPT techniques for photovoltaic system under uniform insolation and partial shading conditions," in *Engineering and Systems (SCES), 2012 Students Conference on*, March 2012, pp. 1-6.

Appendices

Data sheet of 50 Watt solar panel

THE NEW VALUE FRONTIER

KYOCERA

KD50SE-1P

High efficiency multicrystal photovoltaic module

CUTTING-EDGE TECHNOLOGY

Exhaustive research work, continuous further development of production processes and highly automated production enable polycrystalline Kyocera solar modules to attain an exceptional standard of quality and markedly high levels of efficiency.

The integrated Kyocera high-performance solar cells with a standard size of 156 mm x 156 mm achieve over 16 % efficiency, guaranteeing an extremely high annual yield of energy from the photovoltaic system.

To protect against the harshest weather conditions, the cells are embedded between a reinforced glass covering (hailstorm resistance complying with IEC 61215 ed. 2, tested by TÜV) and EVA foil, and are sealed with a PET foil backing. The laminate is set in a sturdy aluminum frame which is easy to assemble.

The junction box on the module backside is equipped with bypass diodes that eliminate the risk of the individual solar cells overheating (hot spot effect). The solar cables ensure flexible installation in the junction box which definitely simplifies the installation of standalone solutions in particular.

Kyocera manufactures all the components at its own production sites – without buying in semi-finished products – to ensure consistently high product quality.

EXAMPLES OF APPLICATION

- Stand-alone systems (electrifying remote houses, holiday homes and allotment systems, etc.)
- Supplying electricity to outlying villages and medical institutions in rural areas and development zones
- Emergency power supply, protection against catastrophes
- Pumping systems (drinking water supply and irrigation)
- Telecommunications (mobile phone networks, booster stations, etc.)
- Oil & gas (corrosion proofing, control, monitoring, etc.)

Pumping System

TUVdotCOM Service: Internet platform for tested quality and service
TUVdotCom-ID: 0000023574
IEC 61215 ed. 2, IEC 61730 and Safety Class II
Kyocera is ISO 9001 and ISO 14001 certified and registered.

TÜV

www.tuv.com
ID 0000023574

CE

KYOCERA SOLAR

We care!

SPECIFICATIONS

in mm

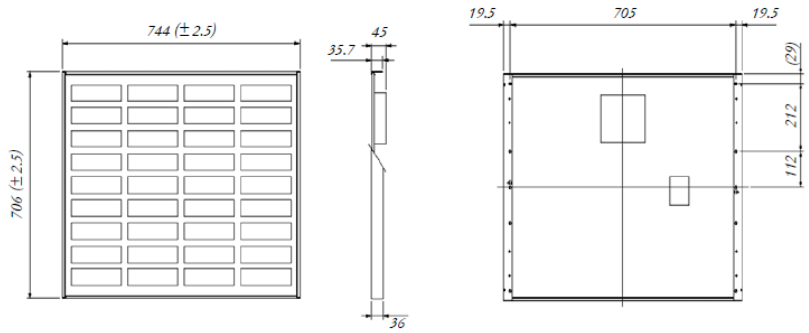

ELECTRICAL CHARACTERISTICS

Current-Voltage characteristics at various cell temperatures

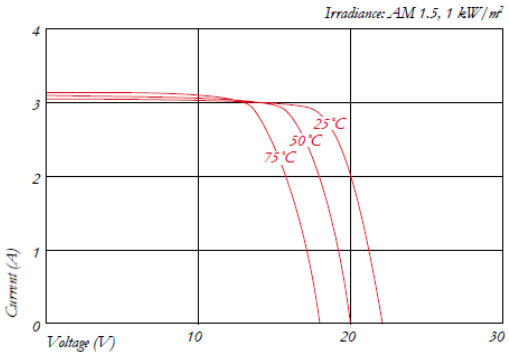

Current-Voltage characteristics at various irradiance levels

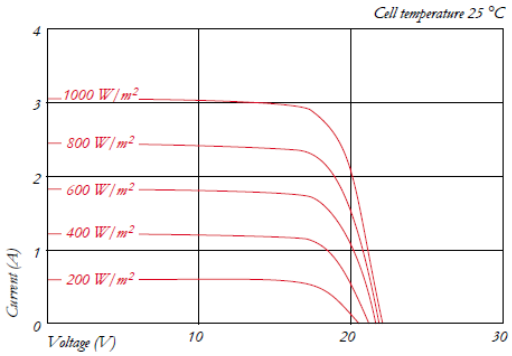

ELECTRICAL PERFORMANCE

PV Module Type		KD50SE-1P
At 1000 W/m² (STC)*		
Maximum Power	[W]	50
Maximum System Voltage	[V]	750
Maximum Power Voltage	[V]	17.9
Maximum Power Current	[A]	2.8
Open Circuit Voltage (V_{OC})	[V]	22.1
Short Circuit Current (I_{SC})	[A]	3.07
At 800 W/m² (NOCT)**		
Maximum Power	[W]	35
Maximum Power Voltage	[V]	15.8
Maximum Power Current	[A]	2.24
Open Circuit Voltage (V_{OC})	[V]	19.9
Short Circuit Current (I_{SC})	[A]	2.50
NOCT	[°C]	49
Power Tolerance	[%]	+10 / -5
Maximum Reverse Current I_R	[A]	6
Series Fuse Rating	[A]	6
Temperature Coefficient of V_{OC}	[V/°C]	-0.80×10^{-1}
Temperature Coefficient of I_{SC}	[A/°C]	1.84×10^{-3}
Temperature Coefficient of Max. Power	[W/°C]	-2.28×10^{-1}
Reduction of Efficiency (from 1000 W/m² to 200 W/m²)	[%]	2.3

DIMENSIONS

Length	[mm]	706 (±2.5)
Width	[mm]	744 (±2.5)
Depth / incl. Junction Box	[mm]	36 / 45
Weight	[kg]	6.5
Connection Type		Screw Terminals
Junction Box		
IP Code		[mm] 150x140x37.2
		IP65

GENERAL INFORMATION

Performance Guarantee	10*** / 20 years****
Warranty	5 years*****

CELLS

Number per Module		36
Cell Technology		polycrystalline
Cell Shape (rectangular)	[mm]	52x156
Cell Bonding		3 busbar

* *Electrical values under standard test conditions (STC): irradiation of 1000 W/m², airmass AM 1.5 and cell temperature of 25 °C*

** *Electrical values under normal operating cell temperature (NOCT): irradiation of 800 W/m², airmass AM 1.5, wind speed of 1m/s and ambient temperature of 20 °C*

*** *10 years on 90 % of the minimally specified power P under standard test conditions (STC)*

**** *20 years on 80 % of the minimally specified power P under standard test conditions (STC)*

***** *In the case of Europe*

Your local Kyocera dealer:

KYOCERA SOLAR

We care!

KYOCERA Fineceramics GmbH
Solar Division
Fritz-Mueller-Straße 27
73730 Esslingen/Germany
Tel: +49 (0)711-93 93 49 99
Fax: +49 (0)711-93 93 49 50
E-Mail: solar@kyocera.de
www.kyocerasolar.de

Data sheet of 210 Watt solar panel

HIT PHOTOVOLTAIC MODULE

HIP-210NH1-BO-1, HIP-205NH1-BO-1

The SANYO HIT (Heterojunction with Intrinsic Thin layer) solar cell is made of a thin mono crystalline silicon wafer surrounded by ultra-thin amorphous silicon layers. This product provides the industry's leading performance and value using state-of-the-art manufacturing techniques.

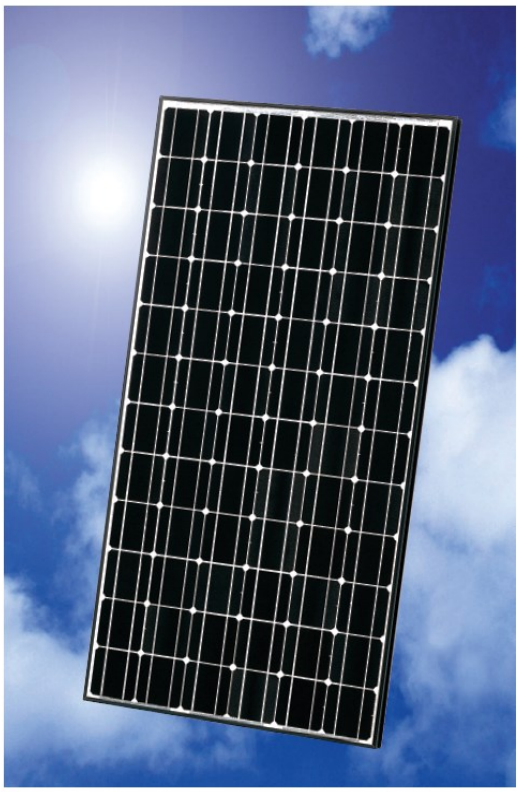

Benefit in Terms of Performance

High efficiency cell

Model	Cell Efficiency	Module Efficiency
HIP-210NH1-BO-1	18.9%	16.5%
HIP-205NH1-BO-1	18.4%	16.1%

The HIT cell and module have very high conversion efficiency in mass production.

High performance at high temperatures

Even at high temperatures, the HIT solar cell can maintain higher efficiency than a conventional crystalline silicon solar cell.

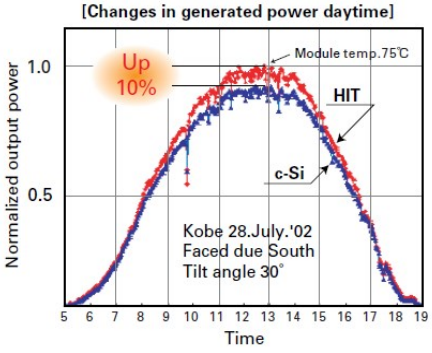

HIT Solar Cell Structure

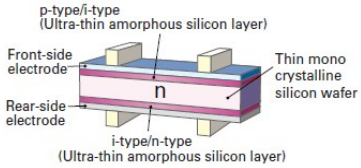

Development of HIT solar cell was supported in part by the New Energy and Industrial Technology Development Organization (NEDO).

Environmental Friendly Solar Cell

More Clean Energy

HIT can generate more clean Energy than other conventional crystalline solar cells.

Special Features

SANYO HIT solar modules are 100% emission free, have no moving parts and produce no noise.The dimensions of the HIT modules allow space-saving installation and achievement of maximum output power possible on given roof area.

Electrical and Mechanical Characteristics

HIP-210NH1-BO-1, HIP-205NH1-BO-1

Electrical data		Models HIP-xxxNH1-BO-1 210	205
Maximum power (Pmax)	[W]	210	205
Max. power voltage (Vmp)	[V]	41.3	40.7
Max. power current (Imp)	[A]	5.09	5.05
Open circuit voltage (Voc)	[V]	50.9	50.3
Short circuit current (Isc)	[A]	5.57	5.54
Warranted minimum power (Pmin)	[W]	199.5	194.8
Output power tolerance	[%]	+10/-5	
Maximum system voltage	[V]	600	
Temperature coefficient of Pmax	[%/°C]	-0.30	
Voc	[V/°C]	-0.127	-0.126
Isc	[mA/°C]	1.67	1.66

Note1: Standard Test Conditions: Air mass 1.5, Irradiance = 1000W/m^2, Cell temperature = 25°C

Note2: The values in the above table are nominal

Dimensions and weight

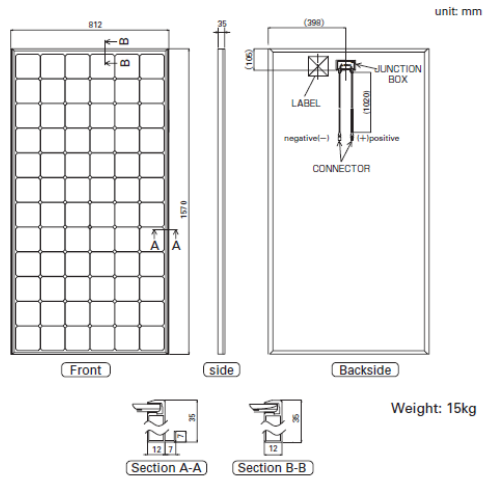

Reference data for model HIP-210NH1-BO-1

Dependence on irradiance

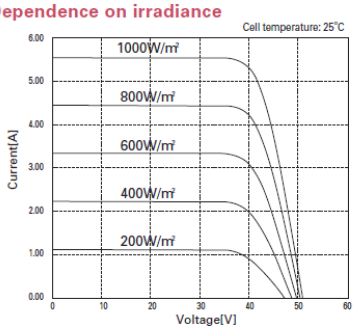

Reference data for model HIP-210NH1-BO-1

Dependence on temperature

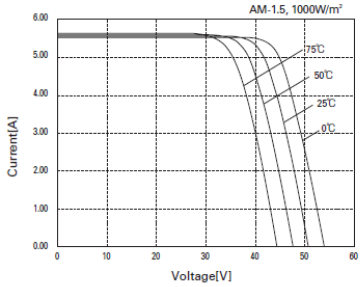

Please consult your local dealer for more information.

Warranty

Power output: 20 years (80% of minimum output power)
Product workmanship: 2 years
(Based on contract)

Certificate Number:PV05-53103-1004

An above number is a certification number by JET.
JET: Japan Electrical Safety&Environment Technology Laboratories

⚠ **CAUTION!** Please read the operating instructions carefully before using the products.

Due to our policy of continual improvement the products covered by this brochure may be changed without notice.

[ASIA & Oceania]
SANYO Sales & Marketing Corporation(Japan)
Tel.81-6-6992-1482 Fax.81-6-6992-1553
SANYO Sales & Marketing(Korea) Corporation
Tel.82-2-2273-6486 Fax.82-2-2273-5996
SANYO Energy (Taiwan) Co., Ltd.
Tel.886-2-8780-8810 Fax.886-2-8780-8850

[Africa]
SANYO South Africa (Pty) Ltd.
Tel.27-11-448-2929 Fax.27-11-448-2860

[Middle East]
SANYO Gulf FZE
Tel.971-4-887-3939 Fax.971-4-887-3969

SANYO

SANYO Electric Co.,Ltd
Clean Energy Company

http://www.sanyo.co.jp/clean/solar/hit_e/index_e.html
email: sola1011115@sanyo.co.jp

20060703

Results of measured efficiency to conventional boost converter and interleaved boost converter under irradiation conditions:

Table 4.4: Conventional boost converter measured hardware experiment efficiency; test is run in Aug of 2012

Irradiation (w/m^2)	Conventional boost converter efficiency (%) with load 195 ohm
100	91.51
150	92.2
200	92.52
300	92.8
400	92.77
500	92.35
600	92.11
700	91.2
800	90.77
900	90.06
1000	89.45

Table 5.4: Interleaved boost converter measured hardware experiment efficiency; test is run in Aug of 2012

Irradiation (w/m^2)	Interleaved boost converter efficiency (%) With load 195 ohm
100	87.51
150	87.81
200	88.49
300	89.51
400	90.59
500	91.51
600	91.8
700	91.95
800	91.9
900	91.85
1000	91.84

Analysis and calculation power losses to conventional boost converter

- The following demonstrates the losses analysis with different loading conditions to the main elements of the interleaved boost converter (inductors, Mosfet switches and diodes): when the output power of PV panel with G=300 w/m² and T=25C° gives maximum power (P_{pv-max}) = 59.99W, maximum power voltage (v_{pv-max}) = 38.5V and maximum power current (i_{pv-max}) = 1.55 A.

Because the assumption of efficiency is 100% then the output power is equal to the input power, so the output voltage of the converter under PV panel with G=300 w/m².

$$P_{out} = \frac{{V_{out}}^2}{R_{Load}}$$

$$V_{out} = \sqrt{59.99 \times 195} \cong 108\ volt$$

$$i_{out} = \sqrt{\frac{59.55}{195}} \cong 0.554\ Amps$$

$$D = 1 - \frac{V_{pv-max}}{V_{out}} = 1 - \frac{38.5}{108} \cong 0.65$$

Losses of inductor:

power losses on inductor with Δi = 9 % can be calculated as follows:

$i_{L-peak} = i_L + \Delta i_{Lp}$= 1.55 + (1.55× $\frac{9}{100}$) =1.689 A

$P_{loss-L} = (i_{L-peak})^2 \times r_L$ = $(1.689)^2$ × (0.3) = 0.855 Watt

Losses of Mosfet switch:

$$P_{Switc-switching\ loss} = \frac{1}{2} V_o i_{in} \left(t_{on} + t_r + t_{off} + t_f\right) f_S$$

$$= \frac{1}{2}(108)(1.55)\left((38 + 52 + 69 + 21)(10^{-9})\right) \times 20 \times 10^3 = 0.301$$

Watt

$$P_{Switch-conduction\ loss} = (r_{ds(on)} D)(i_{in})^2$$

$$= (7.3 \times 10^{-3})(0.65)(1.55)^2 = 5.699 \times 10^{-3}\ \text{Watt}$$

$$P_{gat-loss} = V_g\ Q_g f_s$$

$$= 20 \times (35 \times 10^{-9}) \times 20 \times 10^3 = 0.014\ \text{Watt}$$

Losses of diode:

$$P_{Diode-reverse\ recovery\ loss} = \frac{1}{2} V_{out} i_{RM}\ t_{rr}\ f_s$$

$$= \frac{1}{2}(108)(0.2)(25 \times 10^{-9})(20 \times 10^{3}) = 5.4 \times 10^{-3} \text{ Watt}$$

$$P_{Diode-conduction\ loss} = V_F i_F (1 - D)$$

Here the forward current is equal to the maximum inductor current $(I_F = i_L)$

$$P_{Diode-conduction\ loss} = (0.895)(1.55)(1 - 0.65) = 0.485 \text{ Watt}$$

The efficiency of the interleaved boost converter with output power of the PV panel under G=150 w/m² and T= 25 C° as below:

$$\eta = \frac{P_{pv-max} - (P_{inductor} + P_{switch} + P_{diode})}{P_{pv-max}} \times 100\%$$

$$\eta = \frac{59.99 - (0.855 + (0.301 + 5.69 \times 10^{-3} + 0.014) + (5.4 \times 10^{-3} + 0.485))}{59.99} \times 100\%$$

$$= 97.22$$

- Calculation of losses analysis with different loading conditions to the main elements of the interleaved boost converter (inductors, Mosfet switches and diodes) is as follows, when the output power of the PV panel with G=700 w/m² and T=25C° gives maximum power (P_{pv-max}) = 145.7W, maximum power voltage (v_{pv-max}) = 40.28V, and maximum power current (i_{pv-max}) = 3.618 A.

As assumption of efficiency is 100% then the output power is equal to the input power, so the output voltage of the converter under the PV panel with G=700 w/m².

$$P_{out} = \frac{{V_{out}}^2}{R_{Load}}$$

$$V_{out} = \sqrt{145.7 \times 195} \cong 168.55\ volt$$

$$i_{out} = \sqrt{\frac{145.7}{195}} \cong 0.864\ Amps$$

$$D = 1 - \frac{V_{pv-max}}{V_{out}} = 1 - \frac{40.28}{168.55} \cong 0.76$$

Losses of inductor:

power losses on inductor with Δi = 9 % can be calculated as follows:

$i_{L-peak} = i_L + \Delta i_{Lp}$= 3.618 + (3.618× $\frac{9}{100}$) =3.943 A

$P_{loss-L} = (i_{L-peak})^2 \times r_L$ = $(3.943)^2$ × (0.3) = 4.664 Watt

Losses of Mosfet switch:

$$P_{Switc-switching\ loss} = \frac{1}{2} V_o i_{in} \left(t_{on} + t_r + t_{off} + t_f\right) f_S$$

$= \frac{1}{2}(168.55)(3.618)\left((38 + 52 + 69 + 21)(10^{-9})\right) \times 20 \times 10^3$=1.097 Watt

$$P_{Switch-conduction\ loss} = r_{ds(on)}\ D\ (i_{in})^2$$

$$= (7.3 \times 10^{-3})(0.76)(3.618)^2 = 0.0363 \text{ Watt}$$

$$P_{gat-loss} = V_g\ Q_g f_s$$

$$= 20 \times (35 \times 10^{-9}) \times 20 \times 10^3 = 0.014 \text{ Watt}$$

Losses of diode:

$$P_{Diode-reverse\ recovery\ loss} = \frac{1}{2} V_{out} i_{RM}\ t_{rr}\ f_s$$

$= \frac{1}{2}(168.55)(0.2)(25 \times 10^{-9})(20 \times 10^3) = 8.4\ \times 10^{-3}$Watt

$$P_{Diode-conduction\ loss} = V_F i_F (1 - D)$$

Here the forward current is equal to the maximum inductor current $(I_F = i_L)$

$P_{Diode-conduction\ loss} = (0.895)(3.618)(1 - 0.76)$ = 0.777 Watt

Efficiency of the interleaved boost converter with output power of the PV panel under G=700 w/m² and T= 25 C° as below:

$$\eta = \frac{P_{pv-max} - (P_{inductor} + P_{switch} + P_{diode})}{P_{pv-max}} \times 100\%$$

$$\eta = \frac{145.7 - (4.664 + (1.097 + 0.0363 + 0.014) + (8.4\ \times 10^{-3} + 0.777))}{145.7} \times 100\%$$

$$= 95.47$$

Analysis and calculation power losses to interleaved boost converter

- Calculation of losses analysis with different loading conditions to the main elements of the interleaved boost converter (inductors, Mosfet switches and diodes), when the output power of PV panel with G=300 w/m² and T=25C° gives maximum power (P_{pv-max}) = 59.99W, maximum power voltage (v_{pv-max}) = 38.5V and maximum power current (i_{pv-max}) = 1.55 A.

Because the assumption of efficiency is 100% then the output power is equal to the input power, so the output voltage of the converter under the PV panel with G=300 w/m².

$$P_{out} = \frac{{V_{out}}^2}{R_{Load}}$$

$$V_{out} = \sqrt{59.99 \times 195} \cong 108\ volt$$

$$i_{out} = \sqrt{\frac{59.55}{195}} \cong 0.554\ Amps$$

$$D = 1 - \frac{V_{pv-max}}{V_{out}} = 1 - \frac{38.5}{108} \cong 0.65$$

Losses of inductor:

Then power losses on inductor with Δi = 9 % can be calculated as follows:

$$i_{L1} = i_{L2} = \frac{i_{pv-max}}{2} = \frac{i_{in}}{2} = \frac{1.55}{2} = 0.775A$$

$$i_{L1-peak} = i_{L1} + \Delta i_{L1} = 0.775 + (0.775 \times (9/100)) = 0.844A$$

$$P_{loss-L1} = (i_{L1-peak})^2 \times r_{L1} = (0.844)^2 \times 0.15 = 0.107W$$

$$i_{L2-peak} = i_{L2} + \Delta i_{L2} = 0.775 + 0.0697 = 0.844A$$

$$P_{loss-L2} = (i_{L2-peak})^2 \times r_{L2} = (0.844)^2 \times 0.15 = 0.107W$$

Whole losses on inductors of the interleaved boost converter are as follows:

$$P_{loss-Lw} = P_{loss-L1} + P_{loss-L2} = 0.107 + 0.107 = 0.214\ W$$

Losses of Mosfet switch:

$$P_{Switc-switching\ loss} = 2\frac{1}{2}V_o\left(\frac{i_{in}}{2}\right)\left(t_{on} + t_r + t_{off} + t_f\right)f_S$$

$$= \frac{1}{2}(108)(1.55)\left((38 + 52 + 69 + 21)(10^{-9})\right) \times 20 \times 10^3 = 0.301\ \text{Watt}$$

$$P_{Switch-conduction\ loss} = 2(r_{ds(on)}D)\left(\frac{i_{in}}{2}\right)^2$$

$$= 2(7.3 \times 10^{-3})(0.65)\left(\frac{1.55}{2}\right)^2 = 5.699 \times 10^{-3} \text{ Watt}$$

$$P_{gat-loss} = 2V_g\ Q_g f_s$$

$$= 2 \times 20 \times (35 \times 10^{-9}) \times 20 \times 10^3 = 0.028 \text{ Watt}$$

Losses of diode:

$$P_{Diode-reverse\ recovery\ loss} = 2\frac{1}{2}V_{out} i_{RM}\ t_{rr}\ f_s$$

$$= (108)(0.2)(25 \times 10^{-9})\ (20 \times 10^3) = 0.0108 \text{ Watt}$$

$$P_{Diode-conduction\ loss} = 2V_F \frac{i_F}{2}(1 - D)$$

Here the forward current is equal to the maximum inductor current $(I_F = i_L)$

$$P_{Diode-conduction\ loss} = 2(0.895)(1.55/2)(1 - 0.65) = 0.485 \text{ Watt}$$

Efficiency of the interleaved boost converter with output power of the PV panel under G=300 w/m² and T= 25 C° as below:

$$\eta = \frac{P_{pv-max} - (P_{inductor} + P_{switch} + P_{diode})}{P_{pv-max}} \times 100\%$$

$$\eta = \frac{59.99 - (0.214 + \left(0.301 + 5.69 \times 10^{-3} + 0.028\right) + (0.010 + 0.485))}{59.99} \times 100\%$$

$$= 98.2$$

- The following is losses analysis with different loading conditions to the main elements of the interleaved boost converter (inductors, Mosfet switches and diodes), when the output power of the PV panel with G=700 w/m² and T=25C° gives maximum power (P_{pv-max}) = 145.7W, maximum power voltage (v_{pv-max}) = 40.28V, and maximum power current (i_{pv-max}) = 3.618 A.

As the assumption of efficiency is 100% then the output power is equal to the input power, so the output voltage of the converter under the PV panel with G=700 w/m².

$$P_{out} = \frac{{V_{out}}^2}{R_{Load}}$$

$$V_{out} = \sqrt{145.7 \times 195} \cong 168.55\ volt$$

$$i_{out} = \sqrt{\frac{145.7}{195}} \cong 0.864\ Amps$$

$$D = 1 - \frac{V_{pv-max}}{V_{out}} = 1 - \frac{40.28}{168.55} \cong 0.76$$

Losses of inductor:

Then power losses on the inductor with Δi = 9 % can be calculated as follows:

$$i_{L1} = i_{L2} = \frac{i_{pv-max}}{2} = \frac{i_{in}}{2} = \frac{3.618}{2} = 1.809A$$

$$i_{L1-peak} = i_{L1} + \Delta i_{L1} = 1.809 + (1.809 \times (9/100)) = 1.971A$$

$$P_{loss-L1} = (i_{L1-peak})^2 \times r_{L1} = (1.971)^2 \times 0.15 = 0.582W$$

$$i_{L2-peak} = i_{L2} + \Delta i_{L2} = 1.809 + 0.1628 = 1.971A$$

$$P_{loss-L2} = (i_{L2-peak})^2 \times r_{L2} = (1.971)^2 \times 0.15 = 0.582W$$

Whole losses on inductors of the interleaved boost converter are as follows:

$$P_{loss-Lw} = P_{loss-L1} + P_{loss-L2} = 0.582 + 0.582 = 1.164\ W$$

Losses of Mosfet switch:

$$P_{Switc-switching\ loss} = 2\frac{1}{2}V_o\left(\frac{i_{in}}{2}\right)\left(t_{on} + t_r + t_{off} + t_f\right)f_S$$

$$= \frac{1}{2}(168.55)(3.618)\left((38 + 52 + 69 + 21)(10^{-9})\right) \times 20 \times 10^3 = 1.097\ \text{Watt}$$

$$P_{Switch-conduction\ loss} = 2(r_{ds(on)}D)\left(\frac{i_{in}}{2}\right)^2$$

$$= 2(7.3 \times 10^{-3})(0.76)\left(\frac{3.618}{2}\right)^2 = 0.0363\ \text{Watt}$$

$$P_{gat-loss} = 2V_g\ Q_g f_s$$

$$= 2 \times 20 \times (35 \times 10^{-9}) \times 20 \times 10^3 = 0.028\ \text{Watt}$$

Losses of diode:

$$P_{Diode-reverse\ recovery\ loss} = 2\frac{1}{2}V_{out} i_{RM}\ t_{rr}\ f_s$$

$$= (168.55)(0.2)(25 \times 10^{-9})\ (20 \times 10^{3}) = 0.0168 \text{ Watt}$$

$$P_{Diode-conduction\ loss} = 2V_F \frac{i_F}{2}(1 - D)$$

Here the forward current is equal to the maximum inductor current $(I_F = i_L)$

$$P_{Diode-conduction\ loss} = 2(0.895)(3.618/2)(1 - 0.76) = 0.777 \text{ Watt}$$

Efficiency of interleaved boost converter with output power of the PV panel under G=700 w/m² and T= 25 C° as below:

$$\eta = \frac{P_{pv-max} - (P_{inductor} + P_{switch} + P_{diode})}{P_{pv-max}} \times 100\%$$

$$\eta = \frac{145.7 - (1.164 + (1.097 + 0.0363 + 0.028) + (0.0168 + 0.777))}{145.7} \times 100\% = 97.85$$

The output power ripple of conventional and interleaved boost converter:

The output power of the conventional and interleaved boost converter is obtained under different irradiation conditions. As shown in the figures bellow, the output power ripple amplitude of the interleaved boost converter is lower than the conventional boost converter. Also, the interleaved boost converter has more output ripple frequency and higher output power in comparison with the conventional boost converter with the same input power under irradiation $500\text{w/m}^2, 25\text{C}^\text{o}$. However, the conventional boost converter shows higher output power than the interleaved boost converter with input power under irradiation 100w/m^2, 25C^o. This shows and proves that the interleaved boost converter has small losses at high power levels and large losses at low power levels, while the conventional is vice versa.

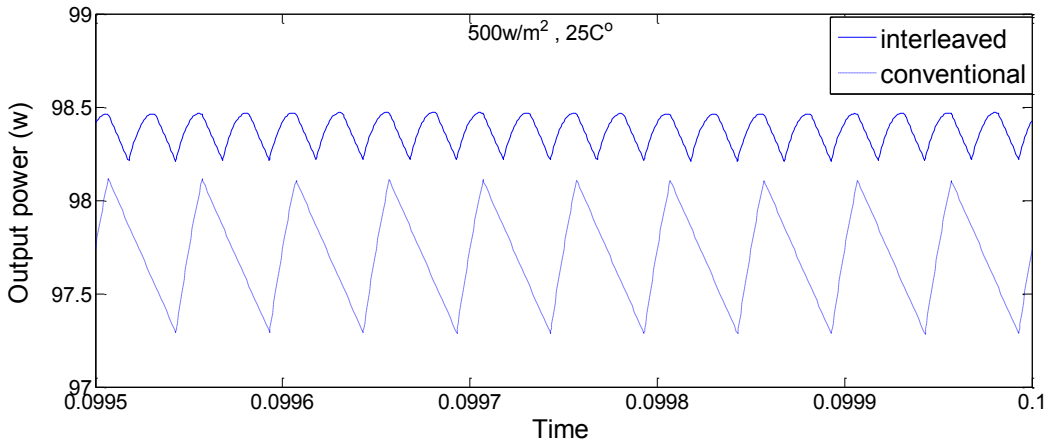

Figure : Output power of conventional and interleaved boost converter under 500w/m^2, 25C^o,

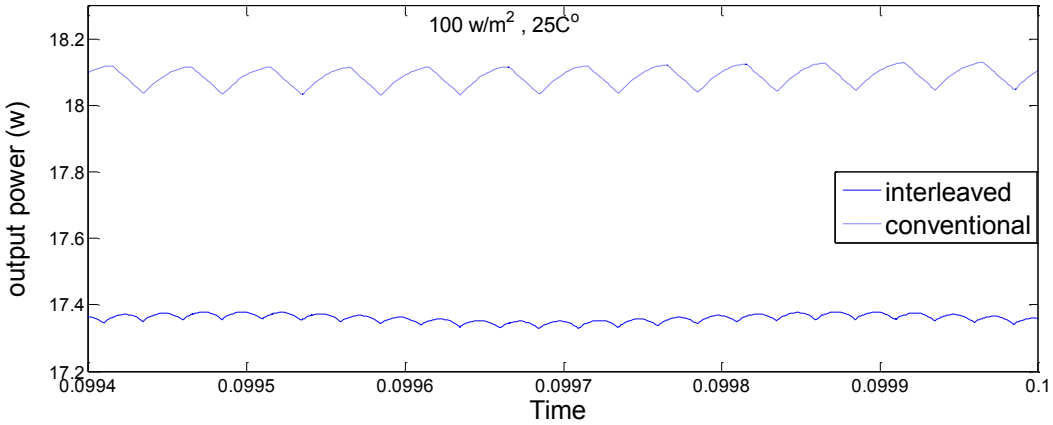

Figure : Output power of conventional and interleaved boost converter under 100w/m^2, 25C^o,